University of Wisconsin
Department of Meteorology
Madison, October 1965

FINAL REPORT 1965

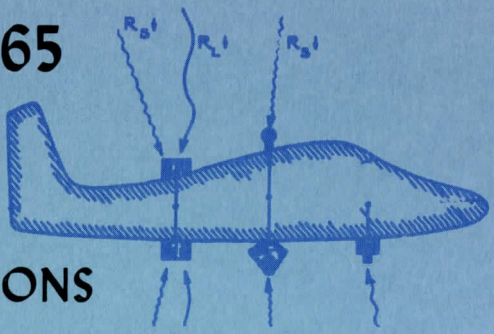

STUDIES OF THE EFFECTS OF VARIATIONS IN BOUNDARY CONDITIONS ON THE ATMOSPHERIC BOUNDARY LAYER

HEINZ H. LETTAU
Project Supervisor

Contributions by
Harry L. Hamilton, Jr.
Warren B. Johnson, Jr.
Donald H. Lenschow

Contract DA-36-039-AMC-00878 (E)
DA Task IVO-1-501-B53A-08

Sponsored by Department of Meteorology
U.S. Army Electronics Research and Development Activity
Fort Huachuca, Arizona

400-2.70

University of Wisconsin
Department of Meteorology
Madison, October 1965

FINAL REPORT 1965

STUDIES OF THE EFFECTS OF VARIATIONS IN BOUNDARY CONDITIONS ON THE ATMOSPHERIC BOUNDARY LAYER

Heinz H. Lettau
Project Supervisor

Contributions by
Harry L. Hamilton, Jr.
Warren B. Johnson, Jr.
Donald H. Lenschow

Contract DA-36-039-AMC-00878(E)
DA Task IVO-14501-B53A-08

Sponsored by Department of Meteorology
U. S. Army Electronics Research and Development Activity
Fort Huachuca, Arizona

GENERAL INTRODUCTION

This "Final Report", together with two previous "Annual Reports" submitted in December, 1964, and November, 1963, conforms with the terms of a three-year contract between the U. S. Army Electronics Research and Development Activity, Fort Huachuca, Arizona, and The University of Wisconsin. The contract period began on 1 October 1962, and ended on 30 September 1965. The defined purpose of the contract was a study of effects of variations in boundary conditions on the three-dimensional structure of the planetary boundary layer which, for practical purposes, can be loosely defined as the atmospheric layer adjacent to the ground, up to approximately 5,000 feet, on the average. It was specified in the statement of work that a coordination of theoretical as well as experimental studies and approaches was required. The outlines of the research work are relatively broad so that the following systematic breakdown into several sub-areas of special effort was found very convenient for reporting on individual quarterly periods of the contract:

1. Theoretical investigation of the wind-profile structure in the entire boundary layer
2. Testing of theoretical models developed under above Item 1.
   - 2.1 Testings using synoptic-type data
   - 2.2 Testings using experimental data
3. Theoretical investigation of diabatic surface layer structure
4. Experimental micrometeorological work
   - 4.1 Experiments dealing with controlled variation in aerodynamic surface roughness on lake ice in the winter season
   - 4.2 Measurements of shear stress effects in stratified air over Lake Mendota in the summer season
   - 4.3 Controlled thermal response experiments on various natural surfaces
5. Measurements in boundary layers using airborne instrumentation

For each one of the above listed sub-areas progress can be, or has been, reported and is documented by the totality of fourteen technical papers submitted in the three "Reports" (five sections of the Annual Report 1963, four in the Annual Report 1964, and five in the present Final Report). Everyone of the individual sections in these three contract reports is accompanied by an abstract in which details of the

scientific problems under investigation, and the main results of the research, are outlined. In the following, an over-all summary is supplied, which is of necessity relatively brief, in view of the wide range of the effort, and represents mainly a classification of research titles by the sub-areas listed above.

1. Theoretical Investigations of Boundary Layer Structure

Strictly theoretical work is reported in Section 4 of "Annual Report 1964", entitled "Preliminary note on the effect of terrain-slope on low-level jets and thermal winds in the planetary boundary layer", and in the major parts of Sections 1 and 2 of the "Final Report" entitled "A universal law relating eddy to mean states, applied to turbulence in ducts", and "Longitudinal versus lateral eddy length scale"; all three are authored by H. Lettau. Theoretical aspects are also presented in parts of Section 3 of the "Final Report", in the paper by W. Johnson, Jr., entitled "Atmospheric boundary layer dynamics over the forests of northeastern Wisconsin."

2.1 Testings of Theoretical Models Using Synoptic-Type Data

U. S. Weather Bureau and synoptic observations for the entire northern hemisphere were utilized by E. Kung in Section 2 of "Annual Report 1963", entitled "Climatology of aerodynamic roughness parameter and energy dissipation in the planetary boundary layer of the Northern Hemisphere"; also, in part, by W. Johnson, Jr., in Section 3 of "Final Report" listed above under (1).

2.2 Testings of Theoretical Models Using Experimental Data

A special surface-layer problem was investigated by H. Lettau in Section 5 of "Annual Report 1963" entitled "Preliminary note on the theory of steady katabatic flow for height-dependent eddy diffusivity". The major contribution in the area of surface-layer research is Section 5 of "Final Report", by H. Hamilton, Jr., entitled "Measurements of infrared radiation-divergence and temperature profiles near an air-water interface".

4.1 Experiments dealing with Controlled Variation in Aerodynamic Surface Roughness of Lake Ice in the Winter Season

In the years preceding the contract period, a relatively novel approach to atmospheric research had been inaugurated at Wisconsin, which is open-air experimentation in natural wind fields, with controlled and reproducible modification of physical interface-parameters (such as aerodynamic surface roughness, or albedo) at a scale significantly larger than that of wind tunnel experimentation. Controlled variations in aerodynamic surface roughness on lake ice were produced by laying out fields

of several hundred obstacles such as bushel baskets of different albedo, or small conifer trees trimmed to uniform size. J. Kearns and R. Deland employed fields of bushel baskets and contributed Section 3 of "Annual Report 1963" entitled "The modification of temperature variance spectra in airflow over artificially controlled surface roughness". In Section 4 of "Annual Report 1963", under the title "Report on two wind-profile modification experiments in air flow over the ice of Lake Mendota", C. Stearns and H. Lettau evaluate work using black and white bushel baskets (permitting control of surface roughness as well as of Richardson number), and conifer trees. In Section 3 of "Annual Report 1964", C. Stearns discusses newer measurements under the title "Report on Wind-profile modification experiments using fields of Christmas trees on the ice of Lake Mendota".

4.2 Measurements of Shear Stress Effects in Stratified Air over Lake Mendota in the Summer Season

Previous micrometeorological field work in air over the open water of Lake Mendota had shown that the problem of measuring shear stress cannot be separated from the problem of measuring simultaneously the eddy transfer of heat from water to air. This transforms the problem into one of studying air-mass modification on the 5 to 10 km scale. In Section 1 of "Annual Report 1964", A. Super has contributed a pertinent study entitled "Preliminary results of air mass modification study over Lake Mendota".

4.3 Controlled Thermal Response Experiments on Various Natural Surfaces

A significant contribution is Section 2 of "Annual Report 1964" by J. Turner, entitled "A thermal response experiment on lake ice".

5. Measurements in Boundary Layers Using Airborne Instrumentation

In view of the sizable vertical extent of the atmospheric boundary layer and the significant degree of horizontal variability of interface structure of natural terrain, sampling by sensors mounted on an airplane, and survey flights with a systematic pattern of alternating horizontal and vertical soundings, is imperative. In Section 4 of "Final Report" entitled "Airborne measurements of atmospheric boundary layer structure", D. Lenschow uses this technique for investigation of two special meteorological problems. The first is coordination with, and support of, W. Johnson's mean-wind-profile study mentioned above in (1). The second is the experimental investigation of a series of air-mass modification cases, on the 100-km scale, predominantly with cold air moving across Lake Michigan in early winter.

For more detailed summaries of results, reference must be made to the abstracts which accompany the individual papers. Eight of the authors or co-authors of articles were graduate students, supported by the contract as research assistants. With parts of their thesis work included in the three contract reports, six of these students completed the requirements for the Ph. D. degree, and the other two that for the M. S. degree at the University of Wisconsin.

Heinz H. Lettau
Madison, Wisconsin

October 1965

Scanner's note:

This page is blank.

TABLE OF CONTENTS

Scanner's note:

This page is blank.

Longitudinal Versus Lateral Eddy Length-Scale

(Second Note on a Vorticity-Transfer-Hypothesis of Turbulence Theory)

H. Lettau

Department of Meteorology and Department of Civil Engineering
University of Wisconsin at Madison

Abstract: A previously introduced vorticity-transfer-and-adaptation hypothesis is briefly summarized and supplemented by consideration of certain spatial derivatives of the components of the eddy displacement vector. The conventional length-scale of turbulence, redefined in the preceding note as a lateral co-variance $\ell = (\overline{x' z'})^{1/2}$, is supplemented by the new concept of a longitudinal length-scale, defined as the variance $L = (\overline{x'^2})^{1/2}$. In correspondence to the Karman constant (which concerns the rate of change of ℓ in the direction lateral to the mean flow) there is a new constant which concerns the rate of change of L in the longitudinal direction. It is proposed to refer to this as the Reichardt constant, because the supplements are of direct importance for turbulence in free flows (such as submerged jets), and because the new hypothesis offers an improvement in comparison with "Reichardt's Momentum Transfer Law" or, "inductive theory," of jet-diffusion. It is shown that the structure of mean profiles in two-dimensional jets can be very satisfactorily predicted by the new theory. The empirically known discrepancy between lateral distributions of heat and momentum is now definitely explained as the result of vorticity-transfer; specifically, by the fact that momentum follows from vorticity-transfer, and therefore does not diffuse in the same manner as a scalar property such as heat per unit mass. The ratio of eddy diffusivities for heat and momentum in the two-dimensional jet has the minimum value of 4/3 at the

axis. Finally, profiles of cross-stream velocity components in free flow are discussed and a new explanation for an old and thus far unresolved discrepancy between empirical and theoretical results is given.

1. Summary and Review of First Note on Vorticity-Transfer-and-Adaption

The new hypothesis of turbulent transfer introduced in a preceding note — Lettau (1964) — can be briefly summarized as follows. Starting out with the classical Reynolds' "bar-operation" for the separation of eddy from mean states, an eddy displacement vector ($\underset{\rightarrow}{r}' \equiv \underset{\rightarrow}{i}x' + \underset{\rightarrow}{j}y' + \underset{\rightarrow}{k}z'$, with $\overline{\underset{\rightarrow}{r}}' = 0$) was formally defined which describes eddy trajectories of fluid elements, and serves to specify the functional relationship between the eddy velocity vector ($\underset{\rightarrow}{v}' \equiv \underset{\rightarrow}{i}u' + \underset{\rightarrow}{j}v' + \underset{\rightarrow}{k}w'$) and the field of mean motion ($\overline{\underset{\rightarrow}{v}} \equiv \underset{\rightarrow}{i}\bar{u} + \underset{\rightarrow}{j}\bar{v} + \underset{\rightarrow}{k}\bar{w}$). Most important is that the suggested new mathematical relationship between $\underset{\rightarrow}{v}'$ and $\overline{\underset{\rightarrow}{v}}$ derives from a principle of "vorticity-transfer-and-adaption." This contrasts with such classical concepts as "conservation of momentum" proposed by Prandtl and others, or "conservation of vorticity" originally suggested by Taylor. With the new hypothesis the physical "fact of life" is considered that in the actual process of eddy displacements a fluid particle will not, and cannot, exactly conserve a property such as vorticity of the level from where it once started. Rather, due to mixing and continuous entrainment, the particle will adapt and adjust its vorticity gradually towards the prevailing or mean conditions along the eddying trajectory. At some point of the irregular travel, the particle will have lost entirely the characteristics of the previous level of origin. It will have assumed a new identity before it undergoes a new eddy displacement, whereupon the play can continue.

When the same notation as explained by Lettau (1964) is here employed, the basic hypothesis was formulated as follows

$$\underset{\rightarrow}{v}' = \underset{\rightarrow}{r}' \times [\nabla \times \overline{\underset{\rightarrow}{v}}] \equiv \underset{\rightarrow}{r}' \times \overline{\underset{\rightarrow}{c}} \,. \qquad (1)$$

In view of the following universal identity of vector analysis, where $\underset{\rightarrow}{v}_1$ and $\underset{\rightarrow}{v}_2$ are two arbitrary three-dimensional or two-dimensional vectors,

$$\nabla \times [\underset{\rightarrow}{v}_1 \times \underset{\rightarrow}{v}_2] \equiv -\underset{\rightarrow}{v}_1 \cdot \nabla \underset{\rightarrow}{v}_2 + \underset{\rightarrow}{v}_1 (\nabla \cdot \underset{\rightarrow}{v}_2) + \underset{\rightarrow}{v}_2 \cdot \nabla \underset{\rightarrow}{v}_1 - \underset{\rightarrow}{v}_2 (\nabla \cdot \underset{\rightarrow}{v}_1), \qquad (2)$$

and upon substitution of $\underset{\rightarrow}{r}'$ for $\underset{\rightarrow}{v}_1$ and $\overline{\underset{\rightarrow}{c}} \equiv \nabla \times \overline{\underset{\rightarrow}{v}}$ for $\underset{\rightarrow}{v}_2$, and con-

sideration of the fact that the divergence of a curl is identically zero, (1) yields

$$\underset{\rightarrow}{c}' \equiv \nabla \times \underset{\rightarrow}{v}' = -\underset{\rightarrow}{r}' \cdot \nabla \underset{\rightarrow}{\bar{c}} + \underset{\rightarrow}{\bar{c}} \cdot \nabla \underset{\rightarrow}{r}' - \underset{\rightarrow}{\bar{c}}(\nabla \cdot \underset{\rightarrow}{r}'), \tag{3a}$$

and, with the model assumption of $\nabla \cdot \underset{\rightarrow}{r}' = 0$ originally proposed by Lettau (1964),

$$\underset{\rightarrow}{c}' \equiv \nabla \times \underset{\rightarrow}{v}' = -\underset{\rightarrow}{r}' \cdot \nabla \underset{\rightarrow}{\bar{c}} + \underset{\rightarrow}{\bar{c}} \cdot \nabla \underset{\rightarrow}{r}' . \tag{3b}$$

The first term on the right-hand sides of (3a and b) expresses Taylor's concept of vorticity conservation. Correspondingly, the second term was interpreted as expressing vorticity adaption, or, the adjustment of eddy displacements produced by the existing mean vorticity of the turbulent flow.

In a reply to critical remarks by Lumley and Stewart (1965), Lettau agreed that $\nabla \cdot \underset{\rightarrow}{r}'$ cannot vanish for all types of turbulent flow. Definite suggestions concerning supplements of the hypothesis shall be the objective of the present note. Before going into detail it will be necessary to complete this brief summary of certain results of the first note.

The preliminary testings of the hypothesis were mainly restricted to a flow type which Hinze (1959) would classify under "wall-turbulence." Specifically, this refers to shear flow in which the vectors of mean motion and mean curl reduce to $\underset{\rightarrow}{i}\bar{u}$, and $\underset{\rightarrow}{j}\bar{u}_z$, respectively, with higher derivatives $\bar{u}_{zz}$, $\bar{u}_{zzz}$, etc., also different from zero. (Note that here, like in the first note, a subscript x, y, or z denotes partial differentiation with respect to one of the independent variables.) If this specialized one-dimensional mean shear flow is also uniform (i.e., $\bar{u}_x = \bar{u}_y = 0$) the assumption that any effects of $\nabla \cdot \underset{\rightarrow}{r}'$ are negligible appears to hold true to a sufficient degree of accuracy. Then, the new hypothesis (1) yields an extremely simple expression for the three components of the eddy velocity vector,

$$u' = -z'\bar{u}_z; \quad w' = x'\bar{u}_z; \quad \text{and,} \quad v' = -\int (u'_x + w'_z)\,dy. \tag{4}$$

It is significant that the two components of the eddy displacement, namely z' and x', are of equal importance for the structure of the considered shear flow as well as the transfer-properties of wall-turbulence. For a schematic illustration, reference can be made to Lettau (1965). The new hypothesis permits us to derive the following systematic hierarchy of four co-variances,

$$\text{Shearing velocity} \equiv u^* \equiv (-\overline{u'w'})^{1/2}, \tag{5a}$$

$$\text{Eddy diffusivity} \equiv K \equiv -\overline{u'x'} = \overline{w'z'}, \tag{5b}$$

$$\text{Mixing length} \equiv \ell \equiv (\overline{x'z'})^{1/2}, \text{ and} \tag{5c}$$

$$\text{Karman constant} \equiv k \equiv (\overline{x'_z z'_z})^{1/2}. \tag{5d}$$

It is normally assumed that among the directly measurable quantities (to be determined as a function of distance z from the wall) are mean speed $\bar{u}$ and consequently, mean shear $\bar{u}_z$, curvature $\bar{u}_{zz}$, etc., and also shearing stress τ, or τ/ρ. Note, that all the above defined co-variances can also be reformulated, strictly and directly in terms of identities involving measurable mean quantities, namely

$$\text{Shearing velocity} \equiv u^* \equiv (\tau/\rho)^{1/2}, \tag{6a}$$

$$\text{Eddy diffusivity} \equiv K \equiv \tau/\rho\,\bar{u}_z \equiv u^{*2}/\bar{u}_z, \tag{6b}$$

$$\text{Mixing length} \equiv \ell \equiv (\tau/\rho)^{1/2}/\bar{u}_z \equiv u^*/\bar{u}_z, \tag{6c}$$

$$\text{Karman constant} \equiv k \equiv \lim_{z \to 0} (-u^* \bar{u}_{zz}/\bar{u}_z{}^2). \tag{6d}$$

In addition to the co-variances (5a to d) certain variances are of importance for practical testings of the hypothesis; reference is made to Lettau (1965). However, only the variances involving the downstream component of the eddy displacement vector will be investigated here; the variances of eddy velocity components will not be needed for the following discussion and their consideration can be omitted here.

2. Suggested supplementation of the eddy transfer-and-adaption hypothesis

It had been briefly indicated before — see Lettau (1965) — that there are some interesting and significant consequences of the new vorticity-transfer-and-adaption hypothesis if the distribution of a scalar property of the fluid, and the transfer of this property by turbulence is also considered. Let $s = \bar{s} + s'$ denote a transferable scalar property, or, fluid admixture. It is imperative to assume that the above defined eddy displacement vector $\underset{\rightarrow}{r}'$ determines also the functional relationship between turbulent fluctuations s' and mean field $\bar{s}$. In

the form of a model assumption it is suggested that a most universally useful relationship is

$$s' = \nabla \cdot \underset{\rightarrow}{r}'(\bar{s}_0 - \bar{s}) \equiv -\underset{\rightarrow}{r}' \cdot \nabla \bar{s} + (\bar{s}_0 - \bar{s})\nabla \cdot \underset{\rightarrow}{r}', \qquad (7)$$

where $\bar{s}_0$ denotes a standard, or constant reference value of the considered admixture. The first term on the right-hand side of (7) obviously expresses conservation of the fluid property along the eddy trajectory, in a form as employed in nearly all conventional discussions of the mechanism of turbulent transfer. The second term is new; it establishes a direct analogy between the structure of equations (7) and (3a or b). It is therefore suggested to interpret the second term in (7) as the expression of adaption or adjustment of either property or eddy displacement, in contrast to, and supplement of, the tendency towards conservation.

It can also be seen that for $\nabla \cdot \underset{\rightarrow}{r}' = 0$ a strictly "gradient-type" eddy transfer will result. Consequently, possible deviations from "gradient-type" eddy diffusion are expressed by the second term of (7) and will imply that $\nabla \cdot \underset{\rightarrow}{r}' \neq 0$. Such deviations are definitely known to exist; especially, if heat per unit mass of a compressible fluid is considered as the transferable property. All convective-type turbulence will be of this nature. There is an obvious similarity between the form of the co-variance $\overline{w's'}$ based on (7) and (4), and an empirical expression of the vertical eddy transfer of heat originally suggested by Priestley and Swinbank (1947). However, the investigation of this analogy shall be postponed to a later study of convective turbulence, because in the present note emphasis will be given to turbulence in a two-dimensional jet. The latter is a case of turbulent free flow which offers a most elementary yet highly significant and rewarding opportunity for the study of unconventional aspects of eddy transfer and structure.

It is evident from a comparison that (7) can be considered as the scalar counterpart to the vectorial relationships (3a and b). Nevertheless, both of these vector-forms for vorticity fluctuations hold true when (1) is valid. It will be shown in the following that, at least for the case of divergent shear flow as in the two-dimensional jet, the expression for the velocity fluctuations must also include an additional term which contains $\nabla \cdot \underset{\rightarrow}{r}'$ as a factor. A supplement of (1) is necessary in order to describe correctly other than wall-turbulence flow, but it should reduce automatically to (1) in cases where $\nabla \cdot \underset{\rightarrow}{r}' = 0$.

As a model assumption, and in analogy to (7), it is suggested to supplement (1) , tentatively, by the following form:

$$\underset{\rightarrow}{v}' = \underset{\rightarrow}{r}' \times [\nabla \times \bar{\underset{\rightarrow}{v}}] - \bar{\underset{\rightarrow}{v}} (\nabla \cdot \underset{\rightarrow}{r}'). \tag{8}$$

The use of (8) in place of (1) will not affect the basic concept of vorticity-transfer-and-adaption. It will only mean that in the expression for $\underset{\rightarrow}{c}' \equiv \nabla \times \underset{\rightarrow}{v}'$ additional terms must appear in comparison with (3a). Admittedly, our attempts to present more convincing arguments for (8) were, thus far, not successful. We want to offer (8) only on the basis of conjecture or, what could benevolently be called an "inductive theory," justified by empirical results. However, it shall be shown in Section 5 that (8) yields predictions which compare very favorably with those derived from another, but definitely more restricted "inductive theory" which was originally suggested by Reichardt. A form like (8) also eliminates a shortcoming of (1) which was noticed by Lumley and Stewart (1965); namely, according to (1) no fluctuations in velocity could be developed in an irrotational mean velocity field. This limitation is avoided in (8).

3. Application of the New Transfer Concepts to Elementary Jet-Flow; Lateral Versus Longitudinal Length-Scale of Turbulence

In order to demonstrate effectively the mathematical and physical consequences of the divergence-term $\nabla \cdot \underset{\rightarrow}{r}'$ let us apply the supplemented expressions (7) and (8) to the special turbulent diffusion which exists, for sufficiently high Reynolds numbers, in the fully established region of a two-dimensional submerged jet under steady-state conditions. Let the jet effectively originate at the y-axis, which therefore would coincide with the center of a slot of small width, and undetermined length in the $\pm$ y direction. Then, the y-component of mean motion as well as any y-derivatives of the mean components $\bar{u}$ and $\bar{w}$ will be equal to zero. The mean flow is represented by the two-dimensional vector,

$$\bar{\underset{\rightarrow}{v}} = \underset{\rightarrow}{i}\,\bar{u} + \underset{\rightarrow}{k}\,\bar{w}, \tag{9a}$$

while the mean curl has only a y-component,

$$\bar{\underset{\rightarrow}{c}} \equiv \nabla \times \bar{\underset{\rightarrow}{v}} = \underset{\rightarrow}{j}(\bar{u}_z - \bar{w}_x) \equiv \underset{\rightarrow}{j}\,\bar{\eta}. \tag{9b}$$

The characteristic of this flow is that $\bar{u}_x < 0$ and, consequently, by virtue of mass continuity, assuming quasi-incompressible fluid, $\bar{w}_z = -\bar{u}_x$. In view of horizontal convergence and lateral divergence of the jet motion it can be expected that the scale of eddy displacements increases systematically downstream, in connection with the lateral spread of the submerged jet.

With the aid of (9a and b) it follows from (8) that

$$u' = -z'\bar{\eta} - \bar{u}\,\nabla\cdot\underset{\sim}{r}', \tag{10a}$$

$$w' = x'\bar{\eta} - \bar{w}\,\nabla\cdot\underset{\sim}{r}'. \tag{10b}$$

The product which has to be taken to obtain the Reynolds' stress is

$$w'u' = -x'z'\bar{\eta}^2 - x'(\nabla\cdot\underset{\sim}{r}')\bar{u}\,\bar{\eta} + z'(\nabla\cdot\underset{\sim}{r}')\bar{w}\,\bar{\eta} + (\nabla\cdot\underset{\sim}{r}')^2\,\bar{u}\,\bar{w}. \tag{11}$$

At the jet-axis (where $z = 0$) the condition of two-dimensional symmetry requires that $\bar{w} = \bar{w}_x = \bar{u}_z = 0$. Consequently, the center value of the Reynolds stress according to (11) will be zero. In the core-region immediately adjacent to the jet-axis it will be found that $\bar{w}$ is much smaller than $\bar{u}$. This can mean that the last two terms on the right-hand side of (11) are negligible in comparison with the first two. Thus, the Reynolds stress in the core-region of the submerged jet will be, to a sufficient degree of approximation,

$$\overline{w'u'} = \overline{-x'z'}\,\bar{u}_z^2 - \overline{x'\,\nabla\cdot\underset{\sim}{r}'}\,\bar{u}_z\bar{u} = -(\ell\,\bar{u}_z)^2 - \overline{x'x'}_x\,\bar{u}_z\bar{u}, \tag{12}$$

where the defining equation (5c) is considered. It is also assumed that the co-variances $\overline{x'y'}_y$ as well as $\overline{x'z'}_z$ average out to zero or, contribute only a negligible fraction to the value of $\overline{x'\,\nabla\cdot\underset{\sim}{r}'}$, in comparison with $\overline{x'x'}_x$.

Let the fluid which forms the two-dimensional jet possess initially an overtemperature $\bar{\Theta}_0$ in comparison with the uniform temperature of the ambient fluid. Due to jet-symmetry $\bar{\Theta}_y = 0$, and it follows from (7) that

$$\Theta' = -x'\bar{\Theta}_x - z'\bar{\Theta}_z - \bar{\Theta}\,\nabla\cdot\underset{\sim}{r}'. \tag{13}$$

In comparison with (10a) it is important to note that (13) contains three

terms, one more than (10a). Thus, the structure of Θ' differs from that of u' inasmuch as the former depends on $\bar{\Theta}_x$ while the latter does not depend on $\bar{u}_x$. It can readily be verified that this discrepancy is a direct consequence of the fact that u' derives from a vorticity-transfer concept. No such discrepancy would appear if u' would behave like a scalar, or, would follow from momentum-transfer concepts.

With the aid of w' in (10b) the product which has to be formed to obtain the Reynolds expression of lateral transfer of heat is,

$$w'\Theta' = -\bar{\eta}(x'^2\bar{\Theta}_x - x'z'\bar{\Theta}_z + x'\nabla\cdot\underset{\rightarrow}{r}'\bar{\Theta}) + \bar{w}\nabla\cdot\underset{\rightarrow}{r}'(x'\bar{\Theta}_x + z'\bar{\Theta}_z + \nabla\cdot\underset{\rightarrow}{r}'\bar{\Theta}) \tag{14}$$

A repetition of the argumentation in connection with the development of (12) from (11), and the application of the bar-operation to (14) yields

$$\overline{w'\Theta'} = -\ell^2\,\bar{u}_z\bar{\Theta}_z - \overline{x'x'}\,\bar{u}_z\bar{\Theta}_x - \overline{x'x'}_x\,\bar{\Theta}\,\bar{u}_z . \tag{15}$$

Here $x'x'$ is the same as x'^2. The significant feature is again that (15) contains one more term than (12), for reasons explained above. However, co-variances involving x' and x'_x appear in both equations (15) and (12). This justifies the introduction of the concept of a longitudinal length-scale, L, of turbulence, in supplement to the length defined by (5c). From now on, the latter shall be referred to as the lateral length-scale of turbulence, or, alternately, the transversal length-scale. It is hoped that herewith the conventional but undescriptive and misleading terminology of "mixing length" can be disposed of. In summary, the use of the spatial components of the eddy displacement vector yields definitions of two different lengths,

$$\text{Lateral length-scale of turbulence} \equiv \ell \equiv (\overline{x'z'})^{1/2}, \tag{16a}$$

$$\text{Longitudinal length-scale of turbulence} \equiv L \equiv (\overline{x'x'})^{1/2}, \tag{16b}$$

$$\text{with } L^2 \equiv (\overline{x'^2}), \quad \text{and } L\,L_x = L_x\,L \equiv \overline{x'x'}_x. \tag{16c}$$

Thus, a reformulation of equations (12) and (15) is

$$\overline{w'u'} = -(\ell\,\bar{u}_z)^2 - L_x L\,\bar{u}_z\bar{u} \tag{17a}$$

$$\overline{w'\Theta'} = -\ell^2\,\bar{u}_z\bar{\Theta}_z - L_x L\,\bar{u}_z\bar{\Theta} - L^2\,\bar{u}_z\bar{\Theta}_x = -\ell^2\,\bar{u}_z\bar{\Theta}_x - L\bar{u}_z(L\bar{\Theta})_x . \tag{17b}$$

Note again a systematic difference inasmuch as (17b) cannot be obtained by substituting Θ for u in (17a), for reasons explained above. Also noteworthy is that the Reynolds stress is not any more a quadratic term. In comparison with shear flow this suggests that the conventional definition of a shearing velocity as in (5a) or (6a) cannot have a direct physical meaning for free turbulence.

4. Basic Theoretical and Empirical Results for the Two-Dimensional Submerged Jet

There exists in the literature a substantial number of theoretical as well as experimental studies of the structure of submerged jets, for the two-dimensional as well as the circular-symmetric case. For an extremely thorough review of the problem, reference can be made to Albertson, Dai, Jensen, and Rouse (1950). The essential facts may also be found in most standard textbooks on fluid dynamics. For brevity, reference will here be made only to the fourth edition of Schlichting (1960). In order to establish a basis for discussion let us consider a strictly two-dimensional steady jet of a fluid which has initially a known over-temperature Θ_0 in comparison with the ambient fluid. We are concerned only with fully established flow, i.e., where the entire central part of the jet has become turbulent. Further entrainment of the surrounding fluid by the expanding eddy region then is balanced inertially by a continuous downstream reduction in $\bar{u}$. It will also be assumed that pressure forces and viscous forces are negligible in comparison with the Reynolds stresses, and that no external forces affect the jet fluid. Specifically, this excludes gravity, or buoyancy forces. This means that in the case of a compressible fluid we are concerned with sufficiently small over-temperatures so that thermal expansion or compression is negligible. Also excluded are molecular conduction, which is assumed negligible in comparison with eddy transfer of heat, and external sources or sinks of heat, for example, effects of radiational heat exchange.

It is realized that there is also a substantial number of studies on the round free jet; reference can be made to Hinze (1959), in addition to the above quoted literature. However, since we are here concerned with a basic testing of the new principle, it will suffice for the time being to restrict the discussion to the most elementary case of the two-dimensional jet.

With the above listed assumptions, mass continuity simply requires that $\bar{u}_x = -\bar{w}_z$. In addition to that of mass, there are the two continuity conditions which express conservation of x-momentum, and of heat per unit mass, of the following form,

$$\overline{(uu)}_x + \overline{(wu)}_z = 0, \tag{18a}$$

$$\overline{(u\Theta)}_x + \overline{(w\Theta)}_z = 0. \tag{18b}$$

After separating mean from eddy values, and assembling the eddy terms on the right-hand sides,

$$(\bar{u}^2)_x + (\bar{w}\,\bar{u})_z = -(\overline{u'u'})_x - (\overline{w'u'})_z \approx -(\overline{w'u'})_z, \tag{19a}$$

$$(\bar{u}\,\bar{\Theta})_x + (\bar{w}\,\bar{\Theta})_z = -(\overline{u'\Theta'})_x - (\overline{w'\Theta'})_z \approx -(\overline{w'\Theta'})_z, \tag{19b}$$

since it will be legitimate to neglect the x-derivative of the co-variances in comparison with the eddy transfer terms and their z-derivatives. Note that there is no systematic difference inasmuch as (19a) could be obtained by substitution of u for Θ in (19b). In view of this it is most interesting (and used to be somewhat puzzling) that detailed and careful measurements have provided indisputable evidence of significant and systematic differences between simultaneous $\bar{u}$ and $\bar{\Theta}$ profiles as functions of lateral distance z, from the axis, for fixed downwind distance, x. Empirical profiles which are normalized with the aid of the center, or maximum, values show that

$$\bar{u}/\bar{u}_{max} \approx (\bar{\Theta}/\bar{\Theta}_{max})^2. \tag{20a}$$

According to Schlichting (1960, page 612) the value of the exponent in (20a) might indicate that eddy diffusivity for heat, K_{heat}, is twice as great as eddy diffusivity for momentum, K_{mom}. It will be shown in the following section that the value of 2 for the exponent in (20a) has a different reason, and that the ratio K_{heat}/K_{mom} equals 4/3 at the center and increases with z. Undisputed is the empirical result that the mean velocity profiles of submerged jets at various values of x in the established flow region can be normalized, and are very satisfactorily approximated by Gaussian or error functions, so that

$$\log_e(\bar{u}/\bar{u}_{max}) \sim -z^2/x^2. \tag{20b}$$

A fixed ratio $\bar{u}/\bar{u}_{max}$ can be taken to indicate the effective width of the jet. Empirically, it has also been established with relatively high accuracy that the center or maximum velocity decreases inversely proportional to the square root of downwind distance, or

$$\bar{u}_{max} \sim x^{-1/2} . \tag{20c}$$

It follows from (20b) that the width of the jet will increase in direct proportion to x.

A review of the pertinent literature indicates that attempts to obtain theoretical solutions of equations (19a and b) which predict realistically the empirical results (20a to c) were generally not as successful as the treatment of the corresponding problems of shear flow in the vicinity of solid bounding walls. Various semi-empirical hypotheses have been proposed in the literature in order to solve equations (19), but yielded predictions which had to be qualified in one or the other aspect. Especially interesting is here the so-called inductive theory by Reichardt; reference is made to Schlichting (1960, page 609). Hinze (1959, page 290) also discusses widely this concept under "Reichardt's momentum transfer law." The main characteristic of Reichardt's approach, which is classified as "purely phenomenological" by Hinze, is the definition of a length,

$$\mathscr{L} \equiv - (\overline{u'w'})/(\overline{u^2})_z , \tag{21a}$$

which is independent of the lateral coordinate, $\mathscr{L}_z = 0$, while $\mathscr{L}_x > 0$. In fact, it was shown that $\mathscr{L}$ is proportional to the width of a submerged two-dimensional jet, so that it increases downstream in proportion to x. Upon introducing (21a) into the basic equation (18a) and neglecting $(\overline{w}\ \bar{u})_z$ in comparison with $(\overline{u^2})_x$,

$$(\overline{u^2})_x = \mathscr{L}(\overline{u^2})_{zz} , \tag{21b}$$

which, for $\mathscr{L} \sim x$ was solved by Reichardt to give

$$\overline{u^2} \sim x^{-1}\, e^{-z^2/2x^2} . \tag{21c}$$

Obviously, (21c) appears to check with (20b) as well as (20c) provided that there are no systematic dependencies, on x or z, of the ratio $(\overline{u^2})/(\bar{u})^2$; the excess of this ratio above unity is conventionally taken as a measure of turbulence-intensity.

It shall be shown in the following section that the employment of the longitudinal length-scale, L, as defined in (16b and c) eliminates the need for (21a) and produces a more satisfactory solution.

5. A New Solution of the Problem of the Heated Two-Dimensional Jet

In view of the limited success of Reichardt's momentum transfer law, and recalling the new hypothesis in the form of equation (12), it is self-suggestive to conclude that in the special case of the submerged jet the co-variance between the components x' and z' of the eddy displacement vector is insignificant. This means that the importance of the lateral length-scale ℓ is restricted only to wall-turbulence, and that ℓ may vanish for free turbulence in favor of the longitudinal length-scale L. Thus, it is suggested to reduce equations (17a and b) to

$$\overline{w'u'} = - L_x L \bar{u}_z \bar{u}, \tag{22a}$$

$$\overline{w'\Theta'} = - L_x L \bar{u}_z \bar{\Theta} - L^2 \bar{u}_z \bar{\Theta}_x = - L \bar{u}_z (L \bar{\Theta})_x. \tag{22b}$$

When again the term $\bar{w}\,\bar{u}_z$ is neglected in comparison with $\bar{u}\,\bar{u}_x$, and continuity, or $\bar{u}(\bar{u}_x + \bar{w}_z) = 0$ is considered, the approximate form of (19a) together with (22a) yields

$$\bar{u}\,\bar{u}_x \equiv (\bar{u}^2/2)_x = (L_x L \bar{u}_z \bar{u})_z \equiv L_x L (\bar{u}^2/2)_{zz}, \tag{23a}$$

since it will be assumed that $L_z = 0$. In accordance with Reichardt's argumentation concerning $\mathscr{L}$ we also assume that L_x is a positive constant. Then, (23a) is solved by

$$\bar{u}(x, z) = \bar{u}_0 (L_0/L)^{1/2} e^{-z^2/4L^2}, \text{ with} \tag{23b}$$

$$\bar{u}_{max}(x) = \bar{u}_0 \sqrt{L_0/L}, \tag{23c}$$

where $\bar{u}_0$ and L_0 are integration constants which refer to effective values at the apparent origin of the jet, i.e., disregarding the region near the slot where turbulence is not yet fully established.

A new physical meaning of the longitudinal length, previously defined as $\overline{(x'x')}^{1/2} \equiv L$, emerges from (23b) inasmuch as L determines directly the width of the submerged jet. For example, $\bar{u}$ reduces to

1/e of its center-value, $\bar{u}_{max}$, if $z = \pm 2L$, at any given x. On the basis of empirical determinations of the downstream spread of two-dimensional jets as discussed by Schlichting (1960, page 605), it may tentatively be concluded that the only free factor of proportionality has the value of

$$L_x = 0.065; \text{ or, } L = 0.065x. \tag{24}$$

With (16c), and recalling (5c and d), it may be seen that L_x occupies a role in free turbulence, and for the longitudinal length-scale L, which is very similar to the role of the Karman constant in wall-turbulence and for the lateral length-scale ℓ. It is therefore proposed that the numerical constant L_x be referred to as the "Reichardt constant." In terms of eddy structure, $L_x = \overline{(x' x^{\dagger})}/(\overline{x'^2}\,\overline{x^{\dagger 2}})^{1/2}$, and it is desirable that its universal nature, and its numerical value be more securely obtained than in (24).

The functional relationship between L and $\mathscr{L}$ is relatively simple if the turbulence-intensity is quasi-independent of x and z. Then it follows from the comparison of (23a) with (21b) that

$$L_x L = \mathscr{L} \; ; \text{ or, } L^2 = 2\int_0^x \mathscr{L}\, dx. \tag{25}$$

Obviously, the direct use of L is preferable, especially since it has been primarily defined as the variance of the downstream component of the eddy displacement vector.

It can readily be verified that (23b and c) are in perfect agreement with the empirical relations (20b and c). However, this success is essentially shared by Reichardt's inductive theory of momentum transfer in free turbulence. The advantage of the vorticity-transfer concept, and the resulting definition of the longitudinal length-scale comes into fullest play if we turn, finally, to the problem of lateral profiles of scalar admixtures to the jet fluid, specifically the temperature distribution in a warm-fluid jet. When again the term $\bar{w}\,\bar{\Theta}_z$ is neglected in comparison with $\bar{u}\,\bar{\Theta}_x$, and $\bar{\Theta}(\bar{u}_x + \bar{w}_z) = 0$ is considered, together with $L_z = 0$, the approximative form of (19b) yields

$$\bar{u}\,\bar{\Theta}_x = L\,\bar{u}_{zz}(L\,\bar{\Theta})_x + L\,\bar{u}_z(L\,\bar{\Theta})_{xz} \approx L\,\bar{u}_{zz}(L\,\bar{\Theta})_x, \tag{26a}$$

since it is readily verified that on the right-hand side the term containing $\bar{u}_z$ vanishes at the center and is, in the entire core-region, relatively small in comparison with the term containing $\bar{u}_{zz}$. If $\bar{u}(x, z)$

is given by (23b), we obtain a first-order approximation to the solution of (26a), valid in close proximity to the center-line,

$$\bar{\Theta}(x, z) = \bar{\Theta}_0 (L_0/L)^{1/3} e^{-z^2/8L^2}, \text{ with} \tag{26b}$$

$$\bar{\Theta}_{max}(x) = \bar{\Theta}_0 \sqrt[3]{L_0/L}. \tag{26c}$$

where $\bar{\Theta}_0$ and L_0 are integration constants which refer to effective values at the apparent origin of the two-dimensional jet. Evidently, the extremely interesting empirical relationship (20a), which appeared to present a paradox in view of the symmetry between (19a) and (19b), is now explained for the center-region of the jet. The different structure of (26b) in comparison with (23b), which corresponds to (20a) can now be traced back to the difference between (22a) and (22b). Incidentally, a graph reproduced by Schlichting (1960, page 612) provides direct evidence that the empirical relationship (20a) holds true only for z/L values which are absolutely smaller than approximately three (3).

In order to demonstrate the quality of the solution, we differentiate (26b) to obtain $\bar{\Theta}_x$ and $(L\bar{\Theta})_x$, using (23b) to obtain $\bar{u}_{zz}$. Then, the two individual terms of (26a) can be expressed as follows,

$$\bar{u}\,\bar{\Theta}_x = (\bar{u}\,\bar{\Theta}\,L_x/L) \cdot (-\tfrac{1}{3} + z^2/4L^2), \tag{27a}$$

$$L\,\bar{u}_{zz}(L\bar{\Theta})_x = (\bar{u}\,\bar{\Theta}\,L_x/L) \cdot (-\tfrac{1}{3} + z^2/24L^2 + z^4/16L^4). \tag{27b}$$

The appearance of the same numerical constant $(-1/3)$ in both expressions indicates that (26b) is indeed a first-order approximation to the solution of (26a)[1].

Interesting is that together with a weaker lateral gradient of temperature (in comparison with that of mean x-momentum in the core-region of the two-dimensional jet) equation (26c) predicts also a smaller downstream decay of the center-value, inasmuch as $\bar{u}_{max}$ is proportional to $x^{-1/2}$, while $\bar{\Theta}_{max}$ should be proportional to $x^{-1/3}$. In addition, the ratio of eddy diffusivities K_{heat}/K_{mom} is not constant but depends on lateral distance. This can be verified with the aid of the defining equations which yield, from (22a),

$$K_{mom} \equiv -\overline{u'w'}/\bar{u}_z = L_x L\,\bar{u}, \tag{28a}$$

[1] See "Note" on page 19.

(which is similar to a form discussed by Schlichting (1960, pages 481, or 605) as originally proposed by Prandtl), while (22b) yields,

$$K_{heat} \equiv - \overline{w'\Theta'} / \bar{\Theta}_z = L_x L \bar{u}_z \bar{\Theta} / \bar{\Theta}_z + L^2 \bar{u}_z \bar{\Theta}_x / \bar{\Theta}_z . \qquad (28b)$$

If the derivatives $\bar{u}_z$, $\bar{\Theta}_z$, and $\bar{\Theta}_x$ are obtained from the partial differentiations of the solutions (23b) and (26b) it follows that

$$K_{heat} / K_{mom} = \frac{4}{3} + z^2 / 2L^2 , \qquad (28c)$$

which obviously is a result restricted to the core-region. It is highly interesting that the ratio of eddy diffusivities has a lower limit of 4/3. In its parabolic increase with lateral distance from the center-line, the ratio (28c) will, at some distance, pass through the value of 2, but, in contrast to earlier models, no special significance can here be attributed to this value. It can be readily verified that the exponent in the empirical relation (20a) has nothing to do with the value of K_{heat}/K_{mom}.

6. Mean Lateral Speed Versus Root-Mean-Square Lateral Speed in Free Jets

Finally, the lateral velocity component w in a two-dimensional submerged jet shall be briefly investigated. Its mean value follows, under the assumed condition of quasi-homogeneous fluid, from mass continuity,

$$\bar{w} = - \int_0^z \bar{u}_x \, dz. \qquad (29a)$$

If the $\bar{u}$-profile (23b) is considered,

$$- \bar{u}_x = (\bar{u} L_x / 2L) \cdot (1 - z^2/L^2) = \bar{w}_z , \qquad (29b)$$

it can be seen that $\bar{w}$ in (29a) is essentially given by the error-integral which can be evaluated without difficulty. In a first-order approximation the value of $\bar{w}(x, z)$ can be estimated for the immediate core-region of the jet with the aid of the following,

$$\bar{w} \approx \bar{u} L_x z / 2L . \qquad (29c)$$

It follows from (29b and c) that $\bar{w}$ is proportional to $\bar{u}$ multiplied by a linear function of the normalized lateral distance z/L; $\bar{w}$ starts out with a zero-value at the jet-axis, and reaches, according to (29b), extreme values at exactly $z = \pm L$, and goes to zero again at large lateral distance.

There is also the continuity condition for z-momentum (in addition to that formulated in (18a) for x-momentum), namely,

$$(\overline{uw})_x + (\overline{w^2})_z = 0, \tag{30a}$$

provided all the assumptions listed at the beginning of Section 4 apply. We shall try to estimate the root-mean-square value of lateral velocity component. For convenience of writing, let $w^* \equiv (\overline{w^2})^{1/2}$, so that (30a) can be reformulated, after rearrangement, as

$$(w^{*2})_z = -(\overline{uw})_x = -(\bar{u}\,\bar{w})_x - (\overline{u'w'})_x. \tag{30b}$$

The first term on the right-hand side of (30b) can be approximated with the aid of (29c) and (23b). Elementary steps yield the following sequence of first-order approximations,

$$\bar{u}\,\bar{w} \approx \bar{u}^2 L_x z/2L, \tag{31a}$$

$$-(\bar{u}\,\bar{w})_x \approx \bar{u}^2 L_x^2 z/L^2, \text{ and,} \tag{31b}$$

$$-\int_0^z (\bar{u}\,\bar{w})_x\, dz \approx \bar{u}^2 L_x^2 z^2/2L^2. \tag{31c}$$

The last term of (30b) is readily expressed with the aid of the characteristic relation of the new vorticity-transfer concept (22a). Elementary steps, and considering that $L_z = 0$, while $L_x = \text{const}$, yield the following sequence of relations,

$$-\overline{u'w'} = L_x L \bar{u}_z \bar{u} = (L_x L \bar{u}^2/2)_z, \tag{32a}$$

$$-(\overline{u'w'})_x = (L_x L \bar{u}^2/2)_{zx} = (L_x L \bar{u}^2/2)_{xz}, \tag{32b}$$

$$-\int_0^z (\overline{u'w'})_x dz = (L_x L \bar{u}^2/2)_x = \bar{u}^2 L_x^2 z^2/2L^2. \tag{32c}$$

Interestingly, the two terms in (30b) contribute equal parts, as evidenced by the comparison of (31c) with (32c). The solution for the root-mean-square velocity, therefore, is,

$$w^{*2} = \bar{u}^2 L_x^2 z^2/L^2; \text{ or, } w^* = \bar{u} L_x z/L. \quad (33a)$$

This is a surprisingly simple expression, with the following relationship obtained by differentiation,

$$(w^*)_z = (\bar{u} L_x/L) \cdot (1 - z^2/2L^2). \quad (33b)$$

Two facts are greatly interesting; first of all, comparison of (33a) with (29c) shows that within the limitations of the approximative assumptions, i.e., in the core-region of the jet, the root-mean-square value should equal twice the mean value, i.e., $w^* = 2\bar{w}$. Secondly, w^* is a function of the normalized lateral distance z/L, similar to $\bar{w}$, but reaching an extreme value exactly at $z = \pm L\sqrt{2}$ — see (33b) — in contrast to the position of the extreme value found above for $\bar{w}$ at $z = \pm L$. The empirical determination of w-distributions in submerged jets is therefore a useful tool to obtain the values of the longitudinal length-scale L.

In this connection, let us discuss briefly some experimental facts. Albertson et al. (1950) describe an observational program resulting from a wartime fog-dispersal project of the Iowa Institute of Hydraulic Research, which involved the measurement of the mean velocity distribution in both two-dimensional and three-dimensional jets, over a considerable range of each independent variable. Purely for convenience, all measurements were made in air, but the authors say that there is no reason to presume that comparable results would not be obtained in any other fluid — whether liquid or gas — of moderately low viscosity. It was found that the distribution of longitudinal velocity (i.e., $\bar{u}$) in the zone of establishment of flow from slots agrees very satisfactorily with the results summarized in Section 4. However, in connection with w-profiles, it is interesting to quote the following from Albertson et al. (1950, pages 653-654), where the term "data" refers specifically to normalized distribution of lateral velocity in zones of established velocity from slots, and underlinings for emphasis are added here.

"Although the data follow the general trend of the theoretical curve, the values computed from the measurements are at least 1 00 percent greater than those indicated by the plotted function — the discrepancy being apparent from comparison of the analytical curve (curve (a) of Fig. 8) with the measured values. No explanation can be given for this disagreement; neither do the computations disclose any likelihood of mathematical error, nor have repeated measurements by different observers led to essentially different results."

On the basis of the preceding developments, a simple explanation can be offered here. It appears that Albertson et al. have plotted as their "analytical curve" the correctly computed normalized distribution of mean lateral velocity, $\overline{w}$, on the basis of mass continuity, following (29a). However, their empirical measured values were actually equal to the at least 100 percent larger root-mean-square velocities w^* as given by (33a), since their equipment consisted exclusively of sensors for dynamic pressure, or, stagnation probes. It is suggested by the results plotted in Fig. 8 of Albertson et al. (1950, page 654) that the puzzling discrepancy corresponds nearly perfectly to the difference between $\overline{w}$ and w^* discussed above, concerning both magnitude and lateral position of extreme values, as a consequence of the vorticity-transfer hypothesis, and the resulting equations (29a) and (33a). Corresponding discrepancies seem to exist for round jets, and it is possible that they might find a similar explanation as offered above, for the two-dimensional jet.

6. Concluding Remarks

It can be concluded that the successful prediction of an empirically well-established relationship such as (20a) and (20b) represent a significant test with positive results favoring the new hypothesis. Essential for this is that, basically, the new concept is one of vorticity transfer which explains why the actual eddy diffusion of momentum can be significantly different from the simultaneous diffusion of a truly scalar property of the fluid. The present discussion is of a preliminary nature, and certain aspects of free turbulence obviously exist which invite more penetrating study. As an interesting example the tendency towards formation of organized vortices at the fringe zones of submerged jets can be mentioned. It appears possible that this phenomenon could be related to the difference between transfer of momentum and vorticity discussed above. The immediate goal of this continuing investigation will be to find a more definite formulation of the basic concept which permits its application not only to free flow and shear zones near walls, but also to turbulent transfer in the center region of duct flow. Another application will deal with turbulent structure of free convection above a maintained horizontal area-source of heat.

REFERENCES

Albertson, M. L., Y. B. Dai, R. A. Jensen, and Hunter Rouse, 1950: Diffusion of Submerged Jets. Transactions, American Society of Civil Engineers, Vol. 115, Paper no. 2409, 639-697.

Hinze, J. O., 1959: Turbulence. New York: McGraw-Hill Book Company, Inc., 586 pp.

Lettau, H., 1964: A New Vorticity-Transfer Hypothesis of Turbulence Theory, J. atmos. Sci., 21, 453-456.

Lettau, H., 1965: Reply (to Lumley and Stewart). J. atmos. Sci., 22, 594-596.

Lumley, J. L., and R. W. Stewart, 1965: On a Conjecture of Lettau. J. atmos. Sci., 22, 592-594.

Priestley, C. H. B., and W. C. Swinbank, 1947: Vertical Transport of Heat by Turbulence in the Atmosphere. Proc. roy. Soc., London, A 189, 543-561.

Schlichting, H., 1960: Boundary Layer Theory, 4th ed., New York: McGraw-Hill Series in Mechanical Engineering, 647 pp.

Note added at Proofreading

After reviewing a draft copy of this section, Mr. W. Ohmstede of the Department of Meteorology at USAERDA, Fort Huachuca, Arizona, has found that, when (23b) is valid and (26a) is considered in the form,

$$\bar{u}\,\bar{\theta}_x = L\,\bar{u}_{zz}(L\bar{\theta})_x,$$

an exact solution exists which is

$$\bar{\theta}(x, z) = \bar{\theta}_0 (L_0/L)^{1/3} (1 - z^2/6L^2)^{1/3}.$$

This agrees with (26c) but differs in an interesting manner from (26a), and results in $K_{heat}/K_{mom} = 3$, independent of lateral distance. A more detailed discussion must be based on the unabridged form of (26a) and shall be presented in a forthcoming report.

Scanner's note:

This page is blank.

A Universal Law Relating Eddy to Mean States, Applied to Turbulence in Ducts

(Third Note on a Vorticity-Transfer Hypothesis of Turbulence Theory)

H. Lettau

Departments of Meteorology, and Civil Engineering
University of Wisconsin at Madison

Abstract: A generalized mathematical form is presented which relates the three-dimensional vector $(\underset{\rightarrow}{v}')$ of fluctuating velocity to the vector $(\underset{\rightarrow}{\bar{v}})$ of mean motion, and also the fluctuation value (s') of a scalar fluid property to the mean value $(\bar{s})$, with the aid of a three-dimensional fluctuating vector of eddy displacements $(\underset{\rightarrow}{r}' \equiv \underset{\rightarrow}{i}x' + \underset{\rightarrow}{j}y' + \underset{\rightarrow}{k}z')$, in the following two precise equations:

$$s' = -\nabla\cdot(\bar{s}\underset{\rightarrow}{r}') \equiv -\underset{\rightarrow}{r}'\cdot\nabla\bar{s} - \bar{s}(\nabla\cdot\underset{\rightarrow}{r}'), \text{ and}$$

$$\underset{\rightarrow}{v}' = \underset{\rightarrow}{r}'\times[\nabla\times\underset{\rightarrow}{\bar{v}}] - \underset{\rightarrow}{\bar{v}}\times[\nabla\times\underset{\rightarrow}{r}'] + \underset{\rightarrow}{r}'(\nabla\cdot\underset{\rightarrow}{\bar{v}}) - \underset{\rightarrow}{\bar{v}}(\nabla\cdot\underset{\rightarrow}{r}').$$

The evident and interesting properties of symmetry are discussed, and it is shown that the hypothesis is essentially one of transfer-and-adaption, for any scalar property, but also essentially for vorticity rather than momentum. A previously employed tentative formulation of the concept (which was applied to free turbulence in a two-dimensional submerged jet) is included as a special case of the above. The present discussion deals with the case of turbulent pressure-gradient flow between two parallel walls. In spite of one-dimensionality of this special mean flow $(\underset{\rightarrow}{\bar{v}} = \underset{\rightarrow}{i}\bar{u})$, the new hypothesis yields explicit expressions for all three fluctuating components $(u', v', \text{and } w')$. Consequently, for the first time, it is possible to predict variances and co-variances, not only for the fluid regions near the wall but definitely also for mid-

channel where the mean shear vanishes. It is shown that the hypothesis produces satisfactory agreement with detailed experimental results such as those reported by Laufer (1950). For example, the hypothesis explains the empirical finding that the mid-channel ratio of variances of longitudinal to either one of the two lateral velocity components is about 3/2. The same numerical value is shown to apply for the mid-channel ratio of eddy diffusivities for heat and momentum, which agrees with empirical data by Ludwieg (1956). Also, some discussion is devoted to the lateral length-scale of turbulence and it is shown that use of the new hypothesis results in a rationalization of the classical concepts of Prandtl, von Karman, and Taylor .

1. Generalized Relationship between Eddy and Mean States of Turbulent Flow

In two preceding discussions — Lettau (1964, and 1965) — a new hypothesis was introduced which serves to specify the functional relationship between the fields of eddy and mean states in turbulent flows. The conventional Reynolds bar-operation is used. The separation of three-dimensional vectors of eddy and mean motion is expressed by the identity:

$$\underset{\rightarrow}{v} = \bar{\underset{\rightarrow}{v}} + \underset{\rightarrow}{v}' \equiv \underset{\rightarrow}{i}(\bar{u} + u') + \underset{\rightarrow}{j}(\bar{v} + v') + \underset{\rightarrow}{k}(\bar{w} + w'); \quad \text{with} \quad \bar{\underset{\rightarrow}{v}}' = 0. \tag{1}$$

The important feature of the new hypothesis is the definition and consideration of a three-dimensional vector which represents eddy displacements of fluid elements,

$$\underset{\rightarrow}{r}' \equiv \underset{\rightarrow}{i}x' + \underset{\rightarrow}{j}y' + \underset{\rightarrow}{k}z'; \quad \text{with} \quad \bar{\underset{\rightarrow}{r}}' = 0. \tag{2}$$

The first of the two preceding notes dealt with turbulence in zones of strong mean shear, i.e., with wall-turbulence in mean flow tangential to solid boundaries. It was shown that the cross-stream component (z', perpendicular to the wall) and the down-stream component (x', parallel to the wall) of the eddy displacement vector (2) are of equal importance for the process of eddy transfer across the mean stream lines. Consequently, a significant parameter is the co-variance, which was referred to as the "lateral length-scale of turbulence",

$$\ell \equiv (\overline{x'z'})^{1/2} \tag{3}$$

and its cross-stream variation, which corresponds, in the immediate

vicinity of the wall, to a linear increase of ℓ with distance (z) from the boundary. It was demonstrated that (2) with (3), and subsequent covariances for eddy diffusivity, as well as the Karman constant, represent a significant improvement of the classical concept of "mixing length", as originally introduced by Prandtl, and, independently, by Taylor.

The original formulation of the hypothesis was tentatively supplemented in a second note — Lettau (1965) — with an investigation of conditions in free turbulence, specifically, the elementary case of a two-dimensional submerged jet. It was shown that for free turbulence of this nature the most significant parameter of eddy transfer and lateral diffusion is a "longitudinal length-scale of turbulence", which is given by the variance, or, the root-mean-square value of the down-stream component of the eddy displacement vector, i.e.,

$$L \equiv (\overline{x'^2})^{1/2} \equiv (\overline{x'x'})^{1/2}, \qquad (4)$$

and its down-stream variation, which corresponds to a linear increase of L with the distance (x) from the jet origin. It was demonstrated that with (2) and (4) a noticeable improvement of Reichardt's concept of a "momentum transfer length" of free turbulence was achieved. Furthermore, a novel explanation was found of the experimentally well-documented and significant difference between lateral eddy diffusion of momentum and heat. This difference appears to result from the fact that basic similarity exists between heat and vorticity, rather than heat and momentum. However, while conditions in and around the zero-shear zone of freely expanding turbulent jets were rather successfully described, it turned out that turbulence in the zero-shear region of non-divergent duct flow could not be understood with the above tentative supplement of the original hypothesis. It appeared that, in addition to possible effects of $\nabla \cdot \underset{\rightarrow}{r}' \neq 0$, there might be effects of $\nabla \times \underset{\rightarrow}{r}' \neq 0$.

In the following a reformulation of the mathematical relationship between the vectors $\underset{\rightarrow}{v}'$ and $\bar{\underset{\rightarrow}{v}}$ is presented. The new model-assumption is more universal. It includes the original and the tentatively supplemented formulation as special cases, namely,

$$\underset{\rightarrow}{v}' = \underset{\rightarrow}{r}' \times [\nabla \times \bar{\underset{\rightarrow}{v}}] - \bar{\underset{\rightarrow}{v}} \times [\nabla \times \underset{\rightarrow}{r}'] + \underset{\rightarrow}{r}' (\nabla \cdot \bar{\underset{\rightarrow}{v}}) - \bar{\underset{\rightarrow}{v}} (\nabla \cdot \underset{\rightarrow}{r}'). \qquad (5)$$

Again, we want to offer (5) on the basis of conjecture, which will be tested by the confrontation of mathematically derived predictions, based on (5), with reality. It should be emphasized that (5) does not contain any element which is contradictory to the previously formulated relationships

between $\underset{\rightarrow}{v}'$ and $\bar{\underset{\rightarrow}{v}}$. On the contrary, it can be said that the original form — Lettau (1964) — concerned conditions in strong shear zones for which both $\nabla\cdot \underset{\rightarrow}{r}'$ and $\nabla\times \underset{\rightarrow}{r}'$ were insignificant, while for the discussion of free flow in the second note — Lettau (1965) — only the term $\nabla\times \underset{\rightarrow}{r}'$ was unimportant.

Obviously, (5) evidences interesting properties of symmetry. The totality (nine each) of all possible spatial partial derivatives (with respect to x, y, z) of the three cartesian components (x', y' and z') which describe the eddy displacement vector, as well as of $\bar{u}$, $\bar{v}$, and $\bar{w}$, which describe the mean velocity vector, appear as factors in (5). However, barring extreme flow conditions (i.e., flow at relatively high Mach number, or, with relatively strong density variations) the third term in (5) will nearly always vanish. Following strictly the elementary rules of vector analysis, the application of the divergence operator to (5) yields exactly, for $\nabla\cdot \bar{\underset{\rightarrow}{v}} = 0$, the remarkably simple and symmetric relationship,

$$\nabla\cdot \underset{\rightarrow}{v}' = \underset{\rightarrow}{r}'\cdot(\nabla^2\bar{\underset{\rightarrow}{v}}) - \bar{\underset{\rightarrow}{v}}\cdot(\nabla^2\underset{\rightarrow}{r}'). \tag{6a}$$

For all practical purposes it can be expected that $\nabla\cdot \underset{\rightarrow}{v}'$ vanishes at any time and at any point within turbulent fields of fluid flow. With $\nabla\cdot \underset{\rightarrow}{v}' = 0$, a convenient reformulation of (6a) is

$$\underset{\rightarrow}{r}'\cdot(\nabla^2\bar{\underset{\rightarrow}{v}}) = \bar{\underset{\rightarrow}{v}}\cdot(\nabla^2\underset{\rightarrow}{r}'). \tag{6b}$$

Both relations (6a and b) employ the conventional expression of the Laplacian operator; for example,

$$\nabla^2\underset{\rightarrow}{v} \equiv \underset{\rightarrow}{i}\nabla^2 u + \underset{\rightarrow}{j}\nabla^2 v + \underset{\rightarrow}{k}\nabla^2 w; \text{ with: } \nabla^2 u \equiv u_{xx} + u_{yy} + u_{zz}, \text{etc.,} \tag{7}$$

where, as in the previous notes, the subscripts indicate partial differentiations with respect to the independent spatial variables x, y, z.

It is convenient to introduce a set of abbreviations which are defined by the following identities,

$$\nabla\times \underset{\rightarrow}{v} \equiv \underset{\rightarrow}{c} \equiv \underset{\rightarrow}{i}\xi + \underset{\rightarrow}{j}\eta + \underset{\rightarrow}{k}\zeta \equiv \underset{\rightarrow}{i}(w_y - v_z) + \underset{\rightarrow}{j}(u_z - w_x) + \underset{\rightarrow}{k}(v_x - u_y), \tag{8}$$

$$\nabla\cdot \underset{\rightarrow}{r}' \equiv d' \equiv x'_x + y'_y + z'_z, \text{ and} \tag{9}$$

$$\nabla\times \underset{\rightarrow}{r}' \equiv \underset{\rightarrow}{R}' \equiv \underset{\rightarrow}{i}a' + \underset{\rightarrow}{j}b' + \underset{\rightarrow}{k}c' \equiv \underset{\rightarrow}{i}(z'_y - y'_z) + \underset{\rightarrow}{j}(x'_z - z'_x) + \underset{\rightarrow}{k}(y'_x - x'_y). \tag{10}$$

Note that (9) and (10) contain exactly the totality of the nine possible partial derivatives of the eddy displacement vector. According to (1) and the Reynolds rules for averaging, (8) serves directly to produce expressions for eddy and mean values of the curl of the velocity vector, $\underset{\rightarrow}{c}'$ and $\underset{\rightarrow}{\bar{c}}$, respectively. Note that, as for any "primed" quantity, the "bar" values vanish, $\overline{\underset{\rightarrow}{c}'} = \overline{d'} = \overline{\underset{\rightarrow}{R}'} = 0$. The above abbreviations are practical because they permit easy writing of complicated formulas. For example, if we take the curl of $\underset{\rightarrow}{v}'$ in (5), and apply the elementary rules of vector analysis, we obtain with the aid of (8) to (10),

$$\nabla\times\underset{\rightarrow}{v}' \equiv \underset{\rightarrow}{c}' = -\underset{\rightarrow}{r}'\cdot\nabla\underset{\rightarrow}{\bar{c}} + \underset{\rightarrow}{\bar{c}}\cdot\nabla\underset{\rightarrow}{r}' - 2d'\underset{\rightarrow}{\bar{c}} - \underset{\rightarrow}{R}'\cdot\nabla\underset{\rightarrow}{\bar{v}} + \underset{\rightarrow}{\bar{v}}\cdot\nabla\underset{\rightarrow}{R}' + \underset{\rightarrow}{\bar{v}}\times\nabla d'. \qquad (11)$$

The first two terms on the right-hand side of (11) demonstrate again that (5), basically, expresses vorticity transfer. If $d' \equiv \nabla\cdot\underset{\rightarrow}{r}'$ and also $\underset{\rightarrow}{R}' \equiv \nabla\times\underset{\rightarrow}{r}'$ were insignificant or zero, (5) and (11) would reduce to

$$\underset{\rightarrow}{v}' = \underset{\rightarrow}{r}'\times\underset{\rightarrow}{\bar{c}}\ ; \text{ and, } \underset{\rightarrow}{c}' = -\underset{\rightarrow}{r}'\cdot\nabla\underset{\rightarrow}{\bar{c}} + \underset{\rightarrow}{\bar{c}}\cdot\nabla\underset{\rightarrow}{r}'. \qquad (12)$$

It was shown previously that in (12) the expression for $\underset{\rightarrow}{v}'$ contrasts significantly with the concept of "conservation of momentum" introduced originally by Prandtl, while the first term on the right-hand side of the expression for $\underset{\rightarrow}{c}'$ corresponds to "conservation of vorticity" introduced by Taylor. The complete form of $\underset{\rightarrow}{c}'$ in (12) was interpreted as denoting "vorticity-transfer-and-adaption"; reference is made to Lettau (1964).

For a comprehensive treatment of turbulent transfer processes, it is imperative to consider, in addition to momentum and vorticity, a scalar property (s) per unit mass of the fluid, and to study the spatial distribution of this admixture. It must be expected that the functional relationship between turbulent fluctuations s' and mean field $\bar{s}$ is governed and determined also by the above defined three-dimensional vector of eddy displacements. In fact, Lettau (1965) has shown that the following generalized form leads to predictions which agree with empirical findings,

$$s' = -\nabla\cdot\bar{s}\,\underset{\rightarrow}{r}' \equiv -\underset{\rightarrow}{r}'\cdot\nabla\bar{s} - \bar{s}\nabla\cdot\underset{\rightarrow}{r}' \equiv -\underset{\rightarrow}{r}'\cdot\nabla\bar{s} - \bar{s}d'. \qquad (13)$$

For $d' = 0$ it follows that s' in (13) reduces to the conventional expression.

For convenience, and practical use, relations (5) — for $\nabla \cdot \underset{\rightarrow}{\bar{v}} = 0$ — and (13) will be also listed in component form

$$u' = (y'\bar{\zeta} - z'\bar{\eta}) - (\bar{v}c' - \bar{w}b') - \bar{u}d', \tag{14a}$$

$$v' = (z'\bar{\xi} - x'\bar{\zeta}) - (\bar{w}a' - \bar{u}c') - \bar{v}d', \tag{14b}$$

$$w' = (x'\bar{\eta} - y'\bar{\xi}) - (\bar{u}b' - \bar{v}a') - \bar{w}d', \quad \text{and} \tag{14c}$$

$$s' = -x'\bar{s}_x - y'\bar{s}_y - z'\bar{s}_z - \bar{s}d'. \tag{14d}$$

The key for a conversion of the abbreviations a', b', c', d', ξ, η, and ζ, into defined spatial derivatives of the vector components (x', y', z', and u, v, and w) is given by relations (8), (9), and (10).

It shall be shown that the system (14) provides an interesting and useful basis for discussion, not only of turbulence near walls and in free flow, as treated previously, but also in the zero-shear zones near the center of a straight duct (or, closed channel) when the flow is generated by a constant pressure gradient.

2. Summary of Principal Empirical Results Concerning Turbulence in One-Dimensional Mean Flow

One-dimensional mean flow is most readily observed in a duct or straight channel, where the fluid is essentially bounded by two parallel walls, and the vector of mean motion is tangential to these boundaries ($\underset{\rightarrow}{\bar{v}} = \underset{\rightarrow}{i}\bar{u}$). Mean speed, $\bar{u}$, will be a symmetric function only of the distance from the walls, so that the vector of mean curl reduces to $\underset{\rightarrow}{\bar{\zeta}} = \underset{\rightarrow}{j}\bar{u}_z$. Steady-state conditions of such mean flow can be caused and maintained by either a constant boundary drag (which results in Couette flow) or by a constant down-stream gradient, p_x, of pressure, p. Even though Couette flow is the simplest possible in theoretical respect, pressure-gradient flow can be easily produced experimentally. For the present discussion the latter has an additional advantage in that it possesses a center-region of essentially zero-value of mean shear. The averaged equation of motion reduces for these steady-state conditions to

$$\overline{(u'w')}_z + p_x - \vartheta\bar{u}_{zz} = 0, \tag{15a}$$

where ϑ = kinematic viscosity of the fluid. At sufficientiy high Reynolds

numbers the flow is said to be "fully developed" which implies that the viscous term in (15a) becomes negligible in comparison with the Reynolds stress term, so that (15a) reduces further to

$$(\overline{u'w'})_z = -\bar{p}_x = \text{const (independent of t, x, y, and z).} \quad (15b)$$

Measurements of the totality of velocity components in turbulent one-dimensional pressure gradient flow (that is, $\bar{u}$, u', v', and w'), in the form of profiles (that is, z-dependencies from wall to center), of mean flow ($\bar{u}$), variances ($\overline{u'u'}$, $\overline{v'v'}$, and $\overline{w'w'}$), and co-variances ($\overline{u'w'}$, etc.), were obtained by several authors. Outstanding among these is still the set of detailed data reported by Laufer (1950), for Reynolds numbers of about 12,000 to 62,000, in a straight channel of rectangular cross section and a 12:1 aspect ratio. Among the many noteworthy empirical results of Laufer's work, only the measurements of root-mean-square values of the fluctuating velocities at the center of the duct will be considered here. Laufer found that in mid-channel, $\overline{v'v'}$ equals $\overline{w'w'}$, while the value of $\overline{u'u'}$ exceeds significantly that of the other two variances. The corresponding root-mean-square values, when normalized upon dividing by mean speed $\bar{u}$, show only a relatively slight dependency on the Reynolds number. For the two higher Reynolds numbers investigated by Laufer we read from his graphs that representative center-values are about as follows:

$$(\overline{u'u'})^{1/2}/\bar{u} = 0.027; \quad (\overline{v'v'})^{1/2}/\bar{u} = (\overline{w'w'})^{1/2}/\bar{u} = 0.022. \quad (16a)$$

Now, $27/22 = 1.227$, and since this value is very close to $\sqrt{3/2} = 1.225$, (16a) may be reformulated as

$$(\overline{u'u'} \,/\, \overline{v'v'})^{1/2} = (\overline{u'u'} \,/\, \overline{w'w'})^{1/2} \approx \sqrt{3/2}. \quad (16b)$$

At the center, $\bar{u}$ reaches the maximum value for the entire cross-section of flow, while the relative magnitudes of all root-mean-square values listed in (16) show broad and relatively flat minimum values. However, only the numerical result quoted in (16a) will be used here; for further detail the reader is referred to the original report by Laufer (1950).

Concerning co-variances, Laufer's measurement showed that only $\overline{u'w'}$ was significant and in general accordance with (15b), the Reynolds stress decreased linearly to zero at the center. In view of the finite values of the variances quoted in (16a) this must mean that at the center the fluctuating velocities u' and w' are statistically uncorrelated with each other, even though they remain finite, and are negatively correlated

at any other points of the channel. Correspondingly it can be concluded that u' and v', as well as v' and w', are statistically uncorrelated with each other at any point of the one-dimensional mean flow.

Similar results were obtained earlier for flow in a straight air-duct of rectangular cross section (24 cm by 100 cm) by Reichardt, as reported in Schlichting (1960, page 466, Figures 18.3 and 18.4). From the graphs reproduced by Schlichting it can be read that in the center of Reichardt's duct $(\overline{u'u'})^{1/2} = 4.3$ cm/sec, and $(\overline{w'w'})^{1/2} = 3.5$ cm/sec, for $\bar{u}_{max} = 100$ cm/sec. Even though the ratios listed in (16a) would differ from Laufer's it can readily be verified that (16b) is confirmed within a reasonable error tolerance, since $4.3/3.5 = 1.23$.

It is realized that there exists an even larger number of studies on one-dimensional mean pressure-gradient flow with circular symmetry, i.e., in straight, round pipes. For this flow condition, later experimental work by Laufer (1954) is also of outstanding quality, and has been widely quoted and discussed in the general textbooks; see, for example, Hinze (1959, chapter 7-9). However, since we are concerned with a basic testing of the new principle, it will suffice, for the time being, to restrict the discussion to the most elementary case of one-dimensional mean duct flow as produced by a constant pressure gradient in a straight channel of rectangular cross section and sufficiently large aspect ratio.

Eddy transfer processes are conventionally studied with the aid of "eddy diffusivity", K, having physical units of cm^2/sec. For the above case of turbulent flow between two parallel walls, this parameter K can be most readily defined for momentum, or any scalar property of the fluid, with the aid of the identities:

$$K_{mom} \equiv -\overline{u'w'}/\bar{u}_z; \quad K_{sca} \equiv -\overline{s'w'}/\bar{s}_z. \tag{17}$$

For the center region of one-dimensional mean pressure-gradient flow the empirical determination of K_{mom}-values is difficult because both, $-\overline{u'w'}$ and $\bar{u}_z$, go to zero. In general, it is well-established that eddy diffusivity is small at the wall (but never smaller than molecular diffusivity); it increases first systematically with distance from the wall, reaches a maximum value shortly before halfway between wall and center, whereupon eddy diffusivity decreases to a still positive and significant minimum value at mid-channel. It must be expected that K_{mom} depends on flow parameters so that the center value will be a function of the Reynolds number or other flow characteristics.

Insofar as the discussions presented in modern textbooks — for example, Hinze (1959), or Schlichting (1960) — reflect the present state of knowledge, it may be concluded that, even for the simple case of one-dimensional duct flow, only the portion of the K_{mom}-profile closest to the wall is reasonably well understood. Here, for about 10 to 20 percent of the entire diameter of the duct, K_{mom} can be successfully normalized with the aid of shearing velocity and distance from the boundary. However, for the remaining about 80 to 90 percent of the diameter, knowledge is restricted to quasi-empirical and qualitative relationships; especially uncertain are conditions in the region of zero-shear in the center.

A special K_{sca} is K_{heat} which is the eddy diffusivity for heat. It applies when internal energy per unit mass of the fluid, c_pT, is substituted for s in (17), with c_p = specific heat and T = absolute temperature. While it turned out to be rather difficult to normalize the distribution of either K_{mom} or K_{heat} individually, the ratio K_{heat}/K_{mom} was found more easily accessible to quantitative treatment and normalization. It has been pointed out by many authorities in the field — see, for example, Ludwieg (1956) — that the accurate knowledge of the ratio K_{heat}/K_{mom} is of great interest for a host of boundary layer problems.

A thorough experimental study on velocity distribution and temperature gradients for controlled heat transfer from wall-to-wall, with pressure-gradient flow in a channel of rectangular cross section, has been conducted by Corcoran, Page, Schlinger, and Sage (1952). Experimental point-values of K_{heat} and K_{mom} were calculated and reported by Page, Schlinger, Breaux, and Sage (1952). From the last quoted report we selected and extracted a representative set of K_{heat}/K_{mom} ratios for points as closely as possible to mid-channel position. Actually, these points were read from tables for $\pm$ 0.05 diameters from the center. The K-ratios together with Reynolds numbers (Re) are summarized below:

Reynolds number:	8,900	9,400	17,100	37,300	52,500
$(K_{heat}/K_{mom})_{mid}$:	1.43	1.41	1.21	1.10	1.05

It must be added that (the only exception being the run at Re = 9,400) the temperature difference between upper and lower wall was kept at a uniform value close to 5°C, with a mean distance (or duct diameter) of 1.7 cm between boundaries.

The pronounced systematic decrease of the ratio K_{heat}/K_{mom} with increasing Reynolds number, experimentally derived by Page et al.,

appears hardly compatible with corresponding data obtained by other authorities using different methods. For example, Ludwieg (1956) based rather reliable estimates of the radial profile of K_{heat}/K_{mom} on measurements of mean velocity and stagnation temperature distribution in pipes with heat-insulated walls, for flows of relatively high Mach numbers. For these conditions, internal heat generation by energy dissipation is relatively large, and energy fluxes due to turbulent diffusion of eddy energy could be evaluated on the basis of the above measurements. The resulting K_{heat}/K_{mom} profile showed a general increase from about 1.08 near the wall to 1.48 near the center, or exactly, from 0.025 diameters off the wall, to 0.025 diameters off the center. The actual Reynolds numbers were relatively high, ranging from 323,000 to 374,000, corresponding to Mach numbers of 0.63 to 0.87. No significant dependency of K_{heat}/K_{mom} on Reynolds number appears evident. A brief summary and discussion of Ludwieg's results can also be found in Schlichting (1960, page 499).

Ludwieg (1956, page 80) comments on the puzzling discrepancy between his result and that of Page et al. summarized above. Especially this concerns the fact that Page et al. find a center value of K_{heat}/K_{mom} which could be close to 3/2 at lowest Reynolds numbers, but, which decreases with Re so that an extrapolation to Re of the order of 300,000 would definitely predict equality of K_{heat} and K_{mom}. In marked contrast, Ludwieg's ratio is still about 3/2 at such Reynolds numbers and independent of them. Ludwieg feels that this considerable discrepancy can hardly be explained by differences in test conditions alone, and supposes that inaccuracies in the experimental method of Page et al. are responsible.

It may be anticipated that in the following section our new model as formulated by (14) shall be applied to the problem of K_{mom} and K_{sca} in one-dimensional flow. It will be shown that the contrasting result of Ludwieg, versus that of Page et al., can have real causes and may be explained by physical deviations in turbulence structure resulting from dissimilarities in $\bar{u}$ and $\bar{s}$ distributions due to different boundary conditions.

We mentioned before that eddy diffusivities — which represent a concept introduced by Boussinesq nearly nine decades ago — proved difficult to normalize. About four decades ago Prandtl made an important advance in showing that a universal result is more readily obtained — at least for the strong shear zone of flow close to the boundary — by a relatively slight change in approach, in comparison to (17). This change amounts to consideration of $\overline{u'w'}/(\bar{u}_z)^2$ rather than $\overline{u'w'}/\bar{u}_z$. The

concept was supplemented a few years later by von Karman's introduction of a similarity rule of turbulent fluctuations. For a detailed account of historical developments reference can be made to Schlichting (1960, pages 477 to 487). Using the notation defined in Section 1, Prandtl's and Karman's laws can be quoted as

$$-\overline{u'w'} = \ell^2 (\bar{u}_z)^2; \quad \text{and,} \quad \ell = -k\bar{u}_z/\bar{u}_{zz}; \quad \text{with } k \approx 0.4, \tag{18}$$

respectively, where ℓ is supposed to be independent of the magnitude of mean or fluctuating velocity, and k is the universal number named Karman's constant.

When $2h$ denotes the narrow width (or diameter) of the channel it is convenient to introduce dimensionless forms of ℓ (by means of the defining relation $F \equiv \ell/h$), and distance from the wall (by the defining relation $\varphi \equiv z/h$) so that φ equals unity at the center of the duct. When the subscript "wall" refers to the boundary value of a quantity and the subscript φ denotes partial differentiation with respect to φ, a reformulation, with the aid of (15b), of Prandtl's law in (18), is

$$\overline{u'w'} = (1-\varphi) \cdot (\overline{u'w'})_{wall} = (F\bar{u}_\varphi)^2, \tag{19a}$$

and of Karman's law in (18),

$$\overline{u'w'} = (1-\varphi) \cdot (\overline{u'w'})_{wall} = -k^2 (\bar{u}_\varphi)^4/(\bar{u}_{\varphi\varphi})^2. \tag{19b}$$

Integration of (19b) is immediately possible and results in Karman's form of the "universal velocity distribution law"; reference is made to Schlichting (1960, page 488). The corresponding integration of (19a) requires an independent mathematical formulation of $F(\varphi)$. In turn, it must be concluded that (19b), too, involves implicitly, but uniquely, a certain function $F(\varphi)$. In fact, the variety of attempts at deriving a "universal velocity distribution law" reported in the literature can readily be discussed in explicit terms of specific F-functions, regardless of whether the individual authors specified them, or used them implicitly. A detailed discussion along these lines was presented by Lettau (1961), and a few of previously employed mathematical models are summarized below.

Year	Authority	Model assumption: $k^{-1}F(\varphi)$ equal to:
1925	Prandtl	
	Original:	φ
	Modified:	$\varphi\sqrt{1-\varphi}$
1930	Von Karman:	$2(1-\sqrt{1-\varphi})\sqrt{1-\varphi}$
1932	Nikuradse:	$(\varphi-\varphi^2/2)[1 - 0.6(\varphi-\varphi^2/2)]$
1959	Lettau	
	General:	$\varphi/[1 + m\varphi^{(m+1)/m}]$
	Duct Flow(m=2):	$\varphi/(1 + 2\varphi^{3/2})$

Prandtl's classical form of the "universal velocity distribution law" is strictly logarithmic in φ; it is produced by integration, with the aid of the original Prandtl model, $F = k\varphi$, only for Couette-flow conditions, that is, for $(\overline{u'w'})_z = 0$. For duct-flow conditions as determined by (15b) it requires consideration of what is listed above as the modified form of Prandtl's $F(\varphi)$. For a discussion of the Nikuradse model, reference can also be made to Schlichting (1960, pages 510 to 512). Lettau (1962) has shown that his generalized form of $F(\varphi)$ applies also to atmospheric boundary layer conditions if $m = 4$; it will be demonstrated in a forthcoming paper how well the same form of $F(\varphi)$ applies to turbulent Couette flow if $m = 1$.

As can readily be seen from the above listing, all F-functions have the common feature that

$$\lim_{\varphi \to 0} \frac{F}{\varphi} = k \qquad (20a)$$

This permits us to conclude that flow conditions are successfully normalized in the immediate neighborhood of the wall. However, considerable discrepancies exist in the center of the duct. Namely, for $\varphi = 1$, $F(\varphi)/k$ is zero for Karman's, as well as Prandtl's modified law, $0.333 = 1/3$ for Lettau's, 0.35 for Nikuradse's, and 1.0 for Prandtl's original law. The difference between the two models by Nikuradse and Lettau is hardly significant; both F-functions, upon integration of (19a), result in velocity distributions that have been shown to be in quite satisfactory agreement with empirical data over the entire cross section of the duct; see Lettau 1961). Therefore, it can be expected that there is a counterpart of (20a) which describes conditions with the approach to mid-channel,

$$\lim_{\varphi \to 1} F_{\varphi} = 0, \tag{20b}$$

with the additional specification that for pressure-gradient flow $(F/k)_{mid} = 1/3$.

The exact determination of the numerical value of Karman's universal constant depends to a relatively slight though significant degree on the form of the F-function accepted for the integration of (19a), or, the mathematical form of the resulting velocity distribution law. Employing exactly the same set of empirical data for which Nikuradse derived the commonly accepted value of $k = 0.40$ with the aid of Prandtl's strictly logarithmic velocity profile, Lettau (1961) has shown that $k = 0.428$ if the velocity profile corresponding to the more realistic function $F = k\varphi(1 + 2\varphi^{3/2})$ is used. Schlichting (1960, page 512) states that with von Karman's form of the "universal velocity distribution law" as deduced from (19b), good agreement with empirical values would require that $k = 0.36$. In view of obvious deficiencies of the laws of Prandtl and von Karman it can be concluded that $k = 0.428$ appears to be the most representative value of this universal constant.

3. Turbulence Characteristics of One-Dimensional Mean Shear-Flow Derived from the Generalized Eddy Displacement Structure

For the application of the new mathematical model it is practical to summarize the properties of one-dimensional mean shear-flow under conditions as detailed in Section 2, namely,

$$\bar{\underset{\rightarrow}{v}} = \underset{\rightarrow}{i}\bar{u}; \quad \nabla\cdot\bar{\underset{\rightarrow}{v}} = \bar{u}_x = 0; \quad \nabla\times\bar{\underset{\rightarrow}{v}} = \underset{\rightarrow}{j}\bar{\eta} = \underset{\rightarrow}{j}\bar{u}_z; \quad \nabla^2\bar{\underset{\rightarrow}{v}} = \underset{\rightarrow}{i}\bar{u}_{zz}. \tag{21a}$$

Let the consideration also include a scalar property of the fluid, which has a lateral gradient due to uniform flux-density maintained by a continuous boundary source or sink. Then,

$$\nabla\bar{s} = \underset{\rightarrow}{k}\bar{s}_z; \quad \nabla^2\bar{s} = \bar{s}_{zz}. \tag{21b}$$

For mean states, specified by (21), the complete system of fluctuating quantities follows from (14) as

$$u' = -z'\bar{u}_z - d'\bar{u} \equiv -z'\bar{u}_z - (x'_x + y'_y + z'_z)\bar{u}, \tag{22a}$$

$$v' = c'\bar{u} \equiv (y'_x - x'_y)\bar{u}, \tag{22b}$$

$$w' = x'\bar{u}_z - b'\bar{u} \equiv x'\bar{u}_z - (x'_z - z'_x)\bar{u}, \tag{22c}$$

$$s' = -z'\bar{s}_z - d'\bar{s} \equiv -z'\bar{s}_z - (x'_x + y'_y + z'_z)\bar{s}. \tag{22d}$$

Furthermore, the condition for a zero-value of the divergence of the fluctuating velocity vector (6b)reduces to

$$x'\bar{u}_{zz} = (x'_{xx} + x'_{yy} + x'_{zz})\bar{u}. \tag{23}$$

Firstly, let us investigate variances and root-mean-square values. If, for convenience, $u'u'$ is written instead of u'^2, and the same is done with all "primed" quantities, squaring of the individual equations in (22) produces

$$u'u' = z'z'\bar{u}_z^2 + 2d'z'\bar{u}_z\bar{u} + d'd'\bar{u}^2, \tag{24a}$$

$$v'v' = (y'_x y'_x + x'_y x'_y - 2y'_x x'_y)\bar{u}^2, \tag{24b}$$

$$w'w' = x'x'\bar{u}_z^2 - 2b'x'\bar{u}_z\bar{u} + b'b'\bar{u}^2, \tag{24c}$$

and a relation for $s's'$ which needs not to be written down because it would be the same as (24a) only with s in place of u.

Application of the bar-operation eliminates those products of fluctuation quantities which are statistically uncorrelated with each other. Further simplification of the system (24) occurs at the center of the duct. Namely, at mid-channel, $\bar{u}_z = 0$ which means that $\bar{u}_{mid} = \bar{u}_{max}$. If anywhere in the duct, conditions of isotropy will here exist, which implies that at mid-channel all variances are equal,

$$\overline{x'_x x'_x} = \overline{x'_y x'_y} = \overline{x'_z x'_z} = \overline{y'_x y'_x} = \overline{y'_y y'_y} = \overline{z'_x z'_x} = \overline{z'_z z'_z} = \kappa^2, \tag{25a}$$

where κ^2 denotes a positive number. Simultaneously, by virtue of isotropy, a family of mixed products vanishes, specifically,

$$\overline{x'_x y'_y} = \overline{x'_x z'_z} = \overline{x'_y z'_x} = \overline{x'_z z'_x} = \overline{y'_y z'_z} = 0. \tag{25b}$$

With (25) it follows from (24) that at the center of the duct,

$$(\overline{u'u'})_{mid} = 3\kappa^2(\bar{u}^2)_{mid}, \tag{26a}$$

$$(\overline{v'v'})_{mid} = (\overline{w'w'})_{mid} = 2\kappa^2(\bar{u}^2)_{mid}. \tag{26b}$$

One verifies readily that (26) agrees satisfactorily with Laufer's empirical result (16b) which was discussed in Section 2, while (16a) permits numerical estimate $\kappa \approx 0.015$. From Reichardt's results also discussed in Section 2, a 0.025 value would follow but, it was pointed out by Laufer, that the duct employed by Reichardt did not have a satisfactory aspect ratio, so that fluctuation conditions were possibly not truly representative. Provided the interpretation by variances such as (25a) stands further testings it is proposed that κ be called the "Laufer constant". In view of the defining equation, $\kappa^2 = (\overline{x'_x x'_x})_{mid}$, κ represents an interesting counterpart to the Karman constant, $k^2 = (\overline{x'_z z'_z})_{wall}$. It appears desirable that the possibly universal nature of κ and its numerical value be more securely tested than before.

Let us turn now to the investigation of co-variances which can be calculated with the aid of the system (22) as follows,

$$\overline{u'v'} = -c'z'\bar{u}_z\bar{u} - c'd'\bar{u}^2, \tag{27a}$$

$$\overline{v'w'} = c'x'\bar{u}_z\bar{u} - b'c'\bar{u}^2, \tag{27b}$$

$$\overline{u'w'} = -x'z'\bar{u}_z^2 + (b'z' - d'x')\bar{u}_z\bar{u} + b'd'\bar{u}^2, \tag{27c}$$

$$\overline{s'w'} = -x'z'\bar{s}_z\bar{u}_z + b'z'\bar{s}_z\bar{u} - d'x'\bar{u}_z\bar{s} + b'd'\bar{s}\bar{u}. \tag{27d}$$

On the basis of physical reasoning and the one-dimensionality of the mean velocity vector, it must be required that $\overline{u'v'} = \overline{v'w'} = 0$ at any level of the considered flow. Thus, it follows from the system (27) that

$$\overline{c'b'} \equiv \overline{(y'_x - y'_y)(x'_z - z'_x)} = 0, \tag{28a}$$

$$\overline{c'd'} \equiv \overline{(y'_x - x'_y)(x'_x + y'_y + z'_z)} = 0, \tag{28b}$$

$$\overline{c'x'} \equiv \overline{y'_x x'} - \overline{x'_y x'} = 0, \tag{28c}$$

$$\overline{c'z'} \equiv \overline{y'_x z'} - \overline{x'_y z'} = 0. \tag{28d}$$

Furthermore, the restrictive requirement that the eddy flux of x-momentum in the z-direction should be of the "gradient-type", is satisfied when in (27c)

$$\overline{b'd'} \equiv \overline{(x'_z - z'_x)(x'_x + y'_y + z'_z)} = 0. \tag{28e}$$

Since the co-variance (28e) appears in both relations, (27c) and (27d) transform into

$$\overline{u'w'} = \overline{-x'z'}\,\bar{u}_z^2 + (\overline{b'z'} - \overline{d'x'})\,\bar{u}_z\bar{u}, \tag{29a}$$

$$\overline{s'w'} = -\overline{x'z'}\,\bar{u}_z\bar{s}_z + \overline{b'z'}\,\bar{s}_z\bar{u} - \overline{d'x'}\,\bar{u}_z\bar{s}. \tag{29b}$$

The second equation proves that gradient-type eddy diffusion for momentum does not automatically imply the same type for the eddy diffusion of a scalar property of the fluid. More about this farther below.

The cartesian components of the eddy displacement vector appear in co-variances of the systems (28) and (29) in such numbers and variety that we may distinguish three basic types. One involves only the magnitudes themselves, as for example, $\overline{x'z'}$; another type shows a combination of one magnitude with one partial derivative, as for example, $\overline{c'x'}$, while the last consists of products of two derivatives, as for example $\overline{c'd'}$, and its constituents. The first type shall be discussed in some detail at the end of this section, in connection with the revised form of the classical Prandtl-Taylor-Karman length-scale of turbulence. Concerning co-variances of the second type it will immediately be seen that certain terms, like $\overline{x'_y x'}$ in (28c), can be reformulated as the derivative of a variance like $\frac{1}{2}(\overline{x'x'})_y$; the physical nature of the assumed one-dimensional flow will require that the bar-value of the latter example is exactly zero. A similar argumentation concerning $\overline{x'_x x'}$, as part of $\overline{d'x'}$ in (29a), will also result in a zero-value because the average, $\overline{x'x'}$, cannot be a function of x. Additionally, and independently, it must be expected, in the form of a general rule for one-dimensional flow, that all co-variances which contain either y' or, any y-derivative, like x'_y and z'_y, will in all likli-hood average out to zero. This means that non-zeros in (29) will be:

$$\overline{b'z'} = \overline{x'_z z'}; \text{ and, } \overline{d'x'} = \overline{z'_z x'}. \tag{30}$$

Other non-vanishing co-variances of the same type as (30) will also be discussed at the end of this section, in connection with length-scale concepts.

Any of the three components (x', y', z') of the eddy displacement vector can appear in the form of a derivative with respect to each of the three spatial coordinates. Thus, the possible total of individual factors in co-variances of the third type amounts to nine. It has been mentioned in connection with (9) and (10) that the four abbreviated terms $a', b', c',$

and d' contain exactly these nine factors, and each appears only once. We may disregard here the squares (or, orthogonal terms) and assume symmetry in mixed products (for example, $x'_z z'_x = z'_x x'_z$), which leaves us with a total of 36 co-variances. According to (28a) and (28b), 10 of these cross-products do vanish on the average when it is assumed that after expansion of the products of sums in the above three expressions, each individual co-variance is zero. Moreover, it is safe to say that mixed products which involve the longitudinal vorticity component a', as defined in (10), will vanish; even though, due to the one-dimensionality of the investigated mean flow, none of the terms in the system (22) contains a' as a factor. However, condition (28e) is of a special nature, and will be satisfied with only four of the six co-variances individually equalling zero; the remaining two will be equal to each other, that is $\overline{x'_x z'_x} = \overline{x'_z z'_z} \neq 0$, which does not restrict the validity of (28e). Therefore, at least two cross-products of the third type will be significant. It shall be demonstrated that these are indeed extremely important in that they will be identified with the Karman constant.

In summary, a picture developes of a very special anisotropy, or only slightly restricted form of isotropy of turbulent displacement structure, for the considered case of one-dimensional mean shear flow. A closer discussion, though, shall be postponed since we prefer to emphasize, in the present introductory appraisal, the direct comparison of model predictions with the best of empirical data available in the literature. Naturally, no direct measurements of eddy displacements exist and cannot exist, not to mention measurements of their spatial derivatives. Therefore, we now turn our attention to eddy diffusivities.

The defining equations (17) yield in combination with (29) and (30),

$$K_{mom} = \overline{x'z'}\,\bar{u}_z + (\overline{x'_z z'} - \overline{z'_z x'})\,\bar{u} \qquad (31a)$$

$$K_{sca} = \overline{x'z'}\,\bar{u}_z + \overline{x'_z z'}\,\bar{u} - \overline{z'_z x'}\,\bar{s}\,\bar{u}_z/\bar{s}_z. \qquad (31b)$$

Obviously, eddy diffusivities must depend markedly on the structure of mean states of flow. The appearance of both, mean velocity $\bar{u}$ and shear $\bar{u}_z$, in (31a) serves to explain why attempts towards normalization were not successful, except for the region near the wall, where $\bar{u}_z$ is large and $\bar{u}$ small. Furthermore, the system (31) shows clearly that K_{mom} will equal K_{sca} only when $\bar{u}/\bar{u}_z$ equals $\bar{s}/\bar{s}_z$, i.e., when strict similarity prevails. If there is dissimilarity, for instance, if $\bar{s}_z$ would have a non-zero value at the center of the duct, where $\bar{u}_z = 0$, the eddy diffusivity ratio can be normalized, and we obtain a highly interesting relation,

$$(K_{sca}/K_{mom})_{mid} = \overline{b'z'}/(\overline{b'z'} - \overline{d'x'}). \qquad (32)$$

It is certainly possible to think of duct flow under such boundary conditions that at mid-channel the derivative $\bar{s}_z$ is finite; a good example is given by the experiments of Corcoran et al. mentioned in Section 2.

Together with the other extreme case of full similarity between s and u, for which the ratio of the eddy diffusivities equals unity, relations (31) show that the ratio of the K's must vary over the cross section of the duct, and can be normalized only at the center of the duct. In this connection, Ludwieg's empirical result, with heat as the scalar property, is interesting insofar as it indicates that the ratio of K_{heat}/K_{mom} at mid-channel is independent of the flow structure and equal to about 3/2. This conforms with (32) provided that

$$(\overline{b'z'})_{mid} = 3(\overline{d'x'})_{mid}; \text{ or, } (\overline{x'_z z'})_{mid} = 3(\overline{z'_z x'})_{mid}. \qquad (33)$$

The alternate form of (33) is explained by (30). Physical-statistical justification for the validity of (33) can be based on independent reasoning, as will be discussed at the end of this section.

It is indeed reasonable to expect a characteristic degree of dissimilarity between heat and momentum distributions for the conditions of Ludwieg's experiment; namely, temperature increased down-stream with unchanging mean flow, due to heat insulated walls, and significant rates of internal production of heat. A closer investigation of these particular conditions, together, possibly, with the necessary modification of the system (22) for the case of circular symmetry of flow, will be postponed; also delayed will be a closer study of the discrepancy between the experimental results of Ludwieg (1956), and Page et al. (1952). Concerning the latter, it may suffice here to mention the possibility that a gradual approach to fuller similarity between heat and momentum distributions may have taken place. In other words, it appears possible that the ratio of K_{heat}/K_{mom} in the experiments by Corcoran et al., decreased from a low-Reynolds number value of nearly 3/2, towards unity with increasing Reynolds number in accordance with a change from quite dissimilar to more similar conditions of heat and momentum distribution (reference is made to the summary in Section 2). This could have been brought about by the selected procedure of keeping the temperature differential from one wall to the other approximately constant, while the mean flow-rate was systematically increased to produce the desired change in Reynolds number. However, these are tentative suggestions, and revisions are possible upon closer investigation of the empirical data and flow conditions in the experiment by Page et al. The important feature is that we have now available a complete yet concise scheme for the

calculation of turbulent transfer characteristics, in a more consistent and rational manner than before.

The same scheme, when previously applied with reasonable success to transfer processes in free turbulence yielded a ratio of 4/3 for K_{heat}/K_{mom} in the center region of a two-dimensional submerged jet, where there is little or no shear. Again, only the ratio, not the diffusivities themselves, could be normalized. Interestingly, the transfer characteristics in the case of free turbulence can be rather completely described by one variance only, namely that of the down-stream component of the eddy displacement vector. This was mentioned at the beginning of Section 1. Concerning more detail about the concept of the "longitudinal length-scale", and its relationship to the "momentum transfer length" introduced by Reichardt, the reader is referred to Lettau (1965). It appears as if the co-variances of components of the eddy displacement vector play a significant role only in wall turbulence, when the mean flow is strictly ducted and the fluid bounded by at least one solid wall.

It must be emphasized here that there is, of course, no absolute justification for the assumption that "gradient-type" eddy diffusion prevails under all flow conditions. Especially when heat is the fluid property considered, the importance of gradient-diffusion will be diminished as conditions of turbulent free convection are approached. It should be remembered that the expressions for eddy transfer (29), and subsequently derived eddy diffusivities (31), are valid only when (28e) is satisfied. The possible effect of non-vanishing terms in $\overline{b'd'}$, in connection with the original forms (27c and d), must and can be investigated if convection is involved, but in other general cases, too, as shall be demonstrated next.

Now, let us investigate the lateral length-scale of turbulence. Employment of the defining equations (18), in connection with (27c), yields

$$\ell^2 \equiv -\overline{u'w'}/\bar{u}_z^2 = \overline{x'z'} - (\overline{x'_z z'} - \overline{z'_z x'})\bar{u}/\bar{u}_z - \overline{b'd'}(\bar{u}/\bar{u}_z)^2, \quad (34)$$

where the simplification (30) is considered, but eddy diffusion is not restricted to be of the gradient-type. Differentiation of (34) once with respect to z yields, exactly,

$$2\ell_z\ell = 2\overline{z'_z x'} - (\overline{x'_{zz} z'} - \overline{z'_{zz} x'})\bar{u}/\bar{u}_z + \quad (35)$$
$$+ [\bar{u}_{zz}(\overline{x'_z z'} - \overline{z'_z x'}) - \bar{u}(\overline{b'_z d'} + \overline{d'_z b'})]\bar{u}/\bar{u}_z^2 - 2\overline{b'd'}(\bar{u}^2/\bar{u}_z^2)_z .$$

At this point let us restrict further developments to the case of gradient-type eddy diffusion of x-momentum; that means that $\overline{b'd'} = 0$, which eliminates the last term in both relations (34) and (35). Note that this step,

taken at this point, preserves the terms with $\overline{b'_z d'}$ and $\overline{d'_z b'}$ in (35), which will prove significant.

In the zone of strongest mean shear, near the wall, the third term in (35) will be relatively small. Thus it can be concluded that a necessary and sufficient condition for both, ℓ and ℓ_z being independent of the flow structure, must be

$$\overline{x'_z z'} = \overline{z'_z x'} \quad ; \text{ subsequently, } \quad \overline{x'_{zz} z'} = \overline{z'_{zz} x'} \; . \tag{36}$$

The second relation in (36) follows directly and exactly from the first, upon differentiation. Thus, for the immediate vicinity of the wall, (34) and (35) reduce to the completely normalized forms,

$$\ell^2 = \overline{x' z'}; \text{ and, } \quad \ell_z \ell = \overline{z'_z x'} = \overline{x'_z z'} \tag{37}$$

Obviously (37) represents no more or less than a reformulation, and rationalization, of the classical Prandtl-von Karman hypothesis (18). A necessary and sufficient prerequisite of (37) is that both derivatives of the eddy displacement vector, divergence as well as lateral vorticity, go to zero in the vicinity of the boundary. Namely, with $\bar{u}_z$ significantly different from zero, (22b) yields, for $b' = 0$,

$$x' = w'/\bar{u}_z; \text{ subsequently, } \quad x'_z = w'_z/\bar{u}_z - w'\bar{u}_{zz}/\bar{u}^2_z, \tag{38a}$$

which, when combined with (22a), for $d' = 0$, results in

$$-x'_z z' = w'_z u'/\bar{u}^2_z - u'w'\,\bar{u}_{zz}/\bar{u}^3_z \; ; \text{ with: } -z' = u'/\bar{u}_z. \tag{38b}$$

Now, for $\nabla \cdot \underset{\rightarrow}{v}' = 0$ we have that $w'_z = - u'_x - v'_y$; in view of flow conditions requiring $\overline{u'u'}$ to be independent of x, this means that $\overline{w'_z u'} = - \overline{v'_y u'}$, and according to the previously accepted rule, the latter covariance must vanish. Consequently (38b) results in

$$-\overline{x'_z z'} = - \overline{u'w'}\,\bar{u}_{zz}/\bar{u}^3_z. \tag{39}$$

In combination with the first form in (34) and the second form in (37), relation (39) permits the elimination of ℓ, whereupon,

$$(\ell_z)^2 = - \overline{u'w'}\,\bar{u}^2_{zz}/\bar{u}^4_z = k^2, \tag{40}$$

which agrees exactly with the expression for the square of the Karman

constant (19b), since the ratio involving the two derivatives of $\bar{u}$ is independent of non-dimensionalization of lateral distance.

The co-variance expression for the Karman constant can be derived in several different ways. A relatively simple manner is to obtain z'_z, using (22a) with $d' = 0$, in a procedure corresponding to the calculation of x'_z in (38a). Then we form the product, and derive the following sequence of developments,

$$x'_z z'_z = - u'_z w'_z / \bar{u}_z^2 + (w'_z u' + u'_z w') \bar{u}_{zz} / \bar{u}_z^3 - u'w' \bar{u}_{zz}^{\,2} / \bar{u}_z^4$$

$$= - u'_z w'_z / \bar{u}_z^2 + (w'u')_z \bar{u}_{zz} / \bar{u}_z^3 - u'w' u_{zz}^{\,2} / \bar{u}_z^4$$

$$= - u'_z w'_z / \bar{u}_z^2 + (w'u' / \bar{u}_z)_z \bar{u}_{zz} / \bar{u}_z^2 . \qquad (41)$$

It is theoretically legitimate, and practical for the analysis of empirical data, to single out the lowest stratum (called the "surface layer") of the shear zone in fully developed wall-turbulence. The thickness of the surface layer is determined by the requirement that height-integration of the stress derivative — which is prescribed by the equation of motion, that is, (15b) in the case considered here — contributes a total stress variation between top and bottom of the layer, which is small in comparison with the value of wall-stress, or boundary drag. Employing the dimensionless height $\varphi = z/h$ as previously introduced for the system (19), the surface layer is defined by $0 \leq \varphi \leq \varepsilon \ll 1$, so that $\varphi(\overline{u'w'})_\varphi / (\overline{u'w'})_{wall} \leq \varepsilon$, where ε is a small positive number of less than the order of the relative probable error of stress measurement; for example, $\varepsilon \approx 0.01$ to 0.1 in practical experiments. Thus, restriction of the discussion of (41) to the surface layer means that

$$(\overline{u'w'})_z \bar{u}_z / \bar{u}_{zz} \ll (\overline{u'w'})_{wall} . \qquad (42a)$$

A similar argumentation as used above, in connection with the zero-value for $\overline{w'_z u'}$, supports the conclusion that $\overline{w'_z u'_z}$ will vanish, at least in the surface layer. Thus, applying the bar-operation to (41) will yield, for the surface layer,

$$\overline{x'_z z'_z} = - (\overline{u'w'})_{wall} \bar{u}_{zz}^{\,2} / \bar{u}_z^4 = k^2 , \qquad (42b)$$

which is the co-variance form of Karman's law quoted in (19b), and thus explains the physical nature of the Karman constant k. The restricted

validity (to the surface layer only) of (37), (40) and (42b) will explain why the direct integration of (19b) between the full limits from $\varphi = 0$ to $\varphi = 1$, and the resulting Karman-form of the "universal velocity distribution law" does not compare favorably with empirical data for the inner region of duct flow. On the other hand, the length-scale expression in (34), when restricted to surface layer conditions, is successfully and completely normalized. This will explain why the Karman similarity concept, as well as the numerical value of the Karman constant apply universally to mean flow of different types provided that the fluid moves tangential to a solid boundary. The list of such types includes Couette flow, pressure gradient flow in ducts, open channel flow, turbulent boundary layer flow, atmospheric boundary and surface layer flow, etc.

Finally, a brief and tentative discussion of the conditions in mid-channel can be added. With the restriction to gradient-type eddy diffusion, infinities for $\bar{u}_z = 0$ will not occur in (35), if in the zero-shear zone we have that

$$\bar{u}_{zz}(\overline{x'_z z'} - \overline{z'_z x'}) = \bar{u}(\overline{b'_z d'} + \overline{d'_z b'}). \tag{43}$$

The co-variances on the right-hand side of (43) are of a new type, in that second-order derivatives of the eddy displacement vector appear as factors. Let us suppose that the isotropy conditions in mid-channel are of such a nature that $\overline{b'_z d'}$ equals to a sufficient degree of approximation $\overline{d'_z b'}$. This will mean the existence of statistical correlations exclusively between second-order and first-order z-derivatives of x' and z', namely, upon expansion,

$$\overline{b'_z d'} = \overline{(x'_{zz} - z'_{xz})(x'_x + y'_y + z'_z)} \approx \overline{x'_{zz} z'_z}, \tag{44a}$$

$$\overline{d'_z b'} = \overline{(x'_{xz} + y'_{yz} + z'_{zz})(x'_z - z'_x)} \approx \overline{z'_{zz} x'_z} \approx \overline{x'_{zz} z'_z}. \tag{44b}$$

With the aid of (44), the relation (43), at mid-channel, reduces to

$$\bar{u}_{zz}(\overline{x'_z z'} - \overline{z'_z x'}) \approx 2\bar{u}\,\overline{x'_{zz} z'_z} \tag{45}$$

Now, let us recall the characteristic relation (6b) in the special form of (23), which expresses the plausible fact that the fluctuating velocity vector is non-divergent. Upon multiplication of (23) by z'_z and averaging,

$$\bar{u}_{zz}\,\overline{z'_z x'} = \bar{u}\,\overline{z'_z(x'_{xx} + x'_{yy} + x'_{zz})} \approx \bar{u}\,\overline{x'_{zz} z'_z}, \tag{46}$$

when the above described special isotropy condition is considered. Combination of (46) with (45) yields, at mid-channel,

$$\bar{u}_{zz}(\overline{x'_z z'} - \overline{z'_z x'}) \approx 2\,\bar{u}_{zz}\,\overline{z'_z x'}; \text{ thus, } \overline{x'_z z'} \approx 3\,\overline{z'_z x'}, \qquad (47)$$

which agrees with (33). Thus the interrelationship between co-variances, which explains the value of 3/2 for the ratio K_{sca}/K_{mom} at mid-channel, compatible with empirical findings, is herewith deduced.

4. Concluding Remarks

It must be emphasized again that the preceding discussion is part of a continuing investigation. The conclusions are tentative, because certain lines of development have not yet been fully followed through. However, the proposed scheme which prescribes individually and exhaustively the complete system of turbulent quantities (s', u', v', and w') was shown to provide a versatile and useful tool for the prediction of a host of empirical facts concerning turbulence characteristics of one-dimensional mean flow, especially for the zero-shear zone in the center of pressure-gradient flow between parallel boundaries. This is in addition to previous results concerning the structure of free turbulence and of eddy transfer processes in a two-dimensional submerged jet. The explanation of well-documented experimental results establishes another point in favor of the new hypothesis, although it is presented still in the form of a conjecture. Further exploration of its potential shall be the aim of future studies.

Acknowledgments. The research reported is in part supported by the Department of Meteorology, U. S. Army Electronics Research and Development Activity, Fort Huachuca, Arizona, under Contract DA-36-039-AM-00878.

REFERENCES

Corcoran, W.H., F. Page, W.G. Schlinger, and B.H. Sage, 1952: Temperature gradients in turbulent gas streams. Methods and apparatus for flow between parallel plates. Ind. Eng. Chem. 44, pages 410-419.

Hinze, J.O., 1959: Turbulence. McGraw-Hill Book Co., Inc., New York.

Laufer, J., 1950: Investigation of turbulent flow in a two-dimensional channel. Nat. Adv. Com. Aeronautics; Tech. Note 2123, Washington, D.C.

Laufer, J., 1954; The structure of turbulence in fully developed pipe flow. Nat. Adv. Com. Aeronautics; Tech. Report No. 1174, Washington, D.C.

Lettau, H., 1961: A generalized mathematical model of the mean-velocity distribution in fully turbulent duct flow. Annual Report, Contract DA-36-039-SC-80282, Univ. of Wisconsin, Madison.

Lettau, H., 1962: Theoretical wind spirals in the boundary layer of a barotropic atmosphere. Beitr. Phys. Atmosph., 35, 195-212.

Lettau, H., 1964: A new vorticity-transfer hypothesis of turbulence theory. J. Atmosph. Sci., 21, pages 453-456.

Lettau, H., 1965: Longitudinal versus lateral eddy length-scale. Unpublished manuscript.

Ludwieg, H., 1956: Bestimmung des Verhaeltnisses der Austausch-koeffizienten fuer Waerme und Impuls bei turbulenten Grenzschichten. Z. F. Flugwiss. 4, pages 73-81.

Page, F., W.G. Schlinger, D.K. Breaux, and B.H. Sage, 1952: Point values of eddy conductivity and viscosity in uniform flow between parallel plates. Ind. Eng. Chem. 44, pages 424-430; see also Report ADI 3294.

Schlichting, H., 1960: Boundary Layer Theory (Fourth edition), McGraw-Hill Book Co., Inc., New York.

ATMOSPHERIC BOUNDARY-LAYER DYNAMICS OVER THE FORESTS OF NORTHEASTERN WISCONSIN*

Warren B. Johnson, Jr.
Department of Meteorology
University of Wisconsin

Abstract: There is a serious need for detailed observations of boundary-layer structure, particularly over surfaces with tall vegetation. Accordingly, an experimental program consisting of seven observational periods spanning about a year's time was carried out over the extensive deciduous forests of northeastern Wisconsin. A total of 209 usable, detailed wind profiles for the lowest 2 km of the atmosphere were obtained by tracking pilot balloons with two theodolites. Supplementary surface-layer measurements of net radiation, wind and temperature furnished sufficient information to estimate the surface heat-budget parameters, as well as atmospheric stability and aerodynamic surface roughness length, which aided in the interpretation of the results of the wind-profile analysis. Additionally, use was made of boundary-layer temperature profiles obtained by means of an instrumented aircraft during some of the observational periods; for the other periods, USWB radiosonde data were employed.

The observations are illustrated in conjunction with profiles of geostrophic wind computed directly from surface and upper-air pressure and temperature measurements, which, although apparently rather inaccurate, were of some use in the analysis of the wind profiles. The analysis for the most part was performed using a modification of Lettau's "antitriptic" method. The basic method permits the indirect determination of geostrophic wind profiles through the assumption of constant thermal

*This work is part of a thesis submitted to the University of Wisconsin in partial fulfillment of the requirements for the Ph. D. Degree, written under the supervision of Professor H. Lettau, Department of Meteorology.

wind; the modification essentially involves the treatment of baroclinic wind profiles as barotropic profiles upon which thermal winds are simply superimposed. The modified method gives acceptable results for all advection regimes, while the original method fails for cases of strong cold-air advection.

Estimates were obtained for several basic boundary-layer parameters, and these are compared with results from previous investigations and with theory. Fairly good agreement with theory for neutral conditions is indicated in most instances. A pronounced diurnal variation of stress, geostrophic drag coefficient, and total rate of energy dissipation is indicated, confirming previous observations and theory. Seasonal changes in the character of the vegetation due to the phenological cycle are shown to have significant effects upon low-level wind structure.

Several noteworthy features of the boundary-layer observations are discussed, such as nocturnal low-level wind maxima and diurnal variations in the height of the upper-level temperature inversion under convective conditions. In addition, results are reported of an experimental evaluation of the behavior of smooth and artificially roughened pilot balloons. Evidence is presented which indicates that the smooth pilot balloons, while serving satisfactorily as horizontal wind sensors in this investigation, had height-varying ascent rates which were more closely associated with atmospheric turbulence structure than with vertical air motions.

1. Introduction

The term "planetary boundary layer" was introduced by Lettau (1939) to describe the lower portion of the troposphere within which the effects of frictional interaction with the earth's surface are manifest and significant. In recent years the research effort in boundary-layer structure has been intensified in association with the increased demand for a better understanding of atmospheric diffusion, of the general circulation, and of the development of large-scale weather systems.

There is considerable interest at present in the mechanisms of energy transfer in the atmosphere. Following White and Saltzman (1956), the atmospheric energy balance may be concisely stated by the equation

$$\int_M [dQ/dt - \partial(k + P + I)/\partial t - D]dm = 0,$$

where Q is the non-adiabatic heating per unit mass; K, P, and I are kinetic, potential and internal energy per unit mass, respectively; D is the rate of frictional energy dissipation, t is time and the integration is over the whole mass M of the atmosphere. In most of the work done to date, this equation has been simplified by disregarding the heating (source) and dissipation (sink) terms. Clearly, future progress in the investigation of this fundamental energy cycle is dependent upon the gaining of additional knowledge concerning the nature and magnitude of these two important terms. In a case study of the total rate of dissipation of kinetic energy in the winter troposphere over the British Isles, Holopainen (1963) found that almost half of the total occurred within the atmospheric boundary layer (below 900 mb), which illustrates the importance of this region in the energy cycle.

Considerations of basic energy-transfer mechanisms in the general circulation are intimately related to the development of numerical weather forecasting. Lettau (1959a) has shown by his estimates of the mean reservoir of atmospheric mechanical energy and of the global mean of energy dissipation that a renewal period for kinetic energy of about three days is indicated. A similar value was found by Holopainen, who points out: "This implies that a numerical prediction of the tropospheric motion field for more than one or two days cannot be very successful unless a proper mechanism for frictional dissipation is incorporated in the model." The general problem here is one of including the surface fluxes in the large-scale system by relating them to the external parameters controlling the flow.

In this regard, Lettau's work in relating empirically (1959a) and theoretically (1962) his concepts of geostrophic drag coefficient C and surface Rossby number $\underline{Ro}_0$ is useful. (The surface Rossby number is defined as $\underline{Ro}_0 = V_{g,0}/z_0 f$, where $V_{g,0}$ is the surface geostrophic wind speed, z_0 the zerodynamic surface roughness length, and f the Coriolis parameter.) Applying Lettau's theoretical relations, Kung (1963) was able to estimate the climatological pattern of mechanical energy dissipation in the lower atmosphere over the Northern Hemisphere, based on his assessments of area-means of aerodynamic surface roughness. In addition to the wind-spiral solution proposed by Lettau (1962), numerous other theories of varying degrees of generality have been offered: Blackadar (1962, 1963), Appleby and Ohmstede (1964), Estoque (1963), Ching (1964) and others. A number of these theories appear to give fairly good comparisons with the available observations, but the quantity of these data is extremely limited. Routine aerological soundings are not sufficiently detailed for boundary-layer work; special observations are necessary. In an earlier study (Johnson, 1962), the wind-

profile analysis was based upon kite observations obtained over 40 years earlier. The recent use of tall instrumented towers has been of some help in this regard; however, even a 2000-ft. structure is not high enough to sample the total vertical extent of the layer of interest, except under certain conditions.

The seriousness of the lack of suitable observations in the atmospheric boundary layer may be judged from the statements of the National Meso-Micrometeorological Facility Survey Group (1964), in connection with plans of the National Center for Atmospheric Research to establish a boundary-layer observational facility. The following excerpt from the report by the Facility Survey Group is pertinent here: "Perhaps the most important problem of micrometeorology is to relate surface fluxes of momentum, heat and moisture to free-air variables and terrain characteristics.... Progress in this field has been extremely slow, because extensive observational programs of surface conditions have generally not been accompanied by sufficient information to determine the geostrophic wind, the thermal wind and the profiles of wind and temperature up to 5000 ft."

Particularly lacking have been detailed boundary-layer observations over very rough boundaries. Lettau (1959b) states, "Little is known about the effective aerodynamical drag of relatively extreme surface roughness types such as the ensemble of trees in wooded areas or, the net effect of the buildings of extended housing developments, and the mean wind profile and turbulence structure above them." The paucity of such observations has prevented the verification, for extreme surface roughness, of any of the theories referred to previously.

The study reported in this thesis is an attempt to fill partially the void described in the preceding paragraphs. An experimental program was undertaken to provide detailed boundary-layer wind profiles up to 2 km and supplementary low-level data over the forested region of northeastern Wisconsin. The seven observational periods were spaced over about a year's time in order that the dependence of the wind-profile structure upon seasonal vegetation changes could be investigated; the duration of the periods was such that diurnal variations in the boundary-layer dynamics could also be examined. Concurrently with the surface-based observations during three of the periods, detailed temperature profiles were obtained through the use of an instrumented aircraft by Donald H. Lenschow of the Department of Meteorology, University of Wisconsin; reference can be made to Paper No. 4 of this volume. Estimated profiles of geostrophic wind were found by an analysis of synoptic-scale radiosonde observations and surface-pressure data, supplemented during the last two periods with a special barograph network. These profiles, while less accurate than desired, were of some use.

The analysis of the observed wind profiles was accomplished through the use of a modified form of the basic geostrophic-departure method used previously by several investigators, and will be described in Section 2. The computational procedure yielded estimates of several characteristic parameters of the atmospheric boundary layer, including the total and local rates of energy dissipation.

2. Analysis of Boundary-Layer Wind Profiles by the Geostrophic Departure Method

2.1 Basic Mathematical Relationships

The problem of estimating the vertical transport of momentum in the atmospheric boundary layer has been attacked in many different ways. One method has seen considerable use in the past, and consists of the determination of the deviations of the observed mean wind in the friction layer from the wind that would occur if strict geostrophic balance were to exist. The momentum flux, as given by the shearing stress, is obtained through the height integration of these deviations. This "geostrophic departure method," as it is termed, has several advantages over other procedures: (1) the height variation of stress, as well as its surface value, may be found; (2) only relatively simple observational equipment is required to obtain the necessary mean wind profiles; and (3) the method gives estimates of stress for a terrain, rather than for a site, as Priestley (1959) points out. However, there are also disadvantages: (1) some of the assumptions necessary for the analysis can become stringent on occasion, and (2) knowledge is required of the geostrophic wind profile, which is difficult to obtain through direct measurements. Concerning the latter point, an extension by Lettau of his earlier work (1950, 1957b) has permitted the indirect estimation of geostrophic wind profiles (Johnson, 1962; Lettau and Hoeber, 1964), which will be discussed subsequently.

Assuming a broad-scale, horizontally-independent flow over a uniformly rough surface, and neglecting mean vertical motion, normal stresses, and the height variation of density ρ in the boundary layer, the horizontal component equations of motion become

$$\rho\, \partial u/\partial t = \rho f(v - V) + \tau'_x, \tag{2.1}$$

$$\rho\, \partial v/\partial t = \rho f(U - u) + \tau'_y. \tag{2.2}$$

Here f is the Coriolis parameter; τ_x, U and τ_y, V are shearing stress and geostrophic wind components in the directions of the horizontal mean wind components u and v, respectively, where u is directed 90 degrees to the right of v; and the primes (') refer to partial differentiation with respect to height. For the case of a coordinate system which may rotate about its vertical unit vector with respect to the earth, i.e., when the horizontal direction θ of v may change, Eqs. (2.1) and (2.2) must be expanded to

$$\rho(\partial u/\partial t + v\partial\theta/\partial t) = \rho f(v-V) + \tau'_x, \tag{2.3}$$

$$\rho(\partial v/\partial t - u\partial\theta/\partial t) = \rho f(U-v) + \tau'_y. \tag{2.4}$$

Defining

$$v_c = v - (1/f)(\partial u/\partial t + v\partial\theta/\partial t), \tag{2.5}$$

$$u_c = u + (1/f)\partial v/\partial t - u\partial\theta/\partial t), \tag{2.6}$$

and substituting into Eqs. (2.3) and (2.4), we obtain

$$\tau'_y = \rho f(u_c - U), \tag{2.7}$$

$$\tau'_x = \rho f(V - v_c). \tag{2.8}$$

The terms u_c and v_c may be regarded as wind components "corrected" for local change, and for re-orientation of the coordinate system. If the wind flow is in steady states, and the component directions are kept constant as in a geographic coordinate system, $u_c = u$ and $v_c = v$.

If the height H is taken to be the level at the "top" of the boundary layer where the frictional effects, hence the stress components, become negligibly small, Eqs. (2.7) and (2.8) may be integrated over entire vertical extent of the layer to give the surface stress components,

$$\tau_{x,0} = \rho f \int_0^H (v_c - V)dz, \tag{2.9}$$

$$\tau_{y,0} = \rho f \int_0^H (U - u_c)dz. \tag{2.10}$$

The stress components at any level z may then be obtained from

$$\tau_x - \tau_{x,0} = \rho f \int_0^z (V - v_c)dz, \tag{2.11}$$

$$\tau_y - \tau_{y,0} = \rho f \int_0^z (u_c - U)dz. \qquad (2.12)$$

Considerable simplification may be achieved if v is always oriented in the direction of the surface wind, for in this case $\tau_{x,0} = 0$ and $\tau_{y,0} = \tau_0$. In this so-called antitriptic* coordinate system, the equations become

$$0 = \rho f \int_0^H (V - v_c)dz; \qquad (2.13)$$

$$\tau_0 = \rho f \int_0^H (U - u_c)dz; \qquad (2.14)$$

$$\tau_x = \rho f \int_0^z (V - v_c)dz; \qquad (2.15)$$

$$\tau_y = \rho f \int_z^H (U - u_c)dz. \qquad (2.16)$$

Now if the coefficient of eddy viscosity K_m is assumed to be a scalar, we have

$$\tau_x = \rho K_m u', \qquad (2.17)$$

$$\tau_y = \rho K_m v'. \qquad (2.18)$$

Equations (2.13) to (2.18) have been used in various combinations and forms for wind-profile analysis by a number of investigators, among the first of whom were Taylor (1916), Richardson (1920) and Sutcliffe (1936). Sheppard et al. (1952) attempted to apply the relations to ob-

* This term, originally defined by Jeffreys (1922), has been used by Lettau with a slightly different connotation. In Jeffreys' original classification of winds, "antitriptic" denotes the case where the frictional force exactly counterbalances the pressure-gradient force (Greek "tripsis" = friction). Lettau has applied the word to a coordinate system which is oriented according to the direction of the frictional force at the earth's surface. The boundary-layer equations using this coordinate system, however, include the Coriolis force as well as the frictional and pressure-gradient forces. It is suggested that confusion might be avoided if this balanced system of three forces is termed "geotriptic," which connotes the inclusion of the effects of the earth's rotation.

servations over the northeast Atlantic, while Sheppard and Omar (1952) and Charnock et al. (1956) analyzed wind structure in the Trades on this basis. In all of the studies to date, the inertia terms in the equations of motion have been neglected. In some cases, the acceleration terms have been examined and found to be small; some of the observations were taken in regions (i.e., the Trades) where approximately locally stationary, horizontally uniform flow normally prevails. To reduce the seriousness of the assumption of unaccelerated mean wind, averages of large numbers of individual profiles have sometimes been used. For example, Charnock et al. analyzed the average wind profile obtained from 387 individual balloon ascents over a 27-day period. Other investigations (Lettau, 1950, 1957b) have been restricted to the examination of profiles obtained under special conditions when the assumption is approximately valid. In the present study, the wind-profile analysis takes into consideration estimated local-change effects, obtained as described in Section 5 from the time rate of change of the mean wind components.

2.2 Lettau's Antitriptic Method

The graphical-numerical procedure outlined here is an extension by Lettau of his earlier work (1950, 1957b) with the Leipzig and Scilly-Island wind profiles. In those papers he showed that estimates of geostrophic wind-component profiles could be obtained from the profiles of observed wind by a trial-and-error orientation of the coordinate system in the assumed direction of the surface geostrophic wind. The correct orientation is found when certain deviations are minimized. The method described in the next paragraphs is simpler and can be used when sufficiently detailed wind-profile data extending up to and beyond the "top" of the boundary layer are available. When the integration is taken from the surface to a level z^*, Eqs. (2.15) and (2.16) become

$$\tau_x^* = \rho f \int_0^{z^*} (V - v_c)\, dz, \tag{2.19}$$

$$\tau_y^* = \rho f \int_{z^*}^{H} (U - u_c)\, dz, \tag{2.20}$$

where τ_x^* and τ_y^* represent the stress components at a level z^* within the boundary layer. From Eqs. (2.17) and (2.18) we obtain

$$\tau_y = \tau_x (v'/u'), \tag{2.21}$$

which may also be written as

$$\tau_y^* = \tau_x^*(v')^*/(u')^*, \qquad (2.22)$$

at the height z^* where the height derivatives $(v')^*$ and $(u')^*$ apply.

Eqs. (2.13), (2.14), (2.19), (2.20) and (2.22) are sufficient to permit the determination of profiles of geostrophic wind and shearing stress components if (1) a height-independent thermal wind, i.e., a linear geostrophic wind profile, is assumed, and (2) the observed wind at some high level H is assumed to be geostrophic. The graphical-numerical procedure is schematically depicted in Fig. 1, which was drawn for the case when $u_G = u$ and $v_G = v$. (It will be noted that Eqs. (1), (2), (3), (4) and (5) in the illustration correspond respectively to Eqs. (2.13), (2.19), (2.22), (2.20) and (2.14) in the text; the discussion below will use the equation numbers in the illustration to avoid confusion.)

With the aid of the two assumptions, a straight line representing the V-profile may be positioned so that Eq. (1) is satisfied, i.e., such that area A equals area B. The surface geostrophic wind component V_0 is thus determined. The lowest point of intersection of the profiles of v and V is taken as the level z^*. The integral in Eq. (2) is determined from area B, hence τ_x^* may be computed. With the aid of the slopes of tangents to the profiles of u and v at the level z^*, τ_y^* can be calculated from Eq. (3). With τ_y^* known, the integral which is equivalent to area C is found using Eq. (4). The straight line representing the U-profile is drawn such that area C has its calculated value, which determines U_0. Finally, the surface stress τ_0 is computed from Eq. (5) utilizing the area (C + D). Eqs. (2.15) and (2.16) may be applied to yield stress component profiles.

This procedure was first used with some success to derive boundary-layer parameters from climatological wind profiles in the central U.S. (Johnson, 1962). It was also applied by Lettau and Hoeber (1964) in their analysis of wind structure in the boundary layer over the small island of Helgoland in the North Sea. The most important assumptions inherent in the method appear to be that of constant thermal wind, which is considered briefly in Section 8, and that given by Eqs. (2.17) and (2.18), which will be discussed next.

2.3 Analysis of the Lakewood Wind Profiles

The concept of proportionality of stress and vertical wind shear (i.e., of a scalar K_m) is still quite controversial. Taylor (1963) used Eqs. (2.17) and (2.18) in an analysis of wind data obtained from the

Assume: (1) Thermal wind constant with height
(2) Wind at level H is geostrophic

Use these equations:

$$(1)\ \rho f \int_0^H (V-v)dz = 0 \qquad (2)\ \tau_x^* = \rho f \int_0^{z^*} (V-v)dz$$

$$(3)\ \tau_y^* = \tau_x^*(v')^*/(u')^* \qquad (4)\ \tau_y^* = \rho f \int_{z^*}^H (U-u)dz$$

$$(5)\ \tau_0 = \rho f \int_0^H (U-u)dz$$

SCHEMATIC OF METHOD:

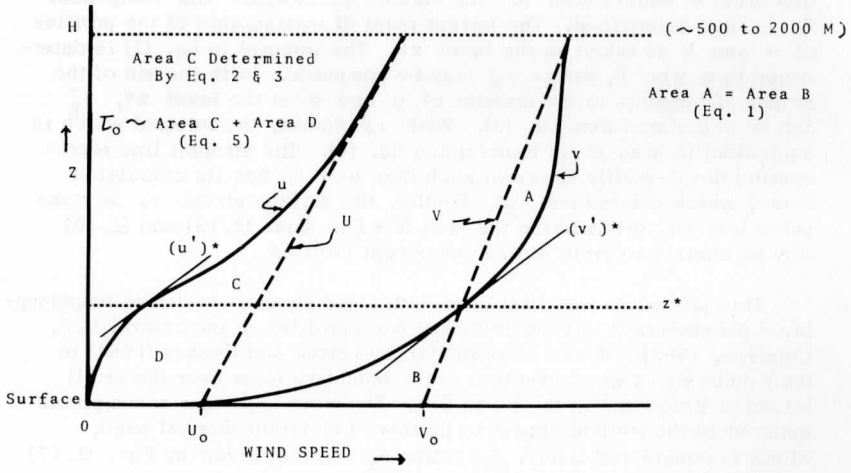

u, U - components perpendicular to surface wind

v, V - components parallel to surface wind

FIG. 1. Schematic of Lettau's antitriptic method for estimating surface geostrophic wind components and shearing stress. See text for details.

instrumented tower at Cedar Hill, Texas. He concluded from his results and from some theoretical arguments that K_m may not always be a scalar. Angell (1964) found negative values for K_m from the analysis of some of his tetroon data, and made the following comments:

> The coefficient of kinematic eddy viscosity may be considered an exchange coefficient and as such implies a transfer of momentum in the direction of the gradient of momentum. If the air motions are unorganized, that is, turbulent in the usual sense, the coefficients of eddy viscosity must always be positive. This is undoubtedly true near the ground, but aloft there is no reason why organized air motions could not exist which would transport momentum against the momentum gradient (the northward eddy transport of angular momentum on the south side of the subtropical jet stream is an example of this).

Similar questions have been raised regarding the validity of the equation for vertical heat flux. Priestley and Swinbank (1947) found that the gradient of potential temperature does not necessarily determine the direction of the heat flux in the atmospheric boundary layer; reference may also be made to Bunker (1956) and Priestley (1959). It is appropriate here to quote from Schlichting (1955) regarding the development of the Navier-Stokes equations:

> Their (St. Venant and Stokes) derivations were based on the same assumption as made here, namely that the normal and shearing stresses are linear functions of the rate of deformation, in conformity with the older law of friction, due to Newton. Since Stokes' hypothesis is evidently completely arbitrary, it is not a priori certain that the Navier-Stokes equations give a true description of the motion of a fluid. It is therefore, necessary to verify them, and that can only be achieved by experiment.

While the assumption of gradient-type transport of momentum has been found in most cases to give useful results regarding duct flow, atmospheric surface-layer flow, and other types of motion in the immediate vicinity of a solid boundary, its relevance to the more unconstrained flow at higher levels in the atmospheric boundary layer has not been demonstrated for all conditions.

One situation which clearly shows a weakness in this concept occurs when strong cold-air advection in the boundary layer causes backing of the wind with height sufficient to offset the normal veering

due to friction. In this case, u' can become equal to or less than zero at a low level, and application of Eq. (2.21) yields infinite or negative values for τ_y. Several instances of this type occurred in the analysis of the Drexel wind profiles (Johnson, 1962); here Lettau's antitriptic method fails to give results when it is used strictly as previously described. The effects of cold-air advection also appear frequently in the Lakewood wind profiles obtained in this investigation, and for many of these cases, attempts at analysis by previously used methods were fruitless.

After a careful examination of the possible consequences, a modification of Lettau's antitriptic method suggested itself and was tested in the analysis of the Lakewood profiles. The change consists of replacing Eqs. (2.17) and (2.18) by the assumed formulations

$$\tau_x = \rho K_m (u - U)', \tag{2.23}$$

$$\tau_y = \rho K_m (v - V)'. \tag{2.24}$$

The analysis procedure is similar to that previously described, except that Eq. (2.22) is replaced by

$$\tau_y^* = \tau_x^* (v-V)'/(u-U)', \tag{2.25}$$

and the slopes V' and U' must now also be determined. It must be admitted that no firm theoretical basis for this hypothesis has been found, although possibilities are still being explored. The assumption that the stress is proportional to the height derivative of the geostrophic departure is tantamount to a rectification of the baroclinic system to a barotropic one; i.e., the distorting effects of a thermal wind, when superimposed on the basic wind spiral, are subtracted.

This assumption is probably not valid for the surface layer flow, upon which the lower boundary exerts more control; Bernstein (1959) found significant effects in certain surface-layer parameters due to a horizontal temperature gradient. However, the results obtained from the analysis of the Lakewood boundary-layer profiles appear realistic. In addition, the method was applied to a reanalysis of some of the Drexel wind profiles, and the results seem to be more reasonable than those obtained previously. A comparison of these values will be given in Section 10.

2.4 Determination of Other Boundary-Layer Parameters, Including Mechanical Eddy Energy Production

It has been shown above how estimates of the surface geostrophic wind components, U_0 and V_0, and the surface stress, τ_0, may be obtained. The angle α_0 between the surface wind direction and the isobars is given by

$$\alpha_0 = \tan^{-1}(U_0/V_0). \tag{2.26}$$

The magnitude G_0 of the surface geostrophic wind is found from

$$G_0 = (U_0^2 + V_0^2)^{1/2}, \tag{2.27}$$

and the geostrophic drag coefficient may be computed from its defining equation,

$$C \equiv (\tau_0/\rho)^{1/2}/G_0. \tag{2.28}$$

When the turbulent energy of the atmospheric boundary layer is in steady states and the turbulence is horizontally homogeneous, a balance is achieved between mechanical eddy energy production plus convective eddy energy production on one side, and divergence flux and rate of dissipation ϵ of eddy energy on the other. The convective eddy energy production term is proportional to

$$gH/c_p \rho T, \tag{2.29}$$

where g is the acceleration of gravity, H the vertical heat flux, c_p the specific heat of dry air at constant pressure, and T the absolute temperature. The mechanical production term may be written as

$$(\tau_x u' + \tau_y v')/\rho. \tag{2.30}$$

It is often assumed that the convective eddy energy production and divergence flux of eddy energy are negligibly small, or that the two cancel each other, in which case the local rate of energy dissipation may be found from the mechanical production term. Using Eq. (2.30), the mechanical production, and hence the local rate of energy dissipation, can be computed at any level where the stress and wind shear are known.

The total rate of energy dissipation E in the boundary layer may be found from an integration of $\rho\epsilon$ over the entire vertical extent of the

layer. Under the assumptions mentioned above, when the work necessary to overcome the frictional force is considered, we have (following Lettau, 1962),

$$-\int_0^H (u\tau'_x + v\tau'_y)dz = \int_0^H (\tau_x u' + \tau_y v')dz = \int_0^H \rho\epsilon\, dz = E. \quad (2.31)$$

Thus E may also be obtained from the term on the left.

3. Description of the Observing Site

3.1 Coverage and Type of Forest

The selection of a suitable site for performing the observational portion of this study involved a number of considerations. The most important of these was location within a relatively extended, reasonably flat area of horizontally uniform forest. In addition, it was desired that the site be as close as possible to a U. S. Weather Bureau radiosonde station from which supplementary aerological data, especially temperature profiles, could be obtained. There were also practical considerations which dictated location within a distance of about 300 miles from the campus of the University of Wisconsin at Madison.

By a thorough inspection of maps of northern Wisconsin, and aerial reconnaissance of this region using the Cessna 310 aircraft of the Department of Meteorology, a suitable site was selected, located at 45°16'N, 88°35'W, in the southern portion of the Nicolet National Forest in northeastern Wisconsin. It is 6 km SW of the village of Lakewood, 95 km NNW of the city of Green Bay (which has a USWB radiosonde station), and 85 km ENE of Wausau. Occasionally this site will be referred to as the "Lakewood site." North of a west-east line through the site, the forest extends virtually unbroken, except for small cleared areas and numerous small lakes, for approximately 200 km (W), 250 km (N), and 80 km (E). The eastern limit of the forest is the water of Green Bay, a portion of Lake Michigan. However, south of a west-east line through the site the forest coverage is not so extensive: 30 km (WSW), 45 km (SW-SSE), and 30 km (SE).

Dyer (1963) treated theoretically the problem of the rate of adjustment of water-vapor profiles as a function of fetch and height for air passing from a dry surface to a wet surface, and found that an overwater fetch of 3.3 and 26.5 km is required for 90% of the total adjustment to be completed at heights of 10 and 50 m, respectively. However, Dyer's results are strictly applicable only in the atmospheric surface

layer. Lettau (1959b) suggests that measurements "should not exceed approximately 1/50 of the upwind distance from significant discontinuities in surface structure." In the present study observations of wind velocity were made at heights up to 2 km above the surface. Applying Lettau's empirical criterion, a fetch of about 100 km over a uniform forest would be required for a wind profile to reach equilibrium all the way to 2 km. However, since the bulk of the frictional effects should be manifest in the lower 1000 m of the wind profile, the criterion would indicate that the wind profiles obtained in this study could be considered to be approximately near equilibrium, except perhaps for winds from the WSW or SE.

According to reports and maps issued by the Wisconsin Conservation Department (1957) and the U. S. Forest Service (1951), the forested area within a 10-km radius of the observing site is principally composed of deciduous-type trees, with aspen predominating. There are isolated conifers, and some northern hardwoods, both types becoming somewhat more abundant further to the north. The aspen trees near the observing site are generally on the order of 8 to 12 m in height. In the octant between south and southwest of the site, at a distance of 20 to 45 km, is a large area of conifers in Menominee County. These trees stand about 15 to 20 m high. As a consequence of the deciduous nature of the forest around the observing site, it was expected that a seasonal change in the aerodynamic roughness of the forest following the phenological cycle would be significant, and detectable in the wind-profile structure. Results in this regard are presented in Section 7.

3.2 Terrain Relief and Slope

Figs. 2 and 3 give an idea of the nature of the terrain around the observing site, as well as showing the striking change in appearance of the forest after the trees shed their leaves in the fall. Generally, the terrain within a 30-km radius of the site may be described as composed of undulations on the order of 25 to 50 m in amplitude and 100 to 200 m in wave length, with the exception of a small range of low hills about 100 to 150 m in height extending NW through NE of the site at a distance of about 15 km. It is felt that the terrain, although certainly not ideal, is sufficiently flat for the purposes of this study.

In order to determine the large-scale slope of the terrain in this area, a plane surface was fitted, using the method of least squares, to terrain elevations. Extreme elevations were excluded; 280 points of

roughly uniform distribution were used in the fitting program. The results showed a definite slope of 3.37 m/km downward to the ESE, or at an azimuth angle of 127.6° from north. Thus, the contour lines are oriented generally from NNE (038°) to SSW (218°). Lettau (1964) has shown that large-scale terrain slope can be an important factor in the formation of low-level jets. Some observations concerning this point will be discussed in Section 9.

3.3 Location of Theodolite Stations

For obtaining the boundary-layer wind profiles used in this study, the method of tracking small pilot balloons with two theodolites was used. In this method, it is important to establish visual contact between the two theodolite stations so that proper adjustments can be made to the instruments to facilitate accurate tracking. For a forested site, this requirement imposes difficulties, but it was met by locating one of the theodolites on a fire lookout tower (see Fig. 2) and the other in a small field south of the tower. Permission to modify and use the lookout tower for this purpose was kindly granted by the U. S. Forest Service, as the tower was not needed for fire-spotting work during the duration of the observational program. The tower is located on top of a small knoll which is covered fairly uniformly with trees right up to the base of the tower. It is constructed of steel and is 30.5 m in height from the ground to the floor of the cab. To permit unrestricted horizontal and vertical visibility, it was necessary to remove the roof of the cab and to install a second floor of heavy boards at window-sill level to serve as the theodolite platform. The stability of the tower was found to be excellent even with high winds, and vibration was not a serious problem.

Theodolite station two was located in the west-central part of a rectangular cleared area of approximate dimensions 200 m (N-S) and 600 m (W-E). The baseline horizontal distance and the elevation difference between the two theodolites were found by triangulation to be 2046 m and 96 m, respectively, with theodolite station two being the lower. The elevation of the base of the tower was compared with that of a bench-mark 5 km away using precision altimeters and was determined to be 437 m MSL.

The orientation of the baseline with respect to true north was determined by observing from the tower theodolite the azimuth angle between another lookout tower on the horizon and theodolite station two, and using a map to obtain the relative orientation of the two

FIG. 2. Aerial view of forest surrounding observing site in summer when trees are in full leaf. Tower used as platform for balloon launching and tracking is at lower left. View is toward SW.

FIG. 3. Aerial view of forest surrounding observing site in winter when deciduous trees are bare. Tower is not visible, but is located on small knoll at lower right. Note isolated conifers. View is toward WSW.

towers with respect to true north. It was found in this way that the tower theodolite was 5.3° west of true north from theodolite station two. This was later verified within tolerable error limits by sightings of Polaris at culmination, which gave a value of 5.45° for this azimuth angle.

4. Description of the Experimental Program

4.1 Balloon Measurements

The experimental program was designed to furnish information about the composition of the atmospheric boundary layer over tall vegetation. The data were to be sufficient to permit an investigation of the dependence of the wind structure upon time of day and upon possible seasonal variations in surface roughness due to the vegetative phenological cycle. To this end, meteorological measurements were made of conditions in the lowest 2 km of the atmosphere over the deciduous forest at the Lakewood site during seven observational periods spaced over about a year's time. Each period was about 12 to 24 hours in duration. The planned length of each period was 24 hours, but due to adverse weather conditions and on occasion, equipment problems, several of the periods were delayed, cut short, or interrupted.

To obtain boundary-layer wind profiles, 30-g pilot balloons were released from the top of the tower and tracked for 12 min (if possible) by two theodolites. The tower also served as a platform for one of the theodolites, as previously described. Since the balloons were filled with helium such that they would ascend at approximately 3 m/sec, each balloon was normally at a height of about 2200 m at the end of the 12-min tracking time. The balloon ascents were grouped into series spaced about 3 hours apart during every observational period except the first, when the series were started at about 2-hr intervals. Within each series, up to six serial balloon releases at about 15-min intervals were made.

Angular readings from the Warren-Knight theodolites (U.S. Army Signal Corps Model ML-474) were made to 0.01 degree during the last six observational periods. Angles were read to 0.1 degree during the first period. Prior to each balloon series, each theodolite was releveled and "lined-in" on the other; any deviations in the elevation-angle readings from the correct value were noted so that later corrections could be made to the data. These corrections always turned out to be very small.

It was desired that the wind profiles be as detailed as possible. Accordingly, an interval of 20 sec between theodolite readings was rather arbitrarily chosen as the shortest interval for which accurate tracking could practically be achieved. Recent work by Barnett and Clarkson (1965) has shown that this probably was a good choice. Using a large number of triple-theodolite observations for intervals of 5, 10, 15, 20, 30, 45, and 60 sec, they analyzed the three sets of double-theodolite observations which could be obtained and found that the 20-sec interval between readings gave the most accurate wind data. The accuracy decreased rapidly with shorter time intervals, but was only slightly less for longer intervals.

For communication between the observers at the two theodolite sites, small radio transceivers were used. These units also served to relay timing signals from one site to the other to insure simultaneity of readings. The signals were generated by a special timing device employing a very accurate, chronometrically-controlled timing motor. To minimize the possibility of errors, theodolite angles were read verbally by each observer into the microphone of a small tape recorder. This procedure also served to reduce the number of personnel required. The accuracy of the Lakewood balloon observations will be considered further in Sections 5 and 6.

There are two principal disadvantages to the method of obtaining wind profiles by tracking pilot balloons with theodolites. First, the presence of low clouds at a certain level will preclude observations above that level. This situation occurred frequently during this observational program. Second, any existing spatial or temporal changes in the wind will show up in the wind profile at different levels. Alternatives are numerous: instrumented tall towers, instrumented kites or captive balloons, radar tracking of balloons, and photographed smoke puffs or rocket trails, to mention a few. All of these techniques, however, have one or more disadvantages (cost, complexity, low maximum height of observations, no nocturnal capability, etc.) which outweigh those of the theodolite-balloon system for the purposes of this study.

Table 1 gives some basic information relative to the wind-profile data obtained during the seven observational periods. The time shown for each series of runs (balloon ascents) was obtained by averaging the release times of the individual balloons in that series, and applies to the series mean of wind profile structure. The heights shown are the maximum heights to which wind data were obtained, disregarding data above 2 km. The low-level wind speed shown was obtained from the anemometer mounted on the tower, at a height of 25 m above the ground

TABLE 1

BASIC OBSERVATIONAL DATA FOR LAKEWOOD WIND PROFILES. METEOROLOGICAL SYMBOLS CONFORM TO STANDARD USAGE.

Obs. Per. No.	Time CST	Date	Ser. No.	No. Runs	Low-level Wind Ht. (km)	Dir. (deg)	Speed (m/sec)	Weather	Included in Group
1	1122	27 Aug 63	1	5	2.0	183.0	3.11	100 ⊕ 6H	1
	1329	27 Aug 63	2	5	2.0	188.7	3.66	100 ⊕ 6H	1
	1517	27 Aug 63	3	5	2.0	192.5	3.97	100 ⊕ 6H	1
	1726	27 Aug 63	4	5	2.0	150.8	2.56	100 ⊕ 6H	
	1928	27 Aug 63	5	5	2.0	199.6	4.44	100 O / O 7H	2
	2122	27 Aug 63	6	4	2.0	218.5	3.90	100 O / O 7H	2
	2325	27 Aug 63	7	5	2.0	229.2	4.63	100 O / O 7H	2
	0130	28 Aug 63	8	4	2.0	225.0	2.62	100 O / O 7H	2
2	1034	10 Sep 63	1	5	2.0	229.9	4.14	/ - O 15	3
	1344	10 Sep 63	2	5	2.0	210.0	4.61	/ - O 15	3
	1634	10 Sep 63	3	5	2.0	238.8	3.72	O 15	3
	2022	10 Sep 63	4	5	2.0	217.5	5.30	O 15	4
	2236	10 Sep 63	5	5	2.0	217.6	4.57	O 15	4
	0124	11 Sep 63	6	3	2.0	228.3	5.31	O 15	4
	0447	11 Sep 63	7	5	2.0	215.8	4.72	/ - ⊕ 7H	5
	0809	11 Sep 63	8	2	1.9	223.8	3.34	50 ⊕ 4R--H	5
3	1847	19 Oct 63	1	5	2.0	206.3	2.29	O 15	6
	2228	19 Oct 63	2	4	2.0	268.9	3.22	O 15	6
	0040	20 Oct 63	3	5	2.0	318.7	5.05	O 15	6
	0359	20 Oct 63	4	4	1.4	016.9	5.96	O 15	7
	0702	20 Oct 63	5	5	1.9	023.6	5.89	/ O 6H	7
4	1447	30 Nov 63	1	3	2.0	318.8	8.49	40 O 10	8
	2147	30 Nov 63	2	5	2.0	296.8	3.91	/ - O 15	9
	0052	1 Dec 63	3	4	2.0	287.6	4.05	O 15	9
	1224	1 Dec 63	4	3	2.0	327.6	3.02	/ - O 15	10
	1458	1 Dec 63	5	5	2.0	330.1	2.80	/ - O 15	10
5	1304	31 Mar 64	1	4	2.0	019.8	3.72	45 O 15	11
	1728	31 Mar 64	2	6	2.0	349.3	2.89	60 O / O 15	11
	2203	31 Mar 64	3	5	1.9	116.3	3.41	O 15	12
	0138	1 Apr 64	4	4	2.0	123.4	2.83	/ - O 15	12
	1510	1 Apr 64	5	6	2.0	162.1	6.33	50 ⊕ 6H	13
6	0947	8 Jun 64	1	6	2.0	139.8	5.55	/ - O 7H	14
	1247	8 Jun 64	2	6	2.0	146.9	6.78	/ - O 8	14
	1620	8 Jun 64	3	4	1.0	148.2	7.20	30 O 4H	
	1916	8 Jun 64	4	5	1.5	140.6	5.36	100 ⊕ 5H	15
	2152	8 Jun 64	5	6	1.3	148.4	4.72	O 5H	15

TABLE 1 (continued)

	0042	9 Jun 64	6	5	1.1	193.4	4.61	O 5H	
7	0856	10 Jun 64	1	5	2.0	351.1	5.17	O 15	16
	1150	10 Jun 64	2	4	2.0	001.6	4.39	O 15	16
	1442	10 Jun 64	3	4	2.0	002.6	2.81	O 15	16
	1742	10 Jun 64	4	4	2.0	058.8	2.08	O 15	
	2118	10 Jun 64	5	4	2.0	124.6	4.02	O 15	17
	2326	10 Jun 64	6	1	2.0	111.9	3.79	O 15	17
	0212	11 Jun 64	7	4	2.0	137.5	3.25	100 O 15	17
	0603	11 Jun 64	8	6	2.0	146.4	2.31	70 O 15	17
	0851	11 Jun 64	9	4	2.0	174.1	3.53	70 ⊕ 8R--	

and about 15 m above the tops of the trees, while the direction represents an average of the first azimuth readings (from the tower theodolite) for the balloons in the series. Since each balloon is normally at a height of about 60 m above the release point at the time of the first theodolite reading, and the release point (top of tower) is 33 m above the surface, the low-level wind direction indicated is actually an average applying at about 50 m above the surface. As will be pointed out later in the discussion of the boundary-layer wind profiles, recording of direction with the aid of a wind vane installed on the tower would have been better. The decision not to do this was prompted by two factors: (1) the necessity for keeping equipment and instruments at a minimum, and (2) the difficulty in locating a vane on the tower where it would neither interfere with the release and tracking of the balloons nor be substantially affected by the influence of the tower upon the wind flow.

The weather conditions listed are visual estimates made at the time of each series, except for ceilings below 6000 ft which were given by the heights at which balloons disappeared into the clouds. The last column in the table illustrates the manner in which the series-mean wind profiles were grouped, a matter which will be discussed in Section 5 along with the method used to convert the balloon data to wind profiles.

The table shows that 209 out of 257 balloons released and tracked during the course of the experimental program were usable. The remaining 48 were discarded due to one of the following reasons: low clouds, poor visibility, equipment malfunction, or loss of balloon by one of the theodolite observers.

4.2 Low-Level Wind Profiles

In order to obtain supporting information on low-level wind structure, for use in estimating atmospheric stability and surface roughness, four Thornthwaite cup-anemometers on 2.2-m booms were mounted at four levels near the ladder on the southwest corner of the tower. To keep the mounts simple, it was necessary to locate the anemometer booms at levels where there were horizontal tower supports. For the first four observational periods, the levels used were 6.3, 12.5, 18.5, and 25.0 m above the ground at the foot of the tower, while during the last three periods the second anemometer was mounted at 10.4 m instead of 12.5 m. The highest tree tops around the base of the tower were at about 11 m. A battery-powered set of electro-mechanical counters gave the revolutions of each anemometer for a 10-min period during each balloon ascent. The average wind speed was obtained from the manufacturer's calibration. Mean low-level wind profiles for each balloon series were obtained by averaging the wind speeds for the several balloon runs.

The anemometers used belong to a set which is regularly employed in other micrometeorological work at the University of Wisconsin. These instruments are subjected to frequent comparison tests, which almost always show agreement among anemometers to within 2 percent of the set-mean. This value is quite acceptable for the large anemometer spacings used here. A more important source of error is the influence of the tower on the wind flow.

Observations by Dabberdt (1965) show that detectable differences in horizontal wind speed can occur up to 5 diameters upstream and up to 12 diameters downstream of a cylindrical tower made of 55-gal drums. Moses and Daubek (1961) compared wind velocity measurements from an Aerovane anemometer mounted at 18.75 ft on a fire-lookout tower (relocated in an open field) with those from a similar instrument at the same level located about 50 m away on top of a slender pole. The tower which they used is somewhat bulkier than the tower at the Lakewood site. The ladder on their tower consists of short sections separated by platforms and goes up the middle of the tower. The Lakewood tower has a straight (merciless) ladder going up its southwest corner. Anemometer exposure on the two towers was approximately similar. For a wind blowing directly through the tower before reaching the anemometer, Moses and Daubek found that the ratio of wind speed measured by the tower anemometer to that measured by the pole-mounted anemometer was 0.55 for tower wind speeds of 0 to 4 mi/hr, 0.67 for speeds of 5 to 9 mi/hr and 0.74 for speeds of 10 to 14 mi/hr. For wind directions

opposite to this, little effect due to the tower was shown. Interestingly, however, they found for winds blowing along the sides of the tower before reaching the anemometer, an average increase of up to 20 percent in the measured wind speed of the tower anemometer as compared with that of the pole anemometer. In addition, discrepancies in measured wind direction of up to 11 deg were noted.

While probably not fully applicable to the wind-speed measurements on the less-massive Lakewood tower, the above results suggest that substantial errors due to the tower effect can occur. Accordingly, the low-level wind profiles obtained in this experimental program must be considered only roughly representative of the true profiles, and it will be necessary to view results derived from them with some caution. Some consolation, however, may be taken from Table 1 which shows that the low-level winds were seldom from the northeast quadrant, for which the tower disturbance should be largest.

4.3 Low-Level Temperature Profiles

The system for measurement of air temperatures at the anemometer levels was kept as simple as possible due to the necessity for transporting all equipment and instruments to and from the site for each observational period and the requirement that they be installed in a minimum of time; permanent installations were not feasible. In addition, commercial AC power was not available at this remote site. A device employing an aspirated, shielded thermistor was fabricated and put into use during the third observational period. Before it was available, temperature measurements were not made during the first period, and a stop-gap technique was employed during the second period. For this period only, air temperatures were measured at the anemometer levels on the tower by using a shielded, hand-ventilated, precision mercury thermometer which was read to 0.05° C.

The thermistor apparatus was suspended by a cable and could be reeled up and down the length of the tower by a windlass, so that readings could be obtained at any level. The device gave satisfactory temperature measurements before and after each balloon series during the third period. Under somewhat different conditions during the fourth observational period, serious technical problems prevented successful measurements. It was necessary to build several new instruments, using separate sensors at each of the four levels, which were successfully in operation during the last three observational periods.

The sensors for the final system are precision mercury thermometers. To slow down their response to turbulent fluctuations, the thermometer bulbs were inserted through holes in rubber corks into small cylindrical vials containing a half-and-half mixture of water and ethylene glycol. The plastic vials are approximately 2.2 cm in diameter and 5 cm high. The response time of one of these modified thermometers was obtained under still-air conditions for a sudden change in ambient air temperature. The time required for 63.3 percent of the change to be registered was 16 min. With moderate ventilation the time constant should be on the order of half this value.

Before, midway through, and after each balloon series the thermometers were read successively at the four different levels. The readings were averaged at each level to obtain a mean low-level temperature profile for each series. Errors due to time changes in temperature should not be important because of the long time constant of the modified thermometers in comparison with the time required to read all of them. The thermometers were periodically compared in a stirred ice-bath, and the small corrections obtained were applied to the temperature-profile measurements. An illuminated, parallax-free magnifying device was built and used during the last two periods to facilitate accurate reading of the thermometers. Repeatable readings to 0.01°C were obtained with the aid of this instrument.

4.4 Estimates of Net Radiation

During all observational periods except the first, a Suomi-Kuhn net radiometer of the shielded, unventilated type was mounted on a 2-m boom near the top of the tower. It was installed at this height so that the bottom plate would be exposed to upward radiation flux from a larger, more representative forest area. Since the instrument was positioned on the south side of the tower, it was never shaded by the cab from direct sunlight. However, substantial errors must be expected due to radiation emitted, reflected and blocked by various portions of the tower structure. The measurements thus must be considered to be only roughly approximate, even though this type of instrument has been shown to possess quite acceptable accuracy except at low sun angles (Suomi and Kuhn, 1958).

A simple electrical circuit was used which measured the current flowing through each of the two thermistors on the top and bottom absorber plates of the radiometer. This current is proportional to the thermistor

resistance, which in turn is a function of the thermistor temperature. A precision reference resistor was employed with a switching arrangement so that frequent checks could be made to insure that the battery voltage stayed within proper limits. Using the manufacturer's calibration curve, the measured currents were converted to thermistor temperatures. The net radiation in units of ly/min was then calculated by utilizing the following empirical equation furnished by the manufacturer:

$$R_n = 0.020\,\sigma\,(T_t^4 - T_b^4) + 0.029(T_t - T_b) + 0.011,$$

where the numerical values are calibration constants, $\sigma = 0.817 \times 10^{-10}$ cal/(cm^2 min °K^4)(Stefan-Boltzmann constant), and T_t and T_b are the absolute temperatures (°K) of the top and bottom absorber plates. Radiometer readings were taken before and after each balloon run. An estimate of mean net radiation for each balloon series was obtained by averaging the net radiation values derived from each of these readings within the series.

4.5 Boundary-Layer Temperature Profiles; Airborne Measurements

Temperature above a height of 25 m was not measured during the first four observational periods. However, during the last three periods, airborne measurements of air temperature and vertical and horizontal wind-velocity fluctuations were carried out by Donald H. Lenschow of the Department of Meteorology, University of Wisconsin. These data were simultaneous with the surface-based observations at the Lakewood site for most of the daytime balloon series within these periods. Air-temperature was measured by means of a fast-response thermocouple fixed on a nose-mounted boom on the Cessna 310 aircraft; for details concerning this and the system for measuring turbulence, reference may be made to Dutton and Lenschow (1962), and Lenschow (1965).

Air temperatures and pressure altitude were continuously recorded as the aircraft made a spiral climb from about 100 m above the ground to a height of about 1700 m. Temperature profiles were obtained by taking values at 30-m height intervals from this record and correcting them for dynamic heating of the thermocouple due to the airspeed of the plane. Adjustments for non-standard lapse rates were also made to the pressure altitude to yield true height above the ground. Profiles of mean air temperature were found by progressive height-averaging of sets of successive temperature measurements at three levels.

For those balloon observations without concurrent airborne measurements at the site, temperature profiles were obtained from the original records of routine radiosonde flights at Green Bay, 95 km SSE of the Lakewood site. These profiles are not as detailed as those from the aircraft measurements; temperature values for height intervals of less than about 120 m were not available. The coded teletype reports, of course, would give even less detail, hence a re-evaluation was made of the original radiosonde records. The spatial separation of Green Bay and the site is a major disadvantage of this method. However, except for situations when there is a front between the two locations, or when the low-level wind at Green Bay has a long over-water trajectory, the Green Bay profiles should be fairly representative of the vertical temperature structure at the Lakewood site. In Section 9, this statement will be substantiated, and the Green Bay temperature profiles and those obtained by the aircraft will be illustrated in conjunction with the balloon wind profiles.

Wind-velocity and temperature fluctuations were measured by the instrumented aircraft in 2-min (8-km) runs approximately parallel to the low-level wind direction (as indicated by a balloon tethered at the tower) at heights of 170, 470, and 1100 m above the surface. These data have been analyzed by Mr. Lenschow to determine values for Reynolds stress and viscous energy dissipation which will be compared in a later section with estimates derived from the balloon wind profiles.

4.6 Synoptic Meteorological Conditions

Essentially the only variable which practically can be controlled in a mesoscale observational program at a given location is the time when measurements are taken. Ideally, the measurements should be attempted only during periods when synoptic conditions are expected to be such that (1) there will be no meteorological impediments to data collection, and (2) the deviations from the assumptions necessary for the analysis will be minimized. An attempt was made to apply this concept in the timing of the observational periods, although the availability of personnel was also a major factor.

For this program, in which balloons were tracked and the resulting wind profiles analyzed by the geostrophic-departure method previously described, point (1) above essentially refers to fair weather. The second point implies an extensive, substantial, approximately horizontally-uniform and (preferably) time-independent horizontal pressure

gradient in the atmospheric boundary layer. Fair weather, or at least the absence of a low cloud layer, was a necessity; a suitable horizontal pressure field had to be considered as a bonus when it occurred. Furthermore, at continental mid-latitudes, particularly in the Great Lakes area, the two conditions are often mutually exclusive due to the common association of fair weather with the centers of high-pressure areas.

Figs. 4 through 10 illustrate the surface pressure patterns prevailing near the beginning and end of each of the seven observational periods. In accordance with common practice, the isobars are labelled with only the last two digits of the pressure in whole millibars. It may be seen that synoptic conditions seldom approximated the ideal state. The most suitable situations occurred during the first and second periods, with shorter intervals at the beginning of period 4 and the ends of periods 5 and 6. The wind profiles obtained during period 3 and the middle of period 5 could not be analyzed because of the existing weak pressure gradients and resulting light winds.

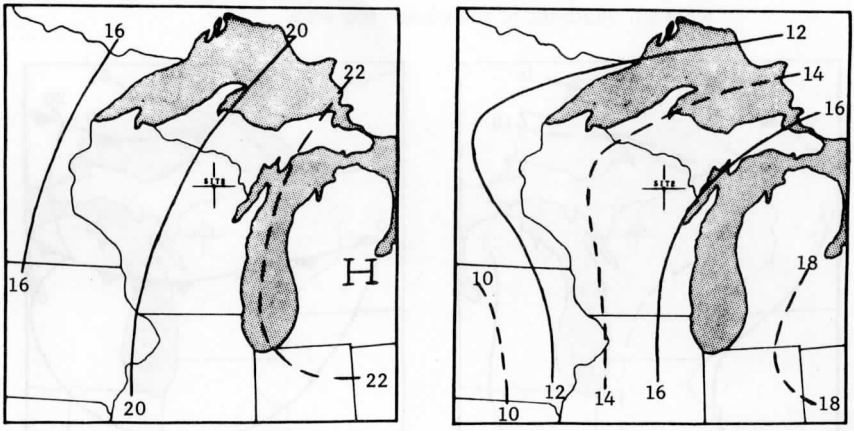

0900 CST, 27 August 1963 0000 CST, 28 August 1963

FIG. 4. National Meteorological Center surface (sea level) analyses for times near the beginning and end of observational period 1. The flow near the surface at the site was from the southwest throughout the period.

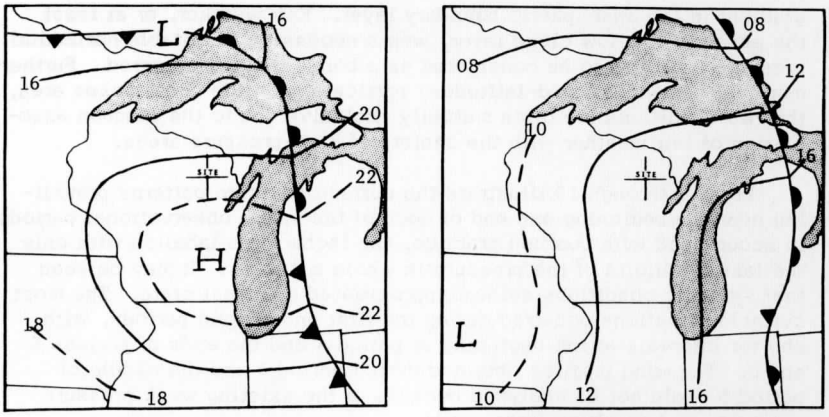

0900 CST, 10 September 1963 0600 CST, 11 September 1963

FIG. 5. National Meteorological Center surface (sea level) analyses for times near the beginning and end of observational period 2. The period was characterized by surface flow from the southwestern quadrant at the observing site.

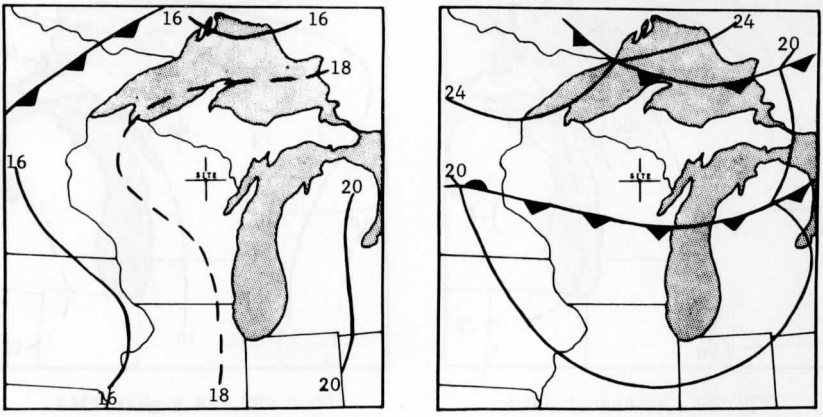

1800 CST, 19 October 1963 0900 CST, 20 October 1963

FIG 6. National Meteorological Center surface (sea level) analyses for times near the beginning and end of observational period 3. As can be seen, the horizontal pressure gradient was very weak and poorly defined throughout the period in the vicinity of the site.

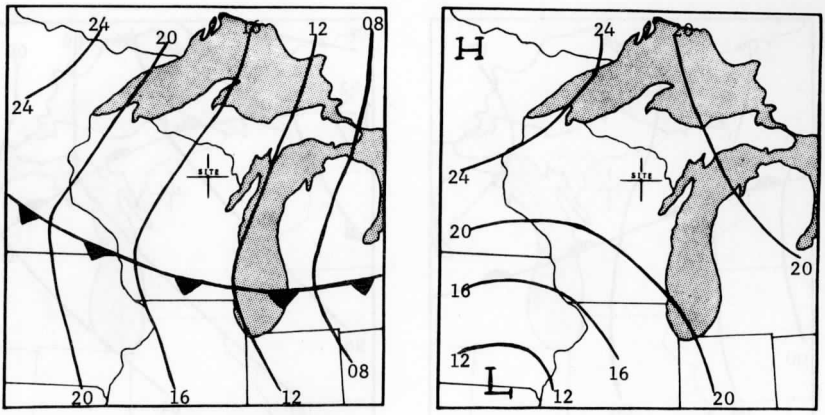

1200 CST, 30 November 1963 1500 CST, 1 December 1963

FIG. 7. National Meteorological Center surface (sea level) analyses for times near the beginning and end of observational period 4. Strong northwesterly flow following a cold-front passage prevailed at the beginning of the period.

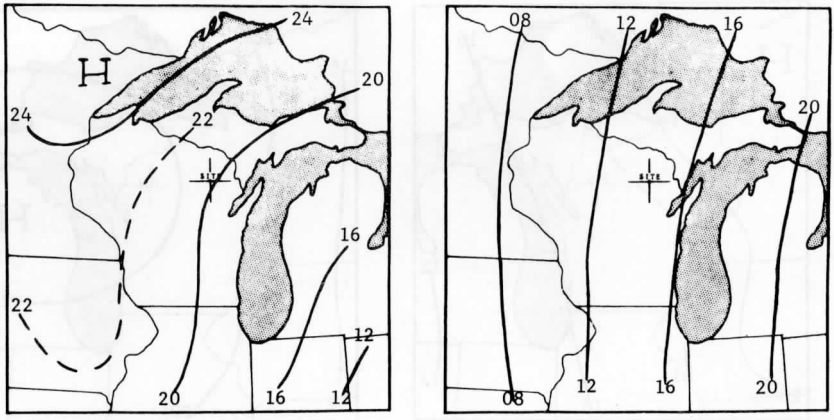

1200 CST, 31 March 1964 1500 CST, 1 April 1964

FIG. 8. National Meteorological Center surface (sea level) analyses for times near the beginning and end of observational period 5. Surface flow changed from northerly to southeasterly as the high moved eastward. The horizontal pressure gradient near the end of the period was very uniform and well defined.

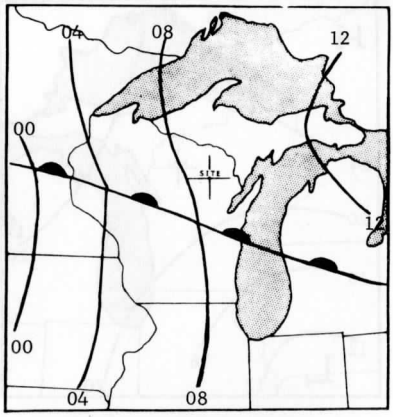

0900 CST, 8 June 1964 0000 CST, 9 June 1964

FIG. 9. National Meteorological Center surface (sea level) analyses for times near the beginning and end of observational period 6. Southeasterly flow at the surface prevailed both before and after the passage of the warm front at the site.

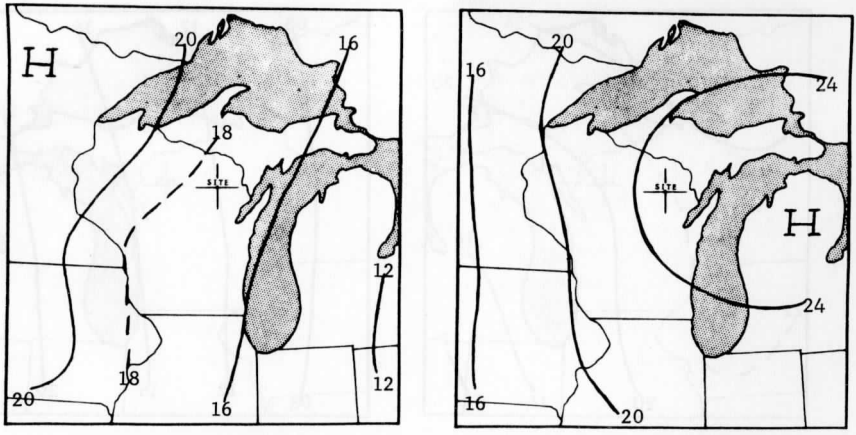

0900 CST, 10 June 1964 0900 CST, 11 June 1964

FIG. 10. National Meteorological Center surface (sea level) analyses for times near the beginning and end of observational period 7. The surface flow shifted from northerly to southeasterly as the high moved eastward during the period.

5. Treatment of Balloon Data

5.1 Computation of Balloon Positions

The basic data obtained by tracking a balloon with two theodolites consist of serial sets of four angles: the azimuth and elevation angles at each theodolite for each time of observation. Any three of these angles can be used to compute the position of a balloon at a given moment. The double-theodolite method thus yields enough information to calculate four such balloon positions from a single four-angle set. The positions computed in such a manner are often significantly different due to the many kinds of errors which may be present in the system. Until recently, virtually all double-theodolite balloon observations were converted to positional data using only three of the angles, although in some instances average balloon positions were obtained from those computed from various three-angle sets. In this investigation, a more accurate and reliable method developed by Thyer (1962) was used to calculate balloon positions. A computational scheme reported recently by De Jong (1964), which also represents an improvement over previous conventional methods, is now available. Some details of Thyer's method and of the manner in which wind profiles were computed will be discussed in this section. All of the calculations that are described were performed either on the IBM 1620 computer at the Meteorology-Space Astronomy Laboratory of the University of Wisconsin, or on the CDC 1604 at the University of Wisconsin Computing Center.

Thyer's (1962) method makes use of all four theodolite angles to estimate the "most probable" location for the balloon. The two angles at each theodolite define a ray from the theodolite to the balloon. If there are absolutely no errors involved in the measurement, the two rays will intersect at the balloon. In practice, of course, this does not occur; an angular uncertainty is associated with each ray which serves to define a cone with vertex at the theodolite. The balloon may be anywhere within the region of intersection of the two cones whose axes are defined by the theodolite angles. Briefly, Thyer's method involves a solution of the vector equations obtained from the geometry of the balloon-theodolite system. The shortest distance between the two rays is determined, and the balloon is considered to be located somewhere on this line. The length of this short line may be regarded as the "closure distance" between the two rays. The position of the balloon on this line is estimated to be at that point which divides the line in the ratio of the radial distances to both theodolites. This procedure is consistent with the supposition of identical angular

uncertainties for the readings from both theodolites, which give similar cones of possible balloon location that diverge with increasing distance from each theodolite.

The method does not fail when the balloon is near or over the baseline, as do conventional computations using only one elevation and two azimuth angles. In addition, a very useful quantity, the closure distance D is obtained. Following a suggestion by Thyer, values of D were listed in the computer output along with values of

$$D_c = 0.05(R_1 + R_2)/57.3, \qquad (5.1)$$

where D_c is the magnitude of the closure distance for an assumed error of 0.05° in each theodolite angle, and R_1 and R_2 are the distances from the balloon to each theodolite. Except during the first observational period, the theodolites were read to the nearest 0.01°, although this involved some estimation since the smallest scale markings were for increments of 0.05°. Due to the many other factors which may contribute to the apparent angular error, such as small inaccuracies in leveling and aligning the instruments, inexact positioning of the crosshairs squarely on the balloon, slight uncertainties in the triangulated horizontal and vertical distances between theodolites, etc., it was felt that an actual error of 0.05° for each theodolite reading would be an acceptable figure. Hence a comparison of the values of D and D_c gave a direct indication of tracking accuracy, and was extremely helpful in discovering and confirming occasional gross, easily-identifiable errors in the angular readings. These errors were then corrected by changing the offending readings by 1°, 5°, or 10°.

In cases when one or both readings from one of the theodolites were missing, the balloon height was interpolated between adjacent computed heights. The horizontal position of the balloon was then calculated from the two angles from the other theodolite. If readings were missing for more than three consecutive observations, the data for that balloon ascent were discarded.

Fig. 11 illustrates the accuracy of balloon tracking during the second observational period, and can be considered typical of that achieved during all of the other periods except the first, when the less-precise theodolite readings gave slightly less-accurate results. At every level, the average closure distance $\bar{D}$ for the 33 ascents in the second period is seen to be substantially less than the average closure distance computed by assuming a 0.05° error in each theodolite reading, $\bar{D}_c$. The actual average angular error θ was estimated to be 0.013° by applying

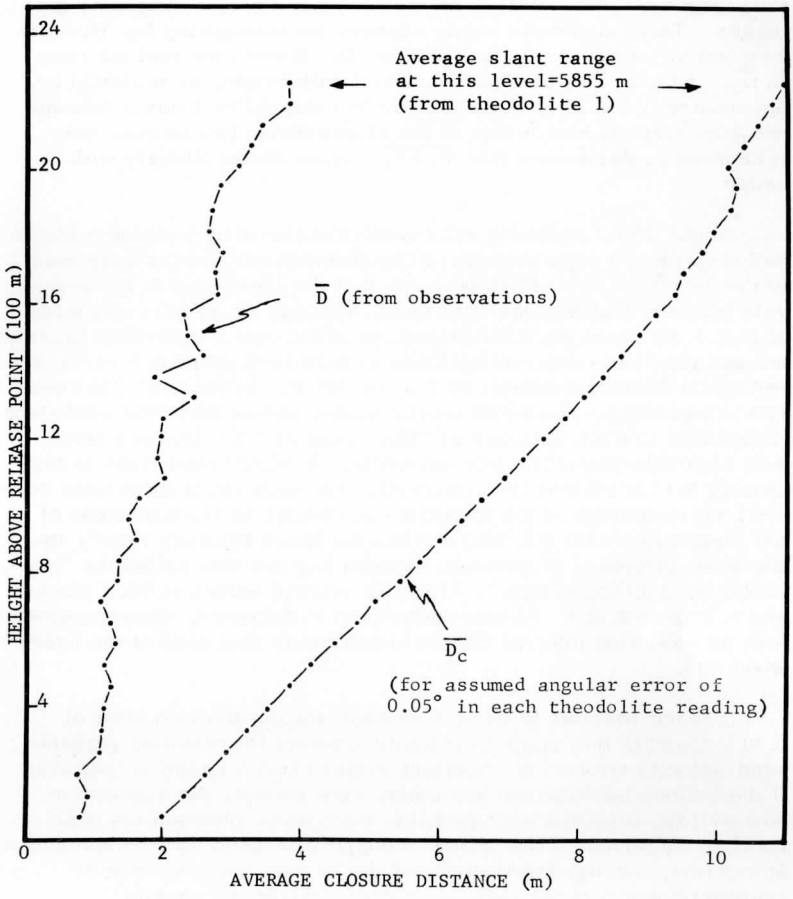

FIG. 11. Illustration of accuracy of theodolite observations for 33 balloon ascents on 10-11 September 1963 (second observational period). Comparing relative magnitudes of $\overline{D}$ and $\overline{D_C}$ gives an estimate of 0.013° for average angular tracking error. The kink in the $\overline{D_C}$ curve at 2000 m is caused by a reduction in the number of observations at and above that level. See text for further explanation.

the relation $\theta = 0.05(\overline{D}/\overline{D_C})$ at each level and height-averaging the results. This equation is easily obtained by considering Eq. (5.1) in conjunction with an analogous one for D. It turns out that the ratio $\overline{D}/\overline{D_C}$, and hence θ, is nearly constant with height, as it should be. Approximately the same estimate may be obtained by a direct (though not quite correct) comparison of the slopes of the two curves, since it happens in this period that $\overline{R_1 + R_2}$ varies almost linearly with height.

Arnold (1948) computed wind vectors obtained by tracking a single balloon with two separate sets of two theodolites. Angles were read to the nearest 0.01°. (It is probable that the conventional 1-min intervals between observations were used, although no mention was made of this.) He found the mean magnitude of the vector difference between the two wind measurements obtained at each level to be 0.4 mi/hr at horizontal balloon distances of 0 to 30,000 ft. Barnett and Clarkson (1965) performed a somewhat similar study, except that they used three theodolites to track balloons and then separated the data into three sets of double-theodolite measurements. Readings were made to the nearest 0.1° at various time intervals. For each set of three wind vectors, the magnitude of the smallest was divided by the magnitude of the largest to obtain the "horizontal wind speed accuracy ratio"; the maximum difference in direction between any two was called the "horizontal wind direction error". Optimum average values of 95.2 percent and 1.4° were found. As was pointed out in Section 4, these resulted from an observing interval (20 sec) identical to that used at the Lakewood site.

It is not possible to use the average angular tracking error of 0.013° found in this study to suitably estimate the resulting probable wind-velocity errors. An important point to keep in mind is that even if the balloon tracking and positioning were perfect, the question of how well the resulting wind profiles, even when averaged (as done here), truly represent the "mean" wind profile would still be unresolved. At any rate, a substantial portion of the angular tracking error is systematic and will not show up in winds obtained by height-differencing of horizontal balloon positions. In view of this fact and the achieved tracking accuracy, together with the rather satisfactory results shown by other investigators' similar but less-precise systems, it can be concluded that the accuracy of the wind measurements is satisfactory provided that the balloons correctly follow the air motions. This last point is considered in some detail in Section 6. It might be mentioned in this regard that consecutive balloon ascents gave quite similar wind profiles, particularly at night when turbulence was light.

5.2 Computation of Wind and Ascent-Rate Profiles

The procedure followed in calculating mean profiles from the positional data for each balloon series is briefly described below.

(1) The computations described earlier produced balloon positions in terms of x, y, and z coordinates parallel with and orthogonal to the horizontal base-line between the two theodolites, with the origin of the coordinate system at the release point. Horizontal wind components parallel with and perpendicular to the base-line were found by dividing the differences in the x and y components of the balloon position by 20 sec, the time between successive observations. Similarly, 20-sec averages of ascent rate, W, were obtained from consecutive balloon heights. Dividing the last observed balloon height by the time elapsed since release gave the height-meaned ascent rate W_m for each balloon. Profiles of $(W-W_m)$, the deviation from the height-meaned ascent rate, were thus determined. Using the known orientation of the base-line with respect to north, profiles of west- and south-wind components, u and v, were computed. The values of u, v, and $(W-W_m)$ were taken to apply at levels corresponding to the mid-points of the height intervals over which they were obtained.

(2) Using linear interpolation between these levels, values of u, v, and $(W-W_m)$ were derived at standard levels spaced 50 m apart. The low-level wind velocity, obtained from the top anemometer on the tower and the first azimuth reading from the tower theodolite, was included in these computations.

(3) For the balloon runs in each series, averages were taken at each standard level, yielding series-mean profiles of u, v, and $(W-W_m)$.

It was pointed out in Section 2 that the local-change terms, $\partial u/\partial t$ and $\partial v/\partial t$, in the horizontal component equations of motion frequently cannot be neglected in the analysis of boundary-layer wind profiles, particularly those observed at mid-latitudes. In this investigation it was hoped that reasonable estimates of the local change could be obtained for use with the mean wind profile for individual series. However, the local-change estimates within one series were often quite large and varied irregularly from level to level. Accordingly, it was necessary to resort to local-change estimates obtained for groupings of series-mean wind profiles.

Table 1 in Section 4 illustrates the manner in which the 46 series-mean profiles were combined into 17 groups. The criteria established

for this procedure are as follows:

(1) The profiles in each group had to be consecutive, with no unduly long time intervals between.

(2) Daytime profiles were grouped separately from nocturnal profiles.

(3) As far as possible, groups were confined to profiles having reasonably compatible low-level wind directions.

(4) Profiles extending to less than 1.2 km were excluded.

It may be seen from the table that the use of these criteria caused rejection of five series from the groupings. Note also that groups 8 and 13 each consist only of a single series which is substantially separated in time from the other series in that period. Although it was not possible to estimate local-change for use with these two groups, it was felt that these profiles were obtained under conditions which warranted their inclusion in the analysis.

Each of the series-mean wind-component profiles was first smoothed by progressive height-averaging of successive sets of wind speeds at three adjacent levels. The smoothed profiles were then transformed into profiles of wind components in an antitriptic coordinate system oriented in the direction of the series-mean low-level wind. It was shown in Section 2 that if u and v are horizontal wind components with respect to a coordinate system oriented in a direction θ, then the effect of local change can be conveniently included in the analysis by the defining equations (2.7) and (2.8) where u_c and v_c may be considered as wind components "corrected" for local change. For an antitriptic system, θ becomes the low-level wind direction.

At each level for each group, the terms $\partial u/\partial t$ and $\partial v/\partial t$ were estimated from the slopes of lines fitted by least squares to the series-mean wind components as a function of time. Similarly, $\partial\theta/\partial t$ was obtained from the series-mean low-level wind directions within each group. These values of $\partial u/\partial t$, $\partial v/\partial t$, and $\partial\theta/\partial t$ were taken to apply at the mean times for each group as determined by averaging the series-mean times. Group-mean profiles of u and v were found by averaging the smoothed series-mean values at each level, as were group-mean profiles of $(W-W_m)$, except that the series-mean values in this case were not vertically smoothed. Sufficient information was obtained in this manner to compute profiles of u_c and v_c for all groups except numbers 8 and 13.

6. Experimental Evaluation of Artificially Roughened Pilot Balloons

6.1 Historical Background

It has been known for decades that ordinary pilot balloons do not rise smoothly through the atmosphere. Frequently the balloons show rapid variations in their horizontal motion, as well as considerable wobble or rotation. This behavior cannot be attributed to effects of atmospheric turbulence, because it occurs on flights into stable air and also on indoor ascents. It apparently is not caused by deformations or lack of absolute sphericity of the rubber balloons, since tests on solid spheres in fluid flow have shown erratic forces of this sort (Shapiro, 1961). In addition, recent work by other investigators, which will be discussed later, has demonstrated that quasi-rigid, superpressure balloons of a high degree of sphericity exhibit similar characteristics when ascending.

Dines (1913) states, "In watching a balloon ascend, it is immediately evident that the motion is very unstable, the balloon ascending in a more or less zigzag course instead of moving steadily upward in a straight line." Dines timed balloon ascents inside a building with the main object of perfecting a formula relating ascent rate to lift and weight. Work by Hesselberg and Birkeland (1917), Cave and Dines (1919), and Frost (1940) had generally the same purpose. Such interest in the ascent rate of pilot balloons was motivated by the fact that in determining winds by tracking a pilot balloon with a single theodolite, the height of the balloon is not measured, but is computed by using an assumed ascent rate.

In discussing the paper by Cave and Dines in 1919, Sir Napier Shaw had this to say: "The ways of balloons are inexplicable... . One cannot rely on repeating a motion with a spherical shape; a special shape is necessary in order to keep the steering satisfactory. There ought to be some steadying apparatus devised to insure that the balloon will go up in a straight line through the air." It was not until recently that, because of requirements of the U. S. aerospace program, balloons have been developed that would fill the need expressed by Shaw over four decades ago.

6.2 Recent Work by J. R. Scoggins

In the course of obtaining detailed wind soundings by balloon for use in rocket launchings, Scoggins (1964, 1965b) found that precise radar tracking of the 2-m mylar superpressure spheres gave very erratic wind-speed profiles. He later obtained somewhat similar results using 100-g neoprene balloons with diameters of more than 1.2 m (MacCready, 1964). In an effort to stabilize the 2-m superpressure balloons, Scoggins taped numerous small paper-cups of conical shape in a uniform pattern to the outside surface of the balloon. Using photography, he found that the artificially roughened balloons, when released into stable air on a clear night, ascended with simpler and steadier trajectories than did the smooth, unmodified balloons. A comparison by Scoggins of wind-speed profiles obtained from radar tracking of the two types of balloons shows much less scatter for the modified balloons than for the unmodified ones. In a recent version of the "Jimsphere" the conical roughness elements are molded directly into the mylar skin (Scoggins (1965a)).

6.3 Tracking Evaluation

In light of Scoggins' work, an experimental investigation was performed to determine if his results affected the validity of the wind profiles obtained as part of this research program, using smaller, 0.7-m-diameter, 30-g pilot balloons. The first problem was to find a method to roughen the surface of the delicate and extensible neoprene balloon. It was finally established that small conical paper cups could be glued directly to the surface of an inflated balloon, using a contact cement. The cups were approximately 9 cm high, and 6 cm in diameter at the base. On all balloons modified in this manner, the cups were approximately uniformly spaced 10 to 15 cm apart, requiring a total of 60 to 70 cups per balloon. Cups and cement contributed an additional 100 to 120 g to the nominal balloon weight of 30 g. A typical artificially roughened pilot balloon is shown in Fig. 12.

Comparison tests involving the modified balloons were performed at the Lakewood site during the fifth and sixth observational periods on 31 March to 1 April 1964, and 8 June 1964. Two series during the fifth period and one series during the sixth were composed of alternate ascents of modified and unmodified balloons, three of each kind being released during each series for a total of 18 flights. In an attempt to keep the ascent rates of the two types within the same range, the balloons to be modified were overinflated and the unmodified ones

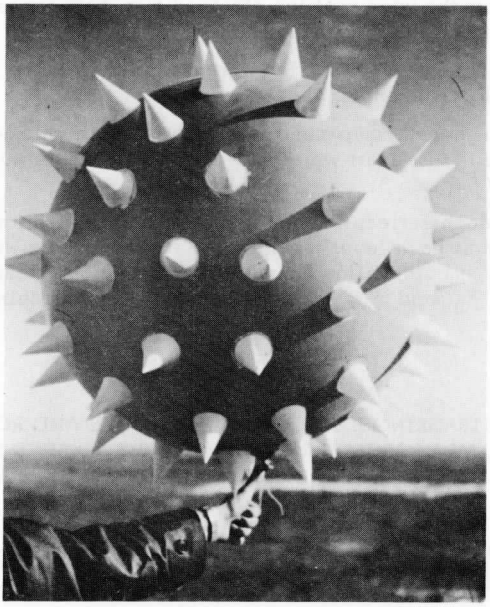

FIG. 12. Artificially-roughened pilot balloon.

underinflated to an undetermined extent. This procedure was not entirely successful, as will be seen in Table 2. The balloons in each series were released at intervals of approximately 15 min and each was tracked for 12 min when possible. Care was exercised to insure accurate tracking by the theodolites. The normal read-out interval of 20 sec was used.

The behavior of the modified balloons when observed visually was very similar to that found by Scoggins for his larger balloons; i.e., their movement was obviously and strikingly much smoother and steadier than that of the unmodified balloons. It was possible to keep the theodolite cross-hairs almost continuously centered on the roughened balloons, while this was nearly impossible with the smooth balloons due to their rapid, small-scale movements. However, careful inspection of the unsmoothed wind profiles obtained from tracking the two types of balloons failed to reveal any significant differences. Calculations of the standard deviations of u and v, the horizontal components of wind

velocity, from the wind profiles obtained from both types of balloons were performed in the following manner:

(1) Component wind profiles were obtained from the tracking data for each balloon ascent in the three series.

(2) From these, component wind profiles with values at standard levels spaced 50 m apart were obtained by linear interpolation, as described in Section 5.

(3) For each series, the mean and standard deviation of u and v were derived at each level for the three rough-balloon wind profiles and for the three smooth-balloon wind profiles. Height-meaned standard deviations, $\bar{\sigma}_u$ and $\bar{\sigma}_v$, were then obtained by averaging over all levels.

TABLE 2

RESULTS OF TRACKING EVALUATION OF SMOOTH AND ROUGH PILOT BALLOONS. MEAN ASCENT RATE AND HEIGHT-MEANED STANDARD DEVIATIONS OF THE HORIZONTAL WIND COMPONENTS ARE GIVEN IN m/sec

Date	Ser. No.	Mean CST	Run Nos.	Balloon Config.	Ascent Rate	$\bar{\sigma}_u$	$\bar{\sigma}_v$
31 Mar 64	2	1728	1, 3, 5	rough	2.86	1.02	0.68
			2, 4, 6	smooth	2.95	0.71	1.01
1 Apr 64	5	1510	1, 3, 5	rough	2.71	1.50	1.01
			2, 4, 6	smooth	3.16	1.19	0.87
8 June 64	5	2152	1, 3, 5	rough	2.38	2.00	1.74
			2, 4, 6	smooth	2.85	1.88	1.11

Table 2 shows the results of these computations. In this experiment, there are four main effects which could contribute to the variance in measured wind velocity at a particular level over the time interval represented by a balloon series: (1) balloon tracking errors, (2) turbulent wind fluctuations, (3) changes in the mean wind with time, and (4) differences due to the manner in which the two types of balloons follow the wind. Since the tracking procedure was identical for the rough and smooth balloons, and since alternate ascents of each type were made, the last effect is the only one which might be expected to cause substantial $\bar{\sigma}_u$ and $\bar{\sigma}_v$ differences for the two types of balloons.

The visual impressions would lead the observer to expect that the standard-deviation values for the rough balloons would be considerably smaller than those for the smooth balloons. However, as can be seen from the table, this is not the case. If anything, the values for the rough balloons seem to be systematically slightly larger. Although this last, rather surprising, result is not sufficiently pronounced to be considered significant, a possible real effect could be indicated. The rough balloons might follow the actual turbulent air motions more exactly than do the smooth balloons, which, although giving the impression of more erratic ascent, could in reality have a damped response to the existing atmospheric turbulence.

On the other hand, the differences in the standard deviations may simply be due to the manner in which they were computed from the wind data. Some smoothing is unavoidably introduced in obtaining winds at standard levels was used here. Since the rough balloons rose somewhat more slowly than did the smooth balloons, the differences between successive observed heights of the rough balloons generally were closer to 50 m in magnitude than were those of the smooth ones. Because of the resulting probability of closer correspondence between standard heights and observed heights for the rough balloons, it is not impossible that the wind profiles obtained from tracking them were smoothed to a lesser extent in the computational program than were the smooth-balloon wind profiles.

An evaluation of the tracking data with regard to balloon ascent rate was also made. For each ascent in the three series, the mean rate W_m was determined by dividing the last measured balloon height by the elapsed time since the balloon was released. Profiles of W, the ascent rate averaged over 20 sec, were obtained in an analogous manner as were u and v, the horizontal wind components; i.e., the height difference in successive balloon positions was divided by the time interval between observations. Hence profiles of deviation from the height-mean ascent rate, $W-W_m$, were found. These profiles were then converted, by using linear interpolation between points, to profiles with points at standard levels spaced 50 m apart, From these, mean profiles for each set of rough and smooth balloons for each series were computed. The lower portions of these are depicted in Fig. 13. There is one slight weakness in the computation method in that the balloons reached somewhat different levels when tracking was terminated and thus W_m is not taken over identical heights for each balloon. However, this could not account for the marked differences shown in the $\overline{W-W_m}$ profiles for the rough and smooth balloons. Above the top level shown in the illustration, the differences were much less pronounced.

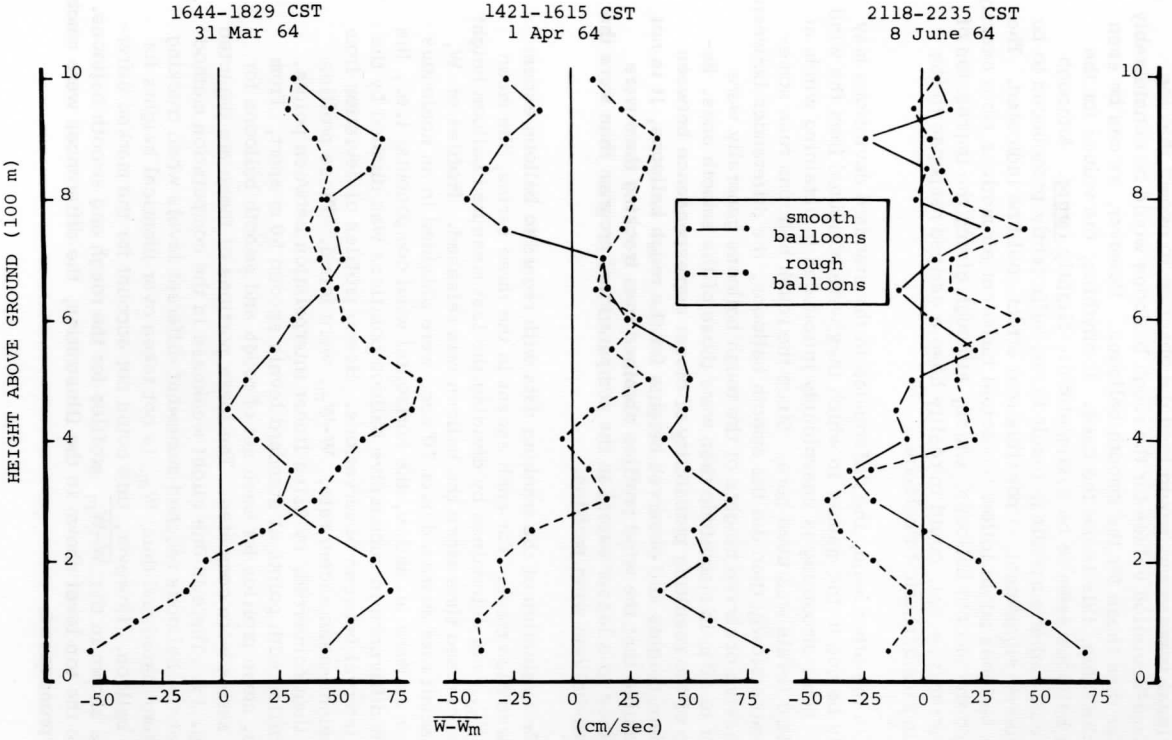

FIG. 13. Profiles of average deviation from height-mean ascent rates of smooth and rough balloons for three different periods. During each period, three smooth and three rough balloons were released alternately. Each profile thus represents the average deviation for three balloon runs.

In their evaluation of the Anegada balloon data, Charnock et al. (1956) interpreted the equivalent of $W-W_m$ to represent vertical air motions. This involves the assumptions that (1) mean vertical air velocity over the whole height interval is negligible, and (2) deviations in the vertical motion of the balloon are due to vertical air motions. Ludlam (1953), after timing indoor ascents of smooth pilot balloons, had this to say: "Moreover, it seems that variations in the rate of rise of a single balloon, or of a succession of balloons, may be ascribed to vertical motions in the air if they considerably exceed some 5 cm/sec, or about 10 ft/min." The results shown in Fig. 13 are apparently at variance with Ludlam's statement and the second assumption used by Charnock et al. in their work, in that the results indicate that either the rough balloons or the smooth balloons (or both) are not accurately following the vertical air motion. This behavior, together with the observed large magnitudes of $\overline{W-W_m}$, implies that the drag coefficients of the two types of balloons may change in different manners with height-variations of turbulence in the boundary layer. The indications are that one must be very careful when ascribing deviation in the ascent rate of balloons to vertical air velocities. This matter will be discussed further in Section 9 in connection with additional observed $\overline{W-W_m}$ profiles and temperature profiles.

6.4 Photographic Comparison

For the purpose of determining the magnitude and nature of the aerodynamically-induced horizontal motions of the smooth pilot balloons, time-exposure photographs were taken of some nocturnal balloon ascents, both indoors and outdoors. A standard light-weight pibal lighting unit, tied as closely as possible to the neck of each balloon, served as a tracer to record the balloon trajectory on the film. The two photographs on the left in Fig. 14 are typical of several which were taken shortly before midnight on 22 May 1964 in the University of Wisconsin Fieldhouse, which has a ceiling 30 m high. All windows in the building were closed and the ventilating system shut down to minimize air movements. It was necessary to attach each balloon to a very light (4-lb test) nylon line wound on a fisherman's spinning reel to permit recovery. The trace on the left in the illustration was made by an unmodified, smooth balloon with an ascent rate of 1.82 m/sec, while that in the center was made by a modified balloon rising at 1.89 m/sec. The full 29.5-m ascent of each balloon is shown in each photograph. The photograph on the right shows simultaneous outdoor ascents of the two types of balloons released 5 m apart under fairly calm conditions on the night of 25 May 1964. The exposure time was about 15 sec.

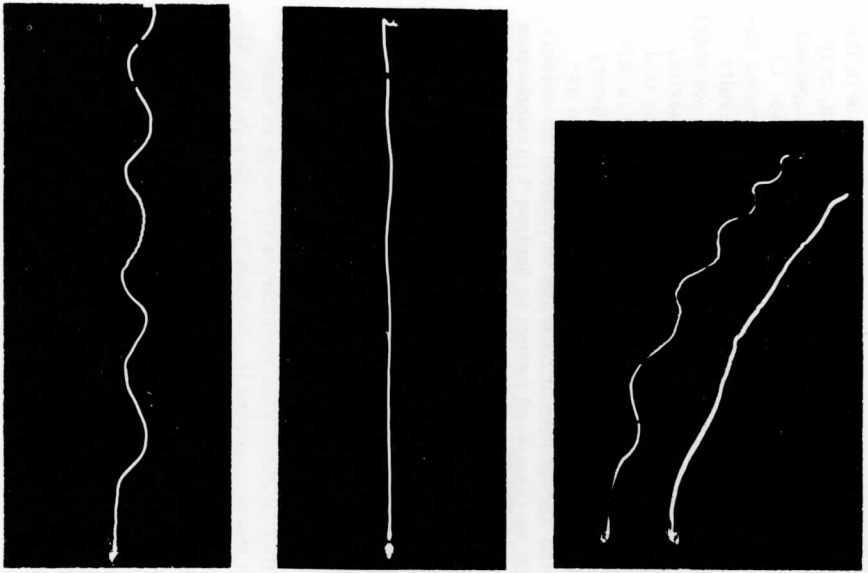

FIG. 14. (a) Ascent of unmodified (smooth) balloon in calm air inside University of Wisconsin Fieldhouse on night of 22 May 1964. (b) Ascent of modified (rough) balloon under same conditions as (a), five minutes later. (c) Simultaneous outdoor ascents under light-wind conditions of unmodified (left) and modified balloons released five meters apart on night of 25 May 1964.

The differences in the trajectories of the smooth and rough balloons are strikingly apparent in the photographs. Visual observation of the smooth balloons released indoors demonstrated that the horizontal oscillations shown in the photographs were actually two-dimensional, such that the trajectories of the balloons were approximately helical in nature. Of interest here is a statement by Dryden et al. (1956) regarding fluid flow around spheres: "It is certain that the flow is no longer stationary at Reynolds numbers greater than 1000, although definite periodicity has not been shown experimentally. It is probable that at times the vorticity comes off in the form of a spiral rather than as discrete rings... . Experiments are needed on the flow in this region. A spiral wake would give rise to a periodic lateral force which should be capable of detection." It is not clear from the context, however, if this comment was meant to apply to flow at Reynolds numbers as great as that of this balloon experiment, which was about 80, 000.

A careful experiment involving indoor ascents of superpressure balloons, reported recently by Murrow and Henry (1965), also showed self-induced smooth-balloon oscillations and smoother trajectories for rough balloons. However, they stated that the oscillations were not of a simple sinusoidal nature, and no reference was made to a spiral trajectory for the smooth balloons. All of their tests involved larger balloons than used in the present study. It is possible that these larger balloons could exhibit a somewhat different type of oscillation, or else the longer wavelengths which are produced by the larger balloons (as will be seen presently) could be more difficult to identify over a limited height. In this regard, a close inspection of the outdoor photograph by Scoggins (1964, 1965b) of the ascent of a smooth 2-m balloon does show evidence of an approximately spiral trajectory, although he made no mention of this.

The oscillations of the smooth balloons in Fig. 14 are about 1.5 m peak-to-peak in amplitude and 6 m in wavelength. A portion of the amplitude is probably due to the rocking of the lighting unit as the balloon turned about its center, although, as previously mentioned, the lighting unit was tied as close to each balloon as possible to keep this effect at a minimum. The observed wavelength and amplitude of oscillation fit in very well with some interesting observations by McVehil et al. (1965) which led them to suggest that the characteristics appear dependent upon the Reynolds number. They tracked 1-m and 2-m superpressure balloons with a Doppler radar system which yielded a continuous record of the radial velocity of the balloon. Spectral analysis of the resulting data showed energy peaks at wavelengths of about 35 m for the 2-m balloon, 15 m for a 1-m balloon with

an ascent rate of 5 m/sec, and 8 and 15 m for the same balloon at higher levels where the ascent rate was 3 m/sec. A peak-to-peak amplitude of approximately 5.5 m for the 2-m balloon can be derived from a time integration of one of the wind-speed oscillations shown in Fig. 1a of their paper. Scoggins (1965b) found the spurious oscillations in his photographs to be about 20 m in wavelength. He also performed a spectral analysis of wind speeds obtained as averages over about 30 m in height from radar tracking of smooth 2-m balloons, and which had been filtered to isolate high-frequency variations not present in smoke-trail profiles observed at about the same time. He found that the major contribution to the total variance was from wavelengths between 100 and 300 m. Such an analysis, of course, would not detect contributions from short wavelengths approaching the length of the averaging interval.

Fig. 15 shows a logarithmic plot of the predominant short wavelength of balloon oscillation as a function of the Reynolds number, together with a summary of the available data. The Reynolds number was computed from the equation $\underline{Re} = dW/\nu$, where d is the balloon diameter, W is the ascent rate and ν is the kinematic viscosity of the air, which was taken to be 0.15 cm^2/sec. The trend line on the graph was estimated by eye. There are only a few data points, but a significant dependency of wavelength upon Reynolds number, in agreement with the suggestion by McVehil et al., is indicated. The peak-to-peak amplitudes of 1.5 m for the 0.6-m pilot balloon and 5.5 m for the 2-m superpressure balloon support the view that a similar dependency may exist for the other parameter of the oscillation. If and when these relationships are verified and refined, they could be very useful in determining the uncertainties to be expected in wind profiles obtained by tracking a smooth balloon of given size and ascent rate, using a particular averaging interval.

6.5 Conclusion

The aerodynamically-induced horizontal oscillations of a smooth, 30-g pilot balloon are evidently minor in magnitude and non-accumulative in nature so that they do not cause appreciable errors in horizontal wind velocities obtained as averages over several wavelengths of the balloon motion. All of the wind profiles obtained in this study were derived from horizontal balloon movement averaged over a period of 20 sec and corresponding to a height interval of about 50 to 60 m, which is sufficiently large compared to the wavelength of balloon oscillation of about 6 m which was found here. This can cause a horizontal wind-speed error of not more than about 10 cm/sec in these wind profiles, which would

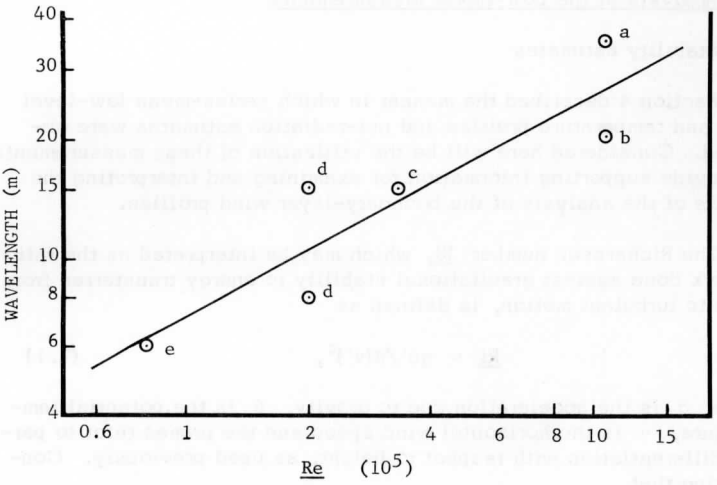

FIG. 15. Variation of predominant wavelength of balloon oscillation with Reynolds number. Points a, c and d according to McVehil et al. (1965), from spectral analysis of Doppler radar data. Point b according to Scoggins (1965b) and point e according to present data, both from examination of time-exposure photographs.

explain why no significant differences were found in the horizontal wind profiles obtained from tracking the two types of balloons. However, the results also indicate that vertical air velocities derived from height changes in the ascent rate of a balloon may not be correct.

Scoggins (1964) has concluded that "a smooth spherical balloon wind sensor is not suitable for measuring detailed wind profiles." His conclusion appears to be correct only if "detailed" is interpreted as implying horizontal velocity averages over height intervals less than about two or three wavelengths of a typical balloon motion. Indications are that the magnitude of the wavelength will depend upon the Reynolds number, i.e., essentially the product of diameter and ascent rate of the particular balloon used.

7. Analysis of the Low-Level Measurements

7.1 Stability Estimates

Section 4 described the manner in which series-mean low-level wind and temperature profiles and net-radiation estimates were obtained. Considered here will be the utilization of these measurements to provide supporting information for examining and interpreting the results of the analysis of the boundary-layer wind profiles.

The Richardson number $\underline{Ri}$, which may be interpreted as the ratio of work done against gravitational stability to energy transferred from mean to turbulent motion, is defined as

$$\underline{Ri} = g\theta'/\theta(v')^2, \tag{7.1}$$

where g is the acceleration due to gravity, θ is the potential temperature, v is the horizontal wind speed and the primes refer to partial differentiation with respect to height, as used previously. Considering that

$$\theta' = \theta(T' + \gamma_d)/T,$$

where T is the absolute temperature and γ_d is the dry adiabatic lapse rate, Eq. (7.1) becomes

$$\underline{Ri} = g(T' + \gamma_d)/T(v')^2. \tag{7.2}$$

When measured values of T and v are available for two levels z_1 and z_2, the finite-difference form of Eq. (7.2) may be written as

$$\underline{Ri} \cong 2g(z_2 - z_1)[(T_2 - T_1) + \gamma_d(z_2 - z_1)]/[(T_1 + T_2)(v_2 - v_1)^2]. \tag{7.3}$$

In this experimental program, v and T were measured at four different levels on the tower. Thus three different Richardson numbers, $\underline{Ri}_1$, $\underline{Ri}_2$, and $\underline{Ri}_3$ could be computed from Eq. (7.3) which were taken to apply at Z_1, Z_2, and Z_3, the mid-levels of adjacent measurement heights. Following Lettau (1957a), a convenient "bulk" stability parameter, defined in this case as

$$(Ri)' = (\underline{Ri}_1 + \underline{Ri}_2 + \underline{Ri}_3)/(Z_1 + Z_2 + Z_3), \tag{7.4}$$

was evaluated for each series during which low-level temperature was

measured. The stability parameter $(Ri)'$ is an approximation to the height derivative of the Richardson number, or, also, to the value of $\underline{Ri}$ at a level of 100 cm, if the Z's are in meters; hence we have

$$\underline{Ri} \cong (Ri)'z, \tag{7.5}$$

$$(Ri)' \cong \underline{Ri}_{100\ cm}. \tag{7.6}$$

Averaging $\underline{(Ri)'}$ over the series in each group gave estimates of mean stability $\overline{(Ri)'}$ to be used with the group-mean wind profiles. The values obtained ranged from -0.008 to +0.010, and will be tabulated later. This range is fairly small, but this is to be expected when averages are taken over periods of several hours, since extreme conditions existing only for a short time will be smoothed. However, the possibility of underestimates due to errors in the measurements cannot be dismissed.

As was brought out in Section 4, low-level temperature structure was not measured during observational periods 1 and 4, hence quantitative estimates of $(Ri)'$ could not be calculated. It is felt, however, that useful qualitative stability estimates can be made, based on the rather well-known general relationships between stability and the observed meteorological variables. For instance, it has been established that near-neutral low-level stratification is encouraged by moderate to strong surface winds accompanied by a reduction in surface heating due to overcast skies. Table 3 shows the qualitative estimates which have been made for time periods associated with the grouped boundary-layer wind profiles, along with some of the observations upon which the estimates are based. Other factors considered were the horizontal visibility and the shape of the low-level wind profile. For what it is worth, the low-level wind profiles for groups 1 and 8 show very little deviation from the logarithmic law, lending some support to the near-neutral stability assignments for these groups. It is recognized that these estimates are certainly not indisputable, and that there is considerable uncertainty in this procedure; however, care was taken to make the assessments as objectively and from as detached a viewpoint as possible.

TABLE 3

QUALITATIVE STABILITY ESTIMATES FOR PERIODS WHEN NO LOW-LEVEL TEMPERATURES WERE OBTAINED.

Cloud-type abbreviations conform to standard usage. Mean 25-m wind speeds are listed in m/sec; mean net-radiation values are in units of ly/min (positive toward the surface). Net radiation was not measured during the first observational period.

Group No.	Mean CST	Date	Wind Speed	Clouds	Net Rad.	Estimated Stability
1	1323	27 Aug 63	3.58	Overcast Ac, As	--	Near neutral
2	2226	27 Aug 63	3.90	Broken Ac, As	--	Slight pos.
8	1447	30 Nov 63	8.49	Scattered Cu	-0.013	Near neutral
9	2319	30 Nov 63	3.98	Scattered Ci	-0.193	Moderate pos.
10	1341	1 Dec 63	2.91	Broken Ci	0.097	Moderate neg.

7.2 Surface Roughness Estimates

The logarithmic law for the variation of wind speed v with height z in an adiabatic surface layer over a boundary with aerodynamic roughness length z_0 is restated by Lettau (1957a) as

$$v = k^{-1}(\tau_0/\rho)^{1/2} \ln [(z+d+z_0)/z_0], \qquad (7.7)$$

where k is the von Karman constant $\cong 0.4$, τ_0 and ρ are surface stress and density, and d is the zero-plane displacement which extends the applicability of the equation to boundaries of tall vegetation. It will be noted that the lower boundary condition is for $v = 0$ when $z = -d$. This implies that d is a length which may be loosely considered to represent the depth of "trapped" air in a vegetative canopy.

The group-mean stability estimates obtained as described in the earlier paragraphs were used to identify and select those groups of low-level wind profiles which were obtained under near-neutral conditions. In view of the rather small range shown by the $\overline{(Ri)}'$ estimates, a criterion similar to but slightly narrower than that established by Lettau (1957a) was employed; $\overline{(Ri)}'$ values between -0.003 to 0.003, or -3 and 3 (10^{-3}/m) were taken to delineate approximately adiabatic conditions. The series-mean low-level wind profiles within each of the groups thus designated were then used to find values for the zero-plane

displacement d. This procedure involved simply the logarithmic extrapolation of the wind profile (as determined by the top three points only) to the height z where v = 0. The wind speed at 6.3 m was not used here due to its measurement within the vegetative (tree) canopy, where it is known that the logarithmic law does not hold. Averaging these results gave group-mean estimates of d.

Using these estimates of zero-plane displacement, the group-mean wind speed at 25 m, and estimates of τ_0 from the analysis of the boundary-layer wind profiles, Eq. (7.7) was employed to evaluate the surface roughness length z_0. The results, grouped according to tree-foliage condition, or, nearly equivalently, according to summer and winter seasons, are shown in Table 4. The zero-plane displacement is seen to decrease by a factor of three after the trees shed their leaves. At the time of the third observational period (19-20 October 1963), about 50 percent of the leaves had fallen, and a mean zero-plane displacement of -248 cm was found using the same procedures as described above. This intermediate value fits in fairly well with the summer and winter averages of -350 and -115 cm. However, the stratification was stable at the time of the observations, casting doubt on the validity of this autumn estimate.

TABLE 4.

Variation of surface roughness length z_0 (cm) and zero-plane displacement d (cm) with tree condition, derived from cases of near-neutral stability as shown by values of $\overline{(Ri)'}$ in units of 10^{-3}/m. The asterisks refer to qualitative stability estimates (see Table 3).

Group No.	Mean CST	Date	Tree Cond.	-d	z_0	$\overline{(Ri)'}$
1	1323	27 Aug 63	Leafed	393	223	*
3	1337	10 Sep 63	Leafed	210	213	-2.3
5	0628	11 Sep 63	Leafed	316	112	2.5
15	2034	8 Jun 64	Leafed	480	94	1.7
			Summer average:	350	160	
8	1447	30 Nov 63	Bare	56	64	*
13	1510	1 Apr 64	Bare	174	147	-2.2
			Winter Average:	115	105	

The qualitative effect of tree foliation on the low-level wind structure may be inferred from Fig. 16, which illustrates typical wind profiles for summer and winter periods. (Only the profiles for odd-numbered series are included for 27-28 August 1963 to avoid crowding.)

The z_0 estimates in the table also are larger for summer, although the distinction between the two seasons is not so well defined as that for d. Based on an analysis of available wind-profile data above tall vegetation, Kung (1961) found the following empirical relation:

$$\log z_0 = -1.24 + 1.19 \log h, \qquad (7.8)$$

where z_0 and the plant height h are in cm and the logarithms are to base 10. As mentioned in Section 3, the aspen trees in the vicinity of the Lakewood site are estimated to be on the order of 8 to 12 m high. The use of Eq. (7.8) gives z_0 values of 162 and 212 cm for tree heights of 8 and 10 m. The z_0 value for the 8-m height agrees very well with the mean value of 160 cm found here for the summer case. Using estimates of land use and vegetation height, and considering seasonal plant differences, Kung and Lettau (1961) obtained maximum summer and minimum winter values for z_0 of 119 and 33 cm for the six-county northeastern district of Wisconsin, which takes in the Lakewood site. A sizeable portion of the southern part of this region is non-forested land, however, so that these estimates must be considered to be somewhat too small to apply strictly to the forested areas.

Since only two near-neutral cases (one of which was qualitatively estimated) were available for the bare-tree situation, a fairly large error may be associated with the winter value of $z_0 = 105$ cm that was found here. In addition, a substantial uncertainty in the summer estimate of 160 cm is indicated by the large variation in the individual values within the average. The possibility does exist, however, of a real dependence of z_0 and d upon wind direction at the tower. This effect would not show up in the wind structure at higher levels, hence the use of average z_0 values is appropriate. With these points kept in mind, the surface roughness lengths estimated here for winter and summer will be utilized in the examination of the results of the analysis of the boundary-layer wind profiles in Section 10.

7.3 The Surface Heat Budget

The condition for heat balance at the earth/air interface is customarily described by

$$R_n = H + S + L + P, \qquad (7.9)$$

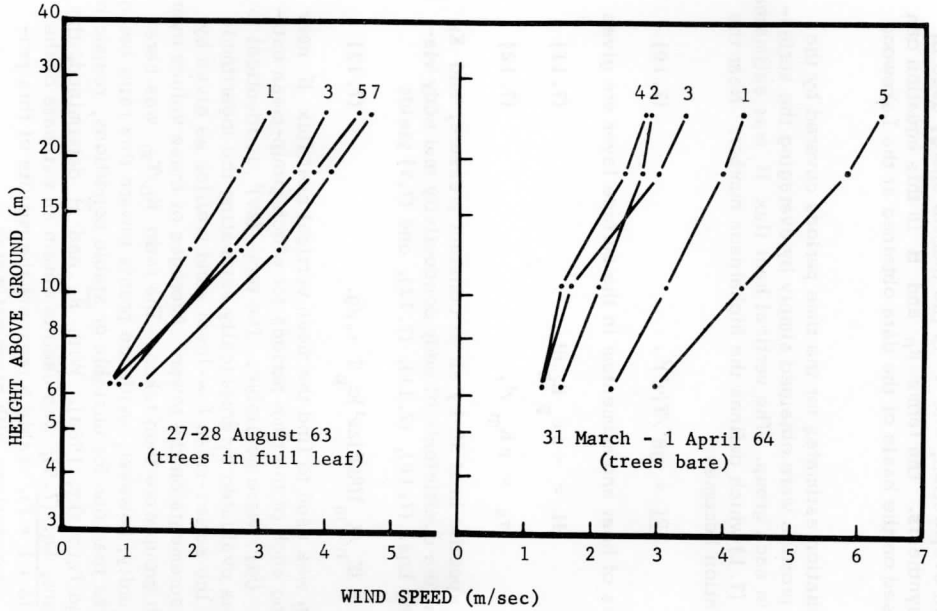

FIG. 16. Illustration of effect of seasonal change in tree foliage on the low-level wind profile. Numbers above individual profiles refer to the balloon series over which the wind averages were obtained.

where R_n is the net radiation, H is the gain of sensible heat by the air, S is the downward flux of sensible heat into the soil, L is the latent heat used in evaporation, and P is the thermal energy used in vegetative photosynthesis. The terms R_n and H in this equation can be roughly assessed on the basis of the data obtained at the Lakewood site.

Mean net-radiation estimates for the time periods covered by the group-mean wind profiles were obtained simply by averaging the series-mean values within each group. The vertical heat flux H was estimated by the use of Eq. (7.1) which defines the Richardson number. Near the surface, this equation becomes

$$\underline{Ri} = g\theta'/T(v')^2. \tag{7.10}$$

The vertical fluxes of heat and momentum in the surface layer are given by

$$H = -\rho c_p K_h \theta' \tag{7.11}$$

and

$$\tau_0 = \rho K_m v', \tag{7.12}$$

where c_p is the specific heat of dry air at constant pressure, and K_h and K_m represent the coefficients of eddy conductivity and eddy viscosity. Combining Eqs. (7.10), (7.11), (7.12), and (7.5) yields

$$H = -(K_h/K_m)(Ri)'(zv')c_p T \tau_0/g. \tag{7.13}$$

This equation was used to find the mean vertical heat flux H near the surface, during each of the time periods for which group-mean estimates of τ_0 and $(Ri)'$ were available. The term $(zv)'$ is identical to $(\partial v/\partial \ln z)$; it was evaluated by graphically estimating the logarithmic slopes of each of the series-mean low-level wind profiles as given by the top three measurements on the tower. Averages of these values over the series in each group were then taken. The ratio K_h/K_m was here considered to be unity; however, evidence points toward this ratio being greater than or less than one for unstable or stable conditions, respectively (see Lumley and Panofsky, 1964). With $\overline{R_n}$ and $\overline{H}$ determined, the balance requirement, Eq. (7.9), was used to obtain an estimate of the remainder term, $\overline{(S + L + P)}$. Table 5 presents the results of this procedure and draws a comparison with other estimates.

With regard to the day cases, the value of surface stress used for group 13 is quite large (9.67 dyne/cm^2), and is probably an overestimate; hence it is probable that the $\overline{H}$ found in this instance is too high. When probable differences in insolation are taken into account, the daytime

TABLE 5

Estimated surface heat budget for the aspen forest at the Lakewood site. The mean values for the stability parameter $\overline{(Ri)'}$ are given in units of $10^{-3}/m$; the estimates for mean net radiation $\overline{(R_n)}$, mean vertical heat flux ($\overline{H}$), and the remainder term $\overline{(S+L+P)}$ are given in ly/min. The duration of each group-period is indicated. The averaged terms are compared with values obtained by Geiger (1965) from the data of Franssila (1936) and Baumgartner (1956). See text for additional details.

Group No.	Date	Duration CST	$\overline{(Ri)'}$	$\overline{R_n}$	$\overline{H}$	$\overline{(S+L+P)}$
3	10 Sep 63	1000-1716	-2.3	0.41	0.08	0.33
11	31 Mar 64	1229-1829	-4.6	0.29	0.07	0.22
13	1 Apr 64	1421-1615	-2.2	0.21	0.20	0.01
14	8 Jun 64	0910-1342	-3.5	0.83	0.18	0.65
16	10 Jun 64	0814-1515	-8.0	0.84	0.12	0.72
	Average, day cases:			0.52	0.13	0.39
	Baumgartner (spruce):			0.64	0.21	0.43
	Franssila (meadow):			0.36	0.06	0.30
4	10 Sep 63	1950-0150	4.2	-0.07	-0.04	-0.03
5	11 Sep 63	0414-0826	2.5	-0.01	-0.07	0.06
15	8 Jun 64	1846-2235	1.7	-0.06	-0.09	0.03
17	11 Jun 64	2055-0658	9.9	-0.01	-0.10	0.09
	Average, night cases:			-0.04	-0.07	0.03
	Baumgartner:			-0.06	-0.01	-0.05
	Franssila:			-0.12	-0.03	-0.09

averages of the Lakewood heat-budget terms compare reasonably well with similar averages summarized by Geiger (1965, pp. 235-238) from observations reported by Franssila (1936) and by Baumgartner (1956). Franssila's measurements were made over a meadow near Tauriala, Finland (61.2°N) during three fair August days in 1934, while those of Baumgartner were taken for a forest of young spruce up to 8.7 m tall in the vicinity of Munich, Germany (47.9°N) during a clear, dry period from 29 June through 7 July 1952.

Because of the likelihood of substantial errors in the measurements, and the approximate nature of the method used to calculate the heat flux, the small values of the estimated heat-budget terms for the Lakewood site at night cannot be viewed with much confidence. The results

indicate in general that for the forest at night, more heat is lost through evaporation than is taken from ground storage, which although possible, seems unlikely. An overestimate of $\bar{H}$ is probable for the nocturnal cases as a consequence of the assumption that $K_h/K_m = 1$; for stable conditions, it is quite possible that this ratio could be as small as 0.6. Conversely, the daytime heat-flux values may be slightly too small on account of the same assumption. Franssila's radiation values at night seem to be a little high, as pointed out by Geiger. In Section 10, the estimates of vertical heat flux which were found here for the surface layer will be compared with those obtained from the airborne measurements.

8. Direct Determination of Geostrophic Wind Profiles

8.1 Surface Geostrophic Wind

As mentioned in Section 2, the geostrophic departure method of wind-profile analysis requires that the geostrophic wind profile be estimated in some manner. It is possible to obtain these estimates indirectly, as was done in this study, by using the modified form of Lettau's antitriptic method which was previously described. An attempt was also made to evaluate the surface geostrophic wind and thermal wind directly, utilizing surface and upper-air observations of pressure and temperature. Although less accurate than desired, these independent assessments were used in the analysis of two of the group-mean wind profiles when the indirect method failed to give results. In the subsequent paragraphs, the procedure will be described, and some of the results are compared with those obtained indirectly from the profiles of observed mean wind. The calculations described were performed on the CDC 1604 digital computer at the University of Wisconsin Computing Center.

Recalling that, near the surface, a geostrophic wind speed error of approximately 5 m/sec results from a horizontal pressure gradient error of only 0.5 mb/100 km, it is not hard to understand the difficulties involved in obtaining accurate estimates of surface geostrophic wind. The problem has been encountered in numerous past investigations, and is particularly acute over sloping terrain. Several methods have been proposed in this regard, e.g. Bellamy (1945) and Sangster (1960). The procedure used in this study involved least-squares fitting of pressures derived from observations at the 17 stations depicted in Fig. 17, and identified by name in Table 6. The stations fall into two general categories: (1) primary — those having mercurial barometers which are under U.S. Weather Bureau control, and (2) secondary — those having aircraft-type altimeters under the control of a commercial airline company. Each

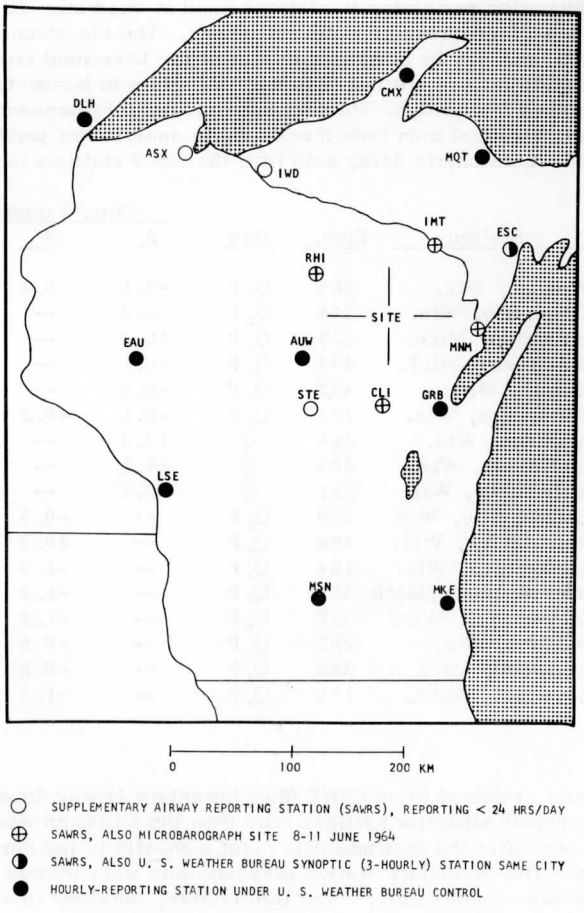

FIG. 17. Network of stations used in the direct determination of surface geostrophic wind estimates at the Lakewood site.

TABLE 6

Basic information pertaining to stations used in quadratic (Q) and plane (P) surface-pressure fitting programs. The elevations are given in m MSL and may be compared to that of the Lakewood site, 437 m. The correction factors are listed in mb; (A) refers to barometer-comparison data furnished by the U. S. Weather Bureau, and (B) represents average corrections obtained from smoothed isobaric analyses of period-mean surface-pressure charts using data from the top 9 stations in the table.

				Corr. Factors		
Ident.	Station	Elev.	Use	A	B	Total
AUW	Wausau, Wis.	365	Q, P	-0.1	-0.4	-0.5
GRB	Green Bay, Wis.	214	Q, P	-0.2	--	-0.2
CMX	Houghton, Mich.	329	Q, P	+0.3	--	+0.3
MQT	Marquette, Mich.	434	Q, P	-0.1	--	-0.1
DLH	Duluth, Minn.	432	Q, P	-0.2	--	-0.2
EAU	Eau Claire, Wis.	273	Q, P	-0.1	+0.2	+0.1
MSN	Madison, Wis.	264	Q	+0.3	--	+0.3
LSE	La Crosse, Wis.	205	Q	+0.1	--	+0.1
MKE	Milwaukee, Wis.	211	Q	-0.2	--	-0.2
CLI	Clintonville, Wis.	250	Q, P	--	-0.3	-0.3
RHI	Rhinelander, Wis.	488	Q, P	--	+0.3	+0.3
MNM	Menominee, Wis.	184	Q, P	--	-1.9	-1.9
IMT	Iron Mountain, Mich.	351	Q, P	--	-1.2	-1.2
STE	Stevens Pt., Wis.	337	Q, P	--	-1.2	-1.2
ASX	Ashland, Wis.	252	Q, P	--	-0.9	-0.9
IWD	Ironwood, Mich.	380	Q, P	--	-0.6	-0.6
ESC	Escanaba, Mich.	183	Q, P	--	-1.4	-1.4

of the latter, referred to as SAWR (Supplementary Airway Reporting) stations, report altimeter settings read from the Kollsman window on the altimeter after the instrument is reset manually to indicate field elevation. The secondary station pressure data were treated as relative measurements only; correction factors, obtained in a manner to be discussed, were applied to yield absolute values.

The analysis was based on hourly altimeter settings obtained from teletype reports. Station pressures were found by using the

standard formula relating the altimeter setting to station pressure and station elevation (Smithsonian Meteorological Tables, 1963, p. 269). These station pressures were then reduced to pressures at the level of the Lakewood site (437 m), using the hypsometric equation. Employed here were the surface temperature at each station, along with an assumed, diurnally varying lapse rate as follows: 1000 to 1600 CST, 1°C/100 m (dry adiabatic); 0000 to 0600 CST, -2°C/100 m; other periods, linear variation with time between these two values.

Mean reduced pressures were then obtained for each station for each observational period, using only those hours during which data from all stations were available. Small correction factors were applied to the pressure data from the primary stations; these corrections were obtained from the U. S. Weather Bureau and represented the results of their latest comparisons of the station barometers with a standard barometer. The mean reduced pressures for each period, with corrections incorporated for the primary stations, were then plotted on a chart, and smoothed isobars were drawn to the data from the primary stations. Deviations of the secondary-station data from the smoothed mean-pressure field could thus be found. These deviations for all periods were averaged to obtain a single correction factor for each secondary station. It was also noted that the corrected mean reduced pressures for Wausau and Eau Claire exhibited small but consistent departures from the smoothed pressure field, hence additional corrections were applied to the measurements from these stations. The decision to make these additional corrections was supported by the following facts: (1) the Wausau barometer was found to be faulty (leaking mercury) and replaced a few months after the observational program was concluded, although the error was not recorded; and (2) the latest comparison data available for the barometer at Eau Claire was obtained in July 1962. Table 6 summarizes the correction factors added to individual pressure values before the fitting procedure was employed.

In this manner, corrected reduced pressures were found for each reporting station for each of the several hours spanning individual group-periods associated with the wind-profile observations. For each of these hours, the use of the method of least squares permitted approximation of the pressure field by mathematical surfaces of the following forms:

$$E_{Plane}(p) = \beta_0 + \beta_1 x + \beta_2 y,$$

$$E_{Quad}(p) = \beta_0 + \beta_1 x + \beta_2 y + \beta_3 x^2 + \beta_4 y^2 + \beta_5 xy,$$

where $E(p)$ is the expected value of pressure p, the β's are computed coefficients, and x and y are geographical coordinates. The quadratic

surfaces were fitted using all available data from the 17 stations, while the southernmost three stations (La Crosse, Madison and Milwaukee) were excluded in the plane fit because of their distances from the Lakewood site. The slopes of each fitted pressure surface at the site was evaluated, and west and south components of the surface geostrophic wind were computed. Averaging these components for the hours spanning each group-period, and utilizing the mean low-level wind direction for each group of wind profiles, group-mean antitriptic geostrophic wind components were found. No allowances were made for the effect of isobaric curvature for the quadratic surfaces.

It may be noted from Fig. 17 that the network of stations from which data were obtained for this procedure covers a large area, roughly 200 km in radius, which is not centered at the Lakewood site. The network is thus poorly suited for the fitting of pressure data, particularly in the case of the plane fit. In addition, the supplementary stations do not report at night, seriously reducing the number of observations available for the computational procedure.

For these reasons, four microbarographs (kindly loaned by the U. S. Weather Bureau) were located in a network symmetric about the site, and were in operation during the last two observational periods. The instruments were placed in the airport offices at Rhinelander, Clintonville, Menominee and Iron Mountain as shown in Fig. 17. The area enclosed by these stations, plus Wausau and Green Bay (which were also included in the network), is about 60 km in radius. Using a portable precision aneroid barometer, the instruments were set relative to the mercurial barometer at Green Bay just prior to the start of the sixth observational period.

The pressure data obtained from this supplementary network were used, in much the same way as that previously described, to estimate group-mean antitriptic surface geostrophic wind components. The smaller scale of this system is more appropriate for the plane-fitting procedure than that described before. However, due to the shorter distances involved, small errors in pressure measurement give quite large geostrophic wind errors, and it is doubtful if any improvement in the accuracy of the geostrophic wind estimates was achieved. Due to pen and bearing friction and gear backlash in the timing mechanisms of the microbarographs used, uncertainties of up to 0.5 mb in pressure and 30 min in time are possible in these measurements. The timing error may be particularly serious because of the rapid pressure changes occurring during the last two periods. Of course, there was also the problem of obtaining representative pressure values from the erratic barograph traces.

TABLE 7

Estimates for each group-period of antitriptic surface geostrophic wind components (U_0, V_0), in m/sec, and angle (α_0) between 50-m wind direction and surface isobars, in deg, obtained as follows: A, indirectly (from wind profile analysis); B, from quadratic fit to synoptic-scale pressure data (17 stations); D, from plane fit to pressure data from microbarograph network (in operation during June periods only).

			U_0				V_0				α_0			
Grp	CST	Date	A	B	C	D	A	B	C	D	A	B	C	D
1	1323	27 Aug 63	6.1	6.7	8.0	--	11.3	7.0	7.5	--	28.4	43.8	47.0	--
2	2226	27 Aug 63	9.1	3.4	2.5	--	10.7	5.3	7.3	--	40.4	32.5	18.8	--
3	1337	10 Sep 63	5.6	6.5	6.8	--	8.2	6.5	7.4	--	34.4	45.0	43.3	--
4	2247	10 Sep 63	5.0	4.5	3.4	--	11.1	4.4	6.1	--	24.2	45.6	28.6	--
5	0628	11 Sep 63	5.0	1.0	1.0	--	12.1	7.2	8.2	--	22.5	7.5	7.1	--
6	2158	19 Oct 63	x	1.2	1.2	--	x	0.3	-0.2	--	x	73.3	98.8	--
7	0530	20 Oct 63	x	0.8	2.2	--	x	4.0	3.3	--	x	11.6	33.2	--
8	1447	30 Nov 63	*	11.7	12.8	--	*	9.0	7.2	--	*	52.5	60.6	--
9	2319	30 Nov 63	5.4	5.8	4.5	--	8.8	7.8	6.9	--	31.5	36.4	33.0	--
10	1341	1 Dec 63	*	0.8	4.3	--	*	0.4	2.2	--	*	62.3	63.6	--
11	1516	31 Mar 64	2.0	2.5	5.6	--	5.7	3.7	3.8	--	18.4	33.8	55.7	--
12	2350	31 Mar 64	x	3.4	4.3	--	x	-0.8	0.4	--	x	103.1	85.1	--
13	1510	1 Apr 64	11.2	14.5	14.7	--	12.5	11.0	8.6	--	41.9	52.7	59.8	--
14	1117	8 Jun 64	5.8	11.6	10.9	9.6	9.5	9.5	9.2	11.0	31.4	50.6	49.8	40.9
15	2034	8 Jun 64	10.4	11.0	11.1	9.3	14.1	7.4	9.6	11.9	36.4	55.9	48.9	38.0
16	1149	10 Jun 64	2.0	3.3	4.9	1.6	5.3	3.4	3.5	3.7	20.7	44.6	54.2	23.0
17	0114	11 Jun 64	2.1	1.8	3.4	0.1	5.9	2.0	2.6	2.9	19.6	42.1	51.8	1.0

x) Wind profile not analyzed because of weak and poorly defined horizontal pressure gradient.
*) No indirect estimate obtained; wind profile analyzed using average U_0 and V_0 from B and C.

Table 7 compares the indirect and direct estimates of antitriptic surface geostrophic wind components obtained for each group-period, as well as the resulting estimates of the angle α_0 between the isobars and the observed low-level wind direction; α_0 was found by using Eq. (2.26). It should be remembered that the direct methods B and C are interdependent in that essentially the same data was used in each case; the same is true for method C, but to a lesser extent since only the Wausau and Green Bay data were used again. It may be seen that the angle α_0 seems to be consistently overestimated by methods B and C, possibly due to a local effect on the pressure measurements at Houghton and Marquette caused by their proximity to Lake Superior.

8.2 Thermal Wind

The data required for computing the height variation of the geostrophic wind in the atmospheric boundary layer over the Lakewood site were obtained from the following seven USWB radiosonde stations:

International Falls, Minnesota (INL),
St. Cloud, Minnesota (STC),
Sault Ste. Marie, Michigan (SSM),
Flint, Michigan (FNT),
Peoria, Illinois (PIA),
Green Bay, Wisconsin (GRB), and
Waverly, Iowa (3WY) (available for observational periods 6 and 7 only).

The locations of these stations with respect to the site are illustrated in Fig. 18.

The coded teletype reports from these stations furnished pressure and temperature information at the surface, 850 mb, 700 mb and, normally, several intermediate levels judged significant due to changes in temperature structure. Using these data for each upper-air observation during, and immediately before and after, each of the observational periods at the Lakewood site, thermal wind components for four 50-mb layers were obtained through the following procedure.

(1) The surface pressure value found for the site by means of the plane-fitting program to the surface pressure data was used as the lowest pressure level.

(2) Mean temperatures were found for each of four successive 50-mb layers above each radiosonde station. A linear change of temperature with the logarithm of pressure was assumed between reported

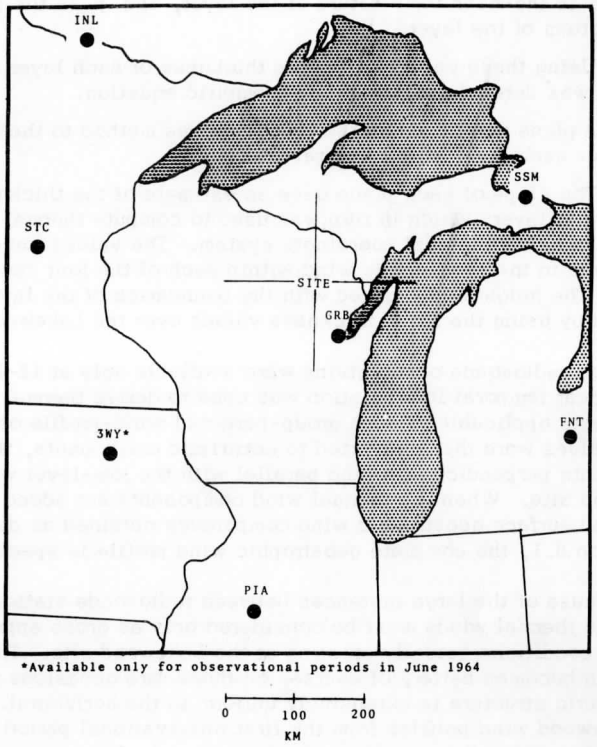

FIG. 18. Network of radiosonde stations used in the direct determination of thermal wind estimates.

levels. The computation was performed using the relation

$$\bar{T} = \int_{p}^{p-50mb} Td(\ln p) \Big/ \int_{p}^{p-50mb} d(\ln p),$$

where $\bar{T}$ is the mean temperature of the layer, and p is the pressure at the bottom of the layer.

(3) Using these values of $\bar{T}$, the thickness of each layer at each location was determined from the hypsometric equation.

(4) A plane was fitted by the least-squares method to the thickness values for each layer at the several stations.

(5) The slope of each plane gave an estimate of the thickness gradient for that layer, which in turn was used to compute thermal wind components in a geographical coordinate system. The values found represent the change in the geostrophic wind within each of the four successive layers. The heights associated with the boundaries of the layers were obtained by using the fitted thickness values over the Lakewood site.

Since radiosonde observations were available only at 12-hr intervals, linear temporal interpolation was used to derive thermal wind components applicable to each group-period of wind-profile observations. These values were then converted to antitriptic components, that is, components perpendicular to and parallel with the low-level wind at the Lakewood site. When the thermal wind components are added to the estimated surface geostrophic wind components obtained as described in Section 8.1, the complete geostrophic wind profile is specified.

Because of the large distances between radiosonde stations, the computed thermal winds must be considered only as gross approximations to conditions actually existing at the Lakewood site. The representation becomes better, of course, on those rare occasions when the atmospheric structure is extensively uniform in the horizontal. Some of the Lakewood wind profiles from the first observational period were analyzed by using the directly estimated thermal wind components, and the results are discussed in Section 10.

It was mentioned in Section 2 that one of the more important assumptions involved in the wind-profile analysis in this study is that of a constant thermal wind, i.e., a linear variation of geostrophic wind with height. To test this assumption, a line was fitted by the method of least-squares to each of the thermal wind components obtained from each set of upper-air observations. The results are shown in Fig. 19.

RESULTS OF LINEAR FIT TO COMPUTED THERMAL WIND COMPONENTS FOR FOUR 50-MB LAYERS

DATE/TIME	RESIDUAL MEAN SQUARE $(M/SEC)^2$ WEST COMP.	SOUTH COMP.
0600 CST 27 AUG 63	0.083	0.136
1800 CST 27 AUG 63	0.221	0.022
0600 CST 28 AUG 63	0.005	0.008
0600 CST 10 SEP 63	0.017	0.026
1800 CST 10 SEP 63	0.006	0.020
0600 CST 11 SEP 63	0.036	0.003
0600 CST 19 OCT 63	0.027	0.084
1800 CST 19 OCT 63	0.161	0.007
0600 CST 20 OCT 63	0.202	0.054
0600 CST 30 NOV 63	0.152	0.022
1800 CST 30 NOV 63	0.301	0.100
0600 CST 01 DEC 63	0.019	0.827
1800 CST 01 DEC 63	0.037	0.264
0600 CST 31 MAR 64	0.023	1.007
1800 CST 31 MAR 64	0.040	1.465
0600 CST 01 APR 64	0.075	0.800
1800 CST 01 APR 64	0.269	0.206
0600 CST 08 JUN 64	0.026	0.020
1800 CST 08 JUN 64	0.020	0.053
0600 CST 09 JUN 64	0.040	0.008
0600 CST 10 JUN 64	0.042	0.027
1800 CST 10 JUN 64	0.103	0.037
0600 CST 11 JUN 64	0.218	0.046
1800 CST 11 JUN 64	0.008	0.047
AVERAGE	0.089	0.220

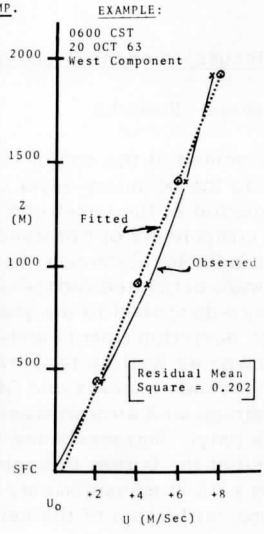

FIG. 19. Results of linear fit to estimated thermal wind components obtained for four 50-mb layers. The example is included to furnish an idea of the departures from linearity associated with the values of residual mean square.

The values of the residual mean square are measures of the goodness of fit of the line, with lower values indicating better fits. The example is included in order to furnish an idea of the goodness of fit relative to the size of the residual mean square. If a value of 0.20 m^2/sec^2 is taken to replace an acceptable fit, it may be seen that there are significant departures from linearity only on a few occasions. However, the inherent smoothing caused by the wide separation of the radiosonde stations and by the computational procedure should be kept in mind. The directly derived estimates of geostrophic wind profiles will be illustrated in conjunction with the Lakewood boundary-layer observations in the next section.

9. Discussion of the Boundary-Layer Observations

9.1 General Remarks

Presented at the end of this section are Figs. 22 and 23 which illustrate the boundary-layer observations for the first and second group-period at the Lakewood site. * Depicted are profiles of the antitriptic components of observed mean wind (u, v), observed mean wind corrected for local change (u_c, v_c), and geostrophic wind (U, V); the latter were estimated independently of the wind measurements by the procedure described in the preceding section. In addition, profiles of average deviation from height-meaned balloon ascent rates $(\overline{W-W_m})$ are shown, as well as temperature soundings from appropriate Green Bay radiosonde ascents and from the airborne measurements at the site. The instrumented aircraft was flown during the last three observational periods only. Surface-based low-level temperature measurements are included at the bottom of each aircraft sounding; it may be seen that the two sets of measurements link up fairly well, indicating that the absolute calibration of the sensing element on the aircraft was satisfactory in most cases.

The geostrophic wind components for groups 1 through 13 were found by using the thermal wind computed from the radiosonde data, in conjunction with estimates of surface geostrophic wind obtained by averaging the results of the plane- and quadratic-surface fits to the synoptic-scale pressure measurements, as described in Section 8. For the last four groups, the surface geostrophic wind components are those obtained by use of the data from the microbarograph network; also shown are estimates by means of the synoptic-scale data.

* Similar graphs have been prepared for each of the seventeen groups. For lack of space, the remaining fifteen are not included here.

Before discussing some of the more distinctive features of the observations, a few additional general remarks are in order. It may be noted from comparing the u and v profiles with those of u_c and v_c that significant local (time) changes in wind-profile structures were found for most groups. This is generally to be expected in continental mid-latitudes. Gross inadequacies of the directly determined geostrophic wind profiles are apparent in many instances, although there are at least three other factors which may possibly contribute to the failure of the corrected observed wind components (u_c, v_c) to become approximately geostrophic at upper levels: (1) the local change may be incorrectly estimated; (2) the inertia terms may not be negligibly small; i.e., the flow may not be horizontally homogeneous; and (3) there may be significant real geostrophic departures due to frictional effects even as high as 2 km.

For the most part, the directly determined geostrophic wind profiles were not used in the analysis, which employed the modified form of Lettau's antitriptic method as described in Section 2. The manner in which the analysis method was applied to the rather complex vertical structure of the Lakewood wind profiles will be briefly discussed in the next section. It should be stated here that the results of the analysis of the nocturnal wind profiles may have been affected to a certain extent by the method by which the low-level wind direction was determined, namely by utilizing the horizontal positions of the balloons 20 sec after release. As mentioned in Section 4, data from a recording wind vane on the tower would have been better. Since the low-level wind directions used in this investigation apply at a height of 50 m above the surface, it is possible that these estimates differ from the true surface wind at night, when relatively large directional shears may occur in the first few tens of meters. The apparent decrease from day to night of the antitriptic u-components for groups 1 and 2 and for groups 3 and 4 may be a manifestation of this effect.

9.2 Low-Level Wind Maxima

The Lakewood wind profiles exhibit the typical diurnal variation which has been observed frequently in the past. The daytime profiles normally show strong shears very near the surface with relatively weak shears above, while the nocturnal observations for the most part are characterized by a maximum in wind speed generally within the lower 500 m. A "low-level jet" was particularly well defined during group-periods 2, 4, 5 and to a lesser extent, 15. Various mechanisms have been proposed to explain such wind structure; perhaps the most widely

accepted at the present time is that of Blackadar (1957). His model takes the primary cause of the low-level jet to be the nocturnal decrease of mixing under inversional conditions, and predicts that the wind vector at the level of the jet will follow an inertial oscillation having a period of one-half pendulum day. This period should thus decrease with latitude; however, Bonner (1965) found that the period of oscillation of the summer low-level jet at International Falls, Minnesota, is about the same as that at Fort Worth, Texas. In addition, the observations at O'Neill, Nebraska, during the late summer of 1953 indicated that the period of the jet oscillation was more on the order of one solar day, rather than the 18 hours predicted by Blackadar's model at that latitude (Barad, 1961). Lettau (1964) has proposed that Blackadar's basic mechanism may be enforced by a diurnal variation of low-level thermal winds, caused by solar heating cycles on a large-scale terrain slope. These thermal winds tend to encourage formation of nocturnal southerly jets on eastward-facing slopes poleward of 30° latitude. Hoecker's (1963) boundary-layer wind-speed cross-sections for the central U. S. indicate that nighttime wind maxima tend to occur over regions of greatest terrain slope, lending support to Lettau's theory.

The large-scale terrain slope for northeastern Wisconsin was evaluated in Section 3.2 to be 3.37 m/km downward to the ESE, with the contour lines oriented along the azimuth directions 218° and 038°. It may be noted from Fig. 23 that the low-level jets for group period 2, (likewise for group periods 4 and 5 which were mentioned previously) have directions (given essentially by the 50-m wind direction) in the neighborhood of 220°. The large-scale terrain slope around the Lakewood site would tend to favor the establishment of jets in just this direction, according to Lettau's mechanism. Although the winds for group 15 are the strongest of all, the maximum is higher and not as sharply defined as that of groups 2, 4 and 5. The 50-m wind direction is about 145°, while that at 600 m is 190°. The strong horizontal pressure gradient in this instance (see Fig. 9) probably dominated over any terrain-slope effects. In group 7, an interesting feature of the wind profile is the maximum at the 50-m level and rapid decrease above. Such a circumstance could also be explained by Lettau's theory; in this case the wind direction is 020°, for which the terrain slope would cause a nocturnal thermal wind opposing the flow. The low-level maxima observed at Lakewood are generally rather closely associated with the heights of the temperature inversion, which indicates that both Blackadar's and Lettau's mechanisms are probably involved.

9.3 Temperature Structure

Before discussing some features of the temperature profiles, it is appropriate to consider the degree to which the Green Bay soundings may be considered representative of the conditions at the Lakewood site 95 km distant, since airborne temperature measurements at the site were made only in conjunction with the daytime balloon series during the last three observational periods. Fig. 20 compares temperature profiles obtained by the instrumented aircraft at Lakewood with those measured at about the same time by radiosondes at Green Bay. There is considerable similarity between the two sets of profiles; however, as would be expected, the radiosonde fails to show some of the fine structure of the temperature profile, such as the sharp inversion during the late afternoon of 10 June.

The wide spread in the profiles for 8 June is probably not entirely real. There is a 2-hr time difference between the measurements at the two locations, but it is not likely that the air at the upper levels above Lakewood would cool by the amount indicated. An error in the absolute calibration of the aircraft or radiosonde sensing elements is possible. At any rate, the shapes of the two profiles are similar. The inversion is apparently due to the warm front depicted in Fig. 9. It should be kept in mind that, due to the difference in elevation between Lakewood and Green Bay, the heights of inversions above the surface at the two sites (as illustrated) may be different even though the inversions are actually at the same level with respect to MSL.

One of the more noteworthy features of the observations, particularly at daytime, is the frequent appearance of two distinct regimes of turbulence structure within the lower 2 km. Significant changes in wind shear often occur in association with temperature inversions at levels from 700 to 1500 m above the surface. These inversions could mark the level of the "peplopause,"* a term coined by Schneider-Carius (1953) to denote the top of the turbulent friction and convection layer, at which haze normally accumulates. The airborne turbulence measurements taken during the last three observational periods demonstrated that turbulence was almost totally absent above the inversion, yet significant below. The inversion is presumably caused by strong vertical mixing below, which works towards the establishment of an adiabatic lapse rate, and by slight subsidence from above.

Ball (1960) studied the diurnal variation of the level of the turbulence inversion, and found that its height varied directly with the

*Greek "peplos" = large shawl or scarf.

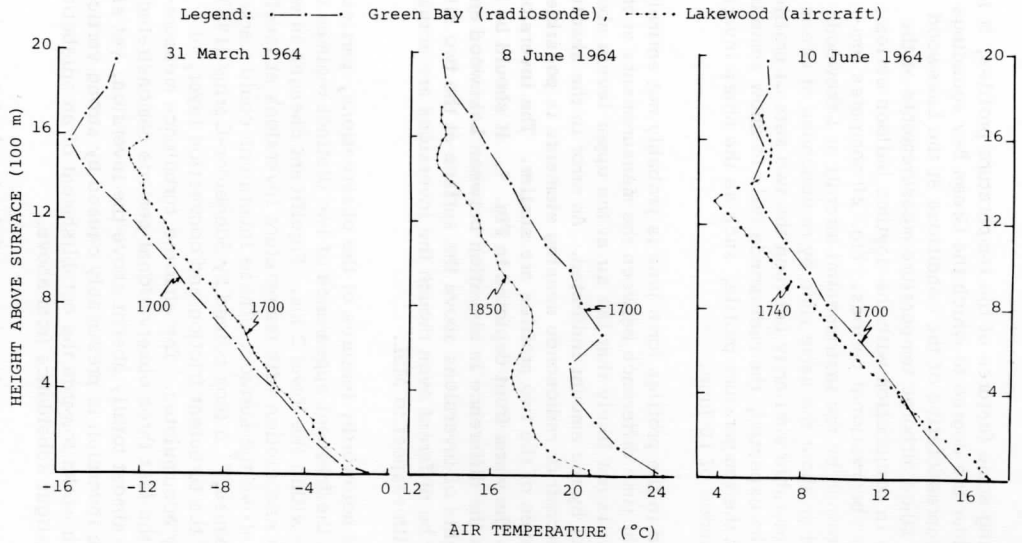

FIG. 20. Comparison of temperature profiles obtained at Green Bay by radiosonde with those obtained at the Lakewood site by an instrumented aircraft, for the three cases when measurements were made at about the same time. Observation times are indicated in CST. Heights above the surface at each location are shown; Green Bay is 223 m lower than the Lakewood site in elevation above MSL. The airborne and surface-based temperature measurements at Lakewood are joined by a dashed line.

intensity of surface heating and the resulting convection. This behavior is also evident in the Lakewood temperature profiles obtained by the aircraft, for example, in group 16. Ball suggests that convective eddy energy which is not dissipated through viscosity is transported upward and destroyed by buoyancy forces at the inversion, where downward transfer of heat and mass is presumed to take place. The process is associated with an upward movement of the inversion, although this may be overcome by sufficiently strong subsidence. For a clear summer day over a dry surface, Ball estimates that when subsidence is weak the height of the inversion will change by about 150 m/hr. The same value may be obtained for the Lakewood observations of 8 and 10 June, but of course the forest cannot be considered as a dry surface.

9.4 Balloon Ascent Rates

The profiles of $\overline{W-W_m}$, representing the average deviations from the height-meaned balloon ascent rates and obtained as explained in Section 5, show significant dependencies upon daytime temperature structure. The association is even more pronounced for individual balloon series. The most striking examples of this effect were observed for groups 10, 11 and 16. On these fairly clear days, convective turbulence was apparently quite vigorous, and the balloons had significantly higher ascent rates in the region below the temperature inversion than at levels above it. Two factors may be offered in explanation of this behavior: (1) real vertical air motions, and (2) changes in the drag coefficients of the balloons due to the separate turbulence regimes above and below the inversions.

With regard to the first point, it hardly seems possible that the large deviations in ascent rate could be ascribed to real vertical motions in the atmosphere existing over such extended periods of time. However, Fig. 21 illustrates what can happen in convective conditions. The graph shows the variation in rate of ascent for two serial releases about 20 min apart on the afternoon of 31 March 1964. Both balloons were inflated to give the normal ascent rate of 3 m/sec, but the mean ascent rate for the first balloon (A) turned out to be only 1.68 m/sec while that for the second (B) was 5.92 m/sec. Evidently balloon A was affected by the downward air motion preceding the overhead passage of a cumulus cloud, while balloon B became entrained in the updraft and entered the base of the cloud at the 1400-m level. If the observed deviations of the ascent rates from the normal 3 m/sec are considered to be caused solely by vertical air motions, then a maximum downdraft of

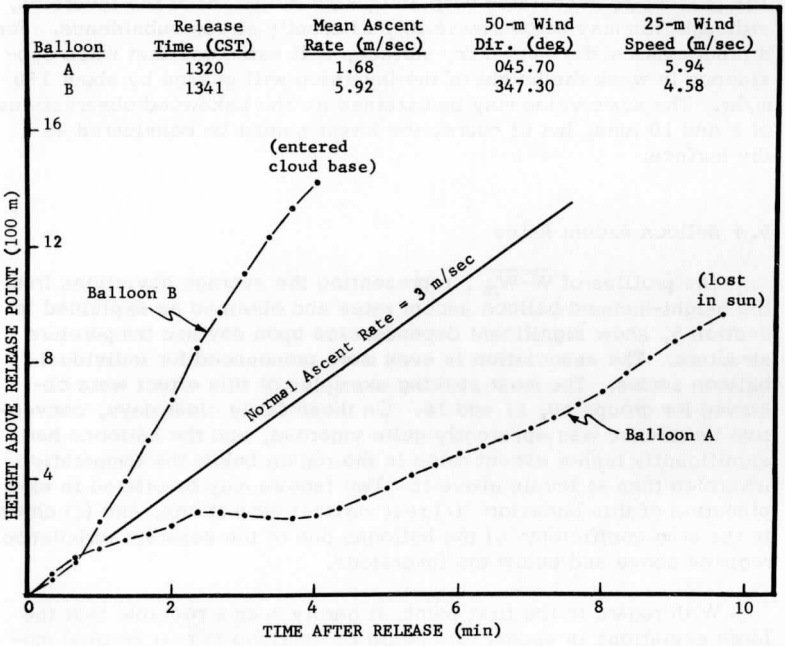

FIG. 21. Balloon height versus time for two serial releases into a sky about 3/10 covered with small to moderate-sized cumulus clouds on the afternoon of 31 March 1964. Balloon B entered the bottom of a cloud about 1/2 km in diameter. Both balloons were inflated to give normal ascent rate of 3 m/sec. Note downward motion of balloon A about 3 minutes after release.

3.5 m/sec and a maximum updraft of about 4 m/sec are indicated for portions of these balloon ascents. Incidentally, because of these effects the data from these balloon runs were not included in the mean profiles for group 11.

The data in Fig. 21 thus suggest that large vertical air motions can exist in the lower portion of the atmosphere, at least as transient states. It has not been demonstrated, however, that mean vertical motions on the order of 1 m/sec can persist over periods of several hours as are represented by the group-mean profiles.

It is known that the critical Reynolds number for a sphere depends upon the turbulence of the air stream (see Dryden et al., 1956, p. 21). For the Lakewood daytime observations, the average balloon ascent rates below and above the temperature inversion are about 3.5 and 2.5 m/sec, respectively, which correspond to drag coefficients of approximately 0.35 and 0.60. Such a change in drag coefficients for the balloons could be explained as follows. Below the inversion the flow is turbulent, causing the Reynolds number of the balloon motion to be supercritical, with the resulting small drag coefficients and high ascent rates. In the relatively smooth air above the inversion, the Reynolds number becomes subcritical, with an increased drag coefficient causing lower ascent rates. Fig. 13 in Section 6 indicates that such a process may indeed be operative, since different height variations in ascent rate were shown by the two types of balloons. This should not happen if the deviations in mean ascent rate were caused by real vertical air motions. The $\overline{W-W_m}$ profiles for the nocturnal group-periods generally indicate almost constant ascent rates, which would be expected when turbulence is light.

It may be that the observed height dependencies of the ascent rates for the Lakewood balloons were caused by both vertical air motions and changes in drag coefficients. At any rate, the effect appears to be significantly associated with the temperature structure. It might even be possible on sunny days to obtain rough estimates of the heights of upper-level temperature inversions (which can often be considered to mark the top of the boundary layer under convective conditions) simply by tracking uninstrumented balloons.

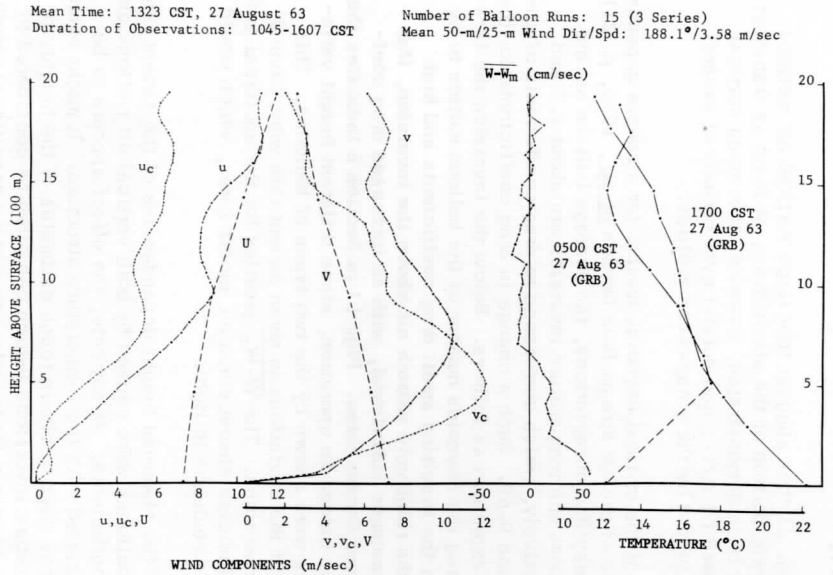

FIG. 22. Profiles of mean observed wind components (u, v), mean observed wind components adjusted for local change (u_c, v_c), and independently derived geostrophic wind components (U, V), perpendicular to and parallel with observed 50-m wind; also profiles of air temperature and of $\overline{W-W_m}$, the average deviation from height-mean balloon ascent rates, all for Group 1. For the Green Bay (GRB) temperature profiles only, the height scale indicates height above the surface at Green Bay, which is 223 m lower than the surface at the observing site.

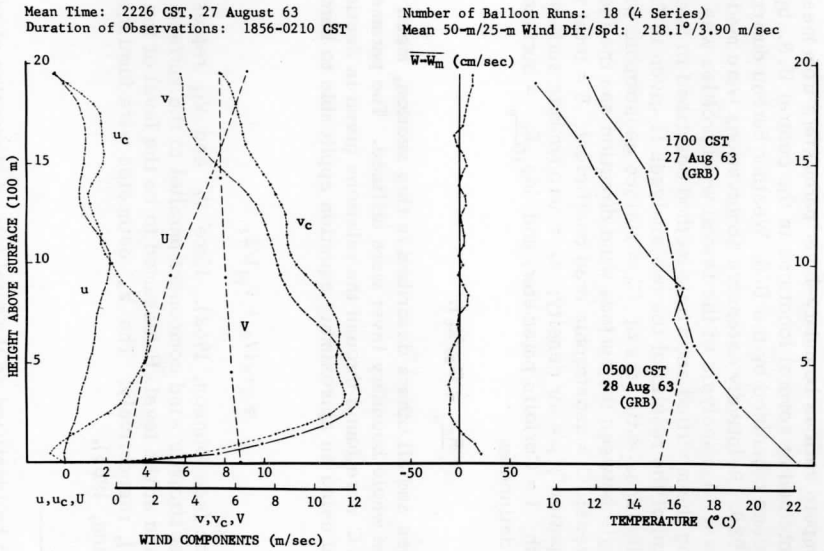

FIG. 23. Profiles for Group 2. For explanation of symbols, see Fig. 22.

10. Results of Wind-Profile Analysis and Comparison With Theory

10.1 Re-analysis of Drexel Wind Profiles

In a previous study (Johnson, 1962), Lettau's antitriptic method was used to compute various boundary-layer parameters from mean wind profiles obtained at several locations in the central U. S. by means of kite observations organized by the U. S. Weather Bureau during the years 1915 to 1920. Relatively extensive observations were made at Drexel, Nebraska. A reanalysis of the Drexel wind profiles was performed, utilizing the modified antitriptic method described in Section 2, and a comparison of the results of the two analyses is given in Table 8. The tabulation includes estimates of G_0 = surface geostrophic wind speed; α_0 = angle between the surface wind direction and the isobars; τ_0 = surface stress; C = geostrophic drag coefficient; E = total rate of energy dissipation*; ρ = air density; z_0 = aerodynamic surface roughness length; f = Coriolis parameter; and $\log_{10}\underline{R_0}_0$ = surface Rossby number defined as

$$\underline{R_0}_0 = G_0/z_0 f. \tag{10.1}$$

In these analyses and all others described in this section, mean air densities for the whole boundary layer were utilized. The parameters G_0, α_0, τ_0 and C were found through the relations given in Section 2; E was estimated using an approximate equation applicable to baroclinic wind profiles,

$$E \cong \tau_0(V_0 + V_H)/2, \tag{10.2}$$

derived by Lettau (see Johnson, 1962). Here V_0 and V_H represent values of the geostrophic wind component parallel to the surface wind, at the surface and at the level H (assumed to be the level of the highest observation), respectively. The z_0 estimates were furnished by E. Kung (see Kung, 1963).

---

*E can also be identified as the total rate of production of eddy-motion energy; however, throughout this section the assumption stated in Section 2.4 will be applied, and E will be considered as approximately equivalent to the total rate of dissipation of mean-motion energy in the boundary layer.

TABLE 8

Comparison of values of boundary-layer parameters derived from Drexel (Nebraska) wind profiles for winter and summer seasons of the years 1915 to 1920. The estimates were obtained as follows: (B) by using the modified antitriptic analysis method, and (A) from a previous analysis (Johnson, 1962) employing the unmodified method. The theoretical values are from Lettau's (1962) model, utilizing the parameters given in the small table at the bottom. The asterisks indicate the cases for which the unmodified method failed to give results. See text for explanation of symbols.

WINTER:

Sfc	G_0		α_0		τ_0		C		E	
Wind Dir	A	B	A	B	A	B	A	B	A	B
N	*	11.0	*	22.3	*	2.76	*	0.045	*	3.12
NE	9.3	9.4	16.9	18.0	1.21	1.47	0.035	0.038	0.99	1.21
E	11.0	11.2	25.4	27.5	1.53	1.87	0.033	0.036	1.13	1.38
SE	13.1	13.7	22.9	27.8	1.67	2.77	0.029	0.036	1.18	1.92
S	13.0	13.3	20.7	24.8	1.80	2.57	0.030	0.036	1.75	2.48
SW	11.7	11.8	19.5	21.8	1.33	1.76	0.029	0.033	1.41	1.86
W	10.5	10.7	19.0	22.0	1.07	1.61	0.029	0.040	1.34	2.01
NW	*	12.0	*	24.5	*	2.40	*	0.038	*	3.42
Mean:	11.4	11.6	20.7	23.6	1.43	2.15	0.031	0.038	1.30	2.18
Theoretical:			25.3		2.06		0.037		2.14	
	(m/sec)		(deg)		(dyne/cm^2)				(watt/m^2)	

SUMMER:

N	*	9.5	*	20.8	*	2.19	*	0.048	*	2.05
NE	*	9.0	*	24.2	*	2.29	*	0.052	*	1.77
E	8.9	9.6	11.1	24.5	1.60	3.35	0.044	0.059	1.13	2.38
SE	10.2	10.5	13.1	18.3	1.41	2.33	0.036	0.045	1.02	1.70
S	11.3	11.5	20.7	22.5	2.63	3.76	0.044	0.052	2.60	3.71
SW	11.9	11.7	21.2	18.9	2.86	2.36	0.044	0.046	3.23	2.66
W	9.6	9.4	21.5	18.6	1.88	1.54	0.044	0.041	2.02	1.50
NW	*	9.9	*	18.4	*	2.32	*	0.048	*	2.68
Mean:	10.4	10.1	17.5	20.8	2.08	2.52	0.042	0.049	2.00	2.31
Theoretical:			28.4		1.87		0.041		1.70	

TABLE 8 (continued)

Season	No. of Profiles	ρ	$\overline{G_0}$	z_0	f	$\log_{10} \frac{R_0}{0}$
Winter	412	1.14	11.5	8	0.963	6.17
Summer	364	1.05	10.3	28		5.58
		(kg/m^3)	(m/sec)	(cm)	(10^{-4}/sec)	

Since the mean G_0 estimates from the two analysis methods were nearly identical for each season, average values, $\overline{G_0}$, for winter and summer were derived and used to compute theoretical values from Lettau's (1962) model, which may be compared with the results from both methods. As indicated, the unmodified antitriptic method (A) failed for profiles showing the effects of strong cold-air advection. It may be noted that for the winter profiles, the theoretical values agree rather well with estimates derived from the modified antitriptic method (B). However, the comparison for summer is less favorable; τ_0, C and E are all larger than predicted, while α_0 is smaller. It is probable that these departures are due at least partly to the fact that the theory refers to neutral conditions, while the observations were all made during the daytime when some degree of atmospheric instability is to be expected, particularly during the summer. From other investigations, it has been fairly well established that the trend evidenced here (i.e., larger τ_0, C, E; smaller α_0) is typical for unstable conditions.

10.2 Analysis of Lakewood Series-Mean Wind Profiles

It may be noted from Fig. 4 that the synoptic pressure pattern over northeastern Wisconsin was fairly constant during the first observational period. With this in mind, analyses by three different methods were carried out for the series-mean wind profiles obtained during this period, neglecting any effects of local (time) change in wind structure. Figs. 22 and 23 for group-periods 1 and 2 indicate that the local change during these periods was probably not negligible, hence substantial systematic errors may be present in the results of the analyses of the series-mean profiles. However, the objective was to study the diurnal variations of the boundary-layer parameters, and the relative magnitudes of the

estimates should provide valid comparisons even if errors in absolute size are inherent.

The analyses were performed by using (A) the modified antitriptic method, (B) the unmodified method, and (C) a method in which the thermal wind components derived directly from radiosonde data were fitted to the upper portions of the wind component profiles. Methods A and B as described in Section 2 require that a level H denoting the "top" of the boundary layer be used in graphically positioning the assumed linear profiles of geostrophic wind components. In the analyses of the Drexel data, the level H was taken to be 1604 m above the surface, corresponding to the highest observational level. At this height the observed wind was assumed to be geostrophic. The procedure used in the analyses of the Lakewood series-mean and group-mean profiles was similarly subjective. Normally, the linear profiles of the geostrophic wind components U and V were fitted to the upper portions of the u_C, v_C profiles (or to the u, v profiles, when u_C, v_C were not available) such that a "balancing of areas" at the upper levels was achieved. In some cases, however, when marked changes in wind structure occurred in association with upper-level temperature inversions, the observed (or corrected) wind in the vicinity of the inversion was assumed to be geostrophic. Admittedly, such subjective procedures are undesirable, but also unavoidable because no other analysis methods are available. Previous investigators encountered the same handicap, and had to rely on a certain degree of subjective smoothing of the wind profiles, loosely equivalent to the procedure chosen here.

Table 9 gives the results of the three analysis methods applied to the series-mean wind profiles of 27 August 1963. For these data, E was found by use of Eq. (10.2). Method B is seen to yield mean values of α_0, τ_0, and C which agree the closest with Lettau's theory, although method A furnished the better comparison for E. The directly derived thermal wind components could not be fitted to the component wind profiles for series 6, hence no estimates were obtained. The values of α_0, τ_0, C and E are generally significantly higher during midday than at morning and evening hours. A diurnal variation of this type for τ_0, C and E agrees with results from many past studies; from his tetroon flights, Angell (1964) found a similar variation of stress at about 3000 ft with time of day. The effect is predicted by diabatic theory; see, for example, Ching (1964). On the other hand, α_0 has been found in most other investigations to decrease with decreasing stability, the opposite of which is indicated in Table 9. A

possible explanation of this discrepancy may be found in the method by which the low-level wind direction was determined at the Lakewood site, which was discussed in Section 9.

10.3 Analysis of Lakewood Group-Mean Wind Profiles

Because of rapidly changing synoptic conditions and weak pressure gradients, it was not possible to analyze the wind profiles for group-periods 6, 7 and 12. The results of the analysis of the other 14 group-mean profiles are summarized in Table 10. All of these profiles with the exceptions of groups 8 and 10 were analyzed by use of the modified form of Lettau's antitriptic method. For the other two groups, it was necessary to resort to surface geostrophic wind estimates derived directly from the pressure data, since the other analysis method gave results which were totally unacceptable. It was not possible to make local-change estimates for groups 8 and 13, each of which consist of only one series-mean profile; hence the analysis for these cases was based on profiles of u and v only. In addition, the local-change effects for group 15 seem to be greatly overestimated, and were not included in the analysis.

The values of E shown in Table 10 were computed numerically by use of the term on the left in Eq. (2.31); the other parameters were calculated in the same manners as before. As in Section 7, $(Ri)'$ values between -3 and 3 ($10^{-3}/m$) were assumed to represent approximately neutral conditions; $(Ri)'$ values in excess of these limits were taken to indicate unstable and stable classes, respectively. Mean estimates of the parameters for each stability class are compared with values derived from Lettau's neutral barotropic model at the bottom of the table. Unfortunately, insufficient data are available to distinguish between the effects of surface roughness and stability on the boundary-layer parameters. For the neutral case, the empirical values are somewhat larger than those predicted by the theory. For the stable and unstable classes, the departures of the mean estimates of C, τ_0, and E from the neutral theory are in the same directions as indicated in tables 8 and 9. Again, the variation of α_0 is erratic and does not conform with the established notion that it should decrease with decreasing stability. In addition to the possible cause of this behavior which was discussed previously, it could be that effects of baroclinicity are also involved. Cold-air advection near the surface is normally accompanied by instability and, correspondingly, warm-air advection with stable conditions. Bernstein (1959) found that α_0 increases with cold-air advection but decreases with diminishing stability, while, normally, one can expect that cold-

TABLE 9

Comparison of values of boundary-layer parameters derived from Lakewood wind profiles of 27 August 1963 (first observational period) by three different methods: (A) modified antitriptic method; (B) unmodified antitriptic method; (C) using thermal wind components derived directly from radiosonde data and fitted to upper portions of each wind component profile. Local change effects are not considered in the analyses. The theoretical values are from Lettau's (1962) model. Series 4 was not included in the analyses because the 50-m wind direction was 150.8°, departing considerably from the smooth trend shown by the other series. See text for explanation of symbols.

		Series No.:	1	2	3	5	6		
		No. of Ascents:	5	5	5	5	4		
		Mean CST:	1122	1329	1517	1928	2122		
		25-m wind speed (m/sec):	3.11	3.66	3.97	4.44	3.90		
		50-m wind dir. (deg):	183.0	188.7	192.5	199.6	218.5		
	Method							Mean	Theor.
G_0 (m/sec)	A		13.0	14.0	10.8	10.9	10.9	11.9	
	B		12.7	13.4	9.9	12.0	12.1	12.0	
	C		13.6	13.7	11.0	8.5	--	11.7	
α_0 (deg)	A		41.6	47.3	34.4	29.2	23.3	35.2	
	B		38.9	43.4	23.7	30.7	24.9	32.3	32.8
	C		26.7	32.2	41.7	24.2	--	31.2	
τ_0 (dyne/cm^2)	A		3.32	8.61	4.85	2.44	1.79	4.20	
	B		2.80	7.28	2.94	2.24	2.72	3.60	3.57
	C		1.57	4.58	5.21	1.35	--	3.18	
C	A		0.042	0.062	0.061	0.043	0.037	0.049	
	B		0.040	0.061	0.052	0.038	0.041	0.046	0.047
	C		0.028	0.048	0.063	0.041	--	0.045	
E (watt/m^2)	A		2.92	7.23	2.98	1.66	1.54	3.27	
	B		2.50	6.90	1.93	1.84	2.19	3.07	3.56
	C		1.43	4.33	4.03	0.76	--	2.64	

TABLE 10

Summary of results of analysis of Lakewood mean wind profiles, and comparison with values from Lettau's (1962) neutral barotropic model. Listed are z_0, aerodynamic surface roughness length; G_0, surface geostrophic wind speed; C, geostrophic drag coefficient; α_0, angle between surface wind and isobars; τ_0, surface shearing stress; E, total rate of energy dissipation in the planetary boundary layer; and (Ri)', bulk stability parameter, equivalent to the Richardson number at a height of 1 m. The stability classes represent stable (S), near-neutral (N) and unstable (U) conditions, determined as specified in Section 7. The analyses were carried out by the modified antitriptic method (A), and by using directly derived surface geostrophic winds (B). The values shown in parentheses for the theory are $\log_{10} \underline{Ro}_0$, where $\underline{Ro}_0$ is the surface Rossby number computed from the indicated values of z_0 and G_0, along with the Coriolis parameter for the site, f = 1.035 (10^{-4}/sec).

Grp. No.	Mean CST	Date	z_0	G_0	C	α_0	τ_0	E	(Ri)'	Stab. Class	Anal. Method
1	1323	27 Aug 63	160	12.8	0.047	28.4	4.25	4.32	--	N	A
2	2226	27 Aug 63	160	13.9	0.048	40.4	5.17	4.62	--	S	A
3	1337	10 Sep 63	160	9.9	0.068	34.4	5.20	3.60	-2.3	N	A
4	2247	10 Sep 63	160	12.2	0.025	24.2	1.06	1.17	4.2	S	A
5	0628	11 Sep 63	160	13.1	0.041	22.5	3.27	3.53	2.5	N	A
8	1447	30 Nov 63	105	14.7	0.063	56.4	10.66	12.37	--	N	B
9	2319	30 Nov 63	105	10.3	0.030	31.5	1.22	0.90	--	S	A
10	1341	1 Dec 63	105	2.9	0.076	63.4	0.61	0.21	--	U	B
11	1516	31 Mar 64	105	6.0	0.082	18.4	3.05	1.24	-4.6	U	A
13	1510	1 Apr 64	105	16.8	0.054	41.9	9.67	8.47	-2.2	N	A
14	1117	8 Jun 64	160	11.1	0.053	31.4	3.82	2.92	-3.5	U	A
15	2034	8 Jun 64	160	17.5	0.036	36.4	4.45	6.42	1.7	N	A
16	1149	10 Jun 64	160	5.7	0.066	20.7	1.62	0.88	-8.0	U	A
17	0114	11 Jun 64	160	6.3	0.058	19.6	1.53	0.63	9.9	S	A
			(cm)	(m/sec)		(deg)	(dyne/cm^2)	(watt/m^2)	(10^{-3}/m)		
Mean (all cases)			140	10.9	0.054	33.5	3.97	3.66			
Theoretical				(4.88)	0.047	32.6	3.16	2.90			
Mean (stable cases)			146	10.7	0.040	28.9	2.25	1.83			
Theoretical				(4.85	0.047	32.8	3.05	2.74			
Mean (neutral cases)			142	14.1	0.052	36.7	6.25	6.45			
Theoretical				(4.98)	0.046	32.0	5.06	6.05			
Mean (unstable cases)			133	6.4	0.069	33.5	2.28	1.31			
Theoretical				(4.67)	0.049	34.0	1.18	0.63			

air advection is associated with decreasing stability. In addition, Blackadar's (1963) theory has α_0 increasing for cold-air advection, and α_0 decreasing for warm-air advection. With regard to the geostrophic drag coefficient C, however, observations agree with theory by indicating that the effects of advection and stability act in the same direction for the two situations described.

The estimates of C derived from the Lakewood group-mean profiles are illustrated as a function of stability in Fig. 24, and a significant relationship is indicated. The values of C for which only qualitative stability estimates were available (see Section 7) were included in the graph by using the following assumed quantitative $(Ri)'$ ranges, in units of $(10^{-3}/m)$; near neutral, -1.5 to 1.5; slight positive stability, 2 to 5; and moderate positive and negative stabilities, 5 to 8, and -5 to -8. Lettau (1959a) found that the O'Neill data suggested a maximum for the ratio C/C_a, where C_a is the adiabatic geostrophic drag coefficient, at a value of about -8 for $(Ri)'$. The range of $(Ri)'$ values associated with the Lakewood group-mean profiles is not sufficient to detect such a peak; otherwise, however, the trend of the curve over its range is similar to Lettau's, although somewhat steeper.

Fig. 25 demonstrates the diurnal variation of the geostrophic drag coefficient. The data points are from the analyses of both the Lakewood group-mean wind profiles and the series-mean profiles of observational period 1. The maximum tends to occur 1 to 3 hours past local noon. In Figs. 26 and 27, mean values of C and α_0 obtained in this investigation are compared with the results of previous studies and with current theories relating these parameters to the surface Rossby number. With regard to the geostrophic drag coefficient, the theoretical neutral barotropic curves of Lettau (1962), Blackadar (1963) and Appleby and Ohmstede (1964) are quite similar. It may be noted that the Drexel winter value for C falls fairly close to these curves; the Lakewood neutral estimate is somewhat higher than predicted. The Lakewood unstable value may well be an overestimate, although it and the Drexel summer estimate show the same relationship with respect to neutral conditions as Ching's (1964) curves for slight instability. Although Ching's model includes greater instabilities, only his curves for slight instability are presented here, since this condition corresponds to the "unstable" estimate for Lakewood. The Lakewood mean value of α_0 for all cases and the Drexel winter estimate fall closely to the neutral barotropic curves of Lettau, Blackadar, and Appleby and Ohmstede, while the summer value of α_0 for Drexel seems to fit Ching's curve for slightly unstable conditions.

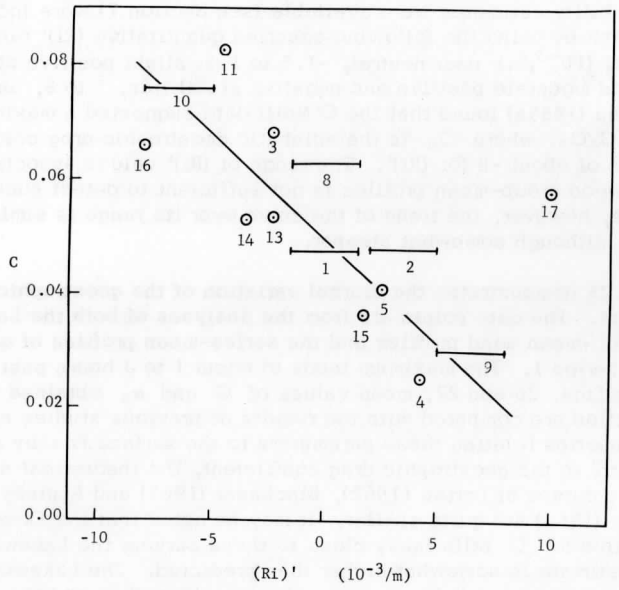

FIG. 24. Geostrophic drag coefficient C as a function of the stability parameter $(Ri)'$. The short horizontal lines represent qualitative stability estimates (see text). The data are identified by group number. The value of C for group 17 appears unreasonable and was not considered when the trend line was positioned by eye.

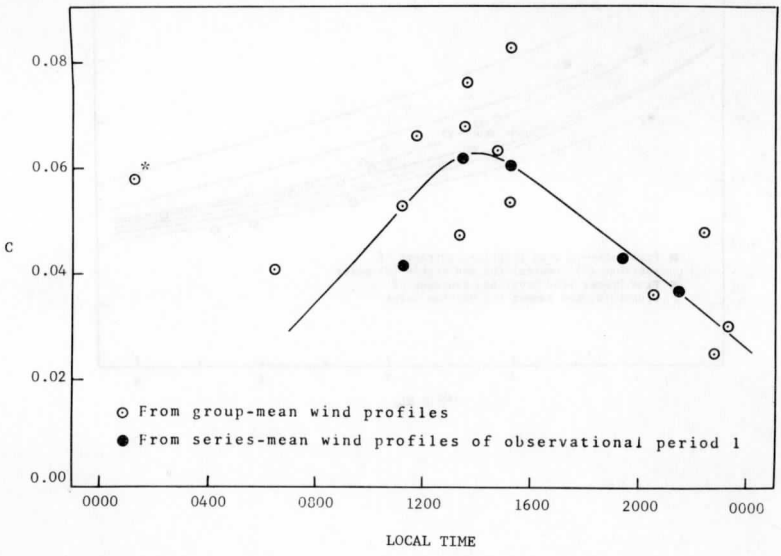

FIG. 25. Geostrophic drag coefficient C as a function of time of day. The point marked with an asterisk is for group 17, and as in Fig. 24, was ignored in the positioning of the trend line by eye.

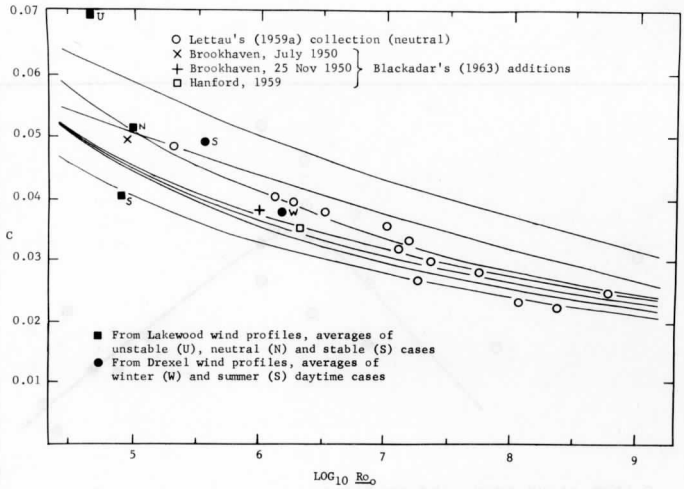

FIG. 26. Geostrophic drag coefficient C as a function of $\log_{10}$ of the surface Rossby number (Ro_0). The theoretical curves, from top right down, are from (1) Ching, 1964 (for slight instability, baroclinic, thermal wind = 5 m/sec/km in direction of surface wind, f = 10^{-4}/sec); (2) Ching, 1964 (slight instability, barotropic); (3) Blackadar, 1963 (neutral baroclinic, thermal wind = 4.2 m/sec/km in direction of surface geostrophic wind, f = 10^{-4}/sec); (4) Lettau, 1962 (neutral barotropic); (5) Appleby and Ohmstede, 1964 (neutral barotropic); (6) Blackadar, 1963 (neutral barotropic); and (7) Blackadar, 1963 (neutral baroclinic, thermal wind = 4.2 m/sec/km in direction opposite to surface geostrophic wind, f = 10^{-4}/sec).

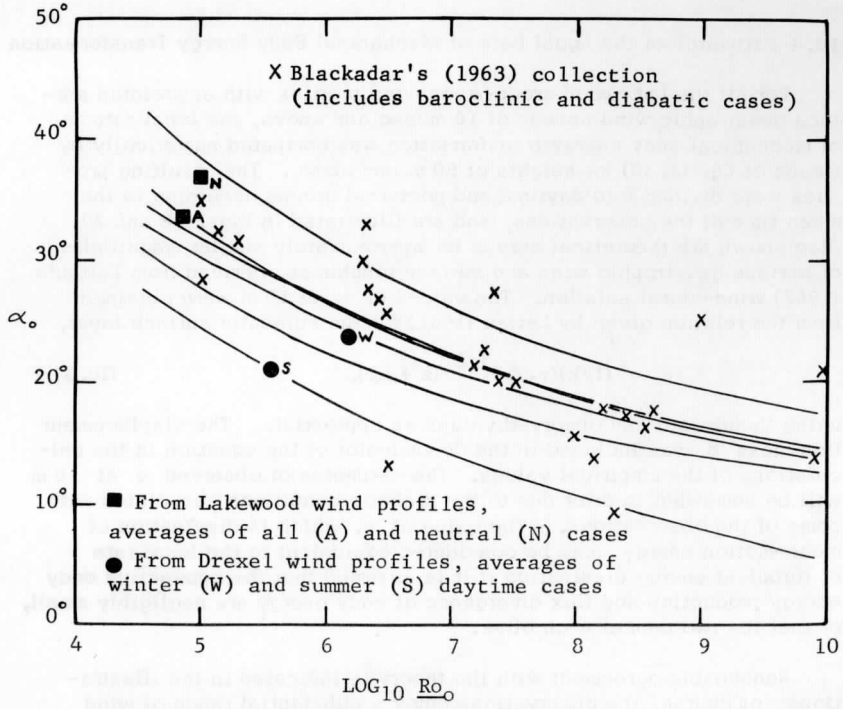

FIG. 27. Angle α_0 between surface wind and isobars as a function of $\log_{10}$ of the surface Rossby number ($\underline{\text{Ro}}_0$). The theoretical curves, from top left down, are from

(1) Blackadar, 1963 (neutral baroclinic, thermal wind = 4.2 m/sec/km in direction of surface geostrophic wind, $f = 10^{-4}$/sec),
(2) Blackadar, 1963 (neutral barotropic),
(3) Lettau, 1962 (neutral barotropic),
(4) Appleby and Ohmstede, 1964 (neutral barotropic),
(5) Blackadar, 1963 (neutral baroclinic, thermal wind = 4.2 m/sec/km in direction opposite to surface geostrophic wind, $f = 10^{-4}$/sec), and
(6) Ching, 1964 (slight instability, barotropic).

10.4 Estimates of the Local Rate of Mechanical Eddy Energy Transformation

For all the Lakewood group-mean wind profiles with associated surface geostrophic wind speeds of 10 m/sec and above, the local rate e of mechanical eddy energy transformation was computed numerically by means of Eq. (2.30) for heights of 50 m and above. The resulting profiles were divided into daytime and nocturnal groups according to the mean time of the observations, and are illustrated in Figs. 28 and 29. Also shown are theoretical curves for approximately similar magnitudes of surface geostrophic wind and surface roughness, derived from Lettau's (1962) wind-spiral solution. The values of e at 10 m were obtained from the relation given by Lettau (1961) for the adiabatic surface layer,

$$e = (1/k)(\tau_0/\rho)^{3/2}/(z + z_0), \qquad (10.3)$$

using theoretical and observed values as appropriate. The displacement thickness d was included in the denominator of the equation in the calculations of the empirical values. The estimates of observed e at 10 m will be somewhat in error due to the diabatic conditions associated with some of the observations. The value of e, which is dissipation of mean-motion energy, may be considered equivalent to the local rate ϵ of turbulent energy dissipation if it is assumed that the convective eddy energy production and flux divergence of eddy energy are negligibly small, or that the two cancel each other.

Reasonable agreement with the theory is indicated in the illustrations; of course, the observations cover a substantial range of wind speeds and normalized representations would have been preferable. The estimates of e near the ground are fairly large during the daytime; this is due to the larger surface stresses for unstable conditions. Both sets of profiles indicate a tendency for e to decrease somewhat faster with height than predicted by the theoretical model.

10.5 Comparison of Results of Airborne and Surface-Based Measurements

From his airborne measurements of turbulent wind and temperature fluctuations, Lenschow (1965) has computed estimates of the local rate of energy dissipation, the Reynolds stress τ, and the vertical heat flux H from the relations

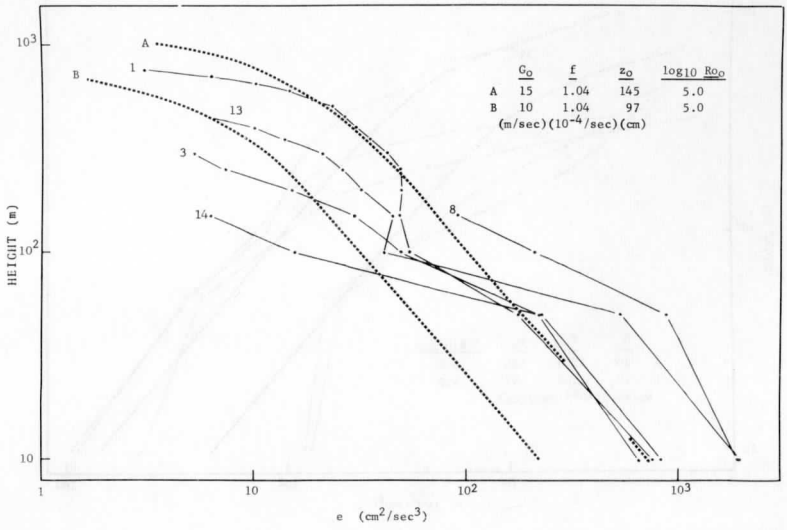

FIG. 28. Height variation of local rate e of mechanical eddy energy production, for daytime observations. The individual profiles are identified by group number. The theoretical (dashed) curves are from Lettau's (1962) model for the indicated values of surface geostrophic wind speed G_0, Coriolis parameter f, aerodynamic roughness length z_0, and the resulting surface Rossby number Ro_0.

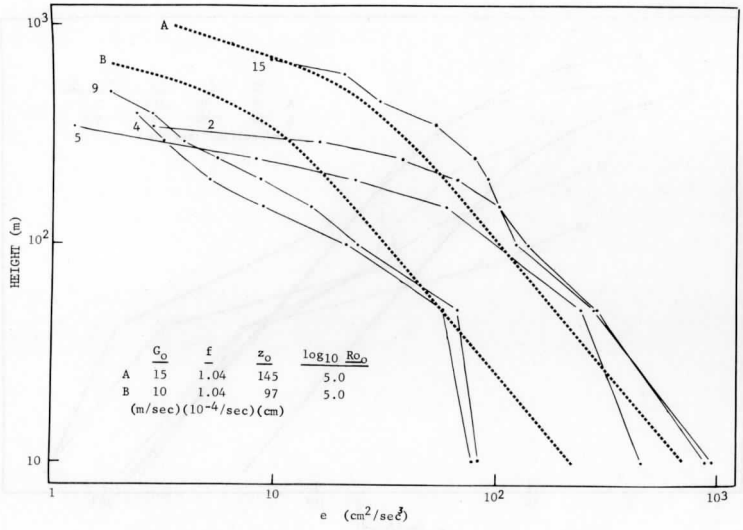

FIG. 29. Height variation of local rate e of mechanical eddy energy production, for nocturnal observations. The individual profiles are identified by group number. The theoretical (dashed) curves are from Lettau's (1962) model for the indicated values of surface geostrophic wind speed G_0, Coriolis parameter f, aerodynamic roughness length z_0, and the resulting surface Rossby number Ro_0.

$$F(n) = c\,\epsilon^{2/3}\,n^{-5/3}, \tag{10.4}$$

$$\tau = -\rho\,\overline{u'w'}, \tag{10.5}$$

$$H = \rho c_p\,\overline{w'T'}. \tag{10.6}$$

Here $F(n)$ is the spectrum function in the inertial subrange; n is the wave number; c is a constant taken equal to 0.47, following Panofsky and Pasquill (1963); and u', w' and T' represent horizontal and vertical wind fluctuations and temperature fluctuations, respectively. The estimates of these parameters derived from the concurrent surface-based and airborne measurements are compared in Table 11.

Since the instrumentation on the aircraft essentially provides only information to compute the stress component in the direction the airplane is travelling, the angle θ between the aircraft heading and the direction of the stress vector obtained from the wind-profile analysis was applied to each value of τ_b to yield a more valid comparison. The stress estimates to be compared, then, are τ_a and $\tau_b \cos\theta$. Although certain sets of values agree fairly well, others show discrepancies. It should be noted here, however, that the comparisons for group-period 15 are not really conclusive, since aircraft measurements were made during only one of the balloon series.

The vertical heat flux estimates for groups 14 and 16 decrease fairly systematically with height, as might be expected. The aircraft data for group 11 were not sufficient for evaluation of the heat flux, hence no estimates are given. Values of convective eddy energy production e_c were found from H_b and H_a by using Eq. (2.29). The estimates e, ϵ, and e_c furnish three terms of the eddy energy balance equation, the remainder being the flux divergence. For group-periods 14 and 16, the dissipation at the higher levels is greater than the local production, hence a flux of eddy energy is required from below. A comparison of e and e_c at the three levels demonstrates that convective eddy energy production becomes relatively more important with increasing height.

11. Summary and Concluding Remarks

The fundamental purpose of this investigation was to add, if only in a modest way, to our store of knowledge concerning the structure of the atmospheric boundary layer, particularly over a relatively rough surface as represented by tall vegetation. An experimental program was carried out over the extensively forested region of northeastern

TABLE 11

Comparison of results of airborne and surface-based measurements at Lakewood site during last three observational periods. The meanings of the symbols are as follows: G_0, surface geostrophic wind speed derived from wind-profile analysis; τ_b and τ_a, stress estimates from balloon and aircraft data; θ, angle between the direction of $\vec{\tau}_b$ and aircraft heading; e, estimated rate of mechanical generation of eddy energy from surface-based measurements; ϵ, local rate of viscous energy dissipation derived from airborne measurements; H_b and H_a, vertical heat flux estimates from surface-based and airborne data; and e_c, rate of convective generation of eddy energy computed from the values of heat flux. The airborne measurements were obtained and analyzed by Lenschow (1965).

Group No.	Mean CST	Date	G_0	Ht.	τ_b	τ_a	θ	$\tau_b \cos\theta$	e	ϵ	H_b	H_a	e_c
				10	3.1	--	--	--	306	--	0.062	--	15
11	1516	31 Mar 64	6.0	170	2.5	1.6	75	0.7	4	144	--	--	--
				470	1.7	-0.1	81	0.3	3	100	--	--	--
				10	3.8	--	--	--	647	--	0.181	--	39
14	1117	8 Jun 64	11.1	170	3.1	0.6	48	2.1	4	96	--	0.039	9
				470	2.2	1.0	69	0.8	9	30	--	-0.010	-2
				10	4.5	--	--	--	940	--	-0.097	--	-21
15*	2034	8 Jun 64	17.5	170	2.8	0.5	34	2.3	98	48	--	0	0
				470	1.5	-0.5	76	0.4	29	12	--	0.025	6
				10	1.6	--	--	--	214	--	0.121	--	26
16	1149	10 Jun 64	5.7	170	1.1	1.6	5	1.1	1	76	--	0.090	20
				470	0.7	1.4	42	0.5	1	68	--	0.021	5
			(m/sec)	(m)	(dyne/cm)		(deg)	(dyne/cm^2)	(cm^2/sec^3)		(ly/min)	(cm^2/sec^3)	

*Airborne measurements were made only in conjunction with the first of the two balloon series within this group-period.

Wisconsin; pilot-balloon observations provided a total of 209 usable, detailed wind profiles for the lowest 2 km of the atmosphere. Supplementary low-level measurements of wind, temperature and net radiation permitted the estimation of surface heat-budget parameters, as well as atmospheric stability and aerodynamic surface roughness length, which aided in the interpretation of the results of the wind-profile analysis. Also used were boundary-layer temperature profiles obtained by means of an instrumented aircraft and from routine radiosonde ascents at a USWB station located at Green Bay, which is in the same section of the state.

Profiles of geostrophic wind computed directly from surface and upper-air pressure and temperature measurements, although apparently rather inaccurate, were of some utility. For the most part, however, the wind-profile analysis was based on a modified version of Lettau's "antitriptic" method, which, incidentally, could perhaps be more adequately specified as a "geotriptic" method. The basic technique permits the indirect determination of geostrophic wind profiles under the assumption of height-independent thermal wind. The modification essentially involves the treatment of baroclinic wind profiles as barotropic profiles upon which thermal winds are simply superimposed. The modified method was found to give acceptable results for all advection regimes, while the basic method frequently fails when the effects of cold-air advection are dominant in the wind profiles.

From the analysis of the Lakewood wind profiles, estimates at low surface Rossby numbers were derived for the boundary-layer parameters of surface stress (τ_0), geostrophic drag coefficient (C), total rate of energy dissipation (E), and angle between low-level wind and isobars (α_0). Fairly good agreement with theory for neutral conditions was indicated in most instances. It was found that C, τ_0 and E showed pronounced diurnal variations, with maximum values occurring near the time of maximum surface heating, confirming previous observations and theory. Seasonal changes in the character of the vegetation due to variations in tree foliation had significant effects on low-level wind structure; however, data were insufficient to separate any such dependencies of the boundary-layer parameters upon surface roughness from the effects of seasonally varying stability.

The Lakewood observations demonstrated again the close association of wind and temperature structure in the boundary layer. Nocturnal low-level wind maxima typically occurred near the tops of temperature inversions; the directions of these "jets" were such that Lettau's (1964) terrain-slope mechanism also appeared to be operative.

Marked changes in daytime wind structure were often associated with upper-level inversions, which in turn exhibited diurnal height variations. Additionally, pronounced reductions in balloon ascent rates at and above the inversions were evident, indicating possible changes in balloon drag coefficients caused by differing turbulence regimes. An evaluation of the relative behavior of smooth and artificially roughened balloons gave evidence supporting this view, indicating that ascribing height changes of balloon ascent rates to real vertical air motions is questionable. On the other hand, the evaluation disclosed that only very small errors in the horizontal mean wind profiles obtained in this study can be expected from the spurious, aerodynamically induced motions of the smooth pilot balloons.

The wind-profile analysis method employed in this investigation furnished results which are generally acceptable, but further work should be done in an attempt to establish a firm theoretical basis for the assumptions used. The baroclinic model developed by Blackadar (1963) assumes strict gradient-type momentum transfer, and gives profiles of exchange coefficient which differ according to the direction of the thermal wind. However, Appleby and Ohmstede (1964) make the following statement:

> It would seem for the case of constant thermal wind, the (barotropic) boundary layer model in terms of the deviation of the wind from the geostrophic wind would remain valid. Consequently, except for extreme thermal wind, it is likely that the baroclinic model can be approximated by inclusion of thermal wind in the barotropic model. The validity of this postulate remains a matter to be tested.

In a sense, this test has been performed in this investigation.

Similar observational programs of wind structure at small surface Rossby numbers should be carried out over other "rough" areas, such as cities. Some work of this type is now in progress at the USWB, utilizing tetroon flights and instrumented towers, but more extensive and detailed observations are needed to provide a basis for more realistic air-pollution models. Through these and additional studies of the structure of the atmospheric boundary layer under a wide range of conditions, a fuller understanding of the relationships linking micrometeorology to synoptic meteorology should be achieved.

12. Acknowledgments

This investigation was carried out under the supervision of Professor Heinz H. Lettau; to him I would like to extend my sincere appreciation for his expert advice, kind guidance, and selfless allocation of time for discussions. I am also indebted to Mr. Ken P. Butterfield, Supervisor, Nicolet National Forest, for his kind permission to modify and use the Archibald fire-lookout tower; the cooperation of District Ranger Cliff Crosby of the Lakewood District was also instrumental in the success of the observational program. In this regard, special thanks are extended to Mr. Fred Alyea for his conscientious efforts in the lonely job of observer at theodolite station two.

I would like to thank Mr. Warren Knapp and Mr. Charles Stearns of the Department of Meteorology, whose technical advice on some of the instrumentation used in the study was quite helpful. Mr. Marvin Burley and Mr. Steven J. Rigney of the U. S. Weather Bureau kindly provided some of the synoptic data needed; appreciation is also extended to Dr. Peter Kuhn and Mr. Kirby Hanson of the Bureau for their efforts in securing the loan of the microbarographs employed during part of the investigation. Special thanks are due to Mr. Donald Lenschow of the Department of Meteorology, whose airborne measurements, particularly those of temperature profiles, contributed substantially to the investigation. Miss Carol Graf did a very commendable job of typing the thesis. The able assistance of Mr. Edward Hilbert in preparing the figures and in performing some of the computations has also been much appreciated.

I would like to express my sincere gratitude to my wife, Ena, whose encouragement and patient understanding of a graduate student's problems have been vital to the completion of this work.

This research has been supported by the Meteorology Department of the U. S. Army Electronics Research and Development Activity, Fort Huachuca, Arizona. In addition, a Graduate Student Fellowship was provided by the Ford Foundation, and is gratefully acknowledged.

REFERENCES

Angell, James K., 1964: Use of tetroons to investigate the kinematics and dynamics of the planetary boundary layer. Mon. Wea. Rev., 92, 465-470.

Appleby, J.F., and W.D. Ohmstede, 1964: Numerical solution of the distribution of wind and turbulence in the planetary boundary layer. Meteorological Research Notes No. 8, Meteor. Dept., USAERDA, Ft. Huachuca, Arizona.

Arnold, A., 1948: On the accuracy of winds aloft at low altitudes. Bull. Amer. Meteor. Soc., 29, 140-141.

Ball, F.K., 1960: Control of inversion height by surface heating. Quart. J. R. Meteor. Soc., 86, 483-494.

Barad, Morton L., 1961: Low-altitude jet streams. Sc. Amer., 205, 120-131.

Barnett, Kenneth M., and Omer Clarkson, Jr., 1965: The relation of time interval to the accuracy of double theodolite observations. Unpublished manuscript, to be presented at 239th Nat. Meeting of the Amer. Meteor. Soc., June 21-25, 1965, Riverside, Calif.

Baumgartner, A., 1956: Untersuchen über den Wärme-u. Wasserhaushalt eines jungen Waldes. Ber. Deutschen Wetter Dienstes, 5, No. 28.

Bellamy, J.C., 1945: The use of pressure altitude and altimeter corrections in meteorology. J. Meteor., 2, 1-79.

Bernstein, Abram B., 1959: The effect of a horizontal temperature gradient on the surface wind. M.S. thesis, Pennsylvania State Univ., 112 pp.

Blackadar, A.K., 1957: Boundary layer wind maxima and their significance for the growth of nocturnal inversions. Bull. Amer. Meteor. Soc., 38, 283-290.

Blackadar, A.K., 1962: The vertical distribution of wind and turbulent exchange in a neutral atmosphere. J. Geophys. Res., 67, 3095-3102.

Blackadar, A. K., 1963: The vertical distribution of wind in a baroclinic adiabatic atmospheric boundary layer. Presented at 211th Nat. Meeting of the Amer. Meteor. Soc., Jan. 21-24, 1963.

Bonner, William D., 1965: Statistical and kinematical properties of the low-level jet stream. Res. Paper 38, Satellite and Mesometeor. Res. Proj., Dept. of Geophys. Sc., Univ. of Chicago, 54 pp.

Bunker, A. F., 1956: Measurements of counter-gradient heat flows in the atmosphere. Austral. J. Phys., 9, 100.

Cave, C. J. P., and J. S. Dines, 1919: Further measurements on the rate of ascent of pilot balloons. Quart. J. R. Meteor. Soc., 45, 277-282.

Charnock, H., J. R. D. Francis and P. A. Sheppart, 1956: An investigation of wind structure in the Trades: Anegada 1953. Phil. Trans. R. Soc. London, 249A, 179-234.

Ching, Jason K. S., 1964: A theory of wind distribution in a single-layered diabatic baroclinic turbulent boundary layer of the atmosphere. M. S. thesis, Pennsylvania State Univ., 65 pp.

Dabberdt, Walter F., 1965: Personal communication. Unpublished work in progress at Dept. of Meteor., Univ. of Wisconsin.

De Jong, H. M., 1964: Application of the theory of adjustment to double theodolite observations. J. Appl. Meteor., 3, 624-632.

Dines, J. S., 1913: Rate of ascent of pilot balloons. Quart. J. R. Meteor. Soc., 39, 101-107.

Dryden, H. L., F. D. Murnaghan and H. Bateman, 1956: Hydrodynamics. New York, Dover Publications, 634 pp.

Dutton, John A., and Donald H. Lenschow, 1962: An airborne measuring system for micrometeorological studies. Sec. 5 of Studies of the Three-Dimensional Structure of the Planetary Boundary Layer, Dept. of Meteor., Univ. of Wisconsin. Final Report, Contract DA-36-039-SC-80282, USAEPG, Ft. Huachuca, Arizona.

Dyer, A. J., 1963: The adjustment of profiles and eddy fluxes. Quart. J. R. Meteor. Soc., 89, 276-280.

Estoque, Mariano A., 1963: A numerical model of the atmospheric boundary layer. J. Geophys. Res., 68, 1103-1113.

Franssila, M., 1936: Mikroklimatische Unteruchungen des Wärmehaushalts. Mitt. Met. Zentralanstalt Helsinki, 20, 1-103.

Frost, R., 1940: The rate of ascent of free balloons, Quart. J. R. Meteor. Soc., 66, 367-369.

Geiger, Rudolph, 1965: The Climate Near the Ground. Cambridge, Harvard University Press, 611 p.

Hesselberg, T., and B. J. Birkeland, 1917: Über die Steigegeschwindigkeit der Pilotballone. Ann. Hydrog., 45, 313. (Abstract by J. S. Dines in Quart. J. R. Meteor. Soc., 44, 1918, 131.)

Hoecker, Walter H., Jr., 1963: Three southerly low-level jet systems delineated by the Weather Bureau special pibal network of 1961. Mon. Wea. Rev., 91, 573-582.

Holopainen, Eero O., 1963: On the dissipation of kinetic energy in the atmosphere. Tellus, 15, 26-32.

Jeffreys, Harold, 1922: On the dynamics of wind. Quart. J. R. Meteor. Soc., 48, 29-46.

Johnson, Warren B., Jr., 1962: Climatology of atmospheric boundary-layer parameters and energy dissipation, derived from Gregg's aerological survey of the U. S. Sec. 7 of Studies of the Three-Dimensional Structure of the Planetary Boundary Layer, Dept. of Meteor., Univ. of Wisconsin. Final Report, Contract DA-36-039-SC-80282, USAEPG, Ft. Huachuca, Arizona.

Kung, Ernest C., 1961: Derivation of roughness parameters from wind profile data above tall vegetation. Sec. 3 of Studies of the Three-Dimensional Structure of the Planetary Boundary Layer, Dept. of Meteor., Univ. of Wisconsin. Annual Report, Contract DA-36-039-SC-80282, USAEPG, Ft. Huachuca, Arizona.

Kung, Ernest C., and Heinz H. Lettau, 1961: Regional and meridional distribution of continental vegetation cover and aerodynamic roughness parameters. Sec. 5, ibid.

Kung, Ernest C., 1963: Climatology of aerodynamic roughness parameter and energy dissipation in the planetary boundary layer over the Northern Hemisphere. Sec. 2 of Studies of the Effects of Variations in Boundary Conditions on the Atmospheric Boundary Layer, Dept. of Meteor., Univ. of Wisconsin. Annual Report, Contract DA-36-039-AMC-00878, USAERDA, Ft. Huachuca, Arizona.

Lenschow, Donald H., 1965: Airborne measurements of the structure of the atmospheric boundary layer. Unpublished Ph. D. thesis in progress, Dept. of Meteor., Univ. of Wisconsin.

Lettau, H. H., 1939: Atmosphärische Turbulenz. Leipzig, Akademische Verlagsgesellschaft, 283 pp.

Lettau, H. H., 1950: A re-examination of the "Leipzig Wind Profile" considering some relations between wind and turbulence in the frictional layer. Tellus, 2, 125-129.

Lettau, H. H., 1957a: Computation of Richardson numbers, classification of wind profiles, and determination of roughness parameters. Sec. 7.4 in Vol. I of Exploring the Atmosphere's First Mile (H. Lettau and B. Davidson, eds.), New York, Pergamon Press, 376 pp.

Lettau, H. H., 1957b: Windprofil, innere Reibung und Energieumsatz in der unteren 500 m über dem Meer. Beitr. Phys. d. Atmos., 30, 78-96.

Lettau, H. H., 1959a: Wind profile, surface stress and geostrophic drag coefficients in the atmospheric surface layer. In Atmospheric Diffusion and Air Pollution, pp. 241-256 (F. N. Frenkiel and P. S. Sheppard, eds.), Vol. 6 of Advances in Geophysics, New York, Academic Press.

Lettau, H. H., 1959b: Research Problems in Micrometeorology, Dept. of Meteor., Univ. of Wisconsin. Final Report, Contract DA-36-039-SC-80063, USAEPG, Ft. Huachuca, Arizona.

Lettau, H. H., 1961: Dissipation of energy by turbulence. J. Meteor., 18, 125-126.

Lettau, H. H., 1962: Theoretical wind spirals in the boundary layer of a barotropic atmosphere. Beitr. Phys. d. Atmos., 35, 195-212.

Lettau, H. H., 1964: Preliminary note on the effects of terrain slope on low-level jets and thermal winds in the planetary boundary layer. Sec. 4 of Studies of the Effects of Variations in Boundary Conditions on the Atmospheric Boundary Layer, Dept. of Meteor., Univ. of Wisconsin. Annual Report, Contract DA-36-039-AMC-00878, USAERDA, Ft. Huachuca, Arizona.

Lettau, H. H., and Heinrich Hoeber, 1964: Über die Bestimmung der Höhenverteilung von Schubspannung und Austauschkoeffizient in der atmosphärischen Reibungsschicht. Beitr. Phys. d. Atmos., 37, 105-118.

Ludlam, F. H., 1953: The rate of rise of pilot balloons. Meteor. Mag., 82, 306-308.

Lumley, John L., and Hans A. Panofsky, 1964: The Structure of Atmospheric Turbulence. New York, John Wiley and Sons, Inc., 239 pp.

McVehil, G. E., R. J. Pilié and G. A. Zigrossi, 1965: Some measurements of balloon motions with Doppler radar. J. Appl. Meteor., 4, 146-148.

MacCready, Paul B., Jr., 1964: Comparison of some balloon techniques. Unpublished manuscript.

Moses, Harry, and Hugh G. Daubek, 1961: Errors in wind measurements associated with tower-mounted anemometers. Bull. Amer. Meteor. Soc., 42, 190-194.

Murrow, Harold N., and Robert M. Henry, 1965: Self-induced balloon motions. J. Appl. Meteor., 4, 131-138.

National Meso-Micrometeorological Facility Survey Group, 1964: Meso-micrometeorological requirements for the atmospheric sciences. Nat. Center for Atmos. Res. Tech. Notes 64-2.

Panofsky, H. A., and F. Pasquill, 1963: The constant of the Kolmogorov law. Quart. J. R. Meteor. Soc., 89, 550-551.

Priestley, C. H. B., and W. C. Swinbank, 1947: Vertical transport of heat by turbulence in the atmosphere. Proc. R. Soc. London, A 189, 543.

Priestley, C. H. B., 1959: Turbulent Transfer in the Lower Atmosphere. Chicago, University of Chicago Press, 130 pp.

Richardson, L. F., 1920: Some measurements of atmospheric turbulence. Phil. Trans. R. Soc. London, 221A, 1-28.

Sangster, Wayne E., 1960: A method of representing the horizontal pressure force without reduction of station pressures. J. Meteor., 17, 166-176.

Schlichting, H., 1955: Boundary Layer Theory. New York, McGraw-Hill Book Co., Inc., 535 pp.

Schneider-Carius, K., 1953: Die Grundschicht der Troposphere. Leipzig, Akademische Verlagsgesellschaft, 168 pp.

Scoggins, James R., 1964: Aerodynamics of spherical balloon wind sensors. J. Geophys. Res., 69, 591-598.

Scoggins, James R., 1965a: Status of Jimsphere development. Bull. Amer. Meteor. Soc., 46, 21.

Scoggins, James R., 1965b: Spherical balloon wind sensor behavior. J. Appl. Meteor., 4, 139-145.

Shapiro, Ascher H., 1961: Shape and Flow, The Fluid Dynamics of Drag. New York, Doubleday and Co., Inc., 186 pp.

Sheppard, P. A., and M. H. Omar, 1952: The wind stress over the ocean from observations in the Trades. Quart. J. R. Meteor. Soc., 78, 583-589.

Sheppard, P. A., H. Charnock and J. R. D. Francis, 1952: Observations of westerlies over the sea. Quart. J. R. Meteor. Soc., 78, 563-582.

Smithsonian Meteorological Tables, 1963: Washington, The Smithsonian Institution, Robert J. List, ed., 527 pp.

Suomi, V. E., and P. M. Kuhn, 1958: An economical net radiometer. Tellus, 10, 160-163.

Sutcliffe, R. C., 1936: Surface resistance in atmospheric flow. Quart. J. R. Meteor. Soc., 62, 3-12.

Taylor, G. I., 1916: Skin friction of the wind on the earth's surface. Proc. R. Soc. London, A92, 196-199.

Taylor, R. J., 1963: An analysis of some wind profiles in the atmospheric friction layer. Report No. AFCRL-63-861, AF Cambridge Research Laboratories, Bedford, Mass.

Thyer, Norman, 1962: Double theodolite pibal evaluation by computer. J. Appl. Meteor., 1, 66-68.

U. S. Forest Service, 1951: Timber survey, Nicolet National Forest, Wis.

White, R. M., and B. Saltzman, 1956: On conversions between potential and kinetic energy in the atmosphere. Tellus, 8, 357-363.

Wisconsin Conservation Dept., 1957: Forest resources of Oconto County. Wisconsin Forest Inventory, Pub. No. 30.

Scanner's note:

This page is blank.

4

AIRBORNE MEASUREMENTS OF ATMOSPHERIC BOUNDARY LAYER STRUCTURE*

Donald H. Lenschow
Department of Meteorology
University of Wisconsin

ABSTRACT: Measurements of vertical and horizontal velocity, air and surface temperature, absolute humidity and incoming and reflected solar radiation within the atmospheric boundary layer, were obtained from a Cessna 310, a twin-engine, 3-passenger airplane, with a cruising speed of 75 m/sec and a range of 1100 km. Nine series of measurements were taken simultaneously with balloon measurements of the mean wind profile over the forest region of Northeastern Wisconsin during early spring and summer, and a series of ten flights were made to measure air mass modification over Lake Michigan, all but two of them during cold air outbreaks in winter.

Airborne measurements of horizontal velocity and temperature in the atmospheric boundary layer are filtered with a digital approximation to an RC high-pass filter, so that they conform in phase and amplitude to the recorded vertical velocity fluctuations. Variances and cross-products of these variables are computed for wavelengths between 28 and 1400 m. About 50 percent of the actual vertical fluxes are found to be included in this bandwidth at heights between 180 and 500 m above the ground. Spectral and co-spectral densities are computed for these variables for 40 wave number intervals. The Kolmogorov hypothesis is used to obtain the rate of kinetic energy dissipation from the structure function of horizontal velocity for a lag of 112 m.

Estimates of vertical velocity variance from balloon measurements are larger than from airplane measurements for unstable

*This work is part of a thesis submitted to the University of Wisconsin in partial fulfillment of the requirements for the Ph. D. degree, written under the supervision of Professor H. Lettau, Department of Meteorology.

conditions and smaller for stable conditions. The spectral densities of velocity and temperature have a slope of -5/3, with the exception of measurements under stable conditions when the horizontal velocity spectrum slope is -2.1. Under stable conditions, it is suggested that the airplane does not measure strictly turbulent fluctuations at the long wavelengths, which would account for the steep negative slope of the spectra and an apparent vertical heat flux. A turbulent kinetic energy budget is calculated; no evidence of a significant vertical transport of kinetic energy up to the inversion level is noted.

Over Lake Michigan, the slope of the spectral density curves is -5/3, except when the wind shear is small, under which conditions the slope is about -2.0. Measurements of the upward heat flux at 350 m and the change in sensible heat above 350 m over the lake are used to estimate the amount of water condensation in the modified air. Long-wave radiation flux divergence is calculated by means of the technique of isothermal flux emissivities. The total sensible and latent heat flux through the downwind boundary of the lake is about 690 ly/day; about 20 percent of this is latent energy. These values are about one-half of what has been estimated in similar studies over the ocean, probably due to the lower surface temperature of the lake (about 4 C, as compared to ocean temperatures of up to 10 C).

1. INTRODUCTION

Micrometeorological investigations utilizing an airplane as a measuring platform have been conducted previously, with few exceptions, without detailed knowledge of conditions at the lower boundary or of mean wind profiles through the boundary layer. As Lettau (1959) points out, "Only when the topographical features of the site and its neighborhood, the subsoil type, the surface cover, and also the weather type including over-all wind speed (or large-scale horizontal pressure gradient), energy supply (or insolation and longwave or net radiation fluxes, etc.), are determined, can the collection of micrometeorological or atmospheric turbulence data lead to conclusive and reproducible results."

Bunker (1957) measured vertical fluxes of heat and momentum from an airplane by means of the average cross-products, $\overline{w'T'}$ and $\overline{w'u'}$, along with the RMS values of the variables w', T', and u' during the Great Plains Turbulence Field Program at O'Neill, Nebraska, and therefore, not only had detailed measurements of the boundary conditions at his disposal, but also was able to compare his results with independently

measured values of the same parameters. His vertical velocity measurements were obtained by measuring the vertical acceleration of the airplane and horizontal air speed fluctuations. Bunker points out, however, that errors are present in such a system because of phugoid oscillations, airplane deformation and unsteady lift.

Airborne measurements of vertical and horizontal velocity fluctuations and the corresponding spectral density functions have been reported more frequently than measurements of $\overline{w'T'}$ and $\overline{w'u'}$ and the corresponding co-spectral densities. Lappe et al. (1959) compared simultaneous tower and airplane measurements of horizontal and vertical turbulence spectra with an airborne system similar to the one used here. Myrup (1965), again with a similar system, measured the structure of turbulence in the lower atmosphere under extremely unstable conditions. Warner and Telford (1962) obtained velocity fluctuations and wet bulb temperatures associated with convective clouds and (1963) measured vertical velocity and air temperature fluctuations over grassland, forest and sea to determine convective patterns from 10 to 300 m above the surface. Telford and Warner (1964) also estimated heat and water vapor flux from airplane data, and, in one case, computed the co-spectral density of $\overline{w'T'}$.

One of the most important parameters of the boundary layer is the rate of generation of turbulent kinetic energy and its conversion to internal and potential energy of the atmosphere. Therefore, a discussion of the methods used to compute this parameter by application of the Kolmogorov similarity hypothesis is included. A comparison is made between the dissipation values obtained from the structure function formulation of the similarity hypothesis and the spectral density formulation.

Few attempts have been made to compare results obtained from an analysis of wind profiles in the boundary layer with simultaneous airplane fluctuation measurements. Charnock et al. (1956) compared values of stress derived from mean wind profiles with values estimated from velocity fluctuations measured by balloon ascents in the Atlantic trade wind region. Simultaneous airplane measurements of stress and turbulence were made by Bunker (1955) in the same locality. A more detailed comparison between the results of airplane measurements and balloon measured mean wind profiles (see the preceding paper by W. Johnson) is presented here, in an attempt to tie together the two basically different approaches to the problem of describing the characteristics of the planetary boundary layer.

Bunker (1955 and 1960) also measured sensible heat and water vapor fluxes over the North Atlantic Ocean to study air mass modification.

Earlier airplane air mass modification measurements were made by Craig (1949) who measured changes in temperature and humidity downwind in a warm air mass passing over a cold ocean bay, and made estimates of eddy diffusivity from the airplane measurements and from wind data. Craig (1946) also investigated the heating of cold air by warmer ocean water.

Most studies of air mass modification have been based primarily on information from atmospheric soundings. Lettau (1944) studied the air modification of two very cold arctic outbreaks from Greenland, out over the Atlantic, to Northwestern Europe. Craddock (1951) studied a series of polar air mass outbreaks off the coast of Northwestern Europe, and Manabe (1957) similar cold air outbreaks over the Sea of Japan. A more complete discussion and list of references of air mass modification studies is presented by Roll (1965). On a smaller scale, Super (1965) has studied air mass modification within 3 m of the surface by measuring horizontal variations of temperature, humidity and wind profiles from a boat crossing a lake 10 km in diameter.

It would be desirable, in airborne studies of air modification, to combine the measurement of atmospheric soundings with measurements of horizontal variations over a scale that is large enough in space and time to eliminate the effect of individual convective-size eddies, on the order of 1 km, by an averaging process, and yet small enough so that large-scale synoptic changes do not occur during the time and over the path of measurement. From the standpoint of airplane measurements, a scale on the order of 100 km would seem to be a reasonable compromise. Such a scale is provided by Lake Michigan. Therefore, a series of airplane measurements was made of air mass modification over the lake during mid-winter cold air outbreaks, in the winter of 1964-65, in an attempt to provide a link between small scale air modification experiments and continental, or oceanic modification studies.

2. Significant Aspects of Turbulence and Boundary Layer Theory

2.1 Equations for Airborne Measurements

One of the most important parameters that must be taken into account in attempting to fit turbulence measurements into any kind of theoretical framework is the hydrostatic stability of the atmosphere. Unfortunately, the most commonly used stability indicator, the "gradient" Richardson number,

$$\underline{Ri} = (g/T_0)((\partial\theta/\partial z)/(\partial V/\partial z)^2), \quad (1)$$

where g = gravity, T = absolute temperature, V = wind speed, and θ = potential temperature, is impossible to measure with instruments now in the airplane. Furthermore, in the usual daytime situation at flight altitudes, the denominator of $\underline{Ri}$ is very small, as compared to tower measurements within 50 m of the ground. The same holds true for the "flux" Richardson number, the ratio of the rate of change of energy due to buoyancy to the rate of energy production by the wind shear, given by

$$\underline{RI} = (g/T_0)(\overline{w'T'})/(\overline{u'w'}\partial V/\partial z). \quad (2)$$

$\underline{RI}$ is equal to $\underline{Ri}$ if the coefficients of eddy diffusivity are the same for the vertical transport of heat and momentum.

Theoretical justification for the use of the Richardson number as a measure of stability is conventionally derived from the diffusion equation for turbulent kinetic energy. Taylor (1952) and Panofsky (1962) have found that near the ground energy production by wind shear is approximately equal to the energy dissipation. Therefore, near the ground (2) becomes

$$\underline{RI} \cong (g/T_0)(\overline{w'T'})/\epsilon \quad (3)$$

where ϵ = kinematic value of the energy dissipation rate. $\underline{RI}$ is the measure of stability used here for airplane measurements. Above the surface, the energy dissipation decreases rapidly with height, but for unstable conditions, the buoyant energy production makes the energy dissipation term larger than the production of energy by wind shear, so that the absolute value of the actual Richardson number will be greater than (3). The advantages of (3) for airplane measurements are that it can be determined solely from airplane measurements and the denominator will not, within the planetary boundary layer, become very much smaller than the numerator.

2.2 Energy Dissipation

A variety of techniques have been utilized to obtain estimates of energy dissipation in the atmosphere. Lettau (1961) and Ball (1961) present summaries of most of the measurements and techniques of measurements up to 1961. Other than diffusion experiments, the estimates of dissipation are based either on equating the energy dissipation to the energy production minus energy diffusion, or, on utilization

of Kolmogorov's similarity hypothesis. In his original paper, Kolmogorov (1941a) presents his similarity hypothesis in terms of the structure functions,

$$B_{dd} = \overline{|u(x+r) - u(x)|^2}; \quad B_{nn} = \overline{|v(x+r) - v(x)|^2}, \tag{4}$$

where "r" is a distance measured along the "x" axis. He assumed that for some range of values of "r," called the inertial subrange, the turbulence is isotropic and the structure functions are functions only of energy dissipation and, therefore, must be of the form $B \sim (\epsilon r)^{2/3}$. Following Batchelor (1953), this function can be transformed by a Fourier transformation to the spectral density function,

$$E(k) = a\epsilon^{2/3} k^{-5/3} \tag{5}$$

where "k" is wave number in rad/cm, E(k) is the spectral density of the longitudinal velocity, and "a" is a universal constant. This procedure also gives the numerical factor relating the spectral density to the structure function, so that

$$B_{dd} = 4.02a \cdot (\epsilon r)^{2/3}. \tag{6}$$

The value of the constant "a" in (5) and (6) has been the subject of much discussion and revision, and has not yet been determined to a degree of precision that has universally satisfied investigators interested in utilizing these equations. MacCready (1953 and 1962), as well as Panofsky and Pasquill (1963), have critically examined, on the basis of measurements from various sources, the magnitude of this constant. At present, $a = 0.47$ appears to be the best estimate.

Although Kolmogorov's hypothesis has been quite generally considered to provide an adequate model for the inertial subrange of atmospheric turbulence, other models exist which predict different power laws. Kraichnan (1959) proposed for the spectral density function,

$$E_2(k) = a_2(\epsilon\sigma_u)^{\frac{1}{2}} k^{-3/2} \tag{7}$$

where $\sigma_u = (\overline{u'^2})^{\frac{1}{2}}$. The spectral density in (7) is a function of turbulence outside the inertial subrange, while Kolmogorov assumed the only effect of such turbulence is to advect the smaller eddies. Since the difference in the exponent of "k" between (5) and (7) is only 1/6, it is obviously difficult to use experimental evidence to decide which model is more realistic. Kraichnan and Spiegel (1962) later developed a mathematical model of turbulence that predicts a $-5/3$ exponent in the inertial subrange.

Other investigators, such as Proudman and Reid (1954) and Tatsumi (1957) have proposed models resulting in a wave number exponent of -2 for the spectral density in the inertial subrange. This differs by 1/3 from the -5/3 spectral density function, and so is more easily tested by experiment.

Various investigators have found that measurements of the spectral density in the isotropic region are close to predictions based on the -5/3 exponent. Pond et al. (1963) present probably the most significant evidence for the validity of the -5/3 hypothesis for atmospheric turbulence from hot-wire anemometer measurements over water. MacCready (1962) summarizes atmospheric spectra reported up to 1962, and has constructed a graph, based on this empirical evidence, to predict the maximum wave-length of the -5/3 region of the spectra as a function of height and stability for both vertical and horizontal turbulence. He estimates the maximum wavelength to be greater than 150 m at heights above 150 m. Lumley and Panofsky (1964) mention that Gurvich (1960) independently obtained a similar result. In addition, they state, "Only a few atmospheric spectra obtained from planes suggest different power laws (see, e.g., Press et al., 1956). In view of the overwhelming evidence for the correctness of the Kolmogorov spectra, these must be explained by improper instrumental response and, in a few cases, by the fact that the frequencies are not sufficiently high for the laws to be applicable." Lappe et al. (1959) utilized a turbulence measuring system similar to the system used here, and found the value of the exponent for their measurements between -5/3 and -2, with most measurements being closer to -5/3 than to -2.0.

2.3 Reynolds' Stress

The Reynolds' stress on a horizontal surface is defined by the two vector components,

$$\tau_x = -\rho \overline{u'w'}; \quad \text{and} \quad \tau_y = -\rho \overline{v'w'}. \tag{8}$$

Since it is possible to measure u' and w' with the airplane, the relationship between the measured and actual value of stress must be considered.

If u', v' and w' are the components of a velocity fluctuation, $\underset{\rightarrow}{V}'$, at some particular point in space and time, and u' is oriented along the axis of flight, then the airplane measurement of w' is independent of airplane direction, if the flight path is approximately horizontal.

The measured dynamic pressure is equal to the magnitude of the entire velocity vector, independent of direction, up to about 30° away from the major axis of the probe, in the particular case of the geometry of the probe used on the airplane; see Dean (1953).

Assume the airplane moves at a speed $\bar{u}_a$ with respect to the earth and with instantaneous velocity $\underset{\rightarrow}{V}$, with respect to the air. Then,

$$\underset{\rightarrow}{V} = (\bar{u}_a + u')\underset{\rightarrow}{i} + v'\underset{\rightarrow}{j} + w'\underset{\rightarrow}{k}, \tag{9}$$

If u'_a is the measured horizontal velocity fluctuation, and it is assumed that $|\underset{\rightarrow}{V}|/\bar{u}_a \cong 1 + u'/\bar{u}_a$, the simplified expression

$$u'_a = u' + (v'^2 + w'^2)/2\,\bar{u}_a \tag{10}$$

is obtained. It follows that

$$\overline{u'^2_a} = \overline{u'^2} + \overline{(v'^2 + w'^2)u'}/2\,\bar{u}_a \tag{11}$$

and

$$\overline{u'_a w'} = \overline{u'w'} + (\overline{v'^2 w'} + \overline{w'^3})/2\,\bar{u}_a. \tag{12}$$

The value of the second terms in the last two equations will be on the order of 1% of the first terms, for airplane speeds on the order of 70 m/sec, and thus can be neglected.

Redefining the direction of u' parallel to the mean wind, $\bar{u}$, the measured component of velocity, or more specifically, of dynamic pressure, in the direction of flight is given by

$$V = (2P_d/\rho)^{\frac{1}{2}} = \bar{u}_a - u'\cos\varphi - v'\sin\varphi, \tag{13}$$

where P_d is the measured dynamic pressure and φ is the angle of the airplane with respect to the mean wind. Since for Reynolds' stress only velocity fluctuations $V - \bar{u}_a$, are of interest, averaging the cross-products over a particular horizontal flight path produces

$$\overline{u'_a w'} = -\overline{u'w'\cos\varphi} - \overline{v'w'\sin\varphi}. \tag{14}$$

Hinze (1959, p. 252) presents the dynamic equations of non-isotropic turbulence for a simplified velocity regime in which $U = U(z)$, $V = W = 0$, and the turbulence is assumed homogeneous in the x and

y directions, but not necessarily in the z direction. He then states, "Because of the symmetry of the flow with respect to planes perpendicular to the y-direction, all correlations involving v and uneven derivatives with respect to y are zero. Hence all terms for the correlations $\overline{u'v'}$ and $\overline{w'v'}$, respectively, are zero." In the more general atmospheric case, the angle, φ, is not necessarily in the direction of the mean wind, but would also be a function of the change in wind direction with height. This represents the $\overline{u'w'}$ component of the Reynolds' stress tensor rotated on a horizontal plane by φ degrees.

3. Techniques of Measurement and Analysis

3.1 Description of Instruments

Most of the sensors used here have been described previously by Dutton and Lenschow (1962), and Lenschow (1962). Since then, two sensors have been added to the probe mounted on the front of the airplane. First, a platinum wire temperature probe (Rosemount Engineering Model No. 102E2AL), utilized as one arm of a Wheatstone bridge circuit, measures instantaneous total air temperature, with a time constant of less than 0.02 sec, and second, a differential pressure transducer (Statham Engineering, Inc., No. PM 283 TC) measures the difference between the static pressure and the dynamic pressure at the front of the airplane.

An error in terminology exists, however, in the section of the first report mentioned above evaluating the frequency response of the vertical velocity probe. The variable λ, on p. 95, is not frequency but angular velocity. Therefore, the actual vertical velocity, w, is related to the measured vertical velocity, w_m, by the equation,

$$w_m(\omega) = w(\omega) \cdot i\omega\tau/(1 + i\omega\tau) \qquad (15)$$

where ω is angular velocity and $\tau = RC$ is the time constant of the single-stage RC high-pass filter, equal to 3.0 sec for the system under consideration. The value of τ was selected to obtain the maximum amount of information without incurring significant errors due to gyro-drift and low frequency variations in airplane velocity and altitude. The problem of gyro-drift for this application is discussed by Kyser (1959). Although the single-stage RC high-pass filter is physically simple, inexpensive and inherently stable, it makes a relatively poor

filter for this application because its response varies slowly as a function of frequency. If the effective cut-off frequency is increased in order to eliminate low frequency errors, significant attenuation will take place at higher frequencies, or, conversely, if the effective cut-off frequency is decreased, low frequency errors may not be sufficiently attenuated. According to the analysis mentioned above, the system should accurately respond to gusts from 0.053 to 26.4 cycles/sec. Fig. 1 indicates that the high-pass filter does not completely attenuate frequencies lower than 0.053 cycles/sec. For this reason, a digital filter, as discussed in Section 3.2, was applied to several series of data to determine the effect of a sharper cut-off frequency on the values of $\overline{w'u'}$ and $\overline{w'T'}$.

The time response equation of the combined probe, differential pressure transducer and galvanometer system can be approximated by a linear, second-order equation of the form,

$$\ddot{P} + \gamma\dot{P} + \omega_0^2 P = F(t), \tag{16}$$

where $\gamma = 34\ \text{sec}^{-1}$ and $\omega_0 = 100$ rad/sec. The values of the two constants were determined by applying a pressure step function to the tip of the probe. These values result in an underdamped solution; consequently the system amplifies the actual pressure, but at frequencies well beyond frequencies of interest for calculations. This could possibly lead to aliasing, as described by Blackmann and Tukey (1958). To reduce this possibility, values of horizontal velocity were visually averaged over the higher frequencies as they were read out.

The horizontal velocity output was also used to change the output of the temperature probe to ambient air temperature by the relation

$$T_t - T_a = u^2/2c_p, \tag{17}$$

where T_t is the indicated temperature and T_a the ambient air temperature. Since the measured velocity is not the true horizontal velocity, it must be corrected before it can be used to obtain T_a. The relationship between pressure and velocity, for velocities significantly less than the speed of sound, is $u = (2P/\rho)^{\frac{1}{2}}$. The transducer is calibrated in terms of the air density, ρ_s, of a standard atmosphere at 1013.25 mb. Therefore, for other densities, $u = u_m(\rho_s/\rho)^{\frac{1}{2}}$, where u_m is the measured velocity. Expressing the correction factor, $(\rho_s/\rho)^{\frac{1}{2}}$, as a function of ambient air temperature, altitude, z, in km above MSL, and sea level pressure in mb,

$$u^2 = 3.52\, u_m^2 T(1 - 0.0226z)^{5.256}/P. \tag{18}$$

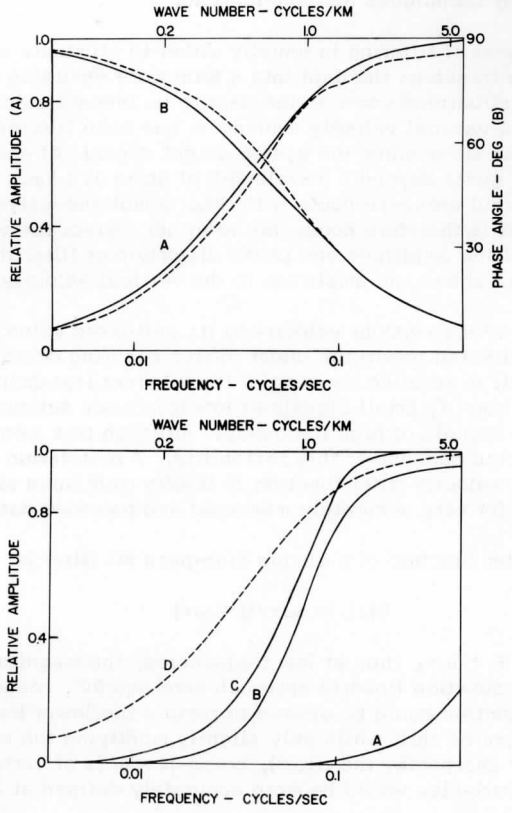

FIG. 1. Frequency response of high-pass filters. In top figure, dashed line is digital approximation to RC filter for $\Delta t = 0.2$ sec., "A" is relative amplitude and "B" is phase angle. In bottom figure, "A" is normal filter with $\sigma = 0.3$, "B" is response of "C" times digital approximation to high-pass filter, "C" is normal filter with $\sigma = 3.33$ and "D" is RC high-pass filter with RC = 3.0 sec.

3.2 Filtering Techniques and Applications

The object of filtering is usually either to eliminate extraneous noise, or to transform the data into a form more desirable for calculation. Both situations occur in the data to be investigated. The recorded output of the vertical velocity transducer has been filtered with a simple RC high-pass filter since the system is not capable of accurately measuring vertical gusts beyond a wavelength of about 1.4 km. In order to obtain meaningful cross-products with other simultaneously-measured variables, it is therefore necessary to either correct the vertical velocity for the resulting amplitude and phase distortion or filter the other variables to conform in phase and amplitude to the vertical velocity.

Restoring the vertical velocity to its unfiltered value may be feasible over a limited bandwidth under ideal measuring conditions, but is very difficult in practice because of the inherent instability involved in trying to amplify small signals of low frequency selectively, and add them to signals of high frequency. Although this method was tried, it was rejected because of this instability. A restoration technique for the vertical velocity filter function is briefly mentioned since it may be of value for very accurately measured and recorded data.

The filter function of a simple high-pass RC filter is

$$R(\omega) = i\omega\tau/(1 + i\omega\tau) \tag{19}$$

As $\omega \to 0$, $R \to i\omega\tau$; thus at low frequencies, the magnitude and phase of the filter function linearly approach zero and 90°, respectively. If the filter function could be altered to restore the lower frequencies and reduce the phase shift while only slightly modifying the cut-off frequency (effectively sharpening the filter), cross-products of vertical velocity with other variables would be more accurately defined at lower frequencies.

The inverse of the high-pass filter function is $R^{-1} = 1 - i/\omega\tau$. In order to approximate a solution to this function in the time domain for a discrete number of points separated by a time interval, Δt, the function, as shown, for example, by Holloway (1958), can be approximated by

$$R_t^{-1}(\omega, \Delta t) = \sum_{k=-n}^{n} w_k \cos \omega k \Delta t + i \sum_{k=-n}^{n} w_k \sin \omega k \Delta t, \tag{20}$$

where the w_k's are the discrete weights of the weighting function.

Since $R^{-1} = 1$ at $\omega = 0$ and $\{w_k : k > 0\} = 0$,

$$R_t^{-1} = 1 + \sum_{k=1}^{n} w_{-k} \cos\omega k\Delta t - i \sum_{k=1}^{n} w_{-k} \sin\omega k\Delta t. \quad (21)$$

The problem now is to select some technique for minimizing the difference between the actual inverse filter function, R^{-1}, and the series approximation for finite time intervals, R_t^{-1}. One simple method is to minimize the imaginary part of the difference by a Fourier series approximation. As an example, let $\Delta t = 0.2$ sec, and $\tau = 3.0$ sec. If $n = 60$ is used, the discrete values of the weighting function are

$$w_{-k} = (2/n) \sum_{i=1}^{n} (1/\omega\tau i)\sin(\pi ik/n) = (1/30) \sum_{i=1}^{60} (4/\pi i)\sin(\pi ik/60). \quad (22)$$

The Fourier series approximation is within 6% of the magnitude and 3% of the phase angle of the actual inverse filter function for $0.10 \leq f \leq 2.5$ cycles/sec.

The alternate approach is filtering the simultaneously measured variables with a digital approximation to the vertical velocity filter. This was found to be more successful for the measurements described here. Transforming (19) to the time domain,

$$w(t) = (1/2\pi) \int_{-\infty}^{\infty} e^{-i\omega t} d\omega - (1/2\pi) \int_{-\infty}^{\infty} 1/(1 + i\omega\tau) e^{-i\omega t} d\omega. \quad (23)$$

Substituting discrete values of $t = n\Delta t$; $n = 0, -1, -2, \ldots$, into this equation, a sequence of weights is obtained, and the transform of this discrete weighting function is

$$R_t = \sum_{k=0}^{-n} w_k \cos\omega k\Delta t + i \sum_{k=0}^{-n} w_k \sin\omega k\Delta t. \quad (24)$$

This filter function is a function of the sampling interval, and, as $\Delta t \to 0$, $n \to \infty$ and $R_t \to R$. The actual RC filter function is given in Fig. 1, along with R_t for $\Delta t = 0.2$, and $n = 52$. For $\Delta t = 0.1$ and $n = 105$, the filter function is roughly halfway between R and the $\Delta t = 0.2$ filter function.

Since the simple high-pass filter function converges to zero linearly at low frequencies, another filter function converging to zero more rapidly was used for comparison purposes, so that the cut-off frequency would

be more clearly defined. A filter function of the form $(1-\exp(-\omega^2\sigma^2/2))$, where σ is a numerical factor determining the cut-off frequency, was selected. The properties of this type of filter, known as a normal filter, are discussed by Holloway (1958). The corresponding weighting function, obtained by a Fourier transformation, is

$$w(t) = \begin{cases} -(2\pi\sigma^2)^{-\frac{1}{2}} \exp(-t^2/2\sigma^2), & \text{for } |t| > 0 \\ 1 - (2\pi\sigma^2)^{-\frac{1}{2}} & \text{for } t = 0 \end{cases} \tag{25}$$

This filter was used with two different values of σ, as illustrated in Fig. 1. The first case, with $\sigma = 3.33$ sec, was used to sharpen the cut-off frequency and thus eliminate any contribution to the variables beyond 1.2 km wavelengths. The second case, with $\sigma = 0.3$ sec, was chosen to eliminate all frequencies below the inertial subrange. As seen in Fig. 2, the filter has negligible response for wavelengths greater than 200 m, which, according to MacCready (1962), is within the region for which the spectral density can be represented by (6).

The combined effect of the total number of data points and the time interval between each point is to filter the variable with a band-pass filter. The statistical effects and useful applications of finite sampling and averaging times are discussed by Pasquill (1962) and Jones and Pasquill (1956). The smoothing function of an infinite sequence of data points over an averaging time, τ, can be expressed by the weighting function

$$w(t) = \begin{cases} 1/\tau, & \text{for } |t| \leq \tau/2 \\ 0, & \text{for } |t| > \tau/2. \end{cases} \tag{26}$$

The Fourier transformation of this function is

$$R = \int_{-\tau/2}^{\tau/2} (1/\tau)\, e^{i\omega t} dt = (\omega\tau/2)^{-1} \sin(\omega\tau/2) \tag{27}$$

The variance of an infinite sequence of data points can be expressed as $\sigma^2 = \sigma_1^2 + \sigma_2^2$, where σ_1^2 is the variance of a subsequence of data points, each point being the average of the original sequence over some arbitrary time interval, τ, and σ_2^2 is the variance of the data points within the interval, τ. Applying (27) to this expression, and solving for σ_2^2, which is the variance actually measured in any physical situation,

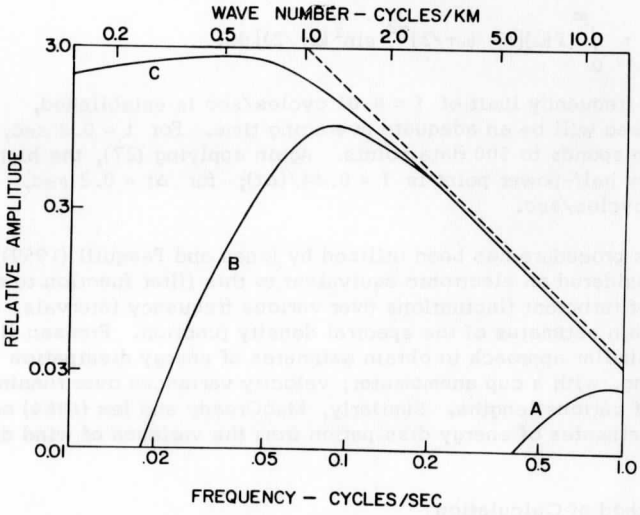

FIG. 2. Effect of filter functions on turbulence spectra. "C" is the response of an RC high-pass filter times $f^{-5/3}$ (dashed line), "B" is "C" times a normal filter with $\sigma = 3.33$, "A" is "C" times a normal filter with $\sigma = 0.3$.

$$\sigma_z^2 = \sigma^2 - \int_0^\infty F(\omega)(\omega\tau/2)^{-2} \sin^2(\omega\tau/2)\, d\omega, \tag{28}$$

where $F(\omega)$ is the spectral density. Since $\sigma^2 = \int_0^\infty F(\omega)d\omega$,

$$\sigma_z^2 = \int_0^\infty F(\omega)[1 - (\omega\tau/2)^{-2} \sin^2(\omega\tau/2)]\, d\omega. \tag{29}$$

If a low-frequency limit of $f = 0.01$ cycles/sec is established, $\tau \geq 100$ sec will be an adequate averaging time. For $t = 0.2$ sec, this corresponds to 500 data points. Again applying (27), the high frequency half-power point is $f = 0.44/(\Delta t)$; for $\Delta t = 0.2$ sec, $f = 2.2$ cycles/sec.

This procedure has been utilized by Jones and Pasquill (1959), who also considered an electronic equivalent to this filter function to obtain values of turbulent fluctuations over various frequency intervals, and thus obtain estimates of the spectral density function. Frenzen (1965) used a similar approach to obtain estimates of energy dissipation by measuring, with a cup anemometer, velocity variances over running means of various lengths. Similarly, MacCready and Jex (1964) obtained estimates of energy dissipation from the variance of wind direction.

3.3 Method of Calculation

3.3.1 Spectral and Cross-Spectral Analysis. Digital computation of the spectral density function has today become so commonplace among experimental scientists and has been so thoroughly and rigorously discussed by Blackmann and Tukey (1958) that a detailed discussion here is not necessary. The more general procedure of jointly estimating the spectral densities, $F_{xx}(k)$ and $F_{yy}(k)$, of a real two-dimensional stationary Gaussian vector process $[x(t), y(t)]$, $-\infty < t < \infty$, along with the co-spectral and quadrature spectral densities, $C_{xy}(k)$ and $Q_{xy}(k)$, for a finite sampling time has been treated in detail by Goodman (1957). Panofsky and Brier (1958) describe various meteorological applications and limitations of the technique. A detailed description of the actual computational technique is given by Cramer, et al. (1961).

The degrees of freedom of the spectral estimates are given by $df = (2N - M/2)/M$, where N is the length of the sample and M is the number of lags used in computing the spectral densities. Assuming the variable is normal, and the sample is drawn at random, the

distribution of the sample spectra estimates about the population spectral density is a chi-square distribution. For example, if $M = 40$ and $N = 500$, an 80% chance exists that the population spectral density will lie between 0.73 and 1.52 times the measured spectral estimate. For $N = 1000$, the confidence levels are 0.79 and 1.33, respectively.

In all cases considered here, 40 lags were used for computation. This figure was arrived at by considering the significance of the spectral estimates, the resolution required to indicate the various features of the spectra and the amount of time necessary to compute the spectral densities. The frequency intervals, f_n, are related to M and the sampling time interval, Δt, by the equation, $f_n = n/(2\Delta tM)$, $n = 0, 1, \ldots, M$. If $t = 0.2$ and $\bar{u} = 70$ m/sec, $k_n = 0.9n$ cycles/km.

In order to determine the significance of the cross-spectral densities, the coherence is defined by

$$CH(k) = (Q_{xy}^2 + C_{xy}^2)/(F_{xx}F_{yy}). \tag{30}$$

An approximate formula for the minimum value of coherence needed for a significant value of coherence at the probability level, p, is given by Panofsky and Brier (1958), as

$$\beta = (1 - p^{1/(df-1)})^{\frac{1}{2}}. \tag{31}$$

In the two previous examples, using a probability of 10% (that is, the chance of obtaining a coherence as large as β from uncorrelated data is one in ten) for $N = 500$, $\beta = 0.30$; for $N = 1000$, $\beta = 0.21$.

If $y = w$, the co-spectral density is proportional to the vertical flux of x as a function of wave number. The total flux is, then, the integral of C_{xw} over all wave numbers. Plotting $k \cdot C_{xw}$ vs. $\log(k)$ results in a more nearly horizontal curve than $\log(C_{xw})$ vs. $\log(k)$, and has the added advantage that the area under the curve is proportional to the vertical flux. This type of curve makes possible estimates of how much of the total flux is contained within the measured bandwidth if the flux reaches a significant maximum within the measured bandwidth.

After computing the spectral densities, the correction for the high pass filter function can easily be applied by multiplying the spectral densities by $(1 + \omega^2\tau^2)/\omega^2\tau^2$, the magnitude squared of the inverse of the filter function. The high-pass filter pre-whitens the data, or flattens the spectra, as shown in Fig. 2. As pointed out by Blackmann and Tukey (1958), this increases the significance of the spectral density estimates.

3.3.2 Cross-Products and Variances. In almost every case, unfortunately, the correlation coefficient between u' and w' is less than 0.2. The situation is similar with w' and T', although in very unstable conditions, the correlation coefficient is sometimes greater than 0.5. For a correlation coefficient of 0.2 to be significant at the 5% level, using the F distribution, about 100 degrees of freedom are required; for a correlation coefficient of 0.1, df = 400.

As a test, data at 120 m over flat, homogeneous farmland at 1200 CST, 10 May 1965, were recorded with the airplane first heading upwind, then downwind, and finally in both directions perpendicular to the wind. Another upwind flight was also made at 300 m. The fourth order moments of the velocity distributions reveal that the fluctuations were almost normal. Therefore, the standard deviation of the correlation coefficient for 400 sample points should theoretically be about $1/(N-2)^{\frac{1}{2}} = 0.05$. Each series was divided into two sections and from this the standard deviation of the correlation coefficient between u' and w' was measured to be actually 0.15. The large difference between the actual and the theoretical standard deviation is due to: (1) one particular segment of all the recorded series happened to be very far from the long-term average of that particular series, and (2) the physical coupling between u' and w' is a function of wave number (or equivalently, of eddy length). Integrating the co-spectral density from 1.15 to 0.384 km wavelengths reveals that 50% of the stress is contained within this interval. Therefore, the effective degrees of freedom of the two series, when computing the correlation coefficient are on the order of 100, which results in a correlation coefficient standard deviation of 0.10 for a section of 500 sample points. This value of 5 sample points per degree of freedom, corresponding to a length of 70 m, appears to be a good estimate for other measurements of the correlation between u' and w'.

During the 10 May 1965 series at 120 m, the correlation coefficient between T' and w' was 0.55 ± 0.04. The coherence indicates that significant correlation exists between T' and w' down to wavelengths of 56 m. This can be verified on Fig. 3 which also suggests the possibility of two peaks in the contribution to eddy heat flux. The peak at 177 m wavelength is hardly statistically significant for this case. However, as will be shown later, the heat flux over Lake Michigan in winter, although smaller in magnitude than the May measurements, can have two significant peaks, perhaps because of a more homogeneous temperature field and a smoother surface. This phenomenon of double peaks has been reported previously from a tower at 16 m height by Cramer, et al. (1962), both in the u' and w' and the w' and T' co-spectral densities under unstable conditions.

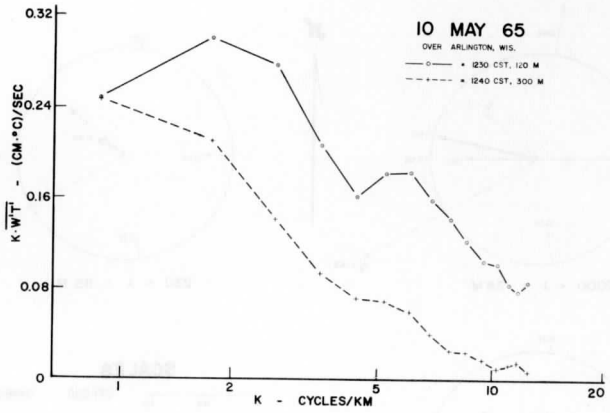

FIG. 3

If it is assumed that the first peak corresponds to heat transfer primarily by convection and the second to heat transfer by mechanically induced turbulent mixing, it is, perhaps, meaningful to ask what amount of momentum flux or stress is contained in each of these regions of the spectrum. The stress is dominated, of course, by the low wave number contributions, but calculation of the stress in the region of 250 m to 115 m gives estimates of less variability, but in the same direction as compared to the longer wavelengths, since the degrees of freedom are greater. Fig. 4 shows the various values of stress over different wave number intervals plotted with respect to the observed mean surface wind and the surface geostrophic wind.

The co-spectral density of both u' and w', and T' and w' at 300 m on 10 May 1965 show a shift to longer wavelengths, as compared to measurements at 120 m, for the total flux. The long wavelength peak for T' and w' at 300 m is apparently above the longest measured wavelength. It is interesting to note, however, that the shorter wavelength peak is relatively insensitive to changes in height. The wavelength of the peak is about 160 m here, as compared to about 145 m for the 16 m tower data as reported by Cramer, et al. (1962).

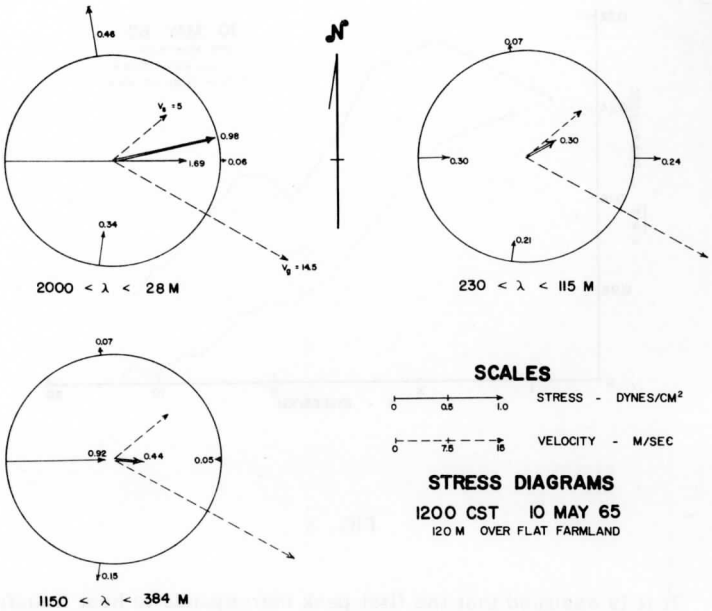

FIG. 4

The spectral densities for 10 May 1965 are plotted in Figures 5a and 5b for velocity, and Fig. 6 for temperature. The spectra can be approximated by a line of -5/3 slope at wavelengths less than 500 m. The ratio of the vertical to the horizontal velocity variance is about 3 for the flight parallel to the wind and about 2 for the flight perpendicular to the wind at a height of 120 m. From the Kolmogorov hypothesis, the value of this ratio in the isotropic region of the spectra would be 4/3 in the first case and unity in the second case. Departure from the theoretical values is apparently due to the turbulence being anisotropic at wavelengths less than 100 m, and measurement errors in the vertical velocity sensor. The calibration error of the velocity sensors is estimated to be less than $\pm$ 5

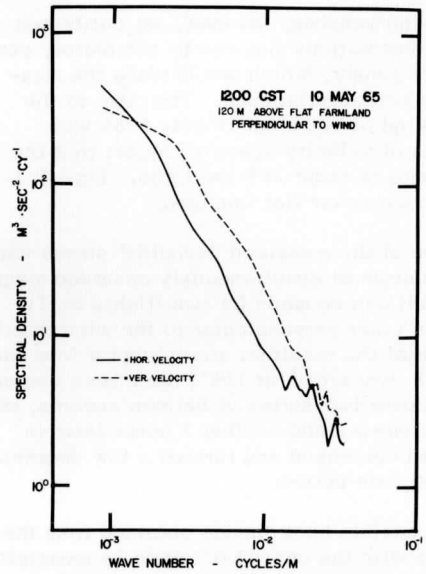

FIG. 5a

Velocity spectra, Arlington, Wis.

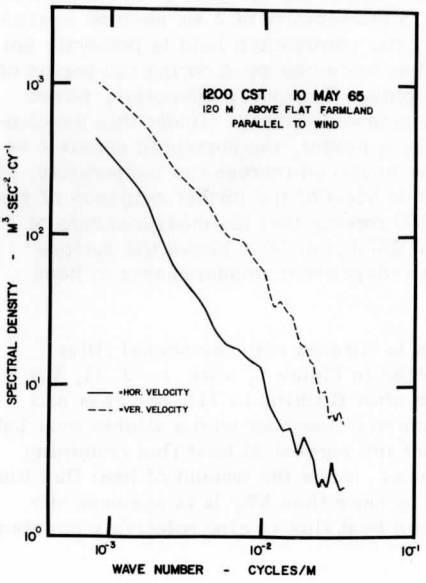

FIG. 5b

Velocity spectra, Arlington, Wis.

percent of the measured value. The sensors, however, we calibrated on the ground; the effect of airplane motions may not be completely cancelled out in the vertical velocity sensor, which would make the measured turbulence greater than the actual turbulence. The ratio of the velocity spectra parallel to the wind at 300 m on 10 May 1965 was about 1.8. Further measurements of velocity spectra suggest that the measured vertical velocity variance is about 20% too large. Fig. 7 illustrates co- and quadrature spectra over flat farmland.

A comparison of the direction of the measured Reynolds' stress with the stress obtained from an evaluation of simultaneously observed mean velocity profiles by Johnson (1965) can be made for two flights on 31 March 1964, one upwind, and the other perpendicular to the wind direction. The magnitude and azimuth of the resultant stress vector from the two orthogonal components is 3.8 dynes/cm^2 at 169°; the stress vector from the wind profiles, averaged over two series of balloon ascents, one at the time of the airplane measurements and another 3 hours later is 2.5 dynes/cm^2 at 190°. The wind decreased and rotated a few degrees toward the east in the intervening time period.

Table 1 is a comparison of sensible heat change obtained from the difference in temperature profiles with the change obtained by measuring the sensible heat flux divergence between two heights at two different times. The temperature profiles in the vicinity of 2 km have no systematic variation throughout the day, the surrounding land is primarily uniformly forested hills, and no clouds were observed during the period of measurement between the two heights. Therefore, advection, phase changes and radiational divergence are neglected. Under this assumption, in the region from 479 to 174 m height, the measured sensible heat flux accounts for about 50% of the observed increase in temperature. This appears to be a reasonable result in view of the further evidence of plots of kF_{Tw} vs. log(k). Bunker (1957) reports that his measurements of $\overline{w'T'}$ over wavelengths from 20 to 2000 m at 30 m above the surface were 50% less than simultaneous independent measurements of heat flux at O'Neill.

If this same series of flights is filtered with the normal filter described in Section 3.2 and plotted in Figure 1, with $\sigma = 3.33$, the percentage of heat flux remaining after filtering is 71% at 174 m and 64% at 479 m. This procedure was also used for winter flights over Lake Michigan, where it was found that the percent of heat flux remaining was 65% at 150 m and 70% at 350 m. Since the amount of heat flux lost in these examples does not vary by more than 6%, it is assumed the estimate of 50% of the total upward heat flux is also relatively constant.

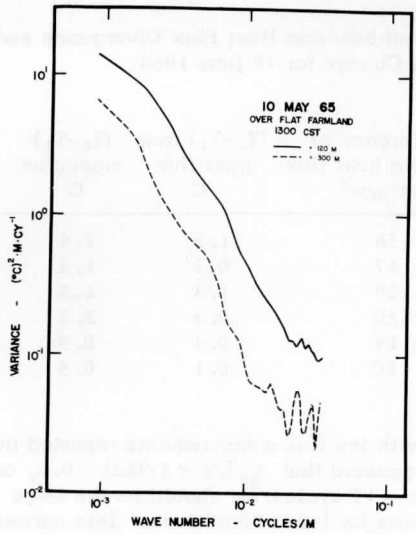

FIG. 6

Temperature spectra, Arlington, Wis.

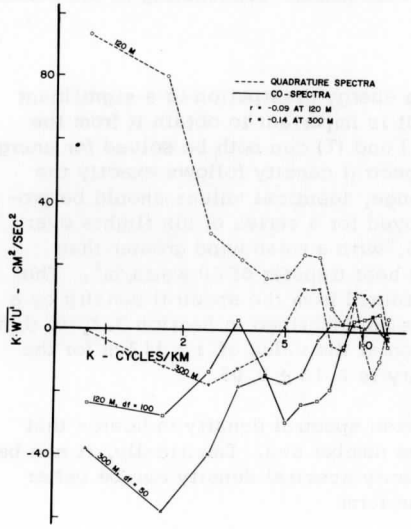

FIG. 7

Co- and quadrature spectra of w' and u' 13:00 CST, 10 May 1965 Arlington, Wis.

TABLE 1. Comparison of Measured Sensible Heat Flux Divergence and Measured Temperature Change for 10 June 1964.

Time Interval CST	Thickness $(z_2 - z_1)$ m	Difference of sensible heat flux watts/m^2	$(T_2 - T_1)$ from heat flux C	$(T_2 - T_1)$ measured C
0905 - 1205	479 - 174	56	1.8	3.4
0910 - 1210	1089 - 479	17	0.3	1.4
1205 - 1505	479 - 174	39	1.3	2.5
1205 - 1505	1089 - 479	20	0.3	2.3
1505 - 1805	479 - 174	14	0.4	0.5
1505 - 1805	1089 - 479	10	0.1	0.5

A comparison can be made with the flux measurements reported by Deacon (1959; Figure 1). He suggested that $t_m\bar{u}/z = 1/(kz) = 0.6$, or, using Figure 3 as an example, $k = 14$ cycles/km should be the large wave number end of the eddy fluxes for lapse conditions. This agrees well with the observed maximum wave number contributing to the vertical flux.

3.3.3 Energy Dissipation. Since energy dissipation is a significant parameter of the boundary layer, it is important to obtain it from the turbulence records. Equations (6) and (7) can both be solved for energy dissipation. Obviously, if the spectral density follows exactly the -5/3 relation in the inertial subrange, identical values should be produced. This procedure was employed for a series of six flights over Lake Michigan on 13 January 1965, with a mean wind greater than 10 m/sec at 350 m and a sensible heat transfer of 20 watts/m^2. The ratio of the energy dissipation obtained from the spectral density by a high-pass digital filtering process as described in Section 3.2, to that obtained from the structure function at the value of $r = 112$ m for the horizontal velocity spectral density is 2.15 ± 0.05.

An examination of the calculated spectral density indicates that flattening occurs at the large wave number end. Empirically, it can be suggested that the horizontal velocity spectral density can be better approximated by an equation of the form

$$E(k) = \begin{cases} a\epsilon^{2/3} k^{-5/3} + B, & \text{for } 0 < k < k_m \\ a\epsilon^{2/3} k^{-5/3}, & \text{for } k \geq k_m \end{cases} \tag{32}$$

where $k_m = \pi/(\bar{u}\Delta t)$ is the largest wave number for which E(k) can be computed and Δt is the sampling time interval. The constant B represents a "white noise" addition to the spectra, probably resulting from a combination of aliasing, as described by Blackmann and Tukey (1958), instrument noise, and data reduction errors. The RMS magnitudes of B in terms of deflection on the recorder output is less than 0.2 cm; the data read-out process is estimated to be accurate to 0.1 cm. Applying the high-pass filtering technique to the example considered above, the ratio of the energy dissipation calculated from both terms of (32) to the energy dissipation calculated from the first term is 2.0. It is evident, therefore, that the spectral estimates of energy dissipation are too large.

This over-estimation is greatly reduced if calculation of energy dissipation is based on the structure function (6) instead of (7). The transformation equation for the structure function is, if (32) is considered,

$$B_{dd} = 2\int_0^\infty E(k)(1 - \cos(kr))dk = 4.02a\epsilon^{2/3} r^{2/3} + 2Bk_m. \tag{33}$$

If $n\Delta t = 1.6$ sec, then r = 112 m and the ratio of energy dissipation calculated from both terms to that of the first term is 1.16. Therefore, the energy dissipation obtained from the structure function is a better estimate of the actual dissipation.

First estimates of energy dissipation were obtained by the high-pass digital filter technique, and were summarized by W. Johnson (1965) in his Table 11. It shall be demonstrated in Section 4.2 that the structure function estimates of dissipation make much better sense when we consider the entire kinetic energy budget of a particular layer in the atmosphere.

If the spectral density is assumed to follow more closely a -3/2 exponent, it is possible to compare the ratio of energy dissipation calculated from the spectra with that calculated from the structure function, as was done for the -5/3 exponent. Using the equations derived for isotropic turbulence, by Batchelor (1953; pp. 46, 49, 50 and 120), the structure function for the longitudinal component of velocity is

$$B_{dd2} = (8\pi)^{\frac{1}{2}} a_2 (\epsilon \sigma_u r)^{\frac{1}{2}} = 5.013\, a_2 (\epsilon \sigma_u r)^{\frac{1}{2}}. \tag{34}$$

Since the magnitudes of a_2 and σ_u are not known, it is not possible to determine the energy dissipation, but taking the ratio of (7) to (34) yields

$$\epsilon_k/\epsilon_r = 8\pi(E_2/B_{dd2})^2 rk^3, \tag{35}$$

where ϵ_k is the energy dissipation obtained from (7) and ϵ_r from (34). Fitting a slope of $-3/2$ to the same series of flights considered above, the value of the ratio is 3.6 ± 0.6. Thus, from the standpoint of obtaining estimates of energy dissipation, the $-5/3$ exponent gives a less ambiguous value than the $-3/2$ spectra.

The horizontal velocity spectral densities measured over Lake Michigan on 14 January 1965 with essentially no wind and a sensible heat flux of 6 watts/m^2 is steeper than a $-5/3$ slope, although for wavelengths less than 200 m, the slope is not far from $-5/3$. If the same procedure as for the previous series is carried out, the energy dissipation derived from the spectral density is again approximately twice the energy dissipation derived from the structure function; a further demonstration of the desirability of computing energy dissipation from the structure function.

Panofsky and Pasquill (1963) quote a formula, apparently first derived by Kolmogorov (1941b), relating "a" in (5), (6) and (7) to the skewness coefficient of the velocity distribution, s, by the equation

$$a = 0.215(-s)^{-2/3}. \tag{36}$$

Using this equation and computing s from all the horizontal velocity fluctuation data for our flights from 8 to 10 June 1964, at a height of 470 m for wavelengths less than 140 m, it was found that the average value was $a = 0.57$; within the limits of one standard deviation of the skewness coefficient, $0.42 < a < 1.0$. Considering the large scatter of the individual values, the general agreement with the accepted value of $a = 0.47$ is tolerable.

4. Description of Sites and Flight Plans

4.1 Lakewood. During 31 March and 8 to 11 June 1964, a series of 12 airplane flights were made in conjunction with the atmospheric boundary layer profile measurements conducted by W. Johnson (1965) over a hilly, uniformly forested region near Lakewood in Northeastern Wisconsin, and described in the preceding paper. The airplane flights

were timed to coincide with a series of balloon releases, to permit direct comparison of balloon and airplane measurements. Records of vertical and horizontal velocity, air and surface temperature, albedo and humidity were obtained over horizontal flight paths of 8.4 km length, as shown in Figure 8, at heights of 180, 480, 1100 and 1600 m in the region of the ascending balloons. These records were sampled every 0.1 sec for the 31 March series and 0.2 sec for the 8 to 11 June series.

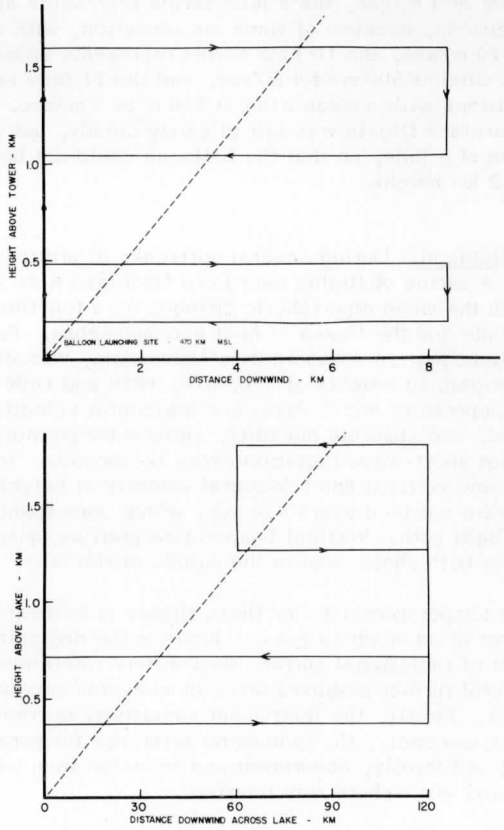

FIG. 8. Cross-sections of flight paths over Lakewood (top) and Lake Michigan (bottom). Dashed line at top represents a balloon ascent with a constant mean wind speed of 10 m/sec. Dashed line at bottom is a line of slope 1/50.

Vertical profiles of temperature and humidity over the balloon launching site up to 1600 m were also recorded; the temperature profiles have been plotted at 30 m intervals by W. Johnson. In addition, a horizontal square pattern of 17 km side-length was flown around the balloon launching site during the June series.

The 31 March series represents unstable conditions with a mean wind at 500 m of 4 m/sec, the 8 June series represents approximately neutral conditions, because of warm air advection, with a mean wind at 500 m of 10 m/sec, the 10 June series represents unstable conditions with a mean wind at 500 m of 4 m/sec, and the 11 June series represents stable conditions with a mean wind at 500 m of 5 m/sec. The weather during the airplane flights was fair to partly cloudy, but very hazy during the afternoon of 8 June, so that the balloons could not be followed up to the desired 2 km height.

4.2 Lake Michigan. During several outbreaks of arctic air in the winter of 1964-65, a series of flights over Lake Michigan were undertaken to measure both the mean atmospheric changes as a function of distance across the lake and the fluxes of heat and momentum. Figure 8 illustrates the flight pattern standard from Milwaukee, Wisconsin, to Muskegon, Michigan, at heights of 350, 670, 1250 and 1800 m above the lake. Air temperature and vertical and horizontal velocity were sampled every second, and absolute humidity, surface temperature and upward and downward short-wave radiation every 12 seconds. In addition, air temperature and vertical and horizontal velocity at heights between 180 and 670 m were sampled every 0.2 sec, which corresponds to 14 m of horizontal flight path. Vertical temperature profiles up to 1800 m were recorded over both shores and in the middle of the lake.

Surface temperature data for these flights is estimated to have an absolute error of as much as $\pm$ 2 C. Besides the difficulties of airborne measurement of radiational surface temperature mentioned by Lenschow (1962), several further problems arise in measurements over Lake Michigan in winter. Firstly, the instrument sensitivity decreases at low temperatures; secondly, the radiometer reference temperature is harder to maintain; and thirdly, absorption and emission from water droplets in the intervening atmosphere may interfere.

Various supporting data were employed to provide a reasonably complete description of the local atmospheric conditions and their variation in time and space. Maps showing the surface isobaric fields and areas of precipitation are presented in Figures 9 and 10. Also,

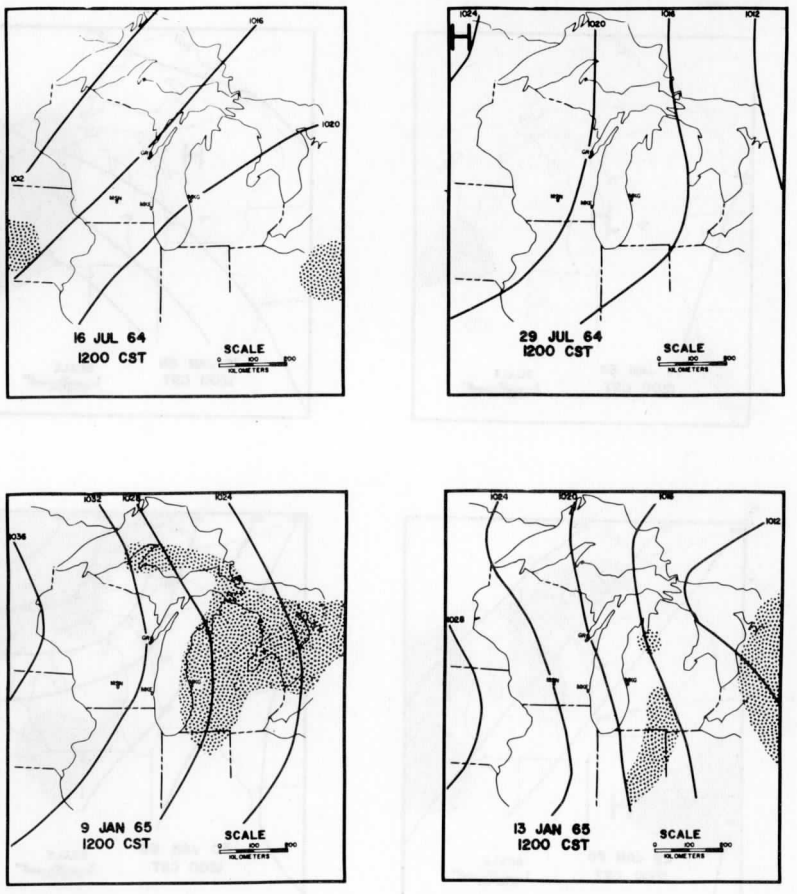

FIG. 9. Surface isobaric fields and areas of precipitation for Lake Michigan area from U.S.W.B. surface analysis at 1200 CST.

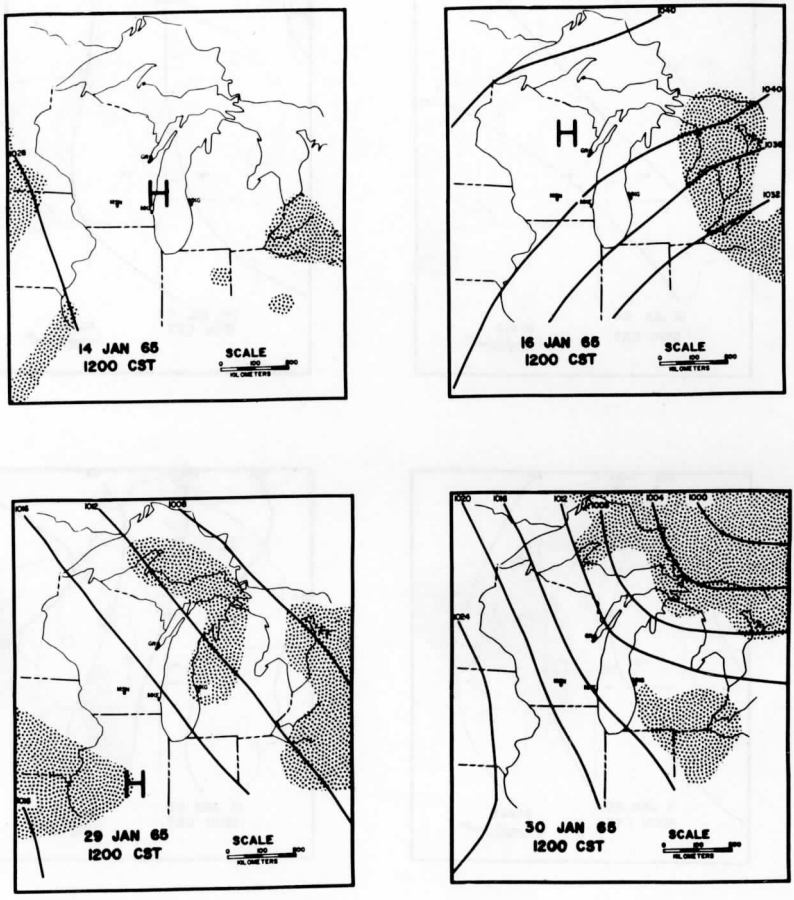

FIG. 10. Surface isobaric fields and areas of precipitation for Lake Michigan area from U. S. W. B. surface analysis at 1200 CST.

various qualitative features were noted, such as estimates of the height, thickness, and type of clouds, the presence of snow showers, and the extent of steam fog and floating ice. The magnitude and direction of the surface wind was estimated by observing the wave pattern on the lake surface. Winds at levels up to 200 m could also be occasionally estimated by observing the smoke plumes from industrial stacks at Milwaukee and Muskegon. Hourly weather observations were obtained from U. S. Weather Bureau Stations at Milwaukee and Muskegon, along with the 0600 CST radiosonde data from Green Bay on the days of flights. Precipitation records for December, 1964 through February, 1965 for Muskegon and Grand Haven, Michigan, and Milwaukee and Shorewood, Wisconsin, were also used.

5. Results of Measurements

5.1 Lakewood

5.1.1 Variances and Vertical Fluxes. The magnitude of both the horizontal and vertical velocity variances, as well as the variance of the vertical velocity of the balloons averaged over the first kilometer of the atmosphere are plotted as functions of time in Figures 11 and 12. The turbulence increases in magnitude with increasing instability, and the ratio of vertical to horizontal variance also increases to a maximum of 2.4 at 180 m at 1230 CST 31 March, and 1.8 at 1205 CST 10 June. For unstable conditions, the turbulence increases more rapidly above 180 m than at 180 m. On 10 June, the maximum vertical turbulence occurs at 1200 CST at 470 m and the maximum horizontal turbulence at 0905 CST at 180 m. The horizontal turbulence for 31 March shows a similar behavior.

Although the mean wind speed at airplane flight levels during the more stable conditions of 8 June is about twice as high as for the other two days, the turbulence is less intense and decreases with height at all times. The ratio of vertical to horizontal variance remains relatively constant at 1.31, which compares favorably with the predicted ratio of 4/3 for the -5/3 region of the spectrum. The ratio of the variance derived from balloon measurements to that derived from airplane measurements reaches a maximum at noon on 10 June, when the lower kilometer of the atmosphere was most unstable and the total energy dissipation within this layer was largest. The energy dissipation, calculated from the horizontal velocity structure function for $r = 112$ m and plotted in Figures 13 and 14, generally is proportional to the horizontal velocity variance to the 3/2 power.

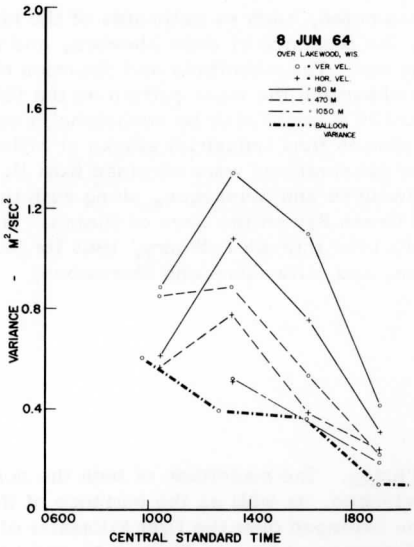

FIG. 11

Velocity variances, Lakewood, Wis.

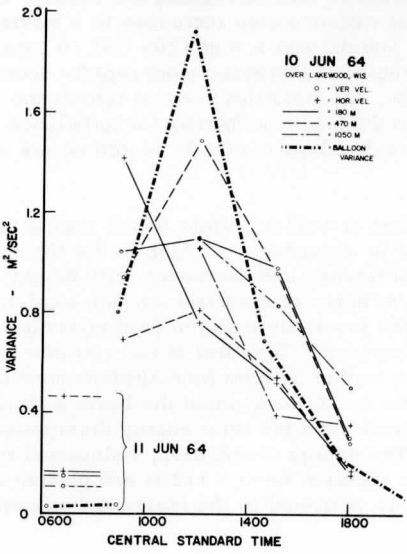

FIG. 12

Velocity variances, Lakewood, Wis.

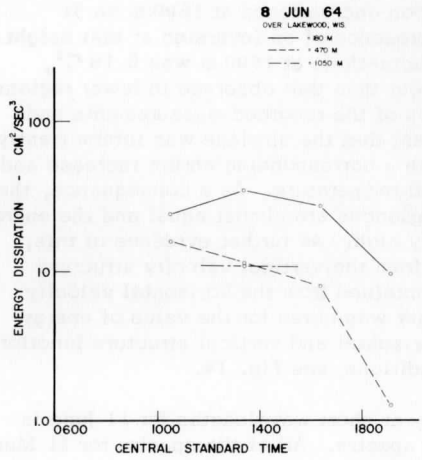

FIG. 13

Energy Dissipation, Lakewood, Wis.

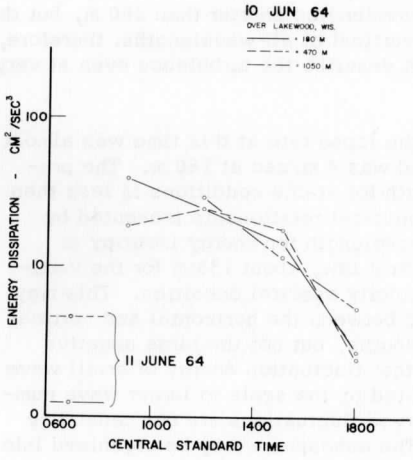

FIG. 14

Energy Dissipation, Lakewood, Wis.

A maximum in energy dissipation and variance at 1600 m on 31 March was apparently due to the presence of an inversion at that height. The variance of the temperature fluctuations at 1600 m was 0.18 C^2, which is an order of magnitude larger than that observed in lower regions of the boundary layer. Examination of the recorded measurements and the mean temperature profile suggest that the airplane was intermittently above and below an inversion, with a corresponding abrupt increase and decrease in horizontal velocity and temperature. As a consequence, the horizontal and vertical velocity variances are almost equal and the energy dissipation value is unrealistically high. As further evidence of this, the energy dissipation calculated from the vertical velocity structure function is only 1/3 of the value obtained from the horizontal velocity structure function. Similar behavior was noted for the value of energy dissipation calculated from the horizontal and vertical structure function for 11 June, under very stable conditions; see Fig. 14.

Further evidence of anisotropy at short wavelengths for 11 June is provided by an examination of the spectra. All of the spectra for 31 March and 8 to 10 June can be approximated by a slope of -5/3 at wavelengths below 500 m. Averages of spectra for the analyzed flights on each of these days showed no significant differences. This is to be expected, since the turbulence should be close to isotropic in this region. An example is shown on Fig. 15 for June 10. The spectra for 0605 CST, 11 June, as illustrated on Fig. 16, are quite different. Not only do they suggest a slope of about -2.5 at wavelengths shorter than 200 m, but the horizontal turbulence exceeds the vertical at all wavelengths; therefore, the Kolmogorov hypothesis does not describe the turbulence even at very small wavelengths.

According to Johnson (1965), the lapse rate at this time was almost isothermal and the mean wind speed was 4 m/sec at 180 m. The predicted maximum isotropic wavelength for stable conditions is less than for lapse conditions. Using the empirical relationship presented by MacCready (1962), the maximum wavelength for energy isotropy is about 100 m, and for the -5/3 spectral law, about 133 m for the vertical and 250 m for the horizontal velocity spectral densities. This may explain the difference in magnitude between the horizontal and vertical velocity spectra at the long wavelengths, but not the large negative slope. The slope value indicates that fluctuation energy of small wave numbers exists which is not escalated up the scale to larger wave numbers. This suggests that the observed fluctuations are not caused by a truly turbulent field of motion. The atmosphere may be organized into relatively uncoupled air strata of relatively large horizontal and small vertical extent, of varying velocities. This type of structure has been

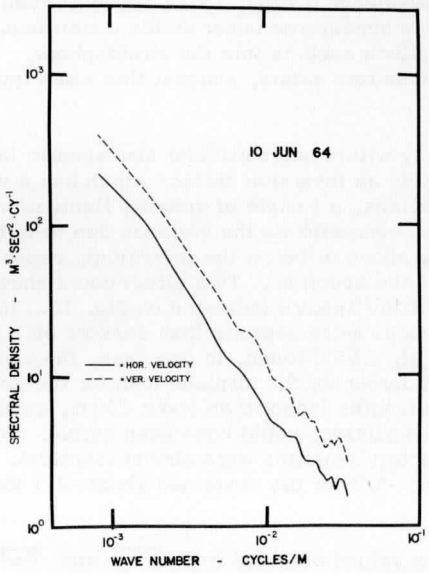

FIG. 15

Velocity spectra, Lakewood, Wis.

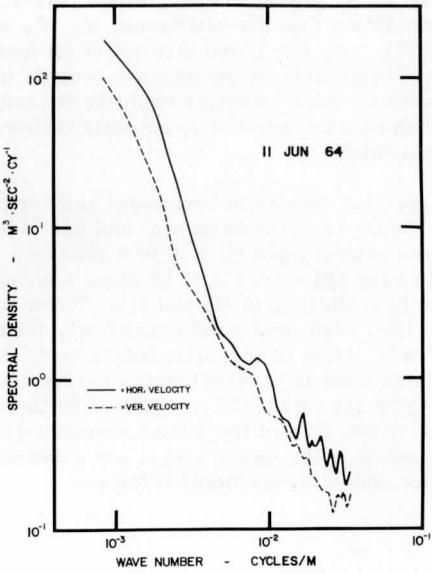

FIG. 16

Velocity spectra, Lakewood, Wis.

observed by Lettau and Schwerdtfeger (Lettau, 1939) during balloon flights in the lower 4 km of the atmosphere under stable conditions. Lettau also points out that balloon ascents into the stratosphere, where a similar isothermal lapse rate exists, suggest this same type of structure.

The airplane does not stay within one particular atmospheric layer, as evidenced by flights close to an inversion surface which has a wavy structure. Under these conditions, a sample of velocity fluctuations measured from an airplane can overestimate the variance due to turbulence actually existing (either above or below the inversion), especially at the long wavelength end of the spectrum. This effect could account for the large negative slope of the spectra indicated on Fig. 16. In a comparison between simultaneous measurements from sensors on a tower and in an airplane, Lappe et al. (1959) found, in one case, the vertical velocity spectral density was larger for the airplane than for the tower data by a factor of 2 for wavelengths longer than about 200 m, under conditions that, from their description, could have been stable. For shorter wavelengths, the spectral densities were almost identical. The spectra showed a slope of $-5/3$ for the tower and about -2.1 for the airplane data.

This also means that flux values obtained from $\overline{u'w'}$ and $\overline{T'w'}$ under stable conditions may be considerably in error, since it is a prerequisite of the Reynolds' formulation that the variations, u', w', and T', are turbulent. Bunker (1957), too, has noted this effect for measurements close to an inversion. Observation of the airplane records indicate the inversion level undulates. Such structure could be the cause of apparent fluxes, even though no eddy transfer is actually taking place, if the undulations are not sinusoidal.

A comparison of the co-spectral density of horizontal and vertical velocity at 180 m is made in Figure 17 between neutral and unstable conditions. The mean wind for the neutral case ($RI = 0$) of 8 June was 9 m/sec, and for the unstable case ($RI = -0.71$) of 10 June, 6 m/sec. The "flux" Richardson number RI is defined in (2) and (3). The measured component of stress for the 8 June flight was 0.52 dynes/cm^2, for the 10 June flights, 2.45 dynes/cm^2. Most of the contribution to the total Reynolds' stress for the unstable case is at wavelengths longer than 500 m, for the neutral case, wavelengths less than 500 m. This is further evidence of a definite separation in the size of the eddies responsible for the transport of heat and momentum. The larger eddies are generated by convection, and the smaller eddies by mechanical forces.

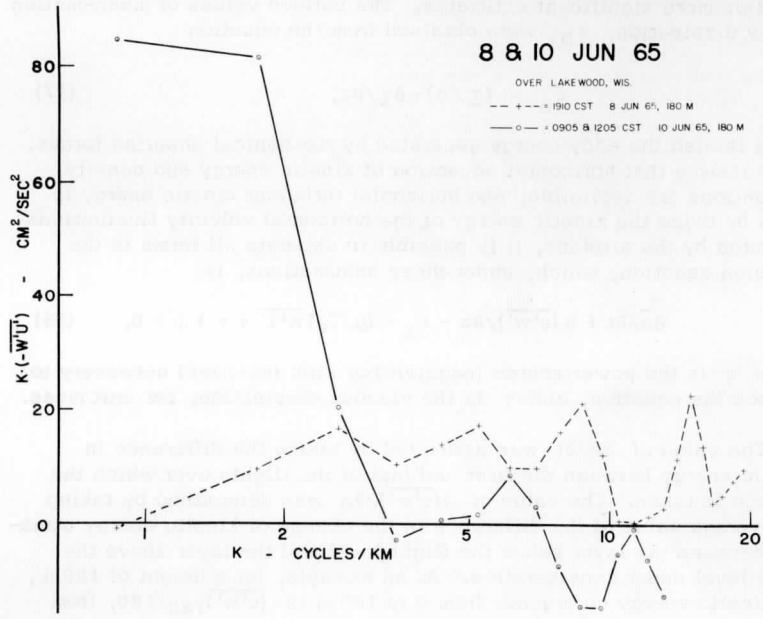

FIG. 17. Co-spectra over Lakewood, Wisconsin.

5.1.2 Turbulent Kinetic Energy Budget. Some of the results obtained from simultaneous balloon and airplane measurements can be related by means of the diffusion equation for turbulent kinetic energy as given by Lumley and Panofsky (1964). Table 2 is a summary of measured parameters, averaged, in most cases, over several series of flights to obtain more significant estimates. The balloon values of mean-motion energy dissipation, ϵ_b, were obtained from the equation

$$\epsilon_b = (\underset{\rightarrow}{\tau}/\rho) \cdot \partial \underset{\rightarrow}{V}/\partial z, \qquad (37)$$

which is also the eddy energy generated by mechanical shearing forces. If we assume that horizontal advection of kinetic energy and density fluctuations are negligible, and horizontal turbulent kinetic energy is given by twice the kinetic energy of the horizontal velocity fluctuations measured by the airplane, it is possible to estimate all terms in the diffusion equation, which, under these assumptions, is

$$\partial \bar{e}/\partial t + \partial (\overline{e'w'})/\partial z - \epsilon_b - (g/T_0)\overline{w'T'} + \epsilon + \psi = 0, \qquad (38)$$

where ψ is the power source (negative) or sink (positive) necessary to balance the equation, and ϵ is the viscous dissipation, per unit mass.

The value of $\partial \bar{e}/\partial t$ was estimated by taking the difference in kinetic energy between the first and last of the flights over which the average is taken. The value of $\partial(\overline{e'w'})/\partial z$ was determined by taking the average value of the difference in the change of kinetic energy transport between the layer below the flight level and the layer above the flight level under consideration. As an example, for a height of 180 m, the kinetic energy divergence from 0 to 180 m is $(\overline{e'w'})_{180}/180$, from from 180 to 470 m, $[(\overline{e'w'})_{470} - (\overline{e'w'})_{180}]/290$. The kinetic energy divergence at 180 m is assumed to be the average of these two values.

Under unstable conditions, according to Table 2, ψ is almost always large and negative. If, however, it is assumed that the measured vertical fluxes contain only 50 percent of the total flux, as suggested in Section 3.3.2, improved values are obtained which are denoted by ψ'. The values of ψ' for the two unstable cases at 170 m height (31 March and 10 June) represent conditions for which the analysis is most reliable because of the larger correlation coefficients. These values are less than 8 percent of the energy dissipation. It therefore appears that the various terms comprising the kinetic energy budget of the lower atmosphere

TABLE 2. Comparison of Parameters Obtained from Mean Velocity Profiles and Fluctuation Analysis

Date (1964)	meters	τ_b (dynes/cm^2)	$\tau_b \cos\theta$ (dynes/cm^2)	τ_a (dynes/cm^2)	$\overline{e'w'}$ m^3/sec^3	$\partial e'w'/\partial z$ (cm^2/sec^3)	$\partial \bar{e}/\partial t$ (cm^2/sec^3)	ϵ_b (cm^2/sec^3)	$gw'T'/T_0$ (cm^2/sec^3)	ϵ (cm^2/sec^3)	ψ (cm^2/sec^3)	ψ' (cm^2/sec^3)	RI
31 March 1230 and 1700 CST	170	2.5	0.94	1.6	0.10	0.3	-1.0	4	11	26	-10	2	-0.42
	470	1.7	0.82	-0.11	-0.10	-2.0	-0.3	3	- 2	21	-18	-17	0.10
	1100				-0.11								
8 June 1030 and 1320 CST	170	3.13	2.10	0.62	-0.07	-2	1.0	4	8	29	-16	- 7	-0.28
	470	2.18	0.78	1.04	-0.08	-1	0.5	9	-2	13	- 4	-5	0.15
	1100												
8 June 1910 and 2210 CST	170	2.81	2.32	0.52				98	0	10	88		0
	470			-0.50*				20	0*	1	28*		0
10 June 0905, 1205 and 1510 CST	170	1.13	1.09	1.60	0.24	7	-1.0	1	19	26	-12	1	-0.73
	470	0.67	0.46	1.38	0.25	-2	-0.8	1	4	20	-12	-5	-0.20
	1100				-0.02								

*Airplane measured values do not include 2210 CST series.

The subscript b refers to parameters obtained from balloon measurements; a refers to airplane measured parameters.

can be reasonably estimated. One interesting result is the absence of large values of vertical kinetic energy advection up to the inversion level, which Ball (1960) thought necessary to account for the daytime increase in inversion height. Rather, it appears that, just as Taylor (1952), and Panofsky (1962) found in the lower atmosphere, energy dissipation is almost equal to the local energy production under neutral and slightly unstable conditions, and that kinetic energy transported from lower levels under unstable conditions is dissipated within the boundary layer, and not at the inversion level. Table 2 also indicates a downward transfer of kinetic energy under stable conditions.

The value of ϵ_b for the stable case of 8 June (1910 CST), is obviously much too high to be accounted for by the energy dissipated. The observed level of turbulence was reduced in late afternoon, and the convective activity was almost zero, yet the mechanical production of kinetic energy appears very large. It is evident, therefore, that the balloon estimate of stress is too large. If the stress measured by the airplane is used instead, so that (37) is multiplied by $\tau_a/(|\vec{\tau}_b|\cos\theta)$, the value of ϵ_b at 180 m is reduced to 22 cm^2/sec^3. The correlation coefficient between u' and w' for this flight was -0.14; a correlation coefficient of -0.65 would be necessary to produce the balloon-measured component of stress. Such a high correlation between u' and w' is unlikely. It should be noted, however, that ϵ_b includes two series of balloon ascents, whereas ϵ was measured only for the earlier series. The wind was observed to increase slightly between the two series, but the stability changed very little. The conclusion, that the stress derived from balloon measurements was too large during such stable situations, is still valid.

5.2 Lake Michigan

5.2.1 Descriptive Results. A parcel of air traveling east at 10 m/sec would take 3.3 hours to cross Lake Michigan. During a time interval of this length, the air shelter temperature at Milwaukee was observed, on one occasion, to increase by 10 C. On another occasion, the surface wind at Milwaukee was reported as 1 m/sec from the west, and at the same time at Muskegon, 3 m/sec from the east. Therefore, in attempting to determine the modification of air passing over a homogeneous surface of this size, it is imperative to consider the effect of velocity and temperature changes in time and space due to large-scale atmospheric phenomena, and the interactions of these phenomena with the modifying surface. In order to solve the problem accurately, not only must the

local derivatives at a particular point be known, as was required, for example, for the simultaneous airplane-balloon measurements, but the changes in these derivatives over the surface under consideration must also be considered.

It is impossible to eliminate entirely the effects of all these variations. However, it is possible to estimate some of them and to ascertain how close to a steady-state condition the atmosphere actually was during a period of measurement. The comparison of vertical temperature profiles on both sides of the lake above the modified layer of air provides an estimate of large scale advection effects. In many cases, vertical temperature profiles were taken several times in the same place over a period of several hours, so that the local time change of temperature could be determined. With the aid of this procedure, a more representative profile could be obtained.

Since a great deal of variation exists from one series of measurements to another, each series will be described separately. The temperature profiles of Figs. 18 and 19, from Lake Michigan in summer, demonstrate how a relatively warm air mass is affected by passing over a relatively cool, smooth surface. A southwest wind of 3 m/sec at the surface during the 16 July flight resulted in a decrease of temperature and inversion height downwind across the lake from Milwaukee to Muskegon. An easterly surface wind and a westerly wind aloft at Milwaukee, and a westerly wind at all levels at Muskegon during the 29 July flight resulted in a decrease in inversion height across the lake from west to east. The temperature below the inversion is higher over Muskegon than over Milwaukee. Milwaukee reached its maximum temperature at mid-morning; then as the east wind developed (most likely a sea breeze), the temperature decreased. The Muskegon temperature reached a maximum at noon, when the surface wind was from the north.

The rest of the flights over the lake were made in winter, with the air, initially, at least 10 C cooler than the water. Examples of vertical temperature profiles for the winter flights are given in Figs. 20 and 21. It should be noted that the ordinate in these figures is altitude above sea level. In the text, vertical distance is given by height above the underlying surface. The 15 December 1964 flight was not completely across the lake because of the heavy cloud cover in the modified air over Muskegon. Warm air advection resulted in a rapid temperature increase in Milwaukee. The total precipitation at Grand Haven, Michigan, on this day amounted to 0.45 cm, which is an absolute maximum for a cold air outbreak during the winter at any of the four precipitation stations considered.

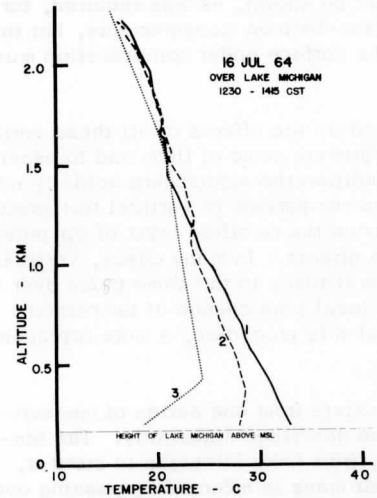

FIG. 18

Temperature profiles
(1) Milwaukee, Wis.
(2) Muskegon, Mich.
(3) RASO Green Bay, Wis.

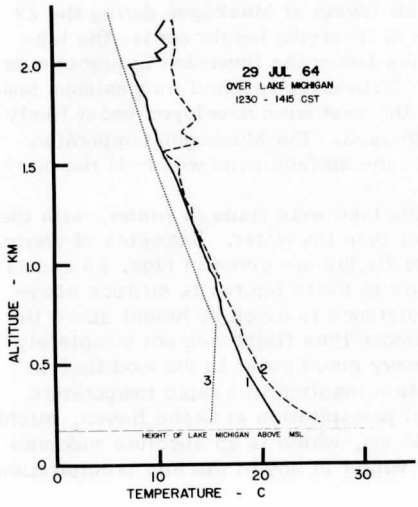

FIG. 19

Temperature Profiles
(1) Milwaukee, Wis.
(2) Muskegon, Mich.
(3) Raso Green Bay, Wis.

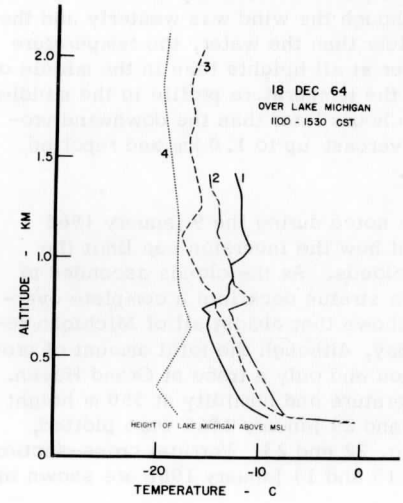

FIG. 20

Temperature Profiles
(1) Milwaukee, Wis.
(2) Mid Lake
(3) Muskegon, Mich.
(4) Raso Green Bay, Wis.

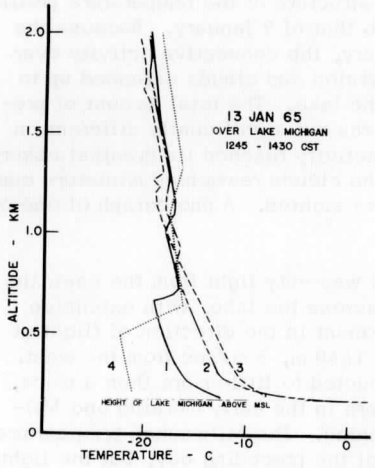

FIG. 21

Temperature Profiles
(1) Milwaukee, Wis.
(2) Mid Lake
(3) Muskegon, Mich.
(4) Raso Green Bay, Wis.

The 18 December 1964 flight was also affected by warm air advection, as indicated in Fig. 20. Although the wind was westerly and the air temperature more than 15 C colder than the water, the temperature downwind over Muskegon was lower at all heights than in the middle of the lake. In this case, however, the temperature profile in the middle of the lake was measured over two hours later than the downwind profile. Muskegon was completely overcast up to 1.0 km and reported 0.38 cm precipitation for that day.

No evidence of advection was noted during the 9 January 1965 series. On this day it was evident how the inversion can limit the vertical growth of the convective clouds. As the clouds ascended to the inversion, they spread out as a stratus deck into a complete overcast. The weather map, Fig. 9, shows that almost all of Michigan received snow at 1200 CST on this day, although the total amount of precipitation was 0.03 cm at Muskegon and only a trace at Grand Haven. Surface temperature, and air temperature and humidity at 350 m height across the lake for 9, 13, 14, 16 and 29 January 1965 were plotted, and examples are illustrated on Fig. 22 and 23. Vertical cross-sections of temperature across the lake for 13 and 14 January 1965 are shown in Fig. 24.

On 13 January, the local time change of temperature at Milwaukee during the two hours of measurements was less than 1 C above 0.7 km and about + 2 C below 0.7 km. The structure of the temperature profile below 0.7 km was almost identical to that of 9 January. Because the cold air was much deeper on 13 January, the convective activity over the water was not limited by the inversion and clouds extended up to 1.5 km over the downwind shore of the lake. The total amount of precipitation at the downwind stations was not significantly different on these two days, but the convective activity reached its greatest observed magnitude on 13 January. Many of the clouds resembled miniature cumulonimbus, and several waterspouts were sighted. A photograph of one of these is given in Figure 25.

On 14 January, the surface wind was very light from the east; the water was calm for most of the way across the lake, with extensive areas of broken ice. The wind component in the direction of flight at 350 m was 3 m/sec from the east; at 1650 m, 5 m/sec from the west. Precipitation at all four stations amounted to little more than a trace, with Muskegon reporting snow showers in the early morning and Milwaukee in the late afternoon and evening. The Milwaukee temperature profile was almost identical to that of the preceding day, but the light wind appears to have caused the spectra of the velocity fluctuations to depart distinctly from the usually observed spectra.

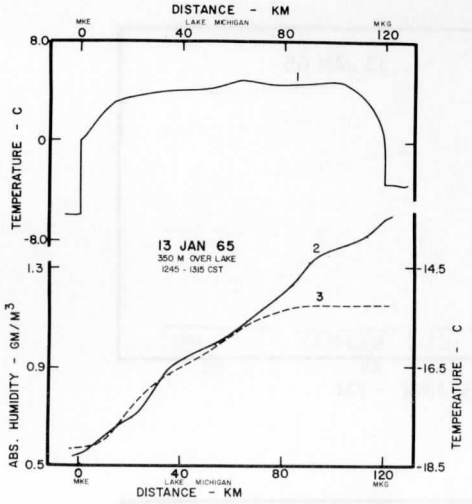

FIG. 22

Downwind Variation across Lake Michigan
(1) surface temperature
(2) air temp. at 350 m
(3) humidity at 350 m

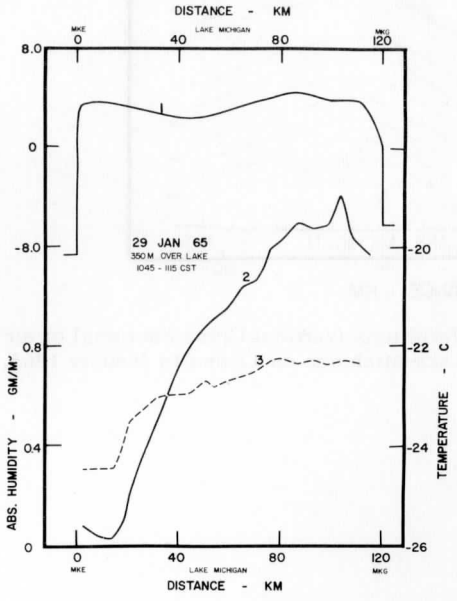

FIG. 23

Downwind Variation across Lake Michigan
(1) surface temperature
(2) air temp. at 350 m
(3) humidity at 350 m

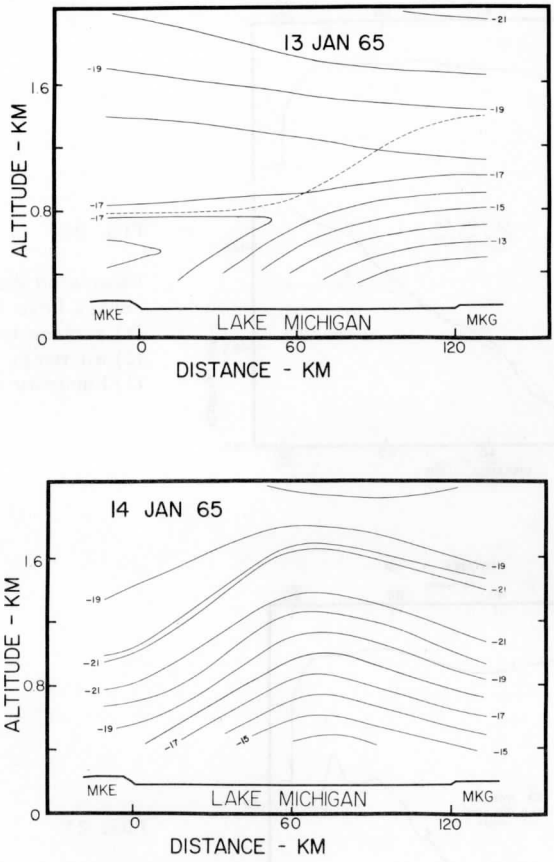

FIG. 24. Height-Distance Variations (Vertical Cross Sections) of air temperature over Lake Michigan on 13 and 14 January 1965.

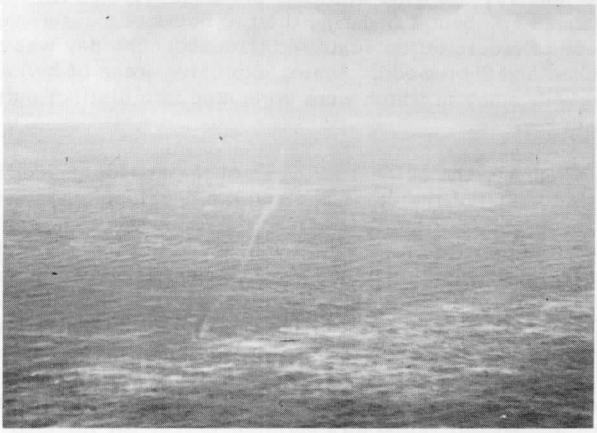

FIG. 25. Waterspout over Lake Michigan on 13 January 1965 about middle of lake.

FIG. 26. Floating ice patterns on Lake Michigan on 16 January 1965. East edge of lake visible in upper left corner. Wind was from the east, or from left to right on photograph.

On 16 January, the wind was from the northeast and the air above 1.3 km warmed up about 2 C during the two hours of measurement. Only a trace of precipitation scattered throughout the day was recorded at Milwaukee and Shorewood. Again, extensive areas of broken ice were observed, many of which were organized into distinct patterns, as shown in Fig. 26.

On 29 January, the coldest air mass of the season passed over the lake. A photograph of the steam fog and the developing convective clouds a few km east of the upwind shore is shown in Fig. 27, taken a day later, but under quite similar conditions. The surface wind was light from the northwest, and patches of broken ice were present over the entire lake, although the lake was frozen solid only about 200 m out from both shores. The ice helped to damp out the wind-formed waves and the surface was almost smooth. The velocity and temperature fluctuations showed the same behavior as on 14 January, although not as pronounced. The maximum height of the clouds was 1.5 km, about 20 km west of Muskegon. From this point eastward, the increasing density of areas of broken ice may have inhibited further convective activity. The total precipitation at Muskegon and Grand Haven was 0.23 and 0.25 cm, respectively.

The velocity spectra for 13 and 14 January are plotted in Figs. 28 and 29. The horizontal and vertical velocity spectra of 13 January and the vertical velocity for 14 January have a slope of $-5/3$, but the horizontal velocity for 14 January has a slope of -2.2. The magnitude of the horizontal velocity variance amounted to only 20 percent of the vertical velocity variance on this day. Apparently, therefore, the conditions for Kolmogorov's hypothesis do not exist; the turbulence is not isotropic, even at wavelengths less than 100 m. It appears the absence of shearing forces somehow inhibits the transfer of energy from long to short wavelengths and from the vertical to the horizontal plane. This may be due to columns of rising warm air, as observed by Townsend (1959) in laboratory experiments involving a heated horizontal surface with no horizontal wind shear. He observed that under these conditions, temperature fluctuations are not reconcilable with the similarity theory of convection. The temperature spectra for both 13 and 14 January have a slope of $-5/3$. Examples of co-spectra of w' and T' over Lake Michigan are presented in Fig. 30.

5.2.2 Quantitative Estimates of Air Mass Modification. The energy transformations resulting from arctic air passing over Lake Michigan can be discussed in terms of equation (38). The most difficult term to evaluate in this equation is the contribution to the liberation of heat due to

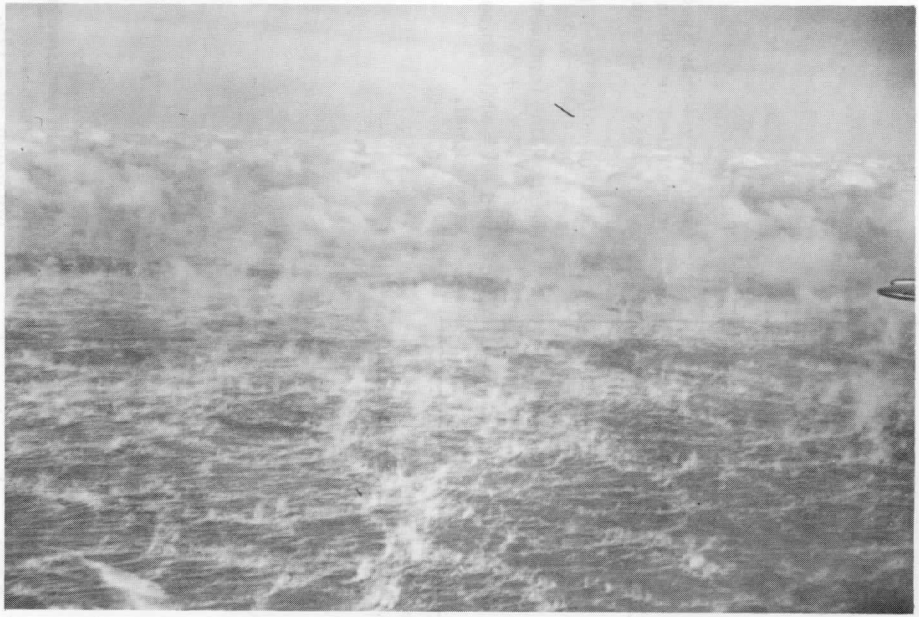

FIG. 27. Convective activity over Lake Michigan on 30 January 1965. View is towards the east, less than 10 km from Milwaukee, with the wind from the west.

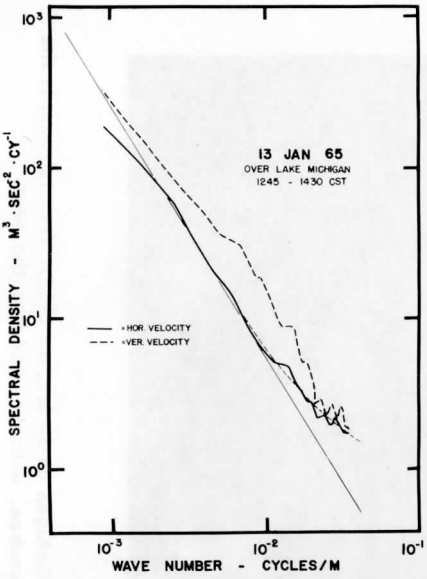

FIG. 28

Average velocity spectra in modified air 200 m above Lake Michigan, df = 235.
Straight solid line represents $a\epsilon^{2/3} k^{-5/3}$
Dashed line represents $a\epsilon^{2/3} k^{-5/3} + B$,
with B = white noise error signal.

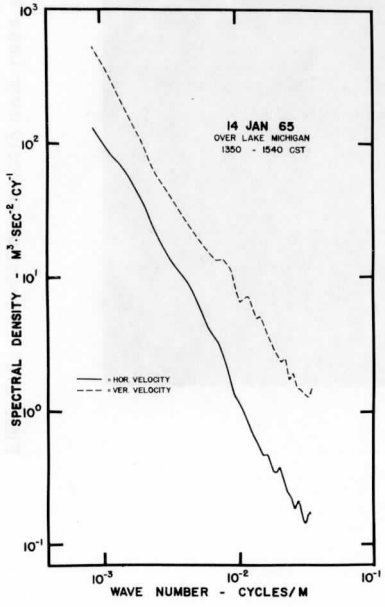

FIG. 29

Average velocity spectra in modified air 300 m above Lake Michigan; df = 170.

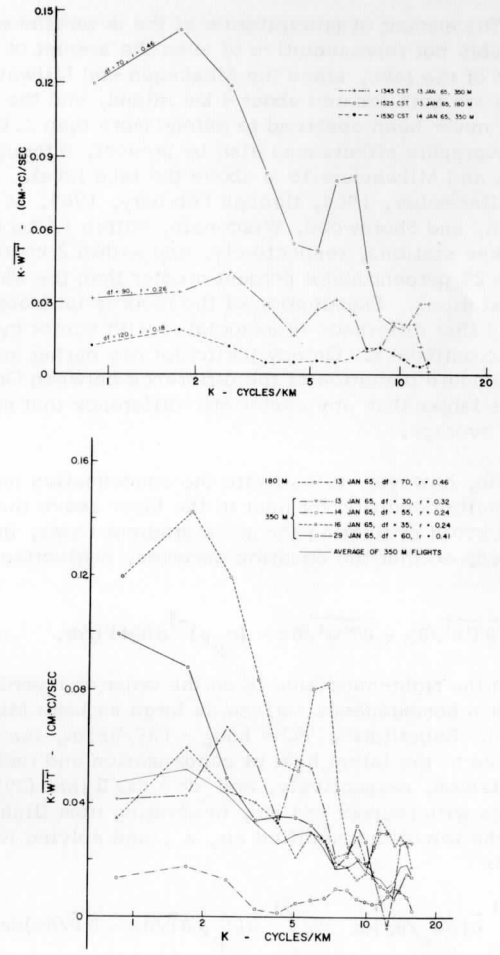

FIG. 30. Co-spectra of w' and T' over Lake Michigan.

condensation. The amount of precipitation at the downwind weather stations is probably not representative of even the amount of precipitation at the shore of the lake, since the Muskegon and Milwaukee weather stations are both located about 4 km inland, and the layer of modified air has never been observed to extend more than 2.0 km above the surface. Orographic effects may also be present, although Muskegon is only 15 m and Milwaukee 36 m above the lake level. Precipitation records for December, 1964, through February, 1965, at Grand Haven, Michigan, and Shorewood, Wisconsin, within 13 km of Muskegon and Milwaukee stations, respectively, and within 2 km of the lake were found to be 27 percent and 8 percent greater than the Muskegon and Milwaukee stations. Examination of the records indicates, however, that almost all of this difference is associated with winter cyclones, rather than arctic outbreaks. On any particular day during an arctic outbreak, the standard deviation of the difference between Grand Haven and Muskegon is larger than any systematic difference that may occur in the long term average.

It is possible, however, to estimate the condensation term by applying the continuity condition for heat to the layer above the lowest flight level. To avoid evaluating the mean gradient terms, the total derivative is used, so that the equation becomes, neglecting density fluctuations,

$$d\bar{T}/dt = -\overline{\partial T'u'}/\partial x - \overline{\partial T'w'}/\partial z - (c_p\rho)^{-1}d(Q+P)/dt. \qquad (39)$$

The first term on the right-hand side is on the order of 1 percent of the second term over a homogeneous surface as large as Lake Michigan, and can be neglected. Substituting $dQ = Ldq_s - (\partial F/\partial z)dt$, the amount of energy change due to the latent heat of condensation and radiation absorption and emission, respectively, and $dt = dx/\bar{u}$ into (39), neglecting local changes with respect to time, integrating from flight level, $z_0 = 350$ m, to the top of the modified air, z, and solving for the latent heat term, yields

$$L_a = L\int_{z_0}^{z_1}\bar{u}(\partial q_s/\partial x)dz = \int_{z_0}^{z_1}\bar{u}(c_p\rho\,\partial\bar{T}/\partial x - \partial\bar{P}/\partial x)dz -$$

$$- c_p\rho\,(\overline{T'w'})z_0 + (F_1 - F_0). \qquad (40)$$

It was observed during the flights that almost all of the condensation takes place above 350 m, so that this expression can be used to estimate the amount of energy added to the air mass by condensation.

The first term on the right-hand side can be obtained by measuring the area between the initial and final vertical temperature profiles, and by using the pressure at the beginning and end of the flight path. The second term was determined from fluctuation data over the middle and downwind sections of the lake, and two times the average measurement was taken, since, as pointed out in Section 3.3.2, the airplane system responded so that only about 50 percent of the total vertical heat flux was directly accounted for. The third term is estimated on the basis of the average cloud cover, height of clouds and vertical temperature and humidity profiles. A computer program developed at the Meteorology Department at Madison, Wisconsin, by Dr. P. M. Kuhn of the U. S. Weather Bureau, was used to compute the upward radiation flux divergence. The technique is based on isothermal flux emissivities, as described, for example, by Haltiner and Martin (1957, p. 120). Concerning the short-wave radiation term, Manabe (1957) has estimated, for a similar case of air mass modification over the Sea of Japan, that its contribution to the flux divergence was less than 10 percent of that of the long-wave. The total radiation flux divergence was found to be negligible at 350 m; the amount of radiation emitted upwards by the clouds and modified air above 350 m is balanced by absorption of the radiation emitted by the surface of the lake. The values of the term of (40) for four cases over Lake Michigan are presented in Table 3, where Q_a and H_a are the first and second terms on the right-hand side of (40).

The magnitude of the total sensible and latent heat fluxes, $Q_S = H_S + L_S$, carried through the downwind boundary, can be estimated from the mean horizontal gradient, c_pT and Lq, respectively. Under the assumption that the contribution by the fluctuation terms and the local time derivative is negligible, integrating over the height of the modified layer of air

$$Q_s = c_p \int_0^{z_1} \rho \bar{u}(\partial \bar{T}/\partial x)dz + L \int_0^{z_1} \bar{u}(\partial q/\partial x)dz. \qquad (41)$$

Both of the derivatives on the right-hand side were measured at 350 m. Since this represents, in most cases, approximately the middle of the modified air mass, it is assumed that estimates of Q_S can be obtained by using the mean measured velocity and derivatives at this height.

The total flux of energy from the lake is given by $Q = Q_S + F_S$, where F_S is the net radiation flux at the upper surface of the modified air, calculated by means of Kuhn's flux emissivity program mentioned previously. An estimate of the total amount of water carried out by the

TABLE 3. Values of energy fluxes calculated from airplane measurements over Lake Michigan during outbreaks of arctic air in January, 1965.

Date:	9 Jan	13 Jan	16 Jan	29 Jan
Geostrophic winds - V_g, m/sec	11.0	18.5	16.4	18.0
Azimuth, deg	10	350	45	320
Measured west comp. of wind at 350 m, m/sec	8	10	- 8	2
Energy fluxes at flight level and above				
Q_a ly/min	0.05	0.13	0.14	0.04
H_a ly/min	0.00	0.06	0.06	0.06
L_a ly/min	0.05	0.07	0.08	-0.02
Precipitation (mm/day				
calculated	1.1	1.5	1.7	-
measured	0.3	1.3	Trace	2.5
Total Energy Fluxes				
H_s ly/min	0.35	0.48	0.32	0.15
L_s ly/min	0.08	0.12	0.09	0.02
F_s ly/min	0.10	0.12	0.12	0.12
Q ly/min	0.53	0.72	0.53	0.30
Water Transported by Clouds (mm/day)	1.2	0.8	0.9	0.2

clouds was made by assuming the average water density of the clouds was 0.5 gm/m^3, and the clouds were moving at the velocity measured at 350 m. Values of these parameters, along with the surface geostrophic wind calculated from the 1200 CST surface weather map, and observed precipitation at the downwind weather station are presented in Table 3.

In this study, the turbulent transfer of sensible heat downward through the inversion has not been considered. This effect may have resulted in the observed downward sensible heat flux of -4.1 watts/m^2, at 350 m on 9 January, the day which showed the greatest observed temperature contrast across the inversion. Bunker (1960) has also observ d a downward sensible heat flux at 400 to 500 m and an upward heat flux at lower levels in cold air masses passing over relatively warm water.

The calculated value of condensed water for the first three cases in Table 3 appears to be reasonable, in view of the observed precipitation and the estimate of the amount of water contained in the clouds over the lake. The sensible heat flux for the 29 January flight, however, is greater than the measured change in heat energy above 350 m. The measured west component of the wind on this day seems small in comparison with the surface geostrophic wind. The surface wind at the Weather Bureau Stations was 2 m/sec from the west at Milwaukee and 3 m/sec from the north at Muskegon. The surface of the lake was much smoother than for the other 3 days considered in Table 3. This was, however, partly due to the damping effect of large areas of floating ice, especially close to Muskegon. The maximum temperature measured at 350 m height was about 20 km west of Muskegon; therefore, it is possible that unmodified arctic air may have lowered the temperature directly over Muskegon. The air over Milwaukee was about 2.0 C warmer than at the same height over Muskegon above the modified layer. These factors both tend to make the measured values of Q_a, H_s and L_s less than the actual values. For these reasons, 29 January is not included in the averaged values of H_s and L_s entered in Table 4.

A comparison between changes of sensible and latent heat obtained here and values obtained by other investigators, as tabulated by Roll (1965, p. 351), is presented in Table 4. Included are also estimates for air flow over Hudson Bay obtained by Bryson and Kuhn (1962). In contrast to the other values, their estimate is a monthly average, for December. The previous modification studies referred to air flow over oceans, with horizontal trajectories of several hundred kilometers. The ocean surface temperatures ranged up to 10 C, and the air masses were about as cold, or colder than those considered here. Therefore, it is not surprising to find the values of fluxes obtained over Lake Michigan to be less than according to previous investigations. The fraction of latent heat to total energy also tends to be somewhat lower than that reported in the other investigations. This may be due to the lower surface temperature and the relatively restricted modification taking place over a distance of 120 km, as compared to oceanic trajectories.

TABLE 4. Comparison of Air Modification Studies Involving Cold Air Passing Over a Relatively Warm Water Surface

Date	Investigator	L_s ly/day	H_s ly/day	Percent of energy due to latent heat
1944	Lettau	720	1340	35
1951	Craddock	265	865	23
	extreme	335	1565	18
1957	Manabe	450	1000	31
1962	Bryson and Kuhn	23	74	24
1965	Lenschow	139	550	20
	extreme	173	690	20

6. Concluding Remarks

Airborne measurements in the atmospheric boundary layer are beset by many problems not encountered by fixed installations. Instrumentation must be portable, fast-responding and rugged, and require a minimum of in-flight attention. For turbulence measurements, it is also necessary to know the instantaneous position of the airplane with respect to the earth. This is not possible to achieve for wavelengths greater than 1.4 km with the system used here for measuring vertical velocity. Therefore, in order that the variables have the same frequency response, the airplane is assumed to have negligible changes in horizontal velocity and altitude with respect to the earth for wavelengths shorter than 1.4 km and the sensor outputs are filtered to eliminate contributions longer than this.

If longer wavelength fluctuations are to be measured accurately, a more sophisticated and considerably more expensive system is required. Within the limitations of the system used here, the spectra of velocity and temperature at airplane flight levels can be measured within the inertial sub-range, and into the energy-containing region of the spectra. However, no peak in the spectra is reached, and only about 50 percent of the vertical fluxes generated by convection are actually measured.

Extending the long wavelength response of the velocity and temperature sensors could probably be done by using higher precision sensors in the vertical velocity system, and measuring horizontal accelerations of the airplane.

In the past, as mentioned in Chapter 1, airplane measurements of water vapor flux have been based on data from a wet bulb sensor. Many problems are associated with this technique; first, both the wet and dry bulbs must have identical response time; second, the wet-bulb must be kept moist at all times; and, third, the system does not work below 0 C. Therefore, an improved system should be considered. A cavity refractometer may offer a more satisfactory solution. The response time is more than adequate, and it has been successfully operated in aircraft. Its response, however, is a function of absolute humidity, air temperature and pressure.

Because of the great versatility of the airplane, many different types of boundary layer problems can be studied. If the measurements are to be applied to a theoretical model of boundary layer structure, it is important to obtain as much information as possible about the ambient conditions of the free atmosphere and the interactions of the earth's surface with the air. It is also desirable to obtain simultaneous but independent measurements of the same atmospheric parameters, in order to check both the measuring technique and the value of the parameters. For this reason, the experiments over Lakewood, Wisconsin, were included in this study, because they provided independent values of stress and energy production by wind shear. In a corresponding manner, the Lake Michigan experiments were arranged so that a study of air mass modification over a relatively smooth, homogeneous surface, provided background information on the magnitude of eddy, convectional energy fluxes. More measurements of this type should be made. Simultaneous balloon and airplane measurements should be extended to different types of terrain under a variety of ambient atmospheric conditions. Simultaneous tower and airplane measurements of turbulence and heat and momentum fluxes would also be desirable. Air mass modification studies over Lake Michigan would be greatly improved if mean wind profiles could be obtained, at least at the upwind and downwind shores of the lake.

It is evident, therefore, that the results reported here are only a first approach to the more general problem of relating changes, both in time and space, of the earth's surface variables to variations in the micrometeorological parameters of the boundary layer. Such knowledge will be the prerequisite both for an improved evaluation of our environment and for control and practical modification of specific microclimates.

Acknowledgments

I wish to express my gratitude to Dr. Heinz Lettau, whose advice and encouragement have been of paramount importance to me during all stages of this work. Original development of the airplane used here as a micrometeorological measuring platform is due to Dr. John A. Dutton. The cooperation of Mr. Roland Mack, who piloted the airplane and willingly volunteered to perform many other tasks not ordinarily required of a pilot, Mr. Sherman Hallen, who did his usual excellent job of modifying the airplane for measuring purposes and mounting instruments on the airplane, and Mr. Charles Hutchins who wrote the sub-routines used to compute the spectra and co-spectra, is gratefully acknowledged. I also thank my wife, Janette, for her assistance and encouragement during the course of this work.

References

Ball, F.K., 1960: "Control of Inversion Height by Surface Heating," Quart. J. Roy. Meteor. Soc., 86, 483.

Ball, F.K., 1961: "Viscous Dissipation in the Atmosphere," J. Meteor., 18, 553.

Batchelor, G.K., 1953: The Theory of Homogeneous Turbulence, Cambridge University Press, London.

Blackmann, R.B. and J.W. Tukey, 1958: The Measurement of Power Spectra, Dover Publications, New York.

Bryson, R.A., and P.M. Kuhn, 1962: "Some Regional Heat Budget Values for Northern Canada." Geograph. Bulletin No. 17, Dept. Mines and Technical Surveys of Ottawa.

Bunker, A.F., 1955: "Turbulence and Shearing Stresses Measured Over the North Atlantic by an Airplane Acceleration Technique," J. Meteor. 12, 445.

Bunker, A.F., 1957: "Aircraft (PBY-6A) Fluctuation and Flux Data—Woods Hole Oceanographic Institution," Sec. 5.3 in "Exploring the Atmosphere's First Mile," (H. Lettau and B. Davidson, eds.) Pergamon Press, London and New York.

Bunker, A.F., 1960: "Heat and Water Vapor Fluxes in Air Flowing Southward Over the Western North Atlantic Ocean," J. Meteor., 17, 52.

Charnock, H., J. R. D. Francis and P. A. Sheppard, 1956: "An Investigation of Wind Structure in the Trades: Anegada, 1953," Roy. Soc. London. Phil. Trans., A249, 179.

Craig, R. A., 1946: "Measurement of Temperature and Humidity in the Lowest 1000 Feet of the Atmosphere over Massachusetts Bay," Papers Phys. Oceanog. Meteor., 10, No. 1.

Craig, R. A., 1949: "Vertical Eddy Transfer of Heat and Water Vapor in Stable Air," J. Meteor., 6, 123.

Cramer, H. E., F. A. Record, J. E. Tillman and H. C. Vaughan, 1961: "Studies of the Spectra of the Vertical Fluxes of Momentum, Heat and Moisture in the Atmospheric Boundary Layer," Annual Report, Contract No. DA-36-039-SC-80209, Dept. of Meteor., Mass. Inst. of Tech.

Cramer, H. E., F. A. Record and J. E. Tillman, 1962: "Studies of the Spectra of the Vertical Fluxes of Momentum, Heat and Moisture in the Atmospheric Boundary Layer," Final Report, Contract No. DA-36-039-SC-80209, Dept. of Meteor., Mass. Inst. of Tech.

Craddock, J. M., 1951: "The Warming of Arctic Air Masses Over the Eastern North Atlantic," Quart. J. Roy. Meteor. Soc., 77, 335.

Deacon, E. L., 1959: "The Measurement of Turbulent Transfer in the Lower Atmosphere," Advances in Geophysics, 6, 211.

Dean, R. C., 1953: Aerodynamic Measurements, Mass. Inst. of Tech., Cambridge, Mass.

Dutton, J. A. and D. H. Lenschow, 1962: "An airborne measuring system for micrometeorological studies," Annual Report, Contract No. DA-36-039-SC-80282, Dept. of Meteor., Univ. of Wis., Madison, Wis.

Frenzen, P., 1965: "Determination of Turbulence Dissipation by Eulerian Variance Analysis," Quart. J. Roy. Meteor., Soc., 91, 28.

Goodman, N. R., 1957: "On the Joint Estimation of the Spectra, Cospectra and Quadrature Spectrum of a Two-dimensional Stationary Gaussian Process," Scientific Paper No. 10, Engineering Statistics Laboratory, College of Engr., New York Univ.

Gurvich, A. S., 1960: "Measurement of the Skewness Coefficient for the Distribution of the Velocity Differences," Doklady ANSSSR, 134, 1073.

Haltiner, G. J. and F. L. Martin, 1957: Dynamical and Physical Meteorology, McGraw-Hill, New York.

Hinze, J. O., 1959: Turbulence, McGraw-Hill, New York.

Holloway, J.L., Jr., 1958: "Smoothing and Filtering of Time Series and Space Fields," Advances in Geophysics, 4, 351.

Johnson, W.B., 1965: "Atmospheric Boundary-Layer Dynamics Over the Forests of Northeastern Wisconsin," Ph.D. Thesis, Dept. of Meteor., Univ. of Wisconsin, Madison, Wis.

Jones, J.I.P. and F. Pasquill, 1959: "An Experimental System for Directly Recording Statistics of the Intensity of Atmospheric Turbulence," Quart. J. Roy. Meteor. Soc., 85, 225.

Kolmogorov, A., 1941a: "The Local Structure of Turbulence in Incompressible Viscous Fluid for Very High Reynolds' Number," Doklady ANSSSR, 30, 301.

Kolmogorov, A., 1941b: "Dissipation of Energy in Locally Isotropic Turbulence," Doklady ANSSSR, 32, 16.

Kraichnan, R.H., 1959: "The Structure of Isotropic Turbulence at Very High Reynolds' Numbers," J. Fluid Mech., 5, 497.

Kraichnan, R.H., and E.A. Spiegel, 1962: "Model for Energy Transfer in Isotropic Turbulence," Physics of Fluids, 5, 583.

Kyser, J.G., 1959: "Measurement of Atmospheric Turbulence," CER-13-59, Giannini Controls Corp., Pasadena, Calif.

Lenschow, D.H., 1962: "Technique and Results of Surface-Temperature Determination with an Airborne Bolometer," Annual Report, Contract No. DA-36-039-SC-80282, Dept. of Meteor., Univ. of Wis., Madison, Wis.

Lettau, H.H., 1939: Atmosphärische Turbulenz, Akademische Verlag. M.B.H., Leipzig.

Lettau, H.H., 1944: "Die Thermodynamische Beeinflussing arktischer Luftmassen über warmen Meeresflachen als Problem der Meteorologischen Stromungs- u. Turbulenzlehre," Schr. Deut. Luftfahrtforschung, 8 (3), 85.

Lettau, H.H., 1959: "Research Problems in Micrometeorology," Final Report, Contract No. DA-36-039-SC-80063, Univ. of Wis., Madison, Wis.

Lettau, H.H., 1961: "Dissipation of Energy by Turbulence," J. Meteor., 18, 125.

Lumley, J.L. and H.A. Panofsky, 1964: The Structure of Atmospheric Turbulence, Interscience Publishers, New York.

MacCready, P. B., Jr., 1953: "Structure of Atmospheric Turbulence," J. Meteor., 10, 434.

MacCready, P. B., Jr., 1962: "The Inertial Subrange of Atmospheric Turbulence," J. Geophys. Research, 67, 1051.

MacCready, P. B., Jr., and H. R. Jex, 1964: "Turbulent Energy Measurements by Vanes," Quart. J. Roy. Meteor. Soc., 90, 198.

Manabe, S., 1957: "On the Modification of Air-Mass Over the Japan Sea When the Outburst of Cold Air Predominates," J. Meteor. Soc. Japan, 35, 311.

Myrup, L. O., 1965: "The Structure of Thermal Convection in the Lower Atmosphere Under Conditions of Light Winds and Strong Surface Heating," Ph. D. Thesis, Univ.of Cal. at Los Angeles, Los Angeles, Cal.

Panofsky, H. A. and G. W. Brier, 1958: "Some Applications of Statistics to Meteorology, The Pennsylvania State University, University Park, Pennsylvania.

Panofsky, H. A., 1962: "The Budget of Turbulent Energy in the Lowest 100 Meters," J. Geophys. Research, 67, 3161.

Pasquill, F., 1962: "Recent Broad-Band Spectral Measurements of Turbulence in the Lower Atmosphere," J. Geophys. Research, 67,

Pond, S., R. W. Stewart and R. W. Burling, 1963: "Turbulence Spectra in Wind over Waves," J. Atmosph. Sci., 20, 319.

Press, H., M. T. Meadows and I. Hadlock, 1956: "A Re-evaluation of Data on Atmospheric Gust Loads for Application in Spectral Calculations," NACA Rep. 1272.

Proudman, I. and W. H. Reid, 1954: "On the Decay of a Normally Distributed and Homogeneous Turbulent Velocity Field," Phil. Trans. Roy. Soc., 247, 163.

Roll, H. U., 1965: Physics of the Marine Atmosphere, Academic Press, New York.

Tatsumi, T., 1957: "The Theory of Decay of Incompressible Isotropic Turbulence," Proc. Roy. Soc., A, 239, 16.

Telford, J. W. and J. Warner, 1964: Fluxes of Heat and Vapor in the Lower Atmosphere Derived from Aircraft Observations," J. Atmosph. Sci., 21, 539.

Taylor, R. J., 1952: "The Dissipation of Kinetic Energy in the Lowest Layer of the Atmosphere," Quart. J. Roy. Meteor. Soc., 78, 179.

Super, A. B., 1965: "A Study of Small-Scale Air Mass Modification Over Lake Mendota," Ph. D. Thesis, Dept. of Meteor., Univ. of Wis., Madison, Wis.

Townsend, A. A., 1959: "Temperature Fluctuations Over a Horizontal Surface," J. Fluid Mech., 5, 209.

Warner, J. and J. W. Telford, 1962: "On the Measurement from an Aircraft of Buoyancy and Vertical Air Velocity in Cloud," J. Atmosph. Sci., 19, 415.

Warner, J. and J. W. Telford, 1963: "Some Patterns of Convection in the Lower Atmosphere," J. Atmos. Sci., 20, 313.

MEASUREMENTS OF INFRARED RADIATION DIVERGENCE AND TEMPERATURE PROFILES NEAR AN AIR-WATER INTERFACE*

Harry L. Hamilton, Jr.
Department of Meteorology
University of Wisconsin

Abstract: A review is given of the assumptions which are conventionally made for the mathematical description of the thermal structure in the layer nearest to the ground, with special consideration of air over water. Micrometeorological equipment was constructed and employed in an experimental program over Lake Mendota to investigate the significance of infrared radiative fluxes and their vertical divergence between 0.4 to 2.8 m above the water. The major characteristic of the equipment is the continuous sweeping or vertical orbiting of sensors (at a rate of about 3 cm/sec) with values of net radiation, dry-bulb and wet-bulb temperatures sampled at height intervals of about 10 cm.

A program was developed based on Funk's method to derive by machine calculation the radiative flux divergences, using the observed temperature and water vapor profiles. In an attempt to generalize the experimental results, two dimensionless parameters (α and δ) are considered which are the logarithmic height derivatives of measured radiative flux (R) and of potential temperature gradient (θ'),

$$\alpha = \partial \log R / \partial \log z; \quad \text{and,} \quad \delta = -\partial \log \theta' / \partial \log z.$$

The second form is also known as the Deacon number of the temperature profile and represents a numerical measure of profile curvature with δ equal to unity for an exactly logarithmic potential temperature profile.

*This work is part of a thesis submitted to the University of Wisconsin in partial fulfillment of the requirements for the Ph. D. degree, written under the supervision of Professor H. Lettau, Department of Meteorology.

A sizable amount of data was obtained during late summer and early fall seasons, for both stable and unstable conditions of the air over water. The experimental evidence obtained in this study appears to show that radiation flux divergence over a water surface is of a magnitude great enough to produce the observed temperature change. Much of the divergence occurs very close to the water surface, where there are relatively large gradients of temperature and moisture. Yet even at 1 to 2 m from the surface, there is detectable divergence. In general, little agreement between calculated and directly observed values of radiation divergence was found, whether derived from single orbits of the sensors, or from up to 20-orbit averages, in spite of a sufficient degree of reproducibility of direct results from individual orbits. Suggestions for future work are outlined.

1. Observed Thermal Structure of the Lowest Atmosphere

Within a few meters of the earth's surface the air tends to assume the temperature characteristics of the surface itself. This is because most surfaces have higher absorption (or emission) coefficients than air. Thus, during the day solar radiation heats the surface to a greater degree than it does the air, and there will be a net heat exchange from the surface to the atmosphere. At night, the surface loses heat by radiative emission at a greater rate than does the air, and there will be a net exchange from air to the surface. Conventionally, it has been assumed that the mechanism for this transfer is turbulent diffusion. Other meteorologists have suggested that infrared fluxes are important in the lowest layers of the atmosphere. It will be the aim of this paper to give some qualitative and quantitative description of the radiation flux divergence as it relates to the establishment of the heat regime near the ground.

Deacon (1953), in a study of wind and temperature profiles near the ground, considered the vertical gradient of temperature inversely proportional to the distance from the surface. He expressed the potential temperature gradient as $\theta' = a\, z^{-\delta}$, where a is a dimensional parameter derived from the eddy heat flux (Q) and the wind structure, and the number δ is assumed a quasi-constant within the surface layer for a given heating rate, but varies with the heating rate. For lapse conditions, $\delta > 1$, while for inversion conditions, $\delta < 1$. Under neutral, or adiabatic, conditions, i.e., potential temperature independent of height, $\delta = 1$. However, this case is significant only for wind or elements other than temperature, since $\theta' = 0$ for the neutral case. Deacon noted some variation of δ with height but did not consider this data adequate to properly evaluate the relationship.

More recent temperature profile data exist which yield more detailed information than was available to Deacon. Among others, Lettau (1957, 1962, 1963) has investigated the problem and has developed several pertinent relationships. He slightly redefines δ, now called the potential temperature Deacon number and alternatively written $\underline{DE}$, as $\delta \equiv -z\theta''/\theta'$, where primes indicate partial derivatives with respect to height, z. Since it is known that Deacon number is a function of stability, there should be a relationship between Deacon number and Richardson number, which is defined as $\underline{Ri} \equiv (g/T_m)(\theta'/V'^2)$, where g is the acceleration of gravity, T_m is the mean Kelvin temperature of the layer under study, and V is wind velocity. By a logarithmic differentiation of Richardson number, it may be seen that $\partial \log \underline{Ri}/\partial \log z \equiv -2\, z\, V''/V' + z\theta''/\theta' \equiv 2\,\underline{De} - \underline{DE}$, where $\underline{De}$ is the wind Deacon number. Thus, unless $2\underline{De} = \underline{DE}$, $\underline{Ri}$ is a function of height and, consequently, δ must also be a function of height. From similarity considerations, most meteorologists assume that $\underline{De} \doteq \underline{DE}$. Therefore, Deacon number is not only dependent on the stability of the atmosphere, but also on the distance from the interface.

The coefficient of eddy conductivity may be defined as $K_H \equiv -Q/c_p\rho\theta'$. While θ' is generally a function of height, from this defining equation it is unclear as to whether K_H is also height-dependent. If the above identity is rearranged and integrated, it is seen that $\theta_z - \theta_0 \equiv -\int_0^z (Q/c_p\rho K_H)dz$. Since the heat flux in the air at any height above a surface may be assumed to be determined by the surface value of the flux and the flux gradient in the intervening air, $Q = Q_0 + \int_0^z Q'dz$. If z is within Lettau's surface layer, then $Q \doteq Q_0$, and $\theta_z - \theta_0 \equiv -Q_0/C_p\rho \int_0^z dz/K_H$. Thus, if K_H as a function of height is known, the potential temperature (and close to the surface, actual temperature) profile can be predicted. The traditional logarithmic profile is obtained by assuming that K_H is directly proportional to height. The various power law profiles are obtained by assuming that K_H varies as some power of the height. All of these profiles are approximations, due to the assumptions made concerning K_H and Q. Virtually all boundary layer theory has been developed with the tacit assumption that the various fluxes are independent of height; the diffusivity coefficients are then adjusted to agree with observational data.

Yet the fluxes are a function of height. Some insight into the problem could possibly be gained by measuring certain fluxes and determining even small vertical gradients. Consider a point near a lake surface quite some distance from the shore on a clear day. If F is the net-

radiation flux density, the temperature change within a small volume, of vertical extent Δz, located at this point is

$$\dot{\bar{T}} = (F_B - F_T)/c_p \rho \Delta z + (Q_B - Q_T)/c_p \rho \Delta z,$$

where subscripts B refer to the bottom, and T to the top of the volume. Alternatively, $c_p \rho \int \dot{\bar{T}} dz = (F_B - F_T) + (Q_B - Q_T)$. During the forenoon, $\dot{\bar{T}} > 0$; in the afternoon, $\dot{\bar{T}} < 0$. At some time past local noon, $\dot{\bar{T}} = 0$ throughout the box, and $(F_B - F_T) + (Q_B - Q_T) = 0$. The question of interest is whether these flux divergences are actually both zero at this time, or whether they are equal in magnitude and opposite in sign.

Although it has just been shown that heat flux should be considered a function of height, the assumption has often been made that the heat flux through the lower layers of the atmosphere is constant and that $\delta = 1$ for the surface layer. Under this assumption, to a first order approximation, the temperature above an interface is proportional to the logarithm of the height. This relationship is not meaningful as z becomes small. This fact, together with the realization that the character of the surface itself will determine in some way the eddy structure of temperature distribution above it, has led to the inclusion of another factor in the expression for temperature variation with height. This is z_0, the surface roughness length, which is a measure of the irregularities in a surface over which the wind is blowing. Deacon (1949) lists the approximate magnitude of the z_0 associated with various types of natural surface, ranging from 0.001 cm for smooth mud flats to 10 cm for long grasses. With z_0 included, the relationship takes the form $(T - T_0) \sim \log(1 + z/z_0)$, T_0 being the surface temperature. From this it may be seen that

$$(T - T_0)/(T_{200} - T_0) = \log(1 + z/z_0)/\log(1 + 200/z_0),$$

where T_{200} is the temperature at a height of 200 cm. Given a temperature difference between the surface and 200 cm, the temperature at any intermediate height will depend on the logarithm of that height and the value of z_0.

Many investigators have obtained experimental evidence that the temperature in the atmosphere's lower layers may largely be described by the logarithmic relationship. However, only a few of these experiments have been carried out over a water surface, and only a very limited number of observations have been taken within a few tens of centimeters of a free water surface. Stearns (1962) and Super (1965) obtained results which closely coincide with this theory for adiabatic

conditions, but their lowest measurements were at a height of 40 cm. Fleagle (1956) determined heating and cooling rates in air layers adjacent to a cold water surface, by means of light refraction, but he did not analyze the characteristics of the temperature profiles.

Any rigid surface is assumed to have a characteristic roughness value (z_0) independent of wind speed. On the other hand, there seems to be some evidence that a surface which may be modified by the wind, such as a lake or large field of grain, has a slightly variable surface roughness. Super finds that over Lake Mendota z_0 increases with increasing wind speed; for speeds below 10 m/sec it has an average value of 0.007 cm. Stearns derived values of z_0 for the same lake between 10^{-2} and 10^{-3} cm. Both investigators obtained these values from wind profile studies, but it is often assumed that these results would apply to the temperature profile as well. Sutton (1953) cites work done by Schiller, which indicated that when z_0 for a surface is less than 0.002 cm, air flow over that surface is aerodynamically smooth and a viscous sublayer exists at the surface.

From the evidence above, it might be expected that an observed temperature profile within centimeters of a free water surface would substantially reflect a logarithmic variation with $(1 + z/z_0)$, and that z_0 would be no less than 10^{-3} cm. This author (1962) has measured temperature profiles which extended from 200 cm above a water surface down through the air/water interface to a depth of 80 cm. Profiles were obtained under many atmospheric conditions, from clear skies to overcast to fog; from moderate wind to calm; and with warm air over cool water and vice versa.

The expected temperature profile was not found. For substantial agreement between the observed profile and the logarithmic profile, z_0 would be less than 10^{-4} cm. In some cases, the observed profiles appeared to have no curvature in the closest few centimeters to the water surface, or, in other words, the existence of a true temperature discontinuity between air and water was suggested.

There were several possible explanations for the deviation from the logarithmic profile. To calculate the logarithmic profile, the temperature at the surface and at one other height must be known. There may have been a thin surface layer of water, less than 1 mm thick, which was at a different temperature from the water at a depth of 10 to 20 cm. Though the sensor had a relatively short response time (0.2 sec) it would have passed through such a layer much too rapidly to have detected it. A so-called skin effect has been noted by several

investigators, among them being Soules (1964), Ball (1954), and Deacon (1962). They have found that the surface temperature of an open body of water is, under light winds, generally between 0.5 and 1.5 C cooler than the temperature at a depth of 20 to 30 cm. This cooling is attributed to the evaporation occurring at the surface. Ball also observed a warm layer when the overlying air was appreciably warmer than the water. Thus, had T_0 actually been higher than the value used, at times with warm air over the lake, and lower than this value, at times with overlying cold air, the logarithmic profile would have more closely resembled the actual profile.

A second possibility was that within a thin layer of air at the water surface the air flow was aerodynamically smooth. In this viscous sublayer the heat transfer would be by molecular diffusion, which could produce a nearly constant temperature gradient. The top of the sublayer would then be significantly warmer or cooler than the actual surface, depending on the air-water temperature difference. The temperature at the top of this viscous sublayer (unresolved by the sensors) would be the bottom temperature for the region of turbulent flow, where height-increasing eddy diffusivity dominates, and where it is permissible to use the logarithmic profile. Again, had this process been occurring, the logarithmic profile and actual profile would have been more in agreement.

A third process which could have been operative would be a heat transfer by radiation. The line of reasoning which leads to the logarithmic profile omits radiative fluxes, and these could be as important as sensible heat fluxes. While not denying the validity of the two above explanations, this third problem was chosen for investigation.

Experimentation was begun to determine whether there was in fact significant infrared radiative flux divergence in the region of a few meters above a free water surface which could possibly modify the temperature regime. After radiometers had been constructed and direct measurements of radiation profiles had been made for several months, the results indicated that confirmation by a second method was advisable. The second method adopted as a calculation of the radiative flux divergence based on temperature and water vapor profiles. Earlier work along these lines by other investigators, equipment for the experiment, and the method for calculating flux divergence are described in the next sections.

2. Previous Investigations of Radiative Flux Divergences

Several investigators have obtained evidence that it is not always valid to assume that radiative flux divergence is negligible. Robinson (1950a) found that radiative heating or cooling of the air may account for a heat transfer of from 10 to 100 times as large as that necessary to produce an observed temperature change. His work was done over short grass, at levels of 20 and 120 cm, and primarily at night to avoid large temperature fluctuations. During periods of strong inversion, he observed flux divergences of about 1.5 mly/min per meter (1 mly = 0.001 ly). Robinson has also noted (1950b) that under cloudless skies, radiative heat transfer appears to be as important as convective or turbulent processes in the transfer of heat from the ground.

Funk (1960) developed a high-precision thermopile radiometer and observed significant radiative divergences at night. He concluded that nighttime cooling of the air was primarily radiative and that the divergences within a few meters of the ground may be capable of cooling rates of 12 C/hr. He believed that these high rates were not observed because of a compensating effect of convective warming of the air, of slightly smaller magnitude. This conclusion is similar to one reached by Rider and Robinson (1951), from a study of heat transfer in an open field.

Studying the temperature distribution over a cold water surface by means of light refraction, Fleagle (1956) observed radiative warming at the surface of up to 10 C/hr, and radiative cooling of 6 C/hr at 10 cm above the water. He believed that the large temperature gradients found near the surface were due to the absorption of infrared radiation.

Infrared flux divergence has been studied by Gaevskaya et al. (1962). They report on experiments which compared observed temperature changes with those predicted by a measured radiative flux divergence and by the computational methods based on temperature and moisture. There was quantitative and qualitative agreement between the different computational methods of Kondratiev, Deacon, and Shekhter, but they all predicted a temperature variation greater than that observed. The measured radiative flux divergence at various times of the day bore little relationship to the calculated values. All radiative temperature changes were at least an order of magnitude greater than the observed ones.

This led to the postulation that the observed temperature changes are due to a combination of radiative flux divergence and convective flux

(eddy diffusion) divergence, each of which depends on the existing temperature profile, yet each of which continually modifies the profile. One of the primary conclusions from the paper was that "temperature changes influenced by radiation and turbulence are not additive; separate calculations of either radiative or turbulent temperature changes have no meaning," since either can account for a heating or cooling rate greater than actually occurs. Unfortunately, no suggestion is given for a possible method of separating the effects.

In an analytic analysis of the physics involved, Godson (1965) shows that the radiative flux divergences can be very important near the ground. By making some simplifying and restrictive assumptions about the vertical distribution of CO_2 and H_2O, the principal atmospheric absorbers, and their absorption characteristics, he obtains cooling rates within a few tens of meters of the ground which average about 2 C/hr. Similar to Gaevskay et al., there is discussion concerning the mutual dependency of the temperature profile and radiant, convective, and diffusive fluxes. A possible explanation of the often-noted nocturnal temperature minimum a few centimeters above the surface (e.g., Lettau 1965) is given in terms of radiative fluxes.

3. Description of Equipment Used in This Study

To measure and calculate the vertical divergence of radiative flux, the vertical distribution of radiation, temperature, and water vapor must be known. The conventional method of obtaining this information is to utilize a series of sensors at fixed levels along a vertical mast. However, there are several disadvantages in this procedure which make questionable the validity of its use for intensive measurements of thin air layers, such as were involved in this study.

One drawback is that the data points are spatially discontinuous. The physical size of each sensor limits the proximity of the adjoining sensor, which means that there is some interval between sensors. Probably the most common practice in circumventing this drawback is to place the sensors in such a fashion that near the ground they are as close together as possible, while further away the spacing increases geometrically with height. Even though many parameters, such as wind, moisture, and temperature, are thought to vary logarithmically with height, any arbitrary selection of positions tends to suppress the fine structure of the profile which would be of prime interest. Furthermore, there are problems of calibration, matching, stability, and zero drift

of the sensors and recorders. Complete characteristics of each component must be known in order that the signals may be properly evaluated.

Experiments performed in an area subject to splashing water (for instance, over a lake surface) can involve other difficulties with an array of sensors. There may develop different electrical conditions in the various cablings, which could produce varying and unknown stray signals in the system. Observed features of a profile could then be due to instrumentation, not to nature. If more than one sensor is used to measure a profile, either an adequate multichannel recorder is needed or a switching device for directing the inputs to a single channel recorder is required. The former is expensive, the latter is difficult to operate rapidly and accurately.

An alternate method which eliminates these problems is to utilize equipment which moves a single sensor through the entire layer under study. Measurements are then spatially continuous; only one set of circuit characteristics is needed; there is only one cable to fail and thereby cause an error in the magnitude of the measured quantity but not in the shape of the profile; and only a single channel recorder is required, with no switching of inputs. Since there is only one sensor, each data point in a profile differs in time from each other point. This disadvantage of the moving system can be made relatively unimportant if the period for a complete orbit of the sensor through the layer is sufficiently short. Glaser (1957) was apparently the first worker to describe an apparatus which moved a single sensor continuously along an essentially vertical orbit. An entirely different principle was used in the sweeping-boom mechanism constructed for the research reported in this paper.

The frame of the lifting apparatus resembled a straight-backed chair, with the boom being a rod protruding out of the back (see Fig. 1). The bottom of the frame (seat of the chair) was 1.2 m long, 0.9 m wide; and 0.9 m high; the back extended 1.4 m above the seat. The 4.6 m boom was caused to move in a vertical arc by a small reversible electric motor. The sensor mounting was at the forward end of the boom, 2.4 m from the frame, and it moved in a nearly vertical, 240 cm path as the boom was operated. The speed of the sensors was 3.5 cm/sec. One complete orbit of the sensors lasted 159.3 sec, with a breakdown as follows: boom moving up, 68.6 sec; pause at top, 11.1 sec; boom moving down, 66.9 sec; pause at bottom, 12.7 sec. The operation of the mechanism was controlled remotely and automatically by a special switching circuit. Manual override of commands was possible. All sensors were designed, constructed, and tested by the author, because commercial products did not appear to have the desired characteristics.

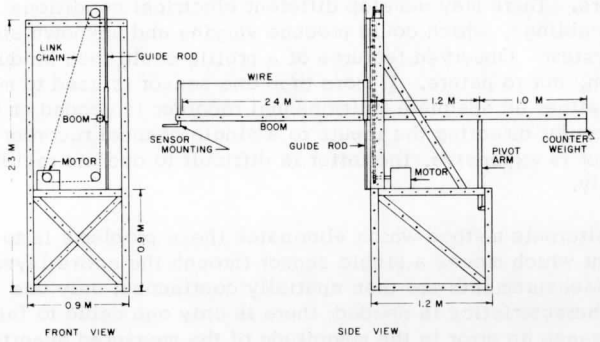

FIG. 1. Sweeping-Boom Mechanism

Thermocouples were used in the temperature sensor. The sensing element itself consisted of five copper-constantan couples in series. Each junction which was exposed to the air was made by soldering #40 copper wire to 2 mil constantan wire, resulting in a junction diameter of about 5 mils. The reference junctions were #30 copper and constantan wires soldered together and enclosed in a small plastic tube. The tube was 1 cm in diameter by 10 cm long, and the reference junctions were encased in epoxy resin within the tube so as to have a large thermal mass. The #30 wire was connected to the fine wire about 4 cm from the sensor junctions. This wire was long enough to allow the reference junction to be up to 4 m away from the sensor. The junctions in the sensor were in a cross arrangement supported by 0.6-cm thick plexiglas. Radiation shields were above and below the junctions. By dipping the sensor into cold water and by alternating hot and cold air streams on the sensor, it was determined that the response time was 0.2 sec.

The radiometers were of the shielded flux plate type described by Suomi et al. (1958), with slight modifications. The flux plates themselves were composed of 2.5 cm × 7.5 cm × 2 mm glass microscope slides, lathe-wound with about 100 turns of 34-gage Advance alloy wire and half-plated with metallic copper. The wound plates were coated with epoxy resin for mechanical protection and electrical insulation. Each plate was suspended in a slot located in the center of a circular polystyrene frame. Over a 8-cm diameter area around the plate the frame was 4 mm thick, which was slightly thicker than the plate itself. The remainder of the inner portion of the frame was 1.2 cm thick. The total diameter of the radiometer was 21.5 cm. Both sides of the flux plate were painted with flat black paint, the spectral absorption characteristics of which were known. The rim of polystyrene supported two polyethylene shields, 13 microns thick, one on either side of the flux plate. The inner polyethylene sheet was 11 mm from the plate and the outer sheet was 18 mm from it.

Polyethylene was used for these shields because it is highly transparent to a wide range of radiation wave lengths and its few absorption bands are not centered on the same wave lengths as are strong atmospheric emitters, such as water vapor and carbon dioxide. Suomi et al. (1958) have studied various materials in search of suitable shielding, and polyethylene has been chosen as the best available.

The top and bottom surfaces of the polystyrene within the radiometers were covered with flat black paint. The purpose of the paint was to minimize reflected radiation from the center partition. A portion of any reflected radiation would in turn be reflected from the polyethylene shields back onto the flux plates, creating false values of net radiation. Under intense solar radiation there was great heating on the top side of the partition. DeGraaf and van der Held (1953) have studied heat transfer in thin cells, and they found that if the Grashof number (defined as $Gr \equiv gd^3\beta\Gamma/\nu^2$ where g is gravity, d is the cell thickness, β is the coefficient of thermal expansion, Γ is the temperature difference across the cell, and ν is kinematic viscosity) is less than 2000, heat transfer remains on the molecular level. For the configuration of the radiometers, a temperature difference of 70 C between the black surface and the outer polyethylene shield would still yield $Gr < 2000$. Therefore, it may be assumed that within the radiometers, all heat transfer was by molecular conduction.

The two radiometers were calibrated by comparison with an Eppley pyrheliometer. The three instruments were leveled and placed side by side about 30 cm apart at the end of a pier which extended about 50 ft out from shore into 7 ft of water. The radiometers were suspended 30 cm

above and beyond the end of the pier. Because of this positioning about 10 percent of the radiation incident on the lower side of the radiometers was from the pier and 90 percent was from the lake surface. The output of each instrument was connected via a manual switch to a Brown Electronex strip chart recorder.

Several calibration runs were made, all on sunny days, beginning in late morning and lasting into the afternoon. The calibration was based on the fact that the incident radiation on such instruments could be changed by the same amount and the resulting change in voltage output noted. The change in radiation was brought about by alternately shading the sensors from direct sunlight. The pyrheliometer had been calibrated by the manufacturer, and recalibrated by Stearns at 2.52 mv per ly/min. The change in insolation was determined from the change in voltage of the pyrheliometer; this same change in insolation produced a change in the voltage output of the radiometers; and thus a calibration figure was obtained.

The shade was provided by a piece of gray cardboard, manually held about one meter above the instruments such that all were in the shade. During a 15-min period of shade, several 1-min samples of the output from each radiometer and the pyrheliometer, in addition to an electrical short of the input, were recorded. The same sequence was followed during a 15-min exposure to direct sunlight. The 30-min cycle was repeated eight to ten times on each of three calibration runs. All three instruments reached thermal equilibrium within about one minute of the change in insolation. With incident angles of more than 60°, the transmittance of polyethylene decreases to small values (Tanner et al., 1960). Therefore, the calibrations were obtained only while the sun was within 45° of the zenith.

The calibration was based on changes of short-wave radiation. From studies of the absorptivity of various paints, Suomi (1957) has found that the voltage output due to a change in long-wave radiation would be 6 percent lower than that due to a similar change in short-wave radiation. The calibrated output of Radiometer #III was 1.78 mv per ly/min, and that of Radiometer #IV was 1.47 mv per ly/min. The time constant was determined to be less than one second. Bushnell (1961) gives a time constant of 0.8 sec for a similar radiometer.

The amount of water vapor in the air was determined by measuring the wet-bulb temperature depression of the air. A small, fast-response sensor was hand-made to fulfill the requirements of this study. Temperature differences were measured with thermocouples made of #30 copper

wire butt-soldered to #30 Advance constantan wire. Three sets were in series, with half of the junctions at air temperature and the other half at the wet-bulb temperature. Water was provided by gravity feed from a reservoir to the junctions by means of cotton wicking. The wicks were enclosed in plastic tubing for the 2- to 3-cm distance from the exit of the reservoir nearly to the junctions. Then the wicking was wrapped around the wires, extending 3/4 cm on either side of the actual junction. Packing in the tubing regulated the flow to the point where excess water did not flow onto the wires, yet the wicking always remained wet. The wet junctions were 2 cm behind the dry junctions, both sets being located in a 2-cm diameter plexiglas tube. The front end of the tube pointed away from the boom, the back end was connected to a ventilating tube. The reservoir was 5 cm long and 2.5 cm in diameter. The output of the system was 0.12 mv/deg difference between wet and dry junctions, and the response time was 1/2 sec. This response time was found by changing the temperature of the air over the sensors. Ventilation of 5 m/sec was provided by a squirrel-cage blower.

The primary recording system for the study was printed tape from a printer connected to a digital voltmeter. The amplified signal was transmitted from the lake tower site on underwater cables to the instrument shelter on shore. At the recording center the signal was divided in half and added to a variable bias. From there, the signal, always between -1.0 and +1.0 volt, went to the digital voltmeter (DVM) thence to the printer. The printer and DVM were connected as far as "reading" times were concerned, so that the DVM "read" its input voltage only when the printer was ready to print. A pulse generator was built to trigger the printers, and the normal triggering rate was once per 3 seconds. Each printer had 2 channels, each of which was capable of recording a 3-digit number plus the sign. The Barnes bolometer was used to determine the temperature of the actual surface of the water. Its sensing head was pointed straight down at a position such that its field of view was near the spot where the profiles were taken. This instrument operates by detecting the difference between the emitted radiation from some object and the radiation of known intensity from an internal source. Since radiative energy is proportional to the fourth power of absolute temperature, this radiation difference may be expressed as a temperature difference, and the bolometer is so calibrated. This bolometer had a range of -10 C to 50 C and detected radiation of wavelengths of 8 to 14 microns.

The temperature of an object indicated on the bolometer is the temperature it would have if it were a perfect black radiator. The actual temperature must be derived from the indicated temperature and the

emissivity of the object. However, if a new calibration of the instrument is made using a water surface as the unknown source, no adjustment for emissivity will be necessary when the instrument is later used in the field for measuring water surface temperatures. Such a calibration was performed. Water in an insulated cannister, which was covered by a truncated cone, was vigorously agitated so that the entire water mass would be at thermal equilibrium. The sensing element of the bolometer was directed at the water surface through a hole in the top of the conical cover. The temperature of the water was slowly varied in stages and allowed to come to thermal equilibrium at each stage; a precision mercury-in-glass thermometer was used to obtain the water temperature. A curve of thermometer temperature vs bolometer temperature was obtained and the relationship found such that

$$T_{therm.} = 10 + 1.03\ (T_{bolom.} - 10.25).$$

One of the reasons cited for moving a single sensor through a layer was that spatially continuous profiles could be obtained. The data could be handled by recording the output with an inked pen on a strip chart and then integrating the area between the trace and some reference exits. It was felt that this process would be unnecessarily difficult and time consuming for the investigation described here. All other advantages of the single-sensor system would still obtain if the signals were recorded digitally at regular intervals. The timing could be arranged such that a recording took place at selected height positions as the sensor moved up, and at those same positions as the sensor moved down.

The pattern selected for this method was such that the recording took place every three seconds. Since the sensor moved at a rate of 3.5 cm/sec, values of net radiation, dry-bulb temperature, and wet-bulb temperature were obtained at 10.5 cm intervals, beginning 40 cm above the water surface. There were 24 readings, including one at the top and one at the bottom of the sweep, as the sensors moved through a total distance of 240 cm. All raw data were punched onto cards for computation by an electronic digital computer. Each card contained an identifying number and 24 three-digit numbers representing radiation, dry-bulb temperatures, or wet-bulb temperatures obtained for one up- or down-sweep of the boom. Vertical and time-wise smoothing of the data was performed before actual calculations took place. Let a_{ij} represent a piece of raw data, where i is the cycle number, having values from 1 to N, the number of cycles in the run, and j is the height position, having values from 1 to 24. Then b_{ij}, the smoothed data value, is

$$b_{ij} = \left(\sum_{m=-2}^{+2} \sum_{n=-1}^{+1} a_{i+m,\, j+n} \right) \Big/ 15, \quad \text{for } 2 < i < N-2, \text{ and } 1 < j < 24.$$

The process is equivalent to a combination of a running time-mean of five points and a running height-mean of three points, with each point having equal weight. The method proved very effective in providing smooth profiles. The five data points for the time-mean were taken over a time interval of 5.6 min, and the three data points for the height-mean were taken over a height interval of 21 cm.

4. Discussion of Errors

Error sources include: unknown emissivity values of the paint on the radiometers; tilting of the radiometer as it moved through the layer; mis-matching of the two radiometers as to output; radiation from equipment occasionally being incident upon a radiometer; a solar radiation input to the temperature sensors; variations in the temperature of the thermocouple reference bath; ventilation rate for the wet-bulb temperature sensor; water supply to the wet-bulb temperature sensor; improper determination of surface temperature.

The black paint used on the flux plates was Fuller's Velvet Black Decoret. Figures given by Suomi (1957) indicate that the absorptivity of this paint varies less than ± 4 percent wavelengths of 1 to 15 microns. If this paint is similar to other black paints, the absorptivity would tend to increase slightly for wavelengths less than 1 micron. A 6 percent increase was taken into account in the calibration; the value used should be within an error tolerance of ± 4 percent.

As the sweeping boom moved the radiometer from lowest position to highest, a parallelogram arrangement, composed of the boom, a rocker arm, a thin wire, and a guide rod, acted to maintain the horizontal orientation of the radiometer and all other sensors. By placing a small circular bubble level at the center of the radiometer and observing the behavior of the bubble during several test cycles, it was determined that the bubble never touched a reference circle inscribed on the glass cover; this indicated that the radiometer was always within 1° of the horizontal position. This small amount of tilt could cause less than 1 percent change in the transmission coefficient of the polyethylene and, hence, a negligible error in the amount of radiation reaching the flux plate.

The two radiometers had different outputs, such that the radiometer which moved through the layer had an output about 20 percent greater than the one which was stationary. If total radiation is constant with time, any height variation of radiation will produce a voltage proportional to the output characteristics of the moving radiometer. The fact that the combined signal of the two radiometers is not zero when the radiometers are exposed to the same amount of net radiation will not enter into the calculation of divergence. This equal-input voltage difference will be subtracted out, and the true vertical variation in net radiation will remain.

If the total amount of radiation varies with time, there will be a voltage output of 0.31 mv/ly, the difference between the two ratings of the radiometers, in addition to any voltage produced by virtue of a vertical variation in net radiation. Runs were not made on days with broken clouds. There can be rapid temporal changes in total radiation which will not be detected by the human eye. However, this effect would introduce a fictitious curvature to the profiles only if the temporal variation of net radiation were of the same frequency as (or some multiple of) the cycling of the radiometer. The handling of the data in computing the divergences would mask other frequencies of temporal flux variation.

Because the transmittance of polyethylene falls rapidly to low values when the angle of incidence is more than about 60°, it may be assumed that the radiometers have an effective "cone of visibility" of about 45°, that is to say, the radiometers are sensitive to all radiation which has an angle of incidence to the radiometer axis of less than 45°. Thus, the moving radiometer intercepts radiation from varying horizontal areas as it sweeps through its path. At its low point, the surface area within the cone is about 0.5 m^2, while at the high point, this surface area increases to about 24 m^2. It was determined that about 20 cm of the legs of the supporting frame for the sweeping boom would be included in the cone when the moving radiometer was at the high point of its path. Because of the small area involved, any radiation reflected or emitted from the legs was considered negligible.

Each radiometer was included in the visibility cone of the other except when the moving radiometer was within about 20 cm of the height of the stationary one. The radiometers were oriented such that if they were each emitting the same amount of radiation, i.e., were at the same temperature, the effect that each would have on the other would cancel, so that the net effect would be zero. The mass of the radiometers plus the temperature gradients experienced within the layer

being sampled plus the rate of motion of the moving radiometer would justify the assumption to be made that the two radiometers were always very close to the same temperature. Thus, the fact that the radiometers were moving in and out of the cones of visibility would produce no error in the net radiation.

There were four radiation shields on the temperature sensor. They consisted of horizontal plates of thin aluminum, two above and two below the five thermocouple junctions which composed the actual sensing element. The outer shields were completely covered with aluminized mylar. The inner shields had aluminized mylar on the sides away from the junctions, while the sides toward the junctions were covered with flat black paint. Aluminized mylar has the property of being highly reflective for short-wave radiation and highly absorptive (or emissive) for long-wave radiation. Therefore, a large percentage of the short-wave radiation falling on the sensor shields is either reflected by the mylar or absorbed by the paint. The amount that is absorbed will not appreciably raise the temperature of the shields above ambient since the mylar loses energy readily through infrared emission. The shields blocked solar radiation from the junctions for sun angles greater than 40°. Direct irradiation of the junctions with a heat lamp, simulating direct solar radiation that might occur at low sun angles, showed that the maximum temperature increase would be 0.2 C. Since this temperature change would be independent of height, it could not cause an error in the shape of the profile; the actual temperatures could be 1 percent less than that indicated by the sensor with sunlight on the junctions.

The temperature sensor was not artificially ventilated. The spacing between the two horizontal inner radiation shields was 2 cm. All runs were made when there was noticeable wind, so that there was always natural ventilation of at least 1 m/sec. With the radiation shields ducting the air horizontally past the junctions, there could be very little convective heat transfer from shield to junctions.

The reference bath for the thermocouples was usually a vacuum bottle containing lake water. The temperature of this reference was determined by a mercury-in-glass thermometer. Since the container was not perfectly insulated, there was a slight diurnal variation in the temperature of the reference. Therefore, its temperature was recorded every hour during a run. This allowed a smooth curve to be fitted to the points, and air temperature was later calculated on the basis of this curve.

It is possible that the temperature changes in the reference bath were not uniform with time. If this were so, the curve fitted to the

observed values would be in error. The maximum observed change in one hour was 0.3°C; this would be the maximum amount by which the computed temperatures could be in error. Most runs were made when the air temperature was between 15° and 25°C.

The wet-bulb temperature sensor was provided with a forced ventilation rate of about 5 m/sec. According to Pasquill (1949), 100 percent of the actual wet-bulb depression will be obtained if the wet-bulb thermometer is ventilated at any rate from 4 m/sec to about 8 m/sec. If the rate drops to 2 m/sec, the observed depression decreases by less than 1 percent. Therefore, the ventilation rate used for the research reported here was considered adequate.

The water for the cotton wicking was brought from the reservoir by a gravity feed. The rate of flow was adjusted so that droplets of water did not form on the wick, yet it remained visibly wet. After about 40 hours of ventilation a noticeable amount of debris collected on the wick. This necessitated either replacing or cleaning the soiled cotton. A small amount of evaporation will suffice to hold a thermometer at the wet-bulb temperature, so that the water supply must nearly cease before the system fails because of insufficient evaporation. The cotton wicking completely covered the junctions and 0.75 cm of the wire on either side of the junctions. By covering the wires on either side of the junctions with the wet wicking, heat flow along the wires from outside of the ventilation chamber was minimized.

The entire sensor was exposed to solar radiation during daylight runs. No effort was made to evaluate what effect this might have had on the signal. It might be assumed that, since all junctions were the same size and exposed to the same solar radiation, there would be no differential heating of the junctions and that no errors would be produced by this exposure to direct sunlight.

The logarithmic extrapolation for T_g (used in the calculation of radiative divergence) was based on $\log z$ rather than $\log(z+z_0)/z_0$. If z_0 is 10^{-2}cm, for values of z of 0.1 cm or greater, a $\log z$ curve is parallel to a $\log(z+z_0)/z_0$ curve to within 4 percent; if z_0 is 10^{-3}cm, the deviation between the two curves is 0.4 percent. The value of z_0 for a lake surface is considered to be less than 0.01 cm. Therefore, errors in the extrapolation procedure were considered to be within a tolerable range.

5. Numerical Integration of the Flux Divergence Equation

There are several graphical methods for determining the radiative flux divergence, based on pressure and water vapor distribution. Perhaps the most widely used is the chart of Elsasser (1940), which was designed primarily for probes through large portions of the atmosphere. Funk (1961) and Brooks (1950) have derived alternative, nongraphical procedures which are rather straight-forward in their use. The calculations reported in this paper were done by the method of Funk rather than that of Brooks, for the former appeared more adapted to micrometeorological work. Instead of requiring accurate knowledge of the emissivity curve, the method requires accurate temperature profile data.

In the following derivation, which follows closely that given by Funk in 1961, optical path length will be measured in centimeters, extending downward from zero at the top of the radiating atmosphere to infinitely long paths at the earth's surface. Subscripts 0, r, and g will stand for the top of the radiating atmosphere, a reference level in the atmosphere, and near the earth's surface, respectively. The downward flux of radiation reaching a reference level from the entire atmosphere above it is given by

$$R\downarrow = \int_0^{\infty} d\lambda \int_0^{u_r} \pi B_\lambda (\partial \tau_\lambda / \partial u)\, du, \qquad (1)$$

where λ is the wave-length at which atmospheric constituents are radiating, B_λ is the black-body intensity of this radiation, u is optical path length, τ_λ is the monochromatic slab transmissivity of the atmosphere and $\partial\tau_\lambda/\partial u$ is the slope of the transmissivity vs path length curve. According to Planck's law, B_λ is a unique-valued function of temperature, while τ and $\partial\tau/\partial u$ are functions of $u_r - u$, where u_r is optical path length at the reference level.

Slab emissivity ϵ for an isothermal slab is defined as being the ratio of the total intensity of emission E at one of its boundaries to the intensity of radiation which would be emitted if the slab were a black body, or $\epsilon = E/(\sigma T^4/\pi)$. Total emitted intensity of a non-black radiator may be given by

$$E = \int_0^{\infty} B_\lambda \epsilon_\lambda \, d\lambda, \qquad (2)$$

where ϵ_λ is the emissivity at wave-length λ. Since by continuity, $a+\tau+r = 1$, where a is absorptivity, τ is transmissivity, and r is

reflectivity, for the atmosphere, we may write $a_\lambda = 1 - \tau_\lambda$, r being zero. At radiative equilibrium, absorbed flux must equal emitted flux, so $a_\lambda = \epsilon_\lambda$. Therefore,

$$E = \int_0^\infty B_\lambda (1 - \tau_\lambda)\, d\lambda; \quad \text{and,} \quad \epsilon = (\pi/\sigma T^4) \int_0^\infty B_\lambda (1 - \tau_\lambda)\, d\lambda. \quad (3) \text{ and } (4)$$

Taking the partial derivative of each side of (4) with respect to path length, we have

$$\partial\epsilon/\partial u = -(\pi/\sigma T^4) \int_0^\infty B_\lambda (\partial\tau_\lambda/\partial u)\, d\lambda. \quad (5)$$

If (5) is multiplied by $\int_0^{u_r} \sigma T^4 du$, (1) may be rewritten in the form

$$R\downarrow = -\int_0^{u_r} \sigma T^4 (\partial\epsilon/\partial u)\, du. \quad (6)$$

A similar analysis holds for the upward radiation ($R\uparrow$) reaching the reference level, with the path of integration downward from $u = u_r$ at the reference level, to $u = \infty$. $R\uparrow$ may be expanded to

$$R\uparrow = \int_r^\infty \sigma T^4 (\partial\epsilon/\partial u)\, du = \int_r^g \sigma T^4 (\partial\epsilon/\partial u)\, du + \int_g^\infty \sigma T^4 (\partial\epsilon/\partial u)\, du. \quad (7)$$

The interval from the reference level to infinite path length has been broken into two segments: from the reference level to near the ground, and from this point to infinity. Evaluating the last term of (7), we obtain

$$\int_g^\infty \sigma T^4 (\partial\epsilon/\partial u)\, du = \sigma T^4 \epsilon \Big|_g^\infty = \sigma T_G^4 (1 - \epsilon) \quad (8)$$

The temperature T_G is the equivalent radiative temperature of the earth's surface. It is the temperature the surface would have if it were a black body radiating as the true surface actually is. It should be noted that T_G is usually not equal to T_g, the surface temperature. It will be equal only if the actual surface is homogeneous and has an emissivity of 1.0. Thus

$$R\uparrow = \sigma T_G^4 (1 - \epsilon) + \int_r^g \sigma T^4 (\partial\epsilon/\partial u) du. \quad (9)$$

The vertical divergence of net radiative flux at level r may be written

$$\partial R/\partial z = R' = (\partial u/\partial z)_r [(\partial R\uparrow/\partial u_r) - (\partial R\downarrow/\partial u_r)].$$

Here z is height above the ground surface, and a function subscripted by r is evaluated at reference level.

Differentiating $R\uparrow$ with respect to u,

$$\partial R\uparrow/\partial u = \int_r^g \sigma T^4 (\partial/\partial u)(\partial \epsilon/\partial u)\, du - \sigma T_G^4 (\partial \epsilon/\partial u). \tag{10}$$

As mentioned at the outset, u increases downward from the top of the radiating atmosphere. Above the reference level, the radiation stream is in the same direction as the increase of u, while below the reference level, it is in the opposite direction. Therefore, above the reference level $\partial \epsilon/\partial u$ has a positive sign affixed, and below the level, it has a negative sign. So we may write

$$\partial R\uparrow/\partial u_r = -\int_r^g \sigma T^4 (\partial/\partial u)(\partial \epsilon/\partial u)\, du - \sigma T_G^4 (\partial \epsilon/\partial u), \text{ and similarly,}$$

$$\partial R\downarrow/\partial u_r = -\int_0^r \sigma T^4 (\partial/\partial u)(\partial \epsilon/\partial u)\, du,$$

so that the vertical divergence is expressed by

$$R' = -\sigma (\partial u/\partial z)_r \left[\int_0^r T^4 (\partial^2 \epsilon/\partial u^2)\, du + \int_r^g T^4 (\partial^2 \epsilon/\partial u^2)\, du + T_G^4 (\partial \epsilon/\partial u) \right]. \tag{11}$$

In this form, R' could be numerically integrated by introducing the appropriate boundary and interval conditions. However, the expression contains $\partial^2 \epsilon/\partial u^2$. To evaluate this requires ϵ for all path lengths to be known to a high degree of accuracy. At the present time, ϵ for small path lengths has not been precisely determined, meaning that $\partial^2 \epsilon/\partial u^2$ could be subject to large errors. Therefore, (11) will be transformed to a more desirable form.

Integrating by parts,

$$\int_0^r T^4 (\partial^2 \epsilon/\partial u^2)\, du = T^4 (\partial \epsilon/\partial u)\Big|_0^r - \int_0^r (\partial T^4/\partial u)(\partial \epsilon/\partial u)\, du$$

$$= -T_0^4 (\partial \epsilon/\partial u) - \int_0^r (\partial T^4/\partial u)(\partial \epsilon/\partial u)\, du,$$

where T_0 is the temperature at the top of the radiating atmosphere.

Similarly,

$$\int_r^g T^4 (\partial^2 \epsilon / \partial u^2)\, du = T_g^4 (\partial \epsilon / \partial u) - \int_r^g (\partial T^4 / \partial u)(\partial \epsilon / \partial u)\, du.$$

Once again integrating by parts,

$$\int_0^r (\partial T^4 / \partial u)(\partial \epsilon / \partial u)\, du = - (\partial T^4 / \partial u)_0 \, \epsilon_r - \int_0^r (\partial^2 T^4 / \partial u^2)\, \epsilon \, du,$$

$$\int_r^g (\partial T^4 / \partial u)(\partial \epsilon / \partial u)\, du = (\partial T^4 / \partial u)_g \, \epsilon_{g,r} - \int_r^g (\partial^2 T^4 / \partial u^2)\, \epsilon \, du.$$

Finally,

$$R' = \sigma (\partial u / \partial z)_r \Big[\underbrace{(T_g^4 - T_G^4)(\partial \epsilon / \partial u)}_{①} + \underbrace{T_0^4 (\partial \epsilon / \partial u)}_{②} + \underbrace{(\partial T^4 / \partial u)_g \, \epsilon}_{③}$$

$$\underbrace{- (\partial T^4 / \partial u)_0 \epsilon}_{④} - \underbrace{\int_0^r (\partial^2 T^4 / \partial u^2)\, \epsilon \, du}_{⑤} - \underbrace{\int_r^g (\partial^2 T^4 / \partial u^2)\, \epsilon \, du}_{⑥} \Big].$$

This is the final integral form of the equation for obtaining radiative flux divergence. Appropriate approximations must now be made so that it may be numerically integrated. For a reference level within a few tens of meters of the earth's surface, u will be relatively large, making $\partial \epsilon / \partial u$ small, and this allows term 2 to be neglected. If the levels over which the integration takes place are made small enough, for instance, such that the temperature change is less than 10 C, T may be linearized through the layer. This allows the following equivalents,

$$(\partial T^4 / \partial u)_g \epsilon = 4 \bar{T}^3 (\partial T / \partial u)_g \epsilon = 4 \bar{T}^3 (\partial T / \partial z)_g (\partial z / \partial u)_g \epsilon,$$

$$(\partial T^4 / \partial u)_0 \epsilon = 4 \bar{T}^3 (\partial T / \partial z)_0 (\partial z / \partial u)_0 \epsilon$$

where $(\bar{\ })$ is the average value for the layer. Further,

$$\int_0^r (\partial^2 T^4 / \partial u^2)\, \epsilon \, du = \int_0^r \Big[\bar{T}^3 (\partial T / \partial u)\, \epsilon \, du = \int_0^r 4 \bar{T}^3 (\partial T / \partial z)(\partial z / \partial u)\, \epsilon \, du$$

$$\doteq 4 \bar{T}^3 \sum_{m=1}^{M} \overline{(\partial z / \partial u)_m \, \epsilon}_m \, \Delta_m (\partial T / \partial z),$$

$$\int_r^g (\partial^2 T^4/\partial u^2)\epsilon \, du \doteq 4\bar{T}^3 \sum_{n=1}^{N} \overline{(\partial z/\partial u)}_n \bar{\epsilon}_n \Delta_n (\partial T/\partial z)$$

where the summation to M refers to successive layers from the reference level to the top of the radiating atmosphere and the summation to N refers to successive layers from the reference level to the ground.

The final simplifying assumption is that above a certain level, radiative flux is constant. Therefore, rather than integrating the radiation through the entire atmosphere, integration will cover only a limited segment of it. Only that portion between the surface and a height Z some meters above the surface will be considered. It is estimated that this assumption will cause errors of no more than 5 to 10 percent of the total divergence. Finally, the form of the equation is found to be

$$R' \simeq \sigma (\partial u/\partial z)_r \Bigg\{ (T_g - T_G)(\partial \epsilon/\partial u) + 4\bar{T} \left[(\partial T/\partial z)_g (\partial z/\partial u)_g \epsilon - (\partial T/\partial z)_Z (\partial z/\partial u)_Z \epsilon \right] - 4\bar{T}^3 \left[\sum_{m=1}^{M} \overline{(\partial z/\partial u)}_m \bar{\epsilon}_m \Delta_m (\partial T/\partial z) + \sum_{n=1}^{N} \overline{(\partial z/\partial u)}_n \bar{\epsilon}_n \Delta_n (\partial T/\partial z) \right] \Bigg\}$$

T_g is the surface temperature or, more precisely, the temperature of the air at an elevation such that the optical path length from that level to the surface is small compared to the optical path length from that level to the reference level. The height arbitrarily chosen was 1 cm. The selection of this height was not critical, since it was used only for the calculation of T_g. Any errors in the determination of T_g will contribute errors to all three terms of the divergence equation, and these errors tend to be compensatory. The temperature at 1 cm was determined by an extrapolation from the temperatures between 50 and 120 cm. A straight line was fitted to these values by the least squares method, then logarithmically extended to a height of 1 cm. The temperatures derived in this fashion were compared with temperatures derived by similar extrapolation to 0.1 and 5 cm. The differences between the temperatures at these other heights and those at 1 cm were less than 0.5 C. Since T_G was known only to $\pm$ 0.5 C, the 1-cm height was considered justified.

The optical path length from the surface to the reference level must be known for the calculation of R', requiring the determination of the surface vapor pressure. The saturation vapor pressure of water at a

temperature of T_G was used. The equivalent radiative temperature of the surface, T_G, was determined directly from bolometer readings. The emissivity values for various optical path lengths in air were obtained from Brooks (1950), Robinson (1950a), and Kuhn (1963). A plot was made of ϵ vs logarithm of u, for path lengths from 0.0001 cm to 1 cm. The curve was in reality three straight line segments, for ease in computing. One segment extended from 0.0001 cm to 0.0008 cm, the next from 0.0008 cm to 0.03 cm, and the last from 0.03 cm to 1.0 cm. For each segment, both ϵ and $d\epsilon/du$ depend on u, and equations were derived to calculate these quantities (see Fig. 2).

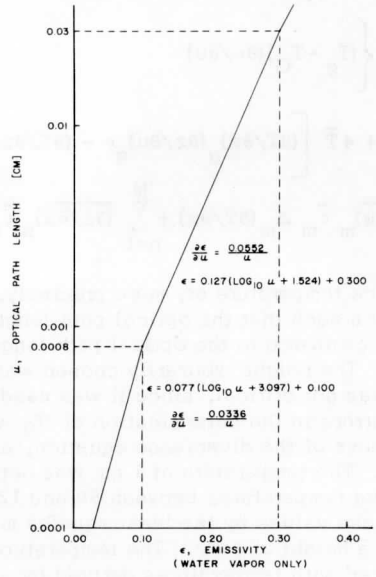

FIG. 2. Relations for Emissivity Computations

An electronic digital computer was programmed to calculate R' at six reference levels. The thickness of the layers used was 21 cm. Smoothed values of temperature and vapor pressure (previously calculated from the wet-bulb temperatures) at 22 levels, from 51 cm to 261 cm above the water, plus T_G values were the input data. T_g was calculated by logarithmic extrapolation from the lowest seven temperature values. The temperatures at all levels were averaged to obtain $\bar{T}$.

From the hydrostatic equation, the universal gas law, and the relationships $du = q\,dp/g$ and $q = 0.6222\,e/(p-e)$, where q is specific humidity, p is air pressure, g is gravity, and e is vapor pressure, the height variation of optical path length may be expressed as $dz/du = -4.62\,T/e$. This was computed for every other level from 61 cm to 251 cm. The lapse rate for 21-cm layers was given by $dT/dz = 4.76\,(T_{i+2} - T_i)$, where i is a height position. $-dT/dz$ for each layer was the difference between the lapse rates at the top and bottom of the layer. The optical path length for each layer was calculated by dividing the distance from the middle of the layer to the reference level, or $\Delta u = (z - z_r)/(dz/du)$. From this value of $-u$, ϵ for that level was determined from the emissivity curve. The product $(\Delta dT/dz)(dz/du)\epsilon$ was formed, summed for all levels, and multiplied by $4\bar{T}^3$. $(du/dz)_r$ was determined by inverting the dz/du value for the reference level. From the emissivity curve, $d\epsilon/du$ for an optical path length extending from the reference level to the surface was calculated. This was then multiplied by the difference between the fourth powers of T_g and T_G. From the lowest and highest levels,

$$[(dT/dz)_g (dz/du)_g \epsilon_{u-u_r} - (dT/dz)_Z (dz/du)_Z \epsilon_{u_r}]$$

was evaluated. Making the appropriate additions and subtractions, and multiplying by du/dz and σ yielded R' for each reference level. A sample calculation is included in Tables 1a and 1b.

6. Results

The research site was located approximately 0.5 km from the south shore of the western portion of Lake Mendota; reference can be made to Stearns (1962). The bottom of the sweeping-boom mechanism was supported, about 20 cm below mean water level, by a 3m by 3m submerged steel-mesh platform. A similar platform, for the support of amplifiers and other equipment not associated with this project, was at the closest point 2m removed, and was entirely clear of the water. Both platforms

TABLE 1a. SAMPLE CALCULATION OF RADIATION DIVERGENCE (Part I)

1	2	3	4	5	6	7	8	9	10
z [cm]	T [C]	e [mb]	$-\partial z/\partial u$ [m/cm]	$\partial T/\partial z$ [deg/m]	$\Delta\partial T/\partial z$ [deg/m]	$z-z_r$ [m]	Δu [cm]($\times 10^3$)	ϵ	Q [deg/cm]
0	23.35	22.80	605						
				2.31					
51	24.53	23.33	591		-1.64				
				0.67		0.52	0.88	0.105	-102.0
72	24.67	23.09	597		-0.29				
				0.38		0.31	0.52	0.085	- 14.7
93	24.75	23.18	596		-0.38				
				0.00		0.10	0.17	0.048	- 10.9
114	24.75	23.24	593		1.19				
				1.19		0.10	0.17	0.048	34.9
135	25.00	23.40	589		-0.95				
				0.24		0.31	0.53	0.086	- 48.2
156	25.05	23.48	587		-0.24				
				0.00		0.52	0.88	0.105	- 14.8
177	25.05	23.44	588		-0.05				
				-0.05		0.73	1.24	0.122	- 3.6
198	25.04	23.38	590		0.24				
				0.19		0.94	1.59	0.138	19.6
219	25.08	23.43	588		-0.09				
				0.10		1.15	1.96	0.149	- 7.9
240	25.10	23.44	588		-0.20				
				-0.10		1.36	2.31	0.158	- 18.6
261	25.08	23.41	589						

Reference level is 114 cm

$$-\sum(\partial z/\partial u)\bar{\epsilon}(\Delta\partial T/\partial z) = -166.2 \text{ deg/cm}$$

TABLE 1b. SAMPLE CALCULATION OF RADIATION DIVERGENCE (Part II)

$T_g = 296.75$ K

$T_G = 293.0$ K

$\partial\epsilon/\partial u\Big|_{u_g - u_r} = -47.5$/cm

$$(T_g^4 - T_G^4)(\partial\epsilon/\partial u) = -148 \times 10^8 \text{ deg}^4/\text{cm} = A$$

$$[(\partial T/\partial z)_g (\partial z/\partial u)_g \epsilon_{u_r - u_g} - (\partial T/\partial z)_Z (\partial z/\partial u)_Z \epsilon_{u_r}] =$$

$(2.31)(605)(0.095) - (-0.10)(573)(0.231) = 146$ deg/cm

$\bar{T} = 298.1$ K

$$4\bar{T}^3[\ ] = 154 \times 10^8 \text{ deg}^4/\text{cm} = B$$

$$4\bar{T}^3 \sum (\partial z/\partial u)\bar{\epsilon}(\Delta\partial T/\partial z) = 176 \times 10^8 \text{ deg}^4/\text{cm} = C$$

$R' = \sigma(\partial u/\partial z)_r (A + B - C)$

$= (8.22 \times 10^{-11} \text{ ly/min deg}^4)(-0.00169 \text{ cm/m})(-148 + 154 - 176) \times 10^8 \text{ deg}^4/\text{cm}$

$R' = 2.28$ mly/min per meter

were painted with a corrosion depressant, which had the color of rust. The platforms rested on four tubular legs and were well anchored in the 3-m-deep water with chains connected to large concrete blocks. They did not noticeably sway in waves driven by winds of up to 8m/sec. Data were obtained during the late summer and fall, so that both stable and unstable conditions were sampled. On several occasions, data were taken continuously for 20- to 30-hr periods, but only a few typical 90-minute segments of the runs will be described here.

Results are shown in the form of vertical profiles of temperature, vapor pressure (e), and radiation divergence. Also, two dimensionless parameters are used in an attempt to generalize the findings. The first of these, α, is defined as $\alpha \equiv zR'/R \equiv \partial \log R/\partial \log z$. This number indicates the relationship between the divergence of radiation and the magnitude of the radiation, or, viewed from another angle, the relative height dependency of radiation. This number can be evaluated for the measured divergence only, since in calculating the divergence by the Funk method, no values of the radiation are obtained, but only R'. The number α_i was evaluated at six levels, from 114 cm to 219 cm. in the form $(z_i/R_i)(R_{i+1} - R_{i-1})/(z_{i+1} - z_{i-1})$, where the subscripts refer to height positions. The (i+1) position differed from the (i-1) position by 105 cm.

The second parameter is the Deacon number for temperature profile structure, defined earlier, and calculated in the form $\delta_i = \frac{z_i}{z_{i+1} - z_{i-1}} \frac{T_{i+2} + T_{i-2} - 2T_i}{T_{i+1} - T_{i-1}}$. The distance between the (i+1) and (i-1) levels was 63 cm, that between the (i+2) and (i-2) levels 105 cm; α_i and δ_i refer to the same height z_i. The time rate of temperature change which would correspond to radiation divergence may be expressed as $\dot{T} = - R'/c_p\rho$. For the situations involved in this study, c_p and ρ may be taken as 0.24 cal/gm deg and 0.0012 gm/cm^3, respectively. Then $\dot{T}$[deg/hr] = - 2.1R'[mly/min per meter].

An example of stable conditions would be those found on September 3, 1964. The period from 1315 to 1445 CST on this day is referred to as Run 50. The day was bright, with high, thin cirrus clouds. The air temperature, T_a, (obtained from a shaded mercury-in-glass thermometer) at a height of 100 cm above the water was 28.4 C, the wind was 3 m/sec from the west-southwest, atmospheric pressure was 969 mb, and the water temperature near the platform, T_w, (also read from the mercury-in-glass

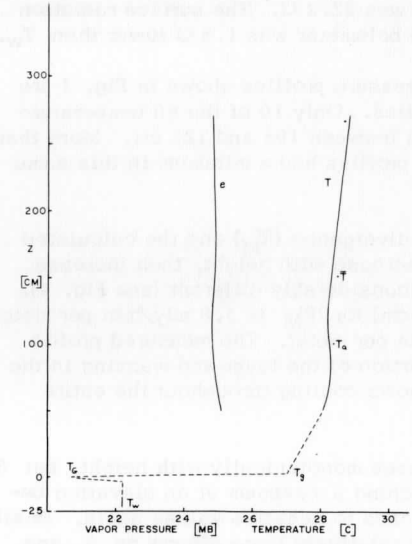

FIG. 3. Run 50
Mean Vapor pressure
and temperature profiles

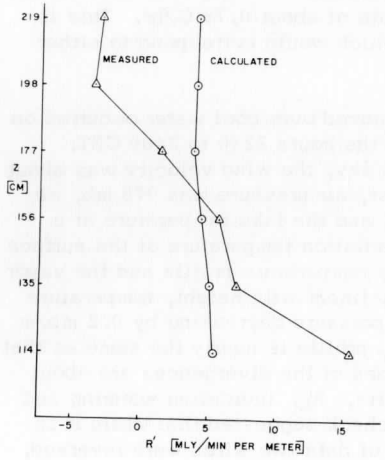

FIG. 4. Run 50
Profiles of Radiation
Flux Divergence

thermometer) at a depth of 15 cm was 22.2 C. The surface radiation temperature as determined by the bolometer was 1.5 C lower than T_w.

The temperature and vapor pressure profiles shown in Fig. 3 are the average of 60 individual profiles. Only 10 of the 60 temperature profiles failed to have a minimum between 105 and 125 cm. More than 65 percent of the vapor pressure profiles had a minimum in this same interval.

Both the measured radiation divergence (R'_M) and the calculated radiation divergence (R'_C) first decrease with height, then increase slightly, but the magnitudes are considerably different (see Fig. 4). The layer-mean (from 114 to 219 cm) for R'_M is 3.8 mly/min per meter, while that for R'_C is 4.3 mly/min per meter. The measured profile indicates cooling in the lower portion of the layer and warming in the upper. The calculated profile shows cooling throughout the entire layer.

Fig. 5 shows that α decreases monotonically with height, but δ increases and changes sign, reaching a maximum at an elevation between 150 and 180 cm, and decreases to negative values again. Small temperature differences can have relatively large effects on δ, and, while the average profile for the entire run is rather smooth, the scatter of individual profiles about the average is large. All values of α are very close to the average value. Between 1500 and 1700 CDT on this day the air at 100 cm cooled at a rate of about 0.75 C/hr. This is roughly 7 C/hr less than the rate which would correspond to either R'_M or R'_C.

Another period when warm air moved over cool water occurred on October 26, 1964. Run 80 covered the hours 2230 to 2400 CST. There were no visible clouds in the sky, the wind velocity was about 1.5 m/sec from the south-southwest, air pressure was 975 mb, air temperature at 100 cm was 13.0 C, and the lake temperature at a depth of 15 cm was 11.7 C. The radiation temperature of the surface was 0.4 C lower than T_w. Both the temperature profile and the vapor pressure profile were approximately linear with height, temperature increasing by 0.08 C/m and vapor pressure decreasing by 0.2 mb/m (see Fig. 6). The shape of the R'_M profile is nearly the same as that of the R'_C profile, and the magnitudes of the divergences are about the same. But the signs are opposite, R'_M indicating warming and R'_C indicating cooling. A careful check suggested that while it is possible that during the collection of data two wires were reversed,

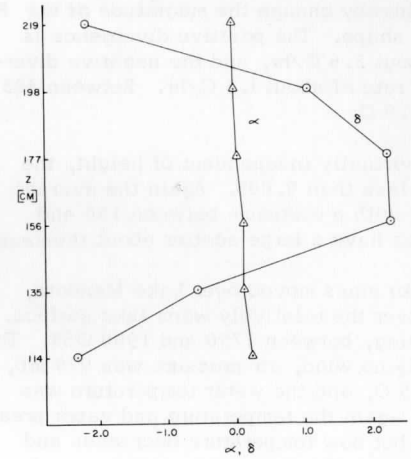

FIG. 5. Run 50 Mean Profiles of α and δ.

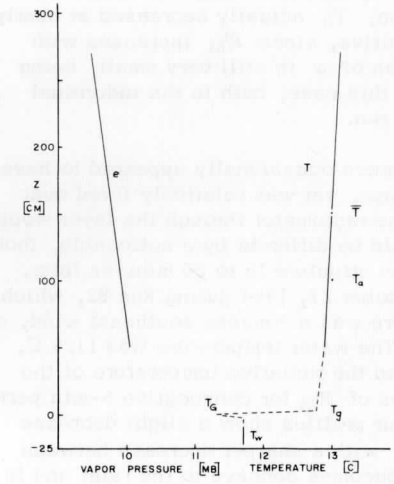

FIG. 6. Run 80 Mean vapor pressure and temperature profiles.

it is improbable. There is no one parameter (such as T_g, T_G, $\bar{T}$, or e) which could be "corrected" and thereby change the magnitude of the $R^{\downarrow}_C$ profile without also changing the shape. The positive divergence is equivalent to a cooling rate of about 2.5 C/hr, and the negative divergence is equivalent to a warming rate of about 1.5 C/hr. Between 2230 and 2330 CST, $\dot{T}_a$ decreased by 0.9 C.

Figure 8 shows that α was virtually independent of height, the variation through the layer being less than 0.005. Again the average profile of δ is relatively smooth with a maximum between 150 and 180 cm, but the individual profiles have a large scatter about the mean.

On October 29, 1964 a cold air mass moved over Lake Mendota, and unstable conditions existed over the relatively warm lake surface. Run 85 occurred in the early evening, between 1730 and 1900 CST. The sky was clear, there was virtually no wind, air pressure was 979 mb, air temperature at 100 cm was 6.5 C, and the water temperature was 11.3 C. Figure 9 illustrates that again the temperature and vapor pressure profiles were nearly linear, but now temperature decreases and vapor pressure increases with height. The radiation temperature of the water suggests that there was a cool layer at the surface, 0.8 C cooler than the water at a depth of 15 cm. Both $R^{\downarrow}_M$ and $R^{\downarrow}_C$ increase with height and are approximately within ± 1 mly/min per meter of each other (see Fig. 10). But in this case the measured divergence indicated cooling of about 1 C/hr, while the calculated divergence indicates warming of about 1 C/hr. During the run, T_a actually decreased at nearly 1/2 C/hr. As expected, α is positive, since $R^{\downarrow}_M$ increases with height. (See Fig. 11.) The variation of α is still very small, being about 0.015. δ is more erratic in this case, both in the individual profiles and in the average for the run.

The measured radiation divergence occasionally appeared to have a profile which slowly changed shape, yet was relatively fixed over short periods. Several orbits of the radiometer through the layer would reveal a mean structure which would be different by a noticeable, though not sizeable, amount from the mean structure 15 to 20 minutes later. An example of this occurred on October 27, 1964 during Run 82, which lasted from 1430 to 1525 CST. There was a 3 m/sec southeast wind, and visibility was 5 km due to haze. The water temperature was 11.9 C, the air temperature was 13.9 C, and the radiative temperature of the surface was 11.6 C. Mean profiles of $R^{\downarrow}_M$ for consecutive 5-min periods are shown in Fig. 12. The first four profiles show a slight decrease in divergence as height increases, with a sharper decrease between 135 and 156 cm. The fifth profile becomes concave to the right and is

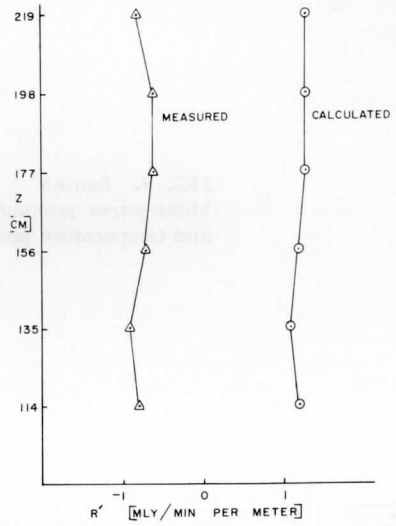

FIG. 7. Run 80 Profiles of Radiation Flux Divergence

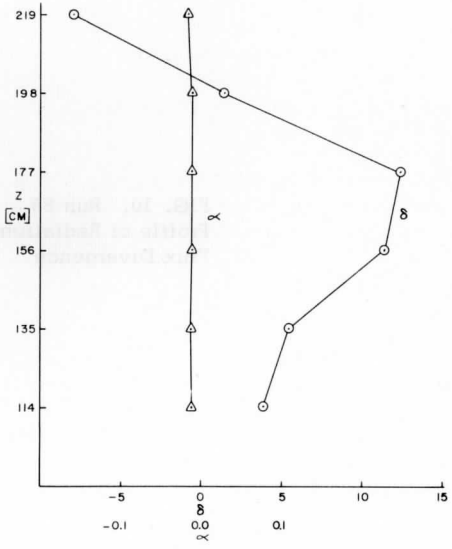

FIG. 8. Run 80 Mean Profiles of α and δ

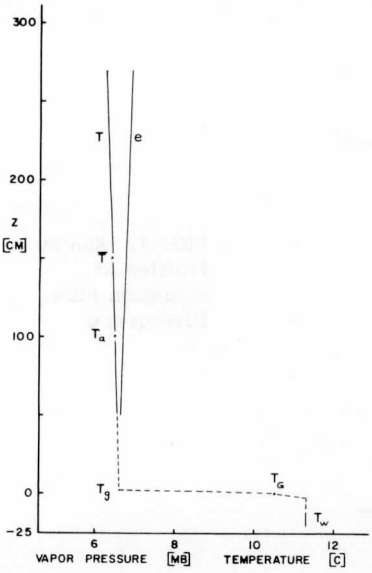

FIG. 9. Run 85
Mean vapor pressure
and temperature profiles

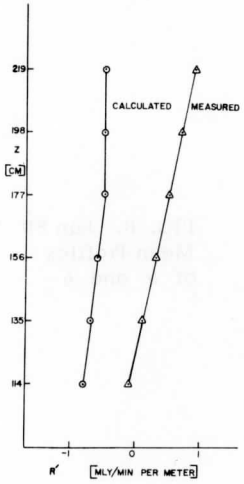

FIG. 10. Run 85
Profile of Radiation
Flux Divergence

nearly 2 mly/min per meter less than the first four. Profile 6 repeats the original pattern. The last five profiles are of the same magnitude as the first group, but while there is a suggestion of the shape of the former profiles in numbers 8 and 9, there is only slight consistency of a general shape.

The radiometers would not operate properly if wet. Data were not obtained when the wind speed was greater than 5 m/sec because waves on the lake might then splash water onto the moveable radiometer. For the range of wind speeds under which data were collected there appears to be no relationship between speed and the magnitude of $R^{\downarrow}_{M}$ or $R^{\downarrow}_{C}$. There is a slight tendency for the variation of $R^{\downarrow}_{M}$ with height to be less when the wind speed is lower; for example, compare the profile in Fig. 4 (wind speed 3 m/sec) with that in Fig. 7 (wind speed 1.5 m/sec).

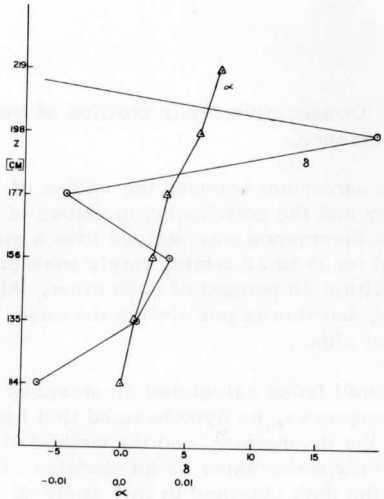

FIG. 11. Run 85. Mean Profiles of α and δ.

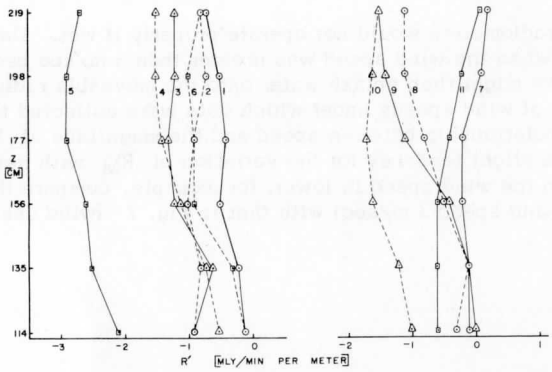

FIG. 12. Run 82. Consecutive 5-min profiles of measured radiation flux divergence.

There is little agreement between the values of R'_M that were obtained in this study and the corresponding values of R'_C. Whether a profile of radiation divergence was derived from a single orbit of the sensor or averaged for 15 to 20 orbits, rarely were corresponding values of R'_M and R'_C within 20 percent of each other. R'_M tends to be large when R'_C is large, but this is not always the case. Often R'_M and R'_C are of different sign.

When Funk (1960) found calculated divergences systematically lower than measured divergences, he hypothesized that haze particles would be contributing to the divergence, and the method of calculation he used took into account only water vapor as an absorber of radiation. Although limited in scope, the data obtained in this study do not show more of a deviation between R'_M and R'_C when the haze is markedly heavy than when it is absent. Also, Zdunkowski et al. (1964) have found that the haze concentration must be increased by nearly 50 times the "normal" value before the cooling rate is doubled from that produced by water vapor alone.

7. Conclusions

The experimental evidence obtained in this study appears to show that radiation flux divergence over a water surface is of a magnitude at least great enough to produce the observed temperature change. Much of the divergence occurs very close to the water surface, where there are relatively large gradients of temperature and moisture. Yet even at 1 to 2 m from the surface there is detectable divergence.

Since small temperature differences can have large effects on profile curvature, Deacon numbers will have real meaning only when calculated for an average temperature profile. The Deacon numbers for temperature reported here were based on 60-min, or 90-min averages of the temperature profiles. It is apparent from the profiles of Deacon number that there is a height variation of profile curvature.

The number α, which measures the relative height dependency of radiation, shows slight variation with elevation and is usually close to a value of zero. The magnitude of α may be somewhat in error, because not sufficient caution was taken in gathering the data to assure accurate determination of the actual net radiation. The changes in net radiation are considered valid, and hence the shape of the α-profile is considered reliable. A dimensionless parameter allowing comparison between its value for measured and computed divergences would be desirable.

Although it was not investigated in any rigorous fashion, the presence of a layer of water at the surface which was different in temperature from the water several centimeters below was noted frequently. Usually the skin layer was cooler, but on several occasions there were indications that it was slightly warmer than the deeper layers.

The question posed in Section 1 as to the relationship between radiation flux and sensible heat flux when temperature change is zero is still unanswered, since sufficient data were not obtained during periods when $\dot{T} = 0$. Gaevskaya has suggested that measuring the fluxes of sensible heat and radiation, and adding the temperature changes that the divergence of each can produce, will not reproduce the observed change. However, this approach, to be based on more detailed measurements, would seem to be precisely what is needed. In other words, the total energy input to and outflow from a volume should be measured, and the temperature changes possible to be affected thereby compared to the actual temperature changes which occur. The

divergences of fluxes of such variables as radiation, heat, and moisture should be measured directly rather than assumed to have some value (such as zero) or determined by measuring the gradient of a related quantity.

It will undoubtedly be difficult to obtain adequate data, but the possibility of validating or invalidating much conflicting theory, assumption, and past experimental data would seem to justify the effort. Further experiments should include measurements of the wind structure at the experimental site, and data on all variables might well be taken at elevations from as close to the surface as possible up to 5 to 10 m. To include advective processes, horizontal sampling would be necessary. Also, though it is hard to conceive of any positive results being produced, horizontal radiation flux measurements might be undertaken simultaneously.

Acknowledgments

I wish to express my gratitude to A. B. Super for much willing and able assistance with the large amount of physical labor involved with this research, rendered while working on his own research projects; to C. R. Stearns for invaluable guidance and aid with instrumentation, as well as aid with the handling of equipment; and to Dr. P. M. Kuhn for advice on various problems of radiation measurement. Above all, I am deeply indebted to Prof. H. H. Lettau, under whose patient tutelage the research reported herein was conducted, for stimulation and encouragement at all times.

References

Ball, F.K.: 1954. Sea surface temperatures. Australian J. Physics, 7(4): 649-652.

Brooks, D.L.: 1950. Tabular method for computing temperature from radiation. J. Meteor. 7:313-321.

Bushnell, R.H., and V. E. Suomi: 1961. Experimental flight verification of the economical net radiometer. J. Geophys. Res. 66(9): 2843-2848.

Deacon, E.L.: 1949. Vertical diffusion in the lowest layers of the atmosphere. Quar. J. Roy. Meteor. Soc. 75: 89-103.

Deacon, E.L., 1953. Vertical profiles of mean wind in the surface layers of the atmosphere. Geophys. Mem. No. 91.

Deacon, E.L.: 1962. Small-scale interactions. The Sea. Vol. 1, Ed. M. N. Hill. Interscience Publishers. New York.

DeGraaf, J.G.A. and E.F.M. van der Held: 1953. The relation between the heat transfer and the convection phenomena in enclosed plane air layers. Applied Sci. Res. A3: 393-412.

Elsasser, W.M.: 1942. Heat Transfer by Infrared Radiation in the Atmosphere. Harvard Meteor. Studies, No. 6. Harvard University Press, Cambridge, Mass.

Fleagle, Robert: 1956. Temperature distribution near a cold surface. J. Meteor. 13: 160-165.

Funk, J.P.: 1960. Measured radiative flux divergence near the ground at night. Quart. J. Roy. Meteor. Soc. 86: 382-389.

Funk, J.P.: 1961. A numerical method for the computation of the radiative flux divergence near the ground. J. Meteor. 18: 388-392.

Gaevskaya, G.N., K. Y. Kondratiev, and K. E. Yakushevskaya: 1962. Radiative heat flux divergence and heat regime in the lowest layer of the atmosphere. Archiv. Meteor., Geophysic, u. Bioclim. 12(1): 95-108.

Glaser, A.H., W. P. Elliott, and A.J. Druce: 1957. The Study of Small Scale Modification of Air Passing over Inhomogeneous Surfaces. Texas A and M College Project 85.

Godson, Warren L.: 1965. The role of radiative flux divergence in the surface layer. Paper given at First Canadian Conference on Micrometeorology.

Hamilton, H.L., Jr.: 1962. Spatially continuous measurements of temperature profiles through an air-water interface. Final Report, Studies of the Three-Dimensional Structure of the Planetary Boundary Layer. Univ. Wisconsin, Dept. Meteor.

Kuhn, P.M.: 1963. Radiometersonde observations of infrared flux emissivity of water vapor. J. Appl. Meteor. 2(3): 368-378.

Lettau, H.H.: 1957. Summary of nondimensional characteristics of boundary layer theory. Exploring the Atmosphere's First Mile. Pergamon Press, London.

Lettau, H.: 1962. Notes on theoretical models of profile structure in the diabatic surface layer. Final Report, Studies of the Three-Dimensional Structure of the Planetary Boundary Layer. Univ. Wisconsin, Dept. Meteor.

Lettau, H.: 1963. Correspondence between theoretic models and actual observations in arctic micrometeorology. Publication in Meteorology No. 65. Stanstead College, Stanstead, Quebec.

Lettau, H.: 1965. Note on the low-level anomaly in vertical temperature profiles under conditions of outgoing radiation. (To be published in Monograph on Antarctic Research, Amer. Geophys. Union).

Pasquill, F.: 1949. A portable indicating instrument for the study of temperature and humidity profiles near the ground. Quar. J. Roy. Meteor. Soc. 75: 239-248.

Rider, N.E., and G.D. Robinson: 1951. Transfer of heat and water vapor above short grass. Quart. J. Roy. Meteor. Soc. 77: 375-401.

Robinson, G.D.: 1950a. Notes on the measurement and estimation of atmospheric radiation. No. 2. Quar. J. Roy. Meteor. Soc. 76: 37-51.

Robinson, G.D.: 1950b. Two notes on temperature changes in the troposphere due to radiation. Centenary Proc. Roy. Meteor. Soc., p. 26-28.

Soules, S.D.: 1964. Sea surface radiation temperatures. Unpublished manuscript.

Stearns, C. R.: 1962. Micrometeorological Installation on Lake Mendota, Section 2 of Final Report, Contract DA-36-039-SC-80282.

Suomi, V. E.: 1957. University of Wisconsin net radiometer. Exploring the Atmosphere's First Mile. Ed. by H. H. Lettau and Ben Davidson. Pergamon Press, London.

Suomi, V. E., D. O. Staley, and P. M. Kuhn: 1958. A direct measurement of infrared radiation divergence to 160 mb. Quar. J. Roy. Meteor. Soc. 84: 134-141.

Super, A. B.: 1965. A study of small-scale air mass modification over Lake Mendota. Doctoral dissertation. Univ. of Wisconsin. 1965.

Tanner, C. B., J. A. Businger, and P. M. Kuhn: 1960. The economical net radiometer. J. Geophys. Res. 65(11): 3657-3667.

Zdunkowski, W., D. Henderson, and J. V. Hales: 1965. The Influence of Atmospheric Constituents upon Long Wave Radiation in Conjunction with the Formation of Radiation Fog. Interim Report No. 1. Intermountain Weather, Inc. Salt Lake City, Utah.

Scanner's note:

This page is blank.

DISTRIBUTION LIST

1. Commanding General
U.S. Army Materiel Comd
ATTN: AMCRD-RV-A
Washington, D.C. 20315 1

2. Chief, Rsch & Development
Department of the Army
ATTN: CRD/M
Washington, D.C. 20310 1

3. Commanding General
U.S.A. Combat Devel Comd
ATTN: CDCMR-E
Fort Belvoir, Va. 22061 1

4. Commanding General
U.S. Continental Army Comd
ATTN: Recon Br ODCS For Intel
Fort Monroe, Virginia 23351 1

5. Commanding General
U.S. Army Electronics Comd
ATTN: AMSEL-EW
Fort Monmouth, N.J. 07703 1

6. Commanding General
U.S. Army Missile Command
ATTN: AMSMI-RRA
Redstone Arsenal, Ala 35809 1

7. Commanding General
U.S. Army T&E Comd
ATTN: NBC Directorate
Aberdeen Prg Gnd, Md 21005 1

8. Commanding Officer
U.S.A. Cold Regions R&E Labs
ATTN: Environmental Rsch Br
Hanover, N.H. 03755 1

9. Commanding General
Natick Laboratories
ATTN: Earth Sciences Div
Natick, Mass. 01762 1

10. Commanding Officer
U.S. Army Ballistic Rsch Labs
ATTN: AMXBR-B
Aberdeen Proving Gnd, Md 21005
1

11. Commanding Officer
U.S. Army Ballistic Rsch Labs
ATTN: AMXBR-IA
Aberdeen Provg Gnd, Md
21005 1

12. Director
U.S.A. Eng Waterways Exper Sta
ATTN: WESSR
Vicksburg, Miss. 39181 1

13. Commanding General
U.S. Army Electronics Comm
ATTN: AMSEL-BL-D
Fort Monmouth, New Jersey
07703 1

14. Commanding Officer
U.S. Army Elect R&D Actv
ATTN: Met Dept
Ft. Huachuca, Ariz 85613 30

15. Commanding Officer
U.S. Army Elct R&D Activity
ATTN: Environmental Sciences
Dept
White Sands Msl Range, N.M.
88002 1

16. Commanding General
U.S. Army Edgewood Arsenal
ATTN: SMUEA-CS-O, Ops. Rsch
Grp
Edgewood Arsenal, Md. 21010
1

17. Commanding Officer
U.S. Army Frankford Arsenal
ATTN: SMUFA-1140
Philadelphia, Pa. 19137 1

18. Commanding Officer
U. S. Army Picatinny Arsenal
ATTN: SMUPA-TV-3
Dover, New Jersey 07801 1

19. Commanding Officer
U. S. Army Dugway Proving Gnd
ATTN: Meteorology Div
Dugway, Utah 84022 1

20. President
U. S. Army Artillery Bd
Fort Sill, Okla. 73504 1

21. Commanding Officer
USA Arty Cbt Developments Agcy
Fort Sill, Okla. 73504 1

22. Commandant
U. S. Army Arty & Msl School
ATTN: Target Acquisition Dept.
Ft. Sill, Okla 73504 1

23. Commanding Officer
US Army CDC Comm-Elct Agcy
Fort Huachuca, Arizona 85613 1

24. Commanding General
USAEPG
ATTN: C, FTFD
Fort Huachuca, Ariz 85613 1

25. Commanding General
Deseret Test Center
Fort Douglas, Utah 84113 1

26. Commanding General
U. S. Army T&E Command
ATTN: AMSTE-EL
Aberdeen Prvg Gnd, Md 21005 1

27. Commanding General
U. S. Army T&E Command
ATTN: AMSTE-BAF
Aberdeen Prvg Gnd, Md 21005 1

28. Commandant
U. S. Army CBR School
ATTN: Micromet Sec, Lt Col Saunders
Ft McClellan, Ala. 36205 1

29. Chief, Comm-Electronics
Department of the Army
ATTN: Elct Sys Directorate
Washington, D. C. 20315 1

30. Asst CofS for Intel
Department of Army
ATTN: ACSI-DSRSI
Washington, D. C. 20310 1

31. Commander
Air Weather Service (MATS)
ATTN: AWSSS/TIPD
Scott AF Base, Ill. 62226 1

32. Commander
AF Cambridge Rsch Labs
ATTN: GRXL
L. G. Hanscom Field
Bedford, Mass. 01730 1

33. Commander
USAF Cambridge Rsch Labs
ATTN: CRZW
1065 Main Street
Waltham, Mass 02154 1

34. Chief of Naval Research
ATTN: CODE 427
Department of Navy
Washington, D. C. 20350 1

35. Commanding Officer
U. S. Naval Weather Service
U. S. Naval Air Station
Washington, D. C. 20390 1

36. Officer in Charge
U. S. Naval Weather Rsch Fac
U. S. Naval Air Sta, Bldg R-28
Norfolk, Virginia 23501 1

37. Director
Atmospheric Sciences Programs
National Sciences Foundation
Washington, D.C. 20550 1

38. Director
Bureau of Rsch & Development
Federal Aviation Agency
Washington, D.C. 20553 1

39. Chief, Fallout Studies Br
Div of Biology & Medicine
Atomic Energy Commission
Washington, D.C. 20545 1

40. Office, Asst SECDEF (R&E)
The Pentagon
ATTN: Tech Library
Washington, D.C. 20301 1

41. Director, Met Systems
Office of Applications (FM)
Natl Aeronautics & Space Adm
Washington, D.C. 20546 1

42. Chief, U.S. Weather Bureau
24th and M Streets
ATTN: Librarian
Washington, D.C. 20235 1

43. Weather Bureau Rsch Sta
c/o Robert A. Taft Sanitary
Engineering Center
4676 Columbia Parkway
Cincinnati, Ohio 45226 1

44. National Cen for Atmos. Rsch
ATTN: Library
Boulder, Colorado 80301 1

45. Defense Documentation Center
Cameron Station
Alexandria, Va. 22314 20

46. Commanding General
U S. Army Munitions Command
ATTN: AMSMU-RE-R
Dover, New Jersey 07801 1

47. Commanding Officer
U.S. Army Biological Labs
ATTN: K. L. Calder
Ft. Detrick, Fredrick, Md.
21701 1

48. Scientific & Tech Info Agcy
Attn: NASA Rep (S-AK/DL)
P.O. Box 5700
Bethesda, Md. 20014 1

49. Commanding General
CDC Experimentation Cen
Fort Ord, Calif 93941 1

50. Director, Meteorology Dept
University of Arizona
Tucson, Arizona 85717 1

51. Director
U.S. Water Conservation Lab
Agricultural Rsch Svc, USDA
Route 2, Box 816-A
Tempe, Arizona 85281 1

52. Director
Pac SW Forest & Range Ex Sta
USDA Forest Service Box 245
Berkeley, Calif 94704 1

53. Director, Meteorology Dept
Univ of California at L.A.
Los Angeles, Calif 90052 1

54. Director, U.S. Salinity Lab
P.O. Box 672
ATTN: Dr. Richards
Riverside, Calif 92502 1

55. Department of Irrigation
ATTN: Dr. W. Pruitt
University of California
Davis, Calif 95616 2

56. Dept of Agricultural Engng
University of California
ATTN; Dr. F. A. Brooks
Davis, Calif 95616 1

57. Meteorology Department
San Jose State College
San Jose, Calif 95113 1

58. Chief, Radio Propagation Lab
U.S. Natl Bureau of Standards
Boulder, Colo. 80301 1

59. Dept of Civil Engineering
Colorado State University
ATTN: Dr. J. E. Cermak
Fort Collins, Colo 80521 1

60. Forest Service Exper Sta
Colorado State University
ATTN: M. Marinelli, Jr.
Rm 221, Forestry Bldg
Fort Collins, Colo 80521 1

61. Director, Meteorology Dept
Florida State University
Tallahassee, Florida 32301 1

62. Director, USDA Field Sta
(Southern Piedmont Soil
Conservation Sta)
P.O. Box 33
Watkinsville, Ga. 30677 1

63. Meteorology Department
University of Hawaii
Honolulu, Hawaii 96822 1

64. Director, Meteorology Dept
University of Chicago
Chicago, Illinois 60607 1

65. Department of Agronomy
Iowa State University
ATTN: Dr. R. H. Shaw
Ames, Iowa 50010 1

66. Director
Soil & Water Consvtn Div
Agricultural Rsch Svc (USDA)
Beltsville, Md. 20705 1

67. Director
Department of Civil Engng
John Hopkins University
Baltimore, Md. 21233 1

68. Executive Secretary
American Met Society
45 Beacon Street
Boston, Mass. 02109 1

69. Round Hill Field Station
Mass. Inst. of Technology
South Dartmouth, Mass. 02748 1

70. Director, Meteorology Dept
University of Michigan
Ann Arbor, Mich. 48105 1

71. Director of Meteorology Dept.
Mass. Inst. of Technology
Cambridge, Mass. 02138 1

72. University of Minnesota
ATTN: Dean Spilhaus
Minneapolis, Minn. 55041 1

73. Director, Meteorology Dept
St. Louis University
St. Louis, Mo. 63120 1

74. Department of Soils
University of Missouri
Columbia, Mo. 62501 1

75. Department of Geophysics
Washington University
St. Louis, Mo. 63120 1

76. Director, Meteorology Dept
New York University
University Heights
New York, N.Y. 10001 1

77. Soil & Water Consvtn Rsch Div
Agricultural Rsch Svc (USDA)
Cornell Univ, Bailey Hall
Ithaca, N.Y. 14851 1

78. Scientific Rsch Institute
Oregon State College
ATTN: Atmos. Sciences Br.
Corvallis, Oregon 97330 1

79. Director, Meteorology Dept
Pennsylvania State Univ
University Sta., Pa 16802 1

80. Department of Oceanography & Met
Texas A & M College
College Station, Tex 77840 1

81. Electrical Engng Rsch Lab
University of Texas
Route 4, Box 189
Austin, Texas 78761 1

82. Department of Meteorology
University of Utah
Salt Lake City, Utah 84116 1

83. Director, Natl Rsch Council
Natl Academy of Sciences
2101 Constitution Avenue
Washington, D.C. 20315 1

84. Director, Meteorology Dept
University of Washington
Seattle, Wash. 99703 1

85. Director, Meteorology Dept
University of Wisconsin
Madison, Wisconsin 53705 1

86. Department of Soils
University of Wisconsin
ATTN: Dr. C. B. Tanner
Madison, Wisconsin 53705 1

87. Officer-in-Charge
Meteorological Curriculum
U. S. Naval Post Graduate Sch
Monterey, Calif. 92801 1

88. Director, Geophysical Rsch
USAF Cambridge Rsch Cen
ATTN: CRZHB (Hanscom Field)
Bedford, Mass 01730 1

89. Deputy for Defense R&E
Office of SECDEF
ATTN: Geophysical Sciences
Washington, D.C. 20315 1

90. USAF Climatic Center
Air Weather Svc (MATS)
ATTN: CCCAD
Annex 2, 225 D., St. S.E.
Washington, D.C. 20315 1

91. Forestry Library
260 Walter Mulford Hall
University of California
Berkeley, Calif 94704 1

92. Commander
AF Cambridge Rsch Labs
ATTN: Chief, Boundary Layer Branch
Bedford, Mass. 01730 1

93. Argonne National Lab
ATTN: Mr. Harry Moses
Meteorology Building
9700 South Cass Avenue
Argonne, Ill. 60440 1

94. Commanding Officer
U.S. Army Chemical School
ATTN: Micromet Br Tech Div
Ft McClellan, Ala 36205 1

95. Prof. J.E. Pearson
University of Illinois
General Engineering Dept
Atmospheric Sciences Lab
Urbana, Illinois 1

96. Brookhaven National Lab
ATTN: Meteorology Group
Upton Long Island, N.Y. 1

97. Director
National Security Agency
ATTN: C3/TDL
Ft. George G. Meade, Md
20755 1

98. U.S. Naval Ordnance Test Sta.
CODE 40306
ATTN: Dr. Richard Jackson
China Lake, Calif 93557 1

99. Office of Chief Engineer
Bureau of Reclamation
ATTN: CODE 755
Bldg 53, Denver Federal Cen
Denver, Colorado 80225 1

100. Weather Bureau Forecast Cen
Rm 911, Federal Office Bldg
Kansas City, Mo. 64106 1

101. Agricultural Research Svc
Snake River Consvtn Rsch Cen
ATTN: Dr. James L. Wright
Route 1, Box 186
Kimberly, Idaho 83341 1

DOCUMENT CONTROL DATA - R&D

(Security classification of title, body of abstract and indexing annotation must be entered when the overall report is classified)

1. ORIGINATING ACTIVITY *(Corporate author)*
University Of Wisconsin, Madison, Wisconsin

2a. REPORT SECURITY CLASSIFICATION
UNCLASSIFIED

2b. GROUP
N/A

3. REPORT TITLE
STUDIES OF THE EFFECTS OF VARIATIONS IN BOUNDARY CONDITIONS ON THE ATMOSPHERIC BOUNDARY LAYER

4. DESCRIPTIVE NOTES *(Type of report and inclusive dates)*
Final Report October 1962 to Sept 1965

5. AUTHOR(S) *(Last name, first name, initial)*
Lettau, Heinz H.; Hamilton, Harry L., Jr.; Johnson, Warren B., Jr.; and Lenschow, Donald H.

6. REPORT DATE	7a. TOTAL NO. OF PAGES	7b. NO. OF REFS
October 1965	249	179

8a. CONTRACT OR GRANT NO.	9a. ORIGINATOR'S REPORT NUMBER(S)
Contract DA-36-039-AMC-00878(E) b. PROJECT NO. 1V0-14501-B53A	N/A
c. Task No. 1V0-14501-B53A-08 d.	9b. OTHER REPORT NO(S) *(Any other numbers that may be assigned this report)* N/A

10. AVAILABILITY/LIMITATION NOTICES Qualified requesters may obtain copies of this report from Defense Documentation Center, Cameron Station, Alexandria, Virginia 22314. Foreign announcement and dissemination of this report by DDC is not authorized.

11. SUPPLEMENTARY NOTES	12. SPONSORING MILITARY ACTIVITY
N/A	Meteorology Department U.S. Army Electronics Research & Development Activity, Fort Huachuca, Arizona

13. ABSTRACT

This report contains a brief survey of research efforts previously reported under the contract, together with five new papers resulting from work done during the concluding year of the contract.

1. Longitudinal Versus Lateral Eddy Length Scale. A previously proposed vorticity-transfer-and-adaptation hypothesis is briefly summarized and supplemented by consideration of certain spatial derivatives of the components of the eddy displacement vector. The conventional length-scale of turbulence, previously redefined as a lateral covariance $\ell = (\overline{x'z'})^{\frac{1}{2}}$, is supplemented by the new concept of a longitudinal length-scale, defined as the variance $L = (\overline{x'^2})^{\frac{1}{2}}$.

2. A Universal Law Relating Eddy to Mean States, Applied to Turbulence in Ducts. A generalized mathematical form is presented which relates the 3-dimensional vector ($\underset{\sim}{v}$) of fluctuating velocity to the vector ($\overline{\underset{\sim}{v}}$) of mean motion, and also the fluctuation value(s) of a scalar fluid property to the mean value ($\overline{s}$), with the aid of a 3-dimensional fluctuating vector of eddy displacements ($\underset{\sim}{r}' \equiv \underset{\sim}{i}x' + \underset{\sim}{i}y' + \underset{\sim}{k}z'$), in the applicable equations.

3. Atmospheric Boundary Layer Dynamics over the Forests of Northeastern Wisconsin. Results are reported for seven observational periods spanning about a year's time over extensive deciduous forests of northeastern Wisconsin. A total of 209 usable detailed wind profiles for the lowest 2 km of the atmosphere were obtained by tracking pilot balloons with two theodolites. Supplementary surface-layer measurements of net radiation, wind, and temperature permit estimates of the surface heat-budget parameters, atmospheric stability, and aerodynamic surface roughness length.

UNCLASSIFIED

Block 13. Abstract (Cont'd)

4. Airborne Measurements of Atmospheric Boundary Layer Structure. Measurements of vertical and horizontal velocity, air and surface temperature, absolute humidity, and incoming and reflected solar radiation within the atmospheric boundary layer were obtained from an airplane. Nine series of airborne measurements were taken simultaneously with balloon measurements of the mean wind profile over the forest of northeastern Wisconsin during early spring and summer, and ten flights were made to measure air mass modification over Lake Michigan. In the analysis of the data, particular attention is paid to computations of rate of generation of turbulent kinetic energy in the boundary layer and its conversion to internal and potential energy. Energy dissipation values obtained from the structure function formulation of the Kolmogorov similarity hypothesis are compared with those computed from the spectral density formulation. Detailed comparison is also made of results obtained from the analysis of wind profiles in the boundary layer and simultaneous airplane fluctuation measurements.

5. Measurements of Infrared Radiation Divergence and Temperature Profiles Near an Air-Water Interface. Equipment was constructed and used in an experimental program over Lake Mendota, Wisconsin, to investigate the significance of infrared radiative fluxes and their vertical divergence in the air between 0.4 and 2.8m above the water. An analysis program based on Funk's method was developed to derive the radiative flux divergences from the observed temperature and water vapor profiles. Based on a sizable amount of data obtained during late summer and early fall seasons, for both stable and unstable conditions, the experimental evidence appears to show that radiation flux divergence over the water surface is great enough to produce the observed temperature change.

Block 14. Key Words (Cont'd)

Section 3	Section 4	Section 5
atmospheric boundary-layer	airborne measurements	micrometeorology
wind profiles	balloon measurements	air-water interface
geostrophic wind profiles	boundary layer structure	infrared radiation
heat budget	energy balance	temperature profiles
balloon measurements	deciduous forest	water-vapor profiles
airborne measurements	air mass over Lake Michigan	radiative flux divergence
radiosonde	spectral density function	air-sea interaction
deciduous forest	Kolmogorov hypothesis	
surface roughness		
energy dissipation		
thermal wind		
geostrophic drag coefficient		

14. KEY WORDS	LINK A		LINK B		LINK C	
	ROLE	WT	ROLE	WT	ROLE	WT
Section 1 and 2 turbulence vorticity-transfer-and-adaptation hypothesis eddy displacement vector lateral co-variance variance eddy diffusivity shearing velocity mixing length Karman constant jet flow turbulent flow shear flow (continued)						

INSTRUCTIONS

1. ORIGINATING ACTIVITY: Enter the name and address of the contractor, subcontractor, grantee, Department of Defense activity or other organization *(corporate author)* issuing the report.

2*a*. REPORT SECURITY CLASSIFICATION: Enter the overall security classification of the report. Indicate whether "Restricted Data" is included. Marking is to be in accordance with appropriate security regulations.

2*b*. GROUP: Automatic downgrading is specified in DoD Directive 5200.10 and Armed Forces Industrial Manual. Enter the group number. Also, when applicable, show that optional markings have been used for Group 3 and Group 4 as authorized.

3. REPORT TITLE: Enter the complete report title in all capital letters. Titles in all cases should be unclassified. If a meaningful title cannot be selected without classification, show title classification in all capitals in parenthesis immediately following the title.

4. DESCRIPTIVE NOTES: If appropriate, enter the type of report, e.g., interim, progress, summary, annual, or final. Give the inclusive dates when a specific reporting period is covered.

5. AUTHOR(S): Enter the name(s) of author(s) as shown on or in the report. Enter last name, first name, middle initial. If military, show rank and branch of service. The name of the principal author is an absolute minimum requirement.

6. REPORT DATE: Enter the date of the report as day, month, year; or month, year. If more than one date appears on the report, use date of publication.

7*a*. TOTAL NUMBER OF PAGES: The total page count should follow normal pagination procedures, i.e., enter the number of pages containing information.

7*b*. NUMBER OF REFERENCES: Enter the total number of references cited in the report.

8*a*. CONTRACT OR GRANT NUMBER: If appropriate, enter the applicable number of the contract or grant under which the report was written.

8*b*, 8*c*, & 8*d*. PROJECT NUMBER: Enter the appropriate military department identification, such as project number, subproject number, system numbers, task number, etc.

9*a*. ORIGINATOR'S REPORT NUMBER(S): Enter the official report number by which the document will be identified and controlled by the originating activity. This number must be unique to this report.

9*b*. OTHER REPORT NUMBER(S): If the report has been assigned any other report numbers *(either by the originator or by the sponsor)*, also enter this number(s).

10. AVAILABILITY/LIMITATION NOTICES: Enter any limitations on further dissemination of the report, other than those imposed by security classification, using standard statements such as:

(1) "Qualified requesters may obtain copies of this report from DDC."

(2) "Foreign announcement and dissemination of this report by DDC is not authorized."

(3) "U. S. Government agencies may obtain copies of this report directly from DDC. Other qualified DDC users shall request through _____."

(4) "U. S. military agencies may obtain copies of this report directly from DDC. Other qualified users shall request through _____."

(5) "All distribution of this report is controlled. Qualified DDC users shall request through _____."

If the report has been furnished to the Office of Technical Services, Department of Commerce, for sale to the public, indicate this fact and enter the price, if known.

11. SUPPLEMENTARY NOTES: Use for additional explanatory notes.

12. SPONSORING MILITARY ACTIVITY: Enter the name of the departmental project office or laboratory sponsoring *(paying for)* the research and development. Include address.

13. ABSTRACT: Enter an abstract giving a brief and factual summary of the document indicative of the report, even though it may also appear elsewhere in the body of the technical report. If additional space is required, a continuation sheet shall be attached.

It is highly desirable that the abstract of classified reports be unclassified. Each paragraph of the abstract shall end with an indication of the military security classification of the information in the paragraph, represented as *(TS)*, *(S)*, *(C)*, *or (U)*.

There is no limitation on the length of the abstract. However, the suggested length is from 150 to 225 words.

14. KEY WORDS: Key words are technically meaningful terms or short phrases that characterize a report and may be used as index entries for cataloging the report. Key words must be selected so that no security classification is required. Idenfiers, such as equipment model designation, trade name, military project code name, geographic location, may be used as key words but will be followed by an indication of technical context. The assignment of links, rules, and weights is optional.